

1 INTRODUCTION

For some 30 years now, we have manufactured piezoelectric ceramics and marketed them under the trade name

PZT (Lead Zirconate Titanate)

All these materials are compounds of lead zirconate and lead titanate manufactured by the most modern production methods. One of their principal advantages is that their **properties can be optimized** to suit specific applications by appropriate adjustment of the zirconate-titanate ratio.

Piezoelectric ceramics **are hard, chemically inert and completely insensitive to humidity or other atmospheric influences**. Their mechanical properties resemble those of the better known ceramic insulators and they are manufactured by much the same processes.

Piezoelectric components **are ideal for all kinds of electromechanical transducers**. Here are just some examples of the many applications you will find our PZT materials used in.

Generators (conversion of mechanical into electrical energy)

- spark igniters
- solid-state batteries

Sonic and ultrasonic transducers (conversion of electrical into mechanical energy)

sonic (< 20 kHz)

- buzzers
- telephone microphones
- high-frequency loudspeakers

ultrasonic

- echo-sounders

measurement of distance in air

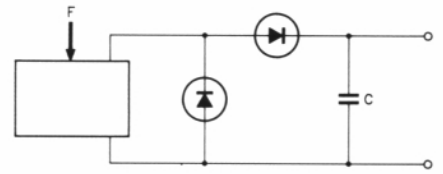
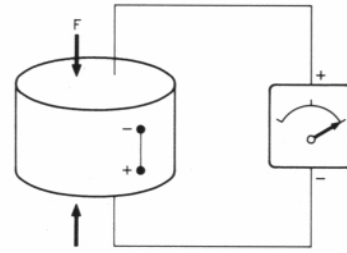
- materials-testing equipment
- atomizers
- welding equipment
- cleaning processes

higher-frequency ultrasonic

- medical applications
- delay lines

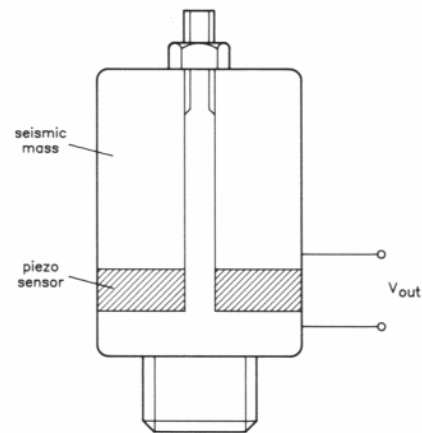
Sensors (conversion of mechanical force or movement into a (proportional) electric signal)

- **acceleration sensor**
- **pressure sensor**
- **knock sensor** (internal-combustion engines)



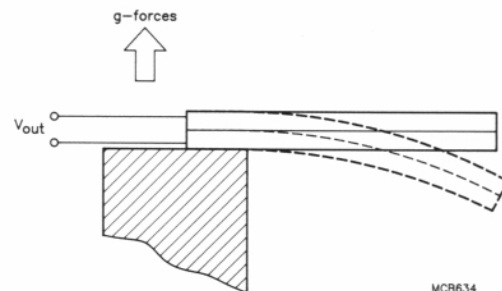
MCB632

PZT as a generator



MCB633

Knock sensor

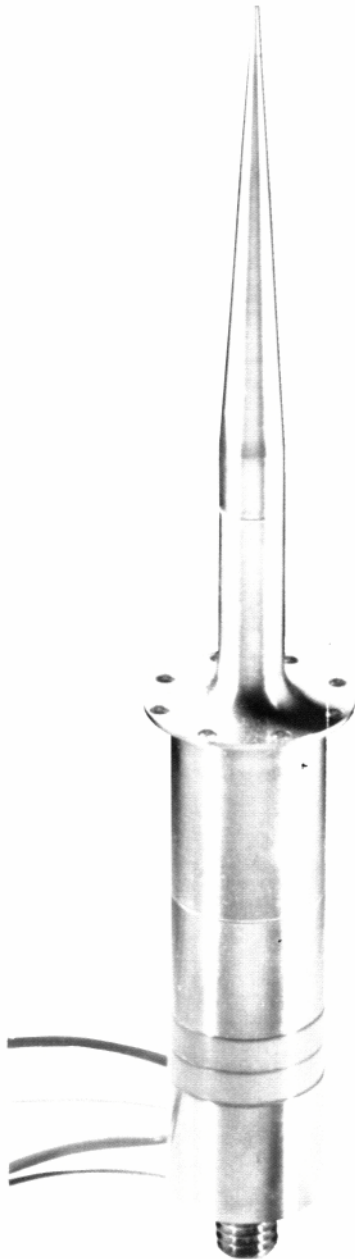
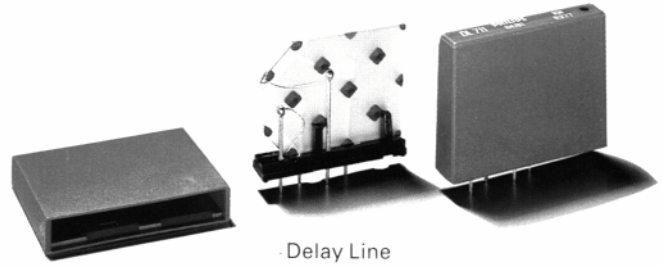


MCB634

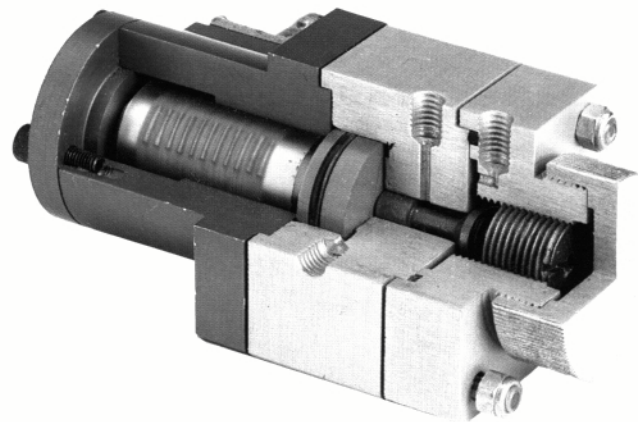
Acceleration sensor

Actuators (conversion of electrical signals into a (proportional) mechanical displacement)

- low-power actuators in:
 - video cassette recorders (**DTF**)
 - pneumatic valves
 - reading aids for the blind
- high-power actuators (**HPAs**)
 - hydraulic valves
 - fuel-injection valves
 - tool adjustment



Welding transducer



Fuel injection valve

2.1 The piezoelectric effect in ceramic materials

The **piezoelectric effect** was discovered by Jacques and Pierre Curie in 1880. They found that **if certain crystals were subjected to mechanical strain, they became electrically polarized and the degree of polarization was proportional to the applied strain.** The Curies also discovered that these same materials deformed when they were exposed to an electric field. This has become known as the inverse **piezoelectric effect**.

The piezoelectric effect is exhibited by a number of naturally-occurring crystals, for instance **quartz, tourmaline and sodium potassium tartrate,** and these have been used for many years as electromechanical transducers. For a crystal to exhibit the piezoelectric effect, its structure should have no centre of symmetry. A stress (tensile or compressive) applied to such a crystal will **alter the separation between the positive and negative charge sites in each elementary cell** leading to a net polarization at the crystal surface. The effect is practically linear, i.e. the polarization varies directly with the applied stress, and direction-dependent, so that compressive and tensile stresses will generate electric fields and hence voltages of opposite polarity. It's also reciprocal, so that if the crystal is exposed to an electric field, it will experience an elastic strain causing its length to increase or decrease according to the field polarity.

2.2 Piezoelectric materials

Besides the crystals mentioned above, an important group of piezoelectric materials are the piezoelectric ceramics, of which PZT is an example. These are **polycrystalline ferroelectric materials** with the perovskite crystal structure - a tetragonal/rhombohedral structure very close to cubic. They have the general formula $A^{2+}B^{4+}O_3$, in which A denotes a large divalent metal ion such as barium or lead, and B denotes a tetravalent metal ion such as titanium or zirconium. It's these materials that are the subject of the present book (Ref. 1).

Materials such as PZT can be considered as a mass of minute crystallites. Above a temperature known as the Curie point, these crystallites exhibit simple cubic symmetry, the elementary cell of which is shown in Fig.2.1(a). This structure is centrosymmetric with positive and negative charge sites coinciding, so there are no dipoles present in the material (which is said to exhibit paraelectric behaviour). Below the Curie point, however, the crystallites take on tetragonal symmetry in which the positive and negative charge sites no longer coincide (Fig.2.2(b)), so each elementary cell then has a built-in electric dipole which may be reversed, and also switched to certain allowed directions by the application of an electric field. Such materials are termed ferroelectric because this electrical

behaviour presents a physical analogy with the magnetic behaviour of ferromagnetic materials. They don't necessarily contain iron as an important constituent. The analogy can, in fact, be carried further, since to some extent the polarization of ferroelectric materials exhibits hysteresis, and their dielectric constants are very high and temperature-dependent (as are the permeabilities of ferromagnetic materials).

The dipoles are not randomly oriented throughout the material. Neighbouring dipoles align with each other to form regions of local alignment known as Weiss domains. Within a Weiss domain, therefore, all the dipoles are aligned, giving a net dipole moment to the domain, and hence a net polarization (dipole moment per unit volume).

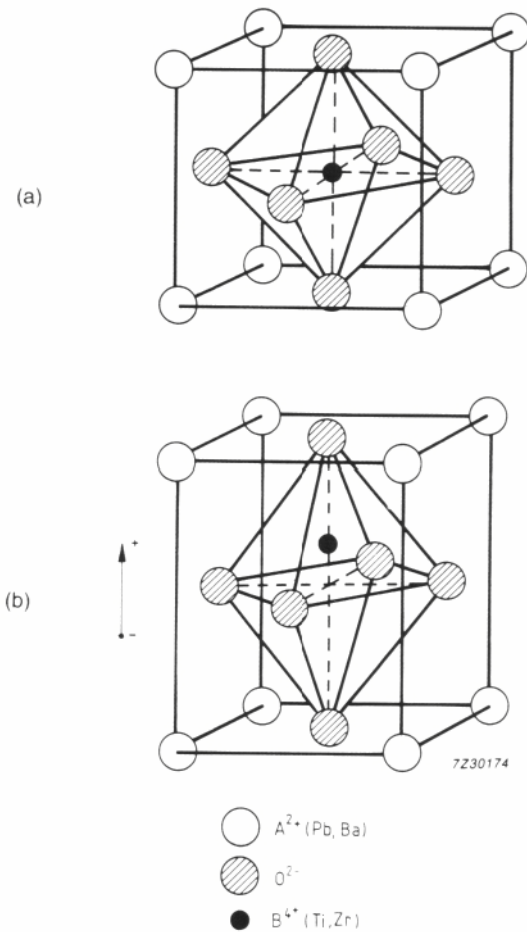


Fig.2.1 PZT elementary cell.

(a) cubic lattice (above Curie temperature);

(b) tetragonal lattice (below Curie temperature)

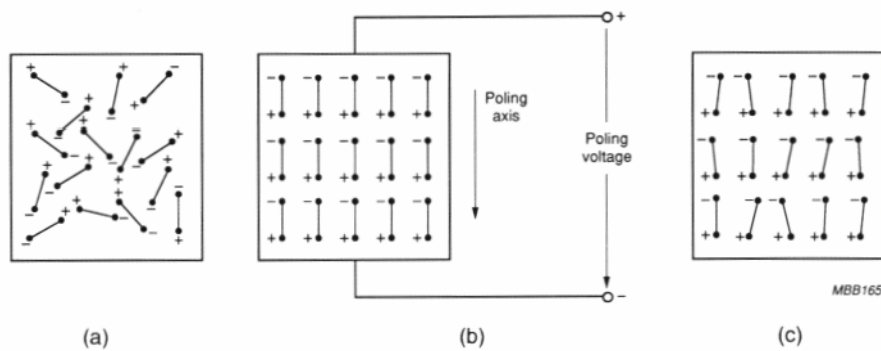


Fig.2.2 Electric dipole moments in Weiss domains.

- (a) before polarization;
- (b) during polarization;
- (c) after polarization

The direction of polarization between neighbouring Weiss domains within a crystallite can differ by 90° or 180° , and owing to the random distribution of Weiss domains throughout the material (Fig.2.2(a)), no overall polarization or piezoelectric effect is exhibited. The ceramic may be made piezoelectric in any chosen direction by a poling treatment which involves exposing it to a strong electric field at a temperature slightly below the Curie point (Fig.2.2(b)). Under the action of this field, domains most nearly aligned with the field will grow at the expense of other domains. The material will also lengthen in the direction of the field. When the field is removed (Fig.2.2(c)), the dipoles remain locked in approximate alignment, giving the ceramic material a remanent polarization and a permanent deformation (i.e. making it anisotropic). The poling treatment is usually the final treatment of PZT component manufacture.

2.3 Dielectric hysteresis

The electric field E and the polarization P are connected in a dielectric medium by the relation:

$$D = \epsilon_0 E + P \quad (2.1)$$

in which ϵ_0 is the permittivity of free space and D is the electric displacement. For a ferroelectric material like PZT, however, P is itself a function of E as shown in Fig.2.3. In this figure, the hysteresis effect, familiar from ferromagnetics, is quite evident. If an initially unpolarized sample of PZT is subjected to an increasing electric field at a temperature slightly below its Curie point, the dipoles become increasingly aligned with the field and the polarization will follow the 'initial curve' shown in Fig.2.3. When the field has increased beyond a certain value, no further increase in polarization will be observed because the dipoles are then all aligned with the field. The material is then said to have reached its saturation polarization P_{s^*} .

If the field is now reduced to zero, the dipoles become less strongly aligned, since in the absence of an external field they're bound to certain preferred directions within the individual crystallites. They do not, however, return to their original alignment (i.e. the alignment before the field was applied) since there are several preferred directions within the crystallites and the dipoles remain in the ones most closely aligned with the original field. Since there is still, therefore, a very high degree of alignment (as can be seen from Fig.2.2(c)), the polarization does not fall back to zero but to a value somewhat lower than the saturation polarization known as the remanent polarization P_r .

If the field is now increased in the opposite direction, the polarization of the sample initially falls to zero and then increases in the negative direction until it reaches a saturation polarization $-P_{s^*}$. If the field is again reduced to zero, the polarization falls to the remanent polarization $-P_r$ and finally, if the field is increased in the positive direction again, the polarization will fall to zero and then eventually return to P_{s^*} .

The curve thus traced out is known as the hysteresis curve. Its shape varies for the different PZT materials (Fig.2.3 is the hysteresis curve for a 'soft' PZT) but the remanent polarization is generally around 0.3 C/m^2 for all PZT materials.

The variation of electric displacement D as a function of electric field strength follows very closely the curve for polarization. For example, at the peak of the hysteresis curve ($E = 1.6 \text{ kV/mm}$), D is only around 0.014 C/m^2 higher than P . At $E = 0$, D and P are equal, i.e. $D = P_r$.

The lower part of Fig.2.3 shows the variation of the sample's relative extension S_3 (i.e. in the direction of polarization) with electric field, and it can be seen that this also exhibits a hysteresis effect corresponding precisely with the effect observed for polarization.

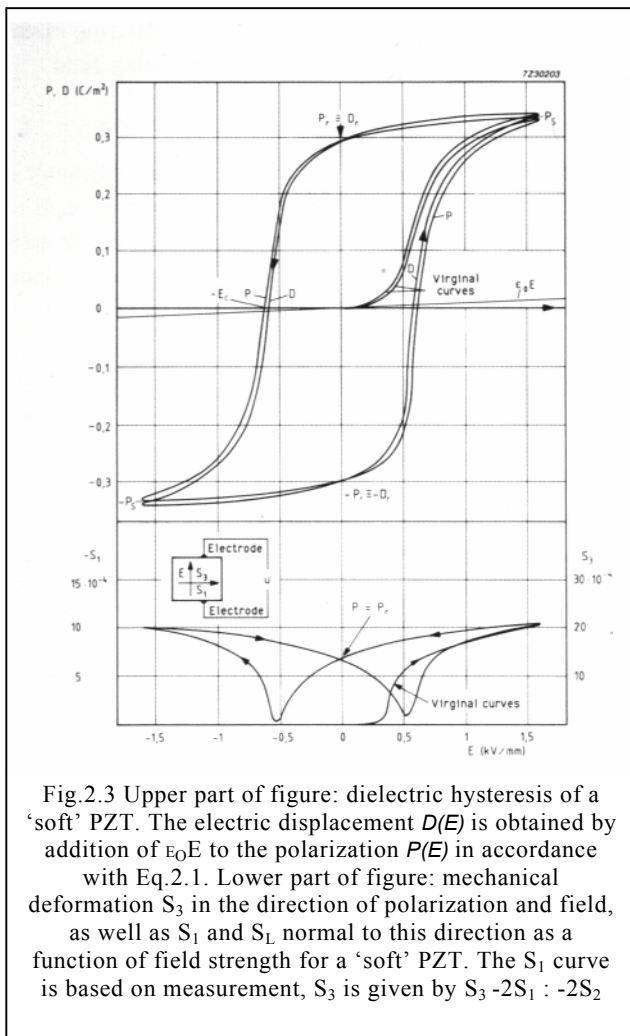


Fig.2.3 Upper part of figure: dielectric hysteresis of a 'soft' PZT. The electric displacement $D(E)$ is obtained by addition of $\epsilon_0 E$ to the polarization $P(E)$ in accordance with Eq.2.1. Lower part of figure: mechanical deformation S_3 in the direction of polarization and field, as well as S_1 and S_L normal to this direction as a function of field strength for a 'soft' PZT. The S_1 curve is based on measurement, S_3 is given by $S_3 - 2S_1 : -2S_2$

Since the volume of the sample remains roughly constant, a relative increase (or decrease) in S_3 will be accompanied by a relative decrease (or increase) in the sample's dimension perpendicular to the field (S_1 and S_2) equal to about half the change in S_3 (the left hand scale in the lower part of Fig.2.3). This is also true, incidentally, for compressive and tensile forces exerted by the sample.

Finally, Fig.2.4 shows how S_1 varies with electric displacement, and again shows the hysteresis effect.

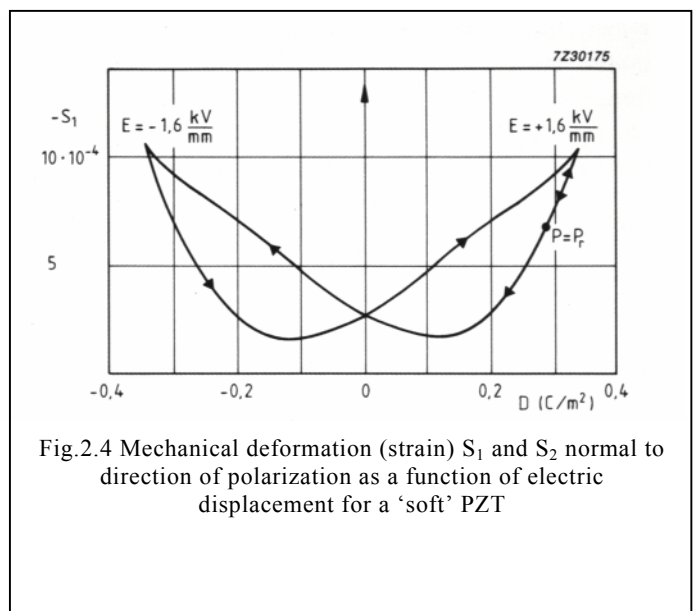


Fig.2.4 Mechanical deformation (strain) S_1 and S_2 normal to direction of polarization as a function of electric displacement for a 'soft' PZT

2.4 Basic behaviour of a piezoelectric ceramic body

Figure 2.5 illustrates the behaviour of a PZT cylinder polarized along its axis. For clarity, the magnitude of the effect has been exaggerated.

Figure 2.5(a) shows the cylinder under no-load conditions. If an external force produces compressive or tensile strain in the material, the resulting change in dipole moment causes a voltage to appear between the electrodes. If the cylinder is compressed so that it resumes its original form, i.e. before poling, the voltage will have the same polarity as the poling voltage (Fig.2.5(b)). If it is stretched, the voltage across the electrodes will have opposite polarity to the poling voltage (Fig.2.5(c)). These are examples of **generator action**: the conversion of mechanical energy into electrical energy. Examples of piezoelectric induced generator action can be found in cigarette and gas lighters, gramophone pick-ups, accelerometers, hydrophones and microphones.

If a voltage of opposite polarity to the poling voltage is applied to the electrodes, the cylinder will shorten (Fig.2.5(d)). If the applied voltage has the same polarity as the poling voltage, the cylinder will lengthen (Fig.2.5(e)).

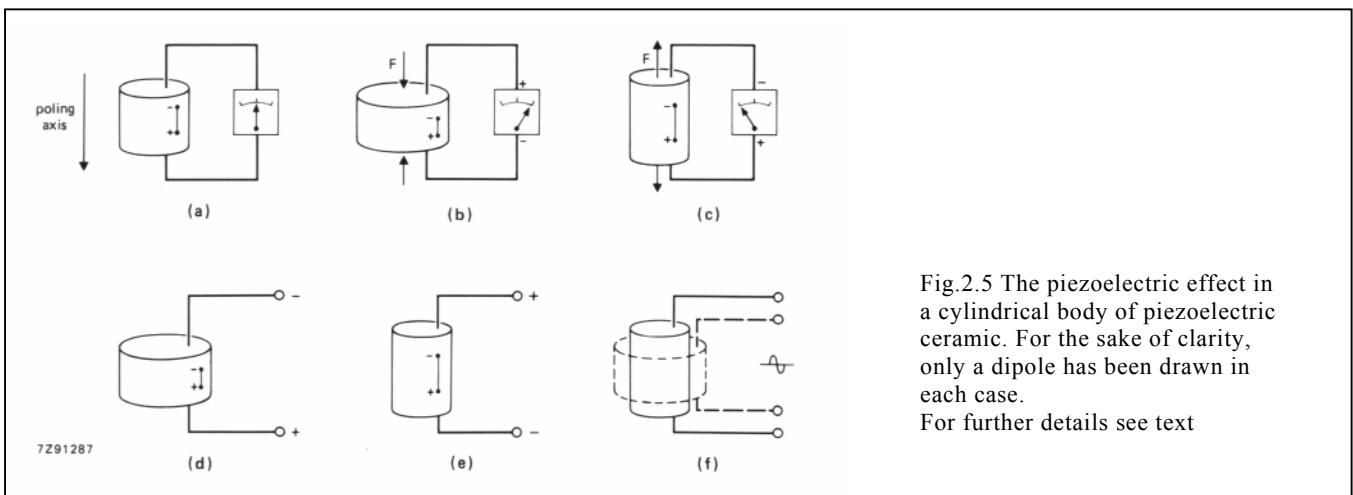
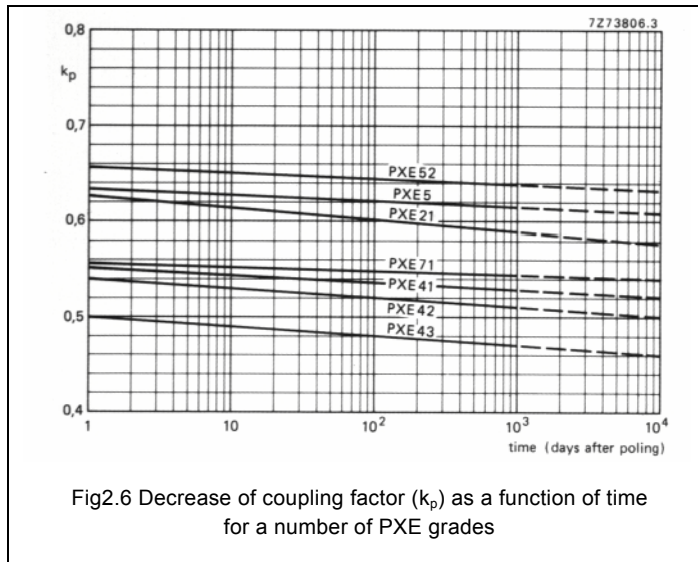


Fig.2.5 The piezoelectric effect in a cylindrical body of piezoelectric ceramic. For the sake of clarity, only a dipole has been drawn in each case.

For further details see text

Finally, if an alternating voltage is applied to the electrodes, the cylinder will grow and shrink at the same frequency as that of the applied voltage (Fig.2.5(f)). These are examples of **motor action**: conversion of electrical energy into mechanical energy.



2.5 Stability

The properties of piezoelectric elements are more or less temperature dependent and time dependent. The stability as a function of time is of particular interest. Fortunately the poling ages approximately logarithmically so that the rate of change in permittivity, coupling factor, frequency constant and so on (Section 2.11), decreases rapidly in the course of time. Powerful ambient influences are likely to change the original ageing pattern. This applies particularly to the permittivity, the mechanical Qfactor and the dielectric loss factor $\tan\delta$.

2.6 Depolarization

As already mentioned, after its poling treatment a PZT ceramic will be permanently polarized, and care must therefore be taken in all subsequent handling to ensure that the ceramic is not depolarized, since this will result in partial or even total loss of its piezoelectric properties. The ceramic may be depolarized electrically, mechanically or thermally.

2.6.1 Electrical depolarization

Exposure to a strong electric field of opposite polarity to the poling field will depolarize a piezoelectric element. The field strength required for marked depolarization depends, among other things, on the material grade, the time the material is subjected to the depolarizing field and the temperature. For static fields, it's typically between 200 and 500 V/mm.

An alternating field will also have a depolarizing effect during the half cycles that it opposes the poling field.

2.6.2 Mechanical depolarization

Mechanical depolarization occurs when the mechanical stress on a piezoelectric element becomes high enough to disturb the orientation of the domains and hence destroy the alignment of the dipoles. The safety limits for mechanical stress vary considerably with material grade.

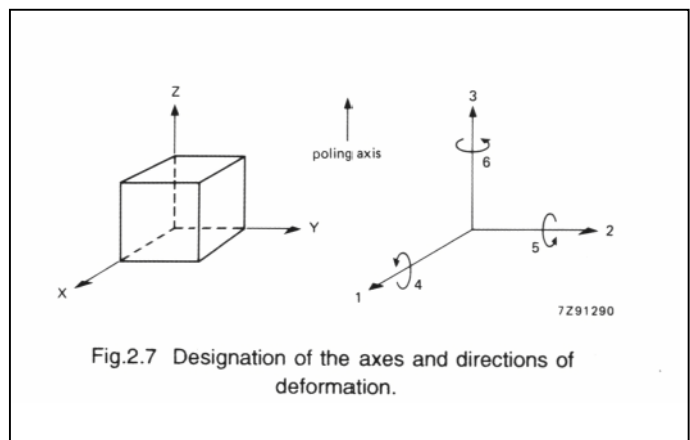
2.6.3 Thermal depolarization

If a piezoelectric element is heated to its Curie point, the domains become disordered and the element becomes completely depolarized. A piezoelectric element can therefore function for long period without marked depolarization only at temperatures well below the Curie point. A safe operating temperature would normally be about half way between 0 °C and the Curie point.

2.7 Piezoelectric constants

Since piezoelectric ceramics are anisotropic, their physical constants (elasticity, permittivity etc.) are tensor quantities and relate to both the direction of the applied stress, electric field etc., and to the directions perpendicular to these. For this reason the constants are generally given two subscript indices which refer to the direction of the two related quantities (e.g. stress and strain for elasticity, displacement and electric field for permittivity). A superscript index is used to indicate a quantity that's kept constant (Ref.2).

The direction of positive polarization is usually chosen to coincide with the Z-axis of a rectangular system of crystallographic axes X, Y, Z. If the directions of X, Y and Z are represented by 1, 2 and 3 respectively, and the shear about these axes by 4, 5 and 6 respectively, the various constants may be written with subscripts referring to these (Fig.2.7).



This system will now be illustrated with a few examples for the main piezoelectric constants.

Permittivity E

The (absolute) permittivity (or dielectric constant) is defined as the dielectric displacement per unit electric field. The first subscript gives the direction of the dielectric displacement, the second gives the direction of the electric field. For example:

ϵ_{11}^T is the permittivity for the dielectric displacement and electric field in direction 1 under conditions of constant stress, and

ϵ_{33}^S is the permittivity for the dielectric displacement and electric field in direction 3 under conditions of constant strain.

The tables in our Data handbook give values for the relative permittivity ϵ/ϵ_0 , i.e. the ratio of absolute permittivity to the permittivity of free space (8.85×10^{-12} F/m).

Compliance s

The compliance s of a material is defined as the strain produced per unit stress. It's the reciprocal of the modulus of elasticity. The first subscript refers to the direction of strain, the second to direction of stress. For example:

s_{11}^E is the compliance for a stress and accompanying strain in direction 1 under conditions of constant electric field, and

s_{36}^D is the compliance for a shear stress about axis 3 and accompanying strain in direction 3 under conditions of constant electric displacement.

Piezoelectric charge constants d

The piezoelectric charge constant is defined as the electric polarization generated in a material per unit mechanical stress applied to it. Alternatively, it is the mechanical strain experienced by the material per unit electric field applied to it. The first subscript refers to the direction of polarization generated in the material (at $E = 0$) or to the applied field strength, the second refers respectively to the direction of the applied stress or to the direction of the induced strain. For example:

d_{33} is the induced polarization per unit applied stress in direction 3. Alternatively it is the induced strain per unit electric field in direction 3.

d_{31} is the induced polarization in direction 3 per unit stress applied in direction 1. Alternatively it is the mechanical strain induced in the material in direction 1 per unit electric field applied in direction 3.

Piezoelectric voltage constant g

The piezoelectric voltage constant is defined as the electric field generated in a material per unit mechanical stress applied to it. Alternatively, it is the mechanical strain experienced by the material per unit electric displacement applied to it. The first subscript refers to the direction of the electric field generated in the material or to the applied electric displacement, the second refers respectively to the direction of the applied stress or to the direction of the induced strain. For example:

g_{31} is the induced electric field in direction 3 per unit stress applied in direction 1. Alternatively it is the mechanical strain induced in the material in direction 1 per unit electric displacement applied in direction 3.

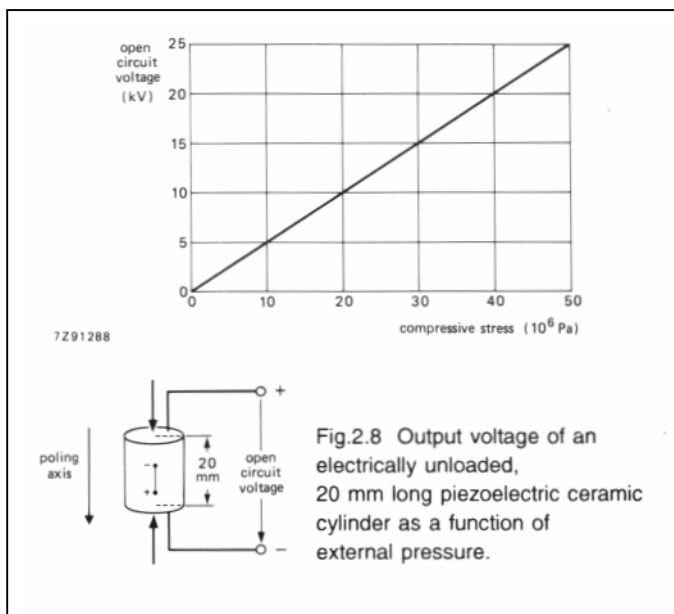
g_{15} is the induced electric field in direction 1 per unit shear stress applied about axis direction 2. Alternatively it is the shear strain induced in the material about axis 2 per unit electric displacement applied in direction 1.

2.8 Examples

To give an indication of the stresses, strains, voltages etc. that accompany piezoelectric transducer action, let's consider the example of a piezoelectric cylinder 20 mm long and 1 cm^2 in cross-section subject to an external stress. This is an example of generator action, i.e. the conversion of mechanical energy into electrical energy. Provided the ends of the cylinder are not connected together, no current flows and the dielectric displacement D is zero.

Figure 2.8 shows that the open-circuit voltage V (and hence the field strength E) is proportional to compressive stress T up to a maximum of 25 kV, which occurs at a stress of 50 MPa ¹⁾ (see Eq.A in the Appendix).

1) 10^6 N/m^2



This can be expressed as:

$$E = -gT \quad (2.2)$$

or, since $V = El$ and $T = F/A$,

$$V = -g \frac{l}{A} F \quad (2.3a)$$

in which F is the force applied to the ends of the cylinder of cross section A and length l , and g is the piezoelectric voltage constant defined in Section 2.7 (dimension m^2/C or Vm/N). Note: by definition, the voltage or electric field generated is said to be positive if its polarity is the same as that of the original poling voltage.

With $g = d/E^T$ (see Appendix, Eq.A), Eq.2.3a can be rewritten as:

$$U = -d \frac{l}{\epsilon^T A} F = -d \frac{F}{C} \quad (2.3b)$$

In which C is the capacitance of the piezoelectric cylinder and E^T is the dielectric constant at (constant) pressure T . So the charge $Q = CV$ on the cylinder (compare Fig.2.8(b)) is given by:

$$Q = -dF = -g\epsilon^T F \quad (2.4)$$

The induced charge therefore is completely independent of cylinder dimensions and hence of its tolerances (in contrast to the induced voltage). In this example, the induced charge is about 2 pC, but this depends heavily on temperature since g and E^T are temperature dependent (with temperature coefficients of opposite sign).

Stresses of 50 MPa are easily obtained with simple presses. Even the bare hand can produce forces of some tens of newtons, and it only takes about 25 N to generate 100 V with the above cylinder. The electrical energy this generates, however, is far too low to be hazardous.

Examples where mechanical energy (movement) is converted into electrical energy or into an electrical signal include: gas cigarette lighters and various domestic gas-ignition devices, gramophone pickups, accelerometers, microphones and hydrophones.

The conversion of electrical energy into mechanical movement is governed by the equation (corresponding to equation A in the appendix):

$$S = dE = d \frac{U}{l} \quad (2.5)$$

in which S is the mechanical strain (Fig.2.9) generated by electric field E or voltage V across the cylinder. The dimensions of the piezoelectric charge constant d are C/N or m/V . Since $S = \Delta l/l$

$$\Delta l = dU \quad (2.6)$$

from which we can deduce that Δl is independent of the dimensions of the PZT cylinder. For a PZT 5A cylinder subject to 16 kV ($E = 800$ V/m), Δl equals about 10 μm .

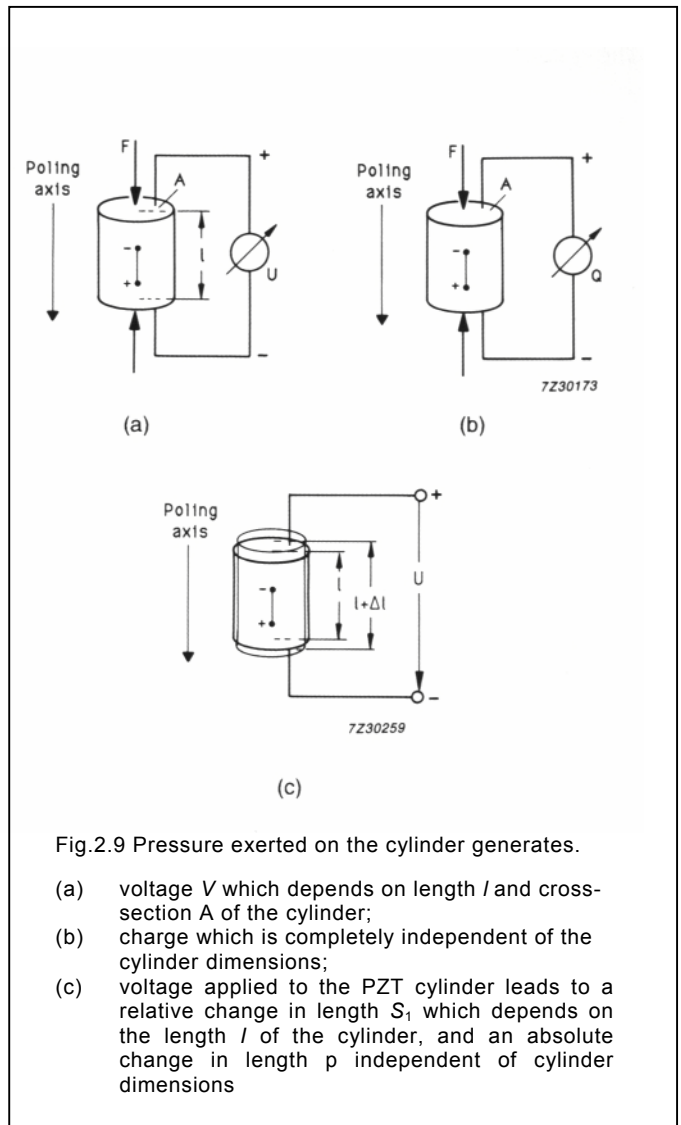


Fig.2.9 Pressure exerted on the cylinder generates.

- (a) voltage V which depends on length l and cross-section A of the cylinder;
- (b) charge which is completely independent of the cylinder dimensions;
- (c) voltage applied to the PZT cylinder leads to a relative change in length S_1 which depends on the length l of the cylinder, and an absolute change in length Δl independent of cylinder dimensions

The figures quoted here refer to static loads; an alternating field generally yields different results. In particular, at the mechanical resonant frequency, the amplitude of oscillation can be expected to be much greater than the static changes. For relatively large mechanical movement (> 1 mm say) special flexional elements are available.

Examples where electrical energy is converted into mechanical energy can be found in atomizers and equipment for ultrasonic cleaning, welding, soldering and ultrasonic drilling.

2.9 Dynamic behaviour of PZT transducers

When exposed to an alternating electric field, a piezoelectric element periodically changes its size in accordance with the frequency of the field. In other words it oscillates and, if the frequency lies in the vicinity of its series resonant frequency (see below for definition) its behaviour can be described by the equivalent circuit of Fig.2.10.

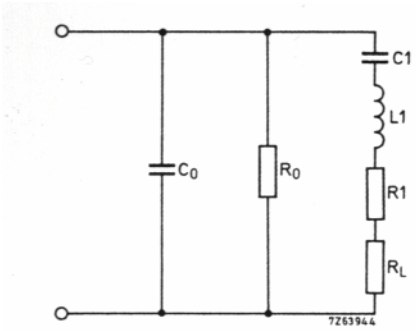


Fig.2.10 Equivalent circuit diagram of a PZT transducer.

C_0 is the capacitance of the transducer below the resonant frequency minus capacitance C_1 ,
 R_1 is the resistance caused by mechanical losses
 R_L the resistance of the working load due to the radiated energy: in vacuum $R_L = 0$,
 C_1 the capacitance of the mechanical circuit and L_1 is the inductance of the mechanical circuit

For such an oscillating system, Fig.2.11 shows the variation of admittance $|Y|$ and impedance $|Z|$ with frequency. The frequency f_m at which the admittance becomes maximum (minimum impedance frequency) lies close to the series resonant frequency

$$f_s = \frac{1}{2\pi} \sqrt{\frac{1}{L_1 C_1}} \quad (2.7)$$

(The frequency at which the impedance in the equivalent circuit becomes zero when R_L is neglected).

The frequency f_n at which the admittance becomes minimum (maximum impedance frequency) lies close to the parallel resonant frequency

$$f_p = \frac{1}{2\pi} \sqrt{\frac{C_0 + C_1}{L_1 C_0 C_1}} \quad (2.8)$$

(The frequency at which the parallel resistance in the equivalent circuit becomes infinite, again neglecting R_L).

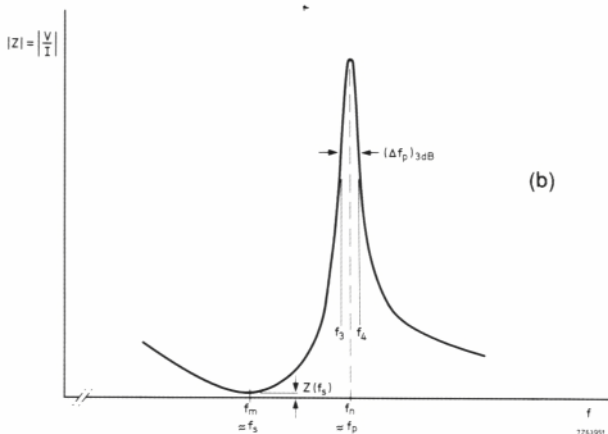
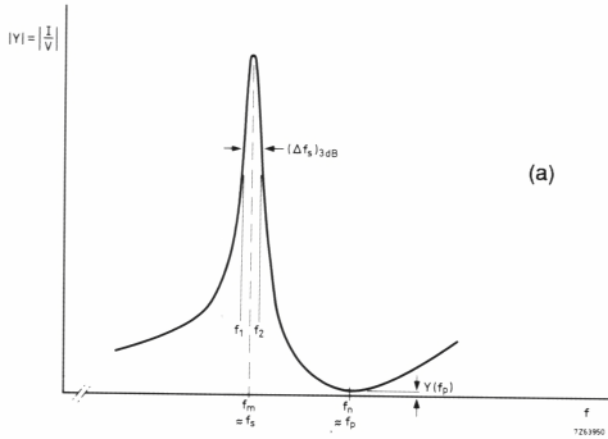


Fig.2.11 Admittance and impedance as functions of frequency. The series resonant frequency f_s lies in the vicinity of the minimum impedance frequency f_m the parallel resonant frequency f_p lies in the vicinity of the maximum impedance frequency f_n . Below f_m and above f_n the transducer behaves capacitively, between f_m and f_n it behaves inductively

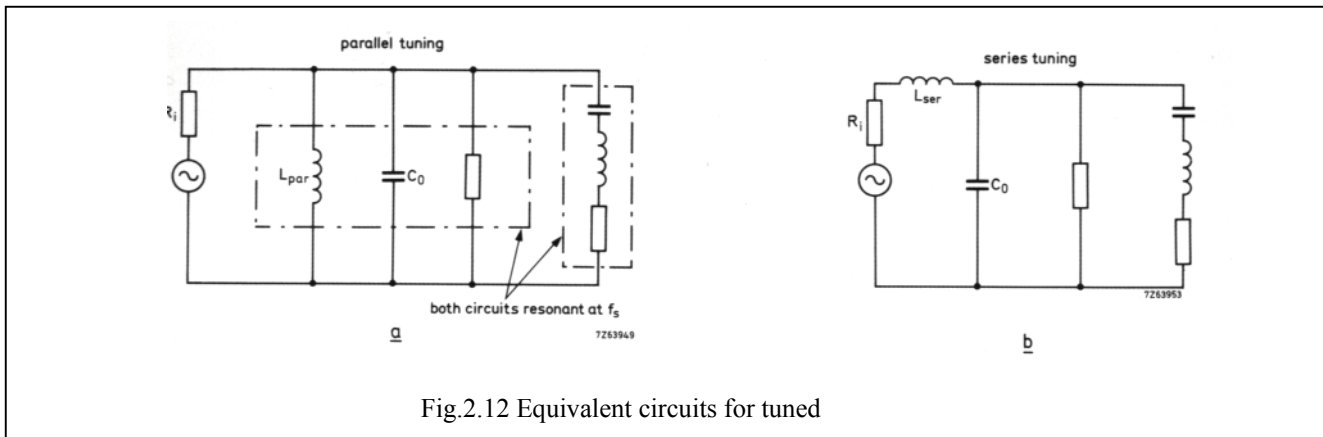


Fig.2.12 Equivalent circuits for tuned

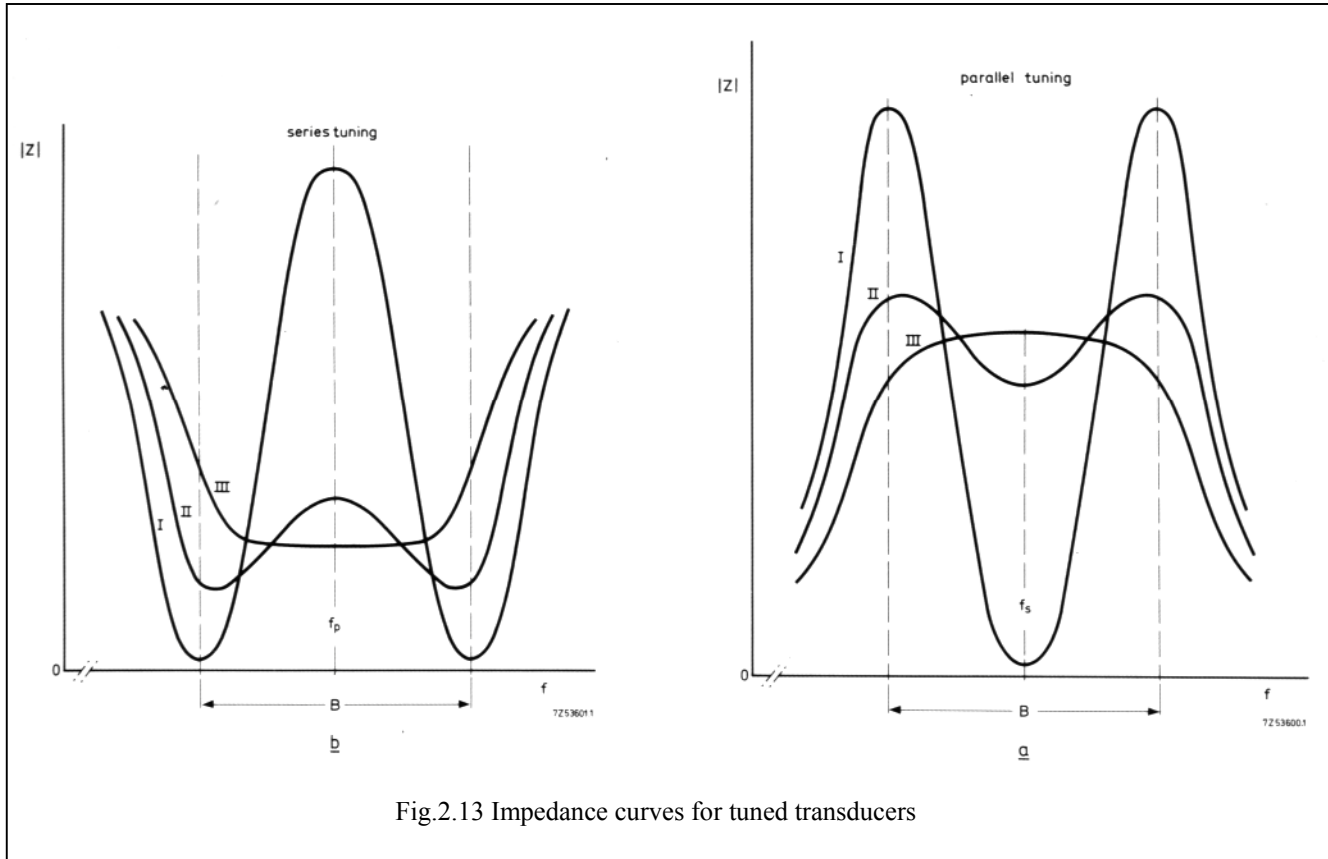


Fig.2.13 Impedance curves for tuned transducers

It's often advisable to tune the transducer with a series or parallel inductance, L_{par} or L_{ser} given by:

$$L_{par} = \frac{1}{\omega_s^2 C_0} \quad (\omega_s = 2\pi f_s) \quad (2.9)$$

$$L_{ser} = \frac{1}{\omega_p^2 C_0} \quad (\omega_p = 2\pi f_p) \quad (2.10)$$

In this way, two coupled resonant circuits are obtained: one mechanical, governed by L_1 , C_1 and R_1 , the other electrical, governed by L_{par} (or L_{ser}), C_0 and the resistor R of the AC voltage generator. The frequency response of such a coupled system resembles that of a band-pass filter.

Figure 2.12 shows the equivalent circuit for a tuned system (series and parallel tuning) and Fig.2.13 shows the

variation of impedance with frequency. Curve I applies to an acoustically unloaded oscillator, curves II or III to an oscillator in which the loading is average or strong.

The impedance of the parallel-tuned system at f_s , is real, and that of the series-tuned system is real at f_p . Although the frequency-response curve depends to some extent on the electrical termination resistance and mechanical load, the effect on bandwidth B , and on f_s and f_p is not great. The bandwidth obtained by electrical tuning is roughly the product of the effective coupling coefficient k_{eff} (see. section 2.11) and the series or parallel resonant frequency, i.e

$$B = k_{eff} f_{sp} \quad (2.11)$$

2.10 Frequency constant N

The resonant frequencies referred to in the previous section depend, of course, on the dimensions of the PZT sample, and experience indicates that they vary inversely with these dimensions. Figure 2.14, for example, shows the variation of impedance with frequency for a PZT5A disc, 1 mm thick and 25 mm in diameter. An impedance-minimum occurs at a series-resonant frequency f_s of

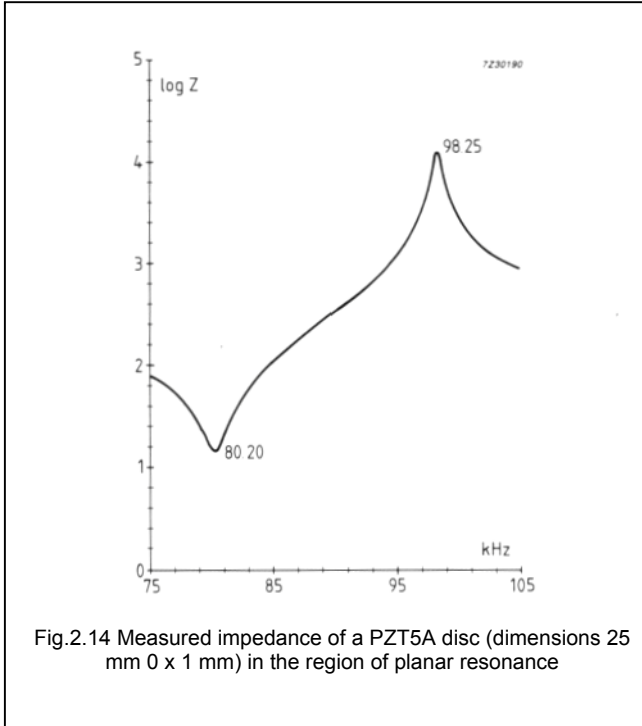


Fig.2.14 Measured impedance of a PZT5A disc (dimensions 25 mm \varnothing x 1 mm) in the region of planar resonance

Known as the planar or radial resonant frequency, it's related to the disc diameter D by

$$f_s = \frac{N_p^E}{d} = \frac{2000}{25 \times 10^{-3}} \approx 80 \text{ kHz} \quad (2.12)$$

N_p^E , which for PZT5A material equals 2000 m/s is known as the planar or radial frequency constant.

Figure 2.15 is similar to Fig.2.14 but with the frequency scale extended to 3 MHz to show higher resonances. The impedance minimum at about 2 MHz is known as the axial resonance, and its frequency is related to the thickness h of the disc by

$$f_s = \frac{N_3^D}{h} = \frac{1850}{1 \times 10^{-3}} \approx 2 \text{ MHz} \quad (2.13)$$

N_3^D is known as the thickness frequency constant and for PZT5A material it equals 1850 m/s ($\approx 1 \times 10^3 \text{ m} \times 2 \times 10^6 \text{ Hz}$).

So the frequency constant is the product of the series resonant frequency f_s and the dimensions governing that frequency. The subscript indicates the type of oscillation at resonance: p for planar oscillations, 3 for oscillations in the Z or axial direction.

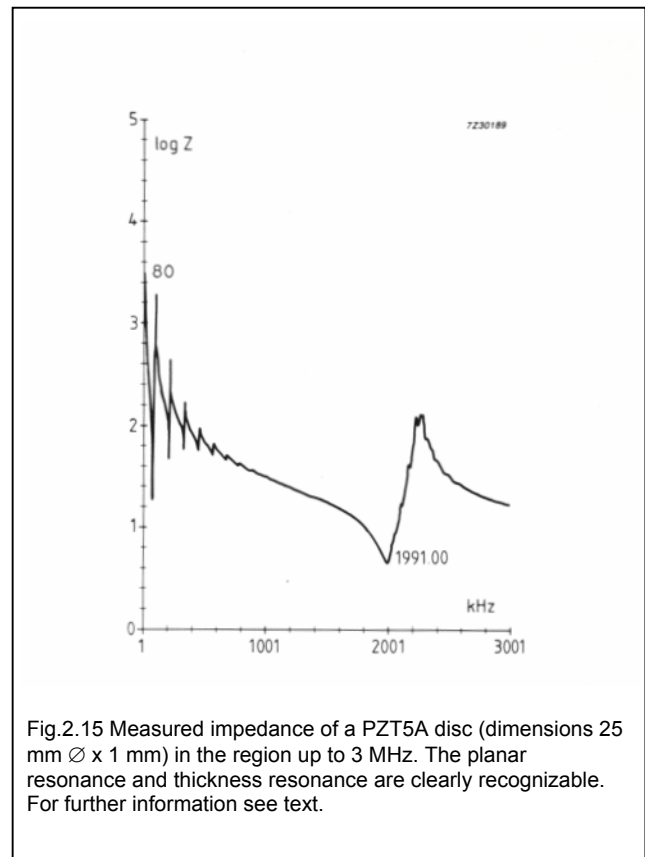


Fig.2.15 Measured impedance of a PZT5A disc (dimensions 25 mm \varnothing x 1 mm) in the region up to 3 MHz. The planar resonance and thickness resonance are clearly recognizable. For further information see text.

Frequency constants are always quoted in our data sheets and data handbook (MA03) on PZT materials, so using the above relations, it's an easy matter to calculate the series resonant frequency of a PZT oscillator. The frequency constant can, in fact, be shown to equal half the sound velocity in the ceramic material (with the exception of N_p).

Figures 2.14 and 2.15 relate to freely oscillating PZT bodies. Behaviour changes quite dramatically if the bodies are constrained. Figure 2.16, for example, shows how the impedance of a diaphragm on which a PZT disc is glued varies with frequency (for details see caption to figure).

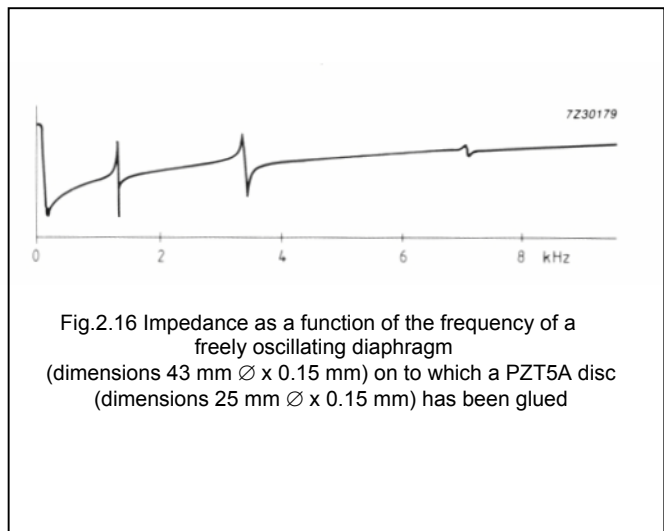


Fig.2.16 Impedance as a function of the frequency of a freely oscillating diaphragm (dimensions 43 mm \varnothing x 0.15 mm) on to which a PZT5A disc (dimensions 25 mm \varnothing x 0.15 mm) has been glued

2.11 Coupling factor k

Another important constant for piezoelectric materials is the coupling factor k_{eff} which is a measure of the effectiveness with which electrical energy is converted into mechanical energy and vice versa. At frequencies well below the resonant frequency of the piezoelectric body, k_{eff} is given by the expression

$$k_{eff}^2 = \frac{\text{energy converted}}{\text{input energy}}$$

(see appendix for derivation).

This expression holds for both electromechanical and mechano-electrical conversions.

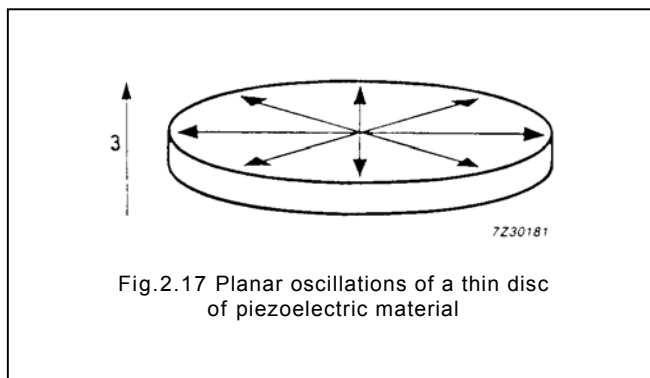
A study of the values of k_{eff} shows that for modern piezoelectric ceramics, up to 50% of the stored energy can be converted at low frequencies. The values of k_{eff}^2 quoted in tables, however, are usually theoretical maxima, based on precisely defined vibrational modes of ideal (i.e. unrealistic) specimens of the material. In practical transducers, the coupling factors are usually lower.

As with other piezoelectric constants, coupling factors carry subscripts. k_{33} , for instance, is the coupling factor for longitudinal vibrations of a very long, very slender rod (in theory infinitely long, in practice, with a length/diameter ratio > 10) under the influence of a longitudinal electric field. k_{31} is the coupling factor for longitudinal vibrations of long rod under the influence of a transverse electric field, and k_{15} describes shear mode vibrations of a piezoelectric body.

Special cases of the coupling factor are the planar coupling factor k_t , and the thickness coupling factor k_r . The planar coupling factor k_p of a thin disc represents the coupling between the electric field in direction 3 (parallel to the disc axis) and simultaneous mechanical effects in directions 1 and 2 (Fig.2.17) that result in radial vibrations. This is known as radial coupling.

The thickness coupling factor k_r represents the coupling between an electric field in direction 3 and the mechanical vibrations in direction 3 of a thin, planar object of arbitrary contour (i.e. an object whose surface dimensions are large compared with its thickness).

The resonant frequency of the thickness mode of a thin planar object is far higher than that of its transverse mode.



What's more, since its overall volume remains substantially constant, expansion/contraction in thickness must always be accompanied by corresponding contraction/expansion in the transverse directions, so the strongly attenuated transverse vibrations at the higher resonant frequency of the thickness mode tend to increase the apparent stiffness of the material. Hence k_t is lower than k_{33} - the coupling factor for longitudinal vibrations of a slender rod (whose longitudinal resonant frequency is much lower and matches more closely its transverse resonant frequency).

Although a high k_{eff}^2 is usually desirable for efficient transduction, it should not be thought of as a measure of efficiency, since the unconverted energy is not necessarily lost (converted into heat) and can in many cases be recovered.

The real efficiency is the ratio of the converted useful energy to the energy taken up by the transducer, and a tuned and well-adjusted transducer working in its resonance region could be more than 90% efficient. Well outside its resonance region, however, its efficiency could be very low.

2.12 Comparison of piezoelectric ceramic and crystalline quartz

This section details some of the important differences between PZT and crystalline quartz, differences that in many instances account for their use in quite widely differing application areas. As we said earlier, the ferroelectric properties of PZT mean that it has a very much higher dielectric constant than quartz (see Table I). Likewise, the coupling factor and piezoelectric charge constant of PZT are considerably higher than those of quartz, and hence volume-for-volume, its performance as a transducer is far superior to that of quartz, allowing expensive amplifiers to be dispensed with.

On the other hand, quartz has a Q factor several times higher than that of PZT.

	Symbol	Unit	Quartz	PZT5A (Navyll)	PZT4(Navyl)
Dielectric Constant	$\epsilon_{33}^T/\epsilon_0$		4.5	1800	1300
Coupling Factor	k_{33}		0.09	0.66	0.60
Charge Constant	d_{33}	10 ⁻¹² C/N	2.0	460	300
Voltage Constant	g_{33}	10 ⁻³ Vm/N	-50	28	25
Quality Factor	Q		10 ⁴ -10 ⁶	80	600

For significance of indices see section 2.6

These differences in material properties naturally lead to PZT and quartz being used in different application areas. Quartz, for example, is ideal for high-Q, high precision mechanical resonators, as used for frequency stabilizers in clocks and watches.

PZT materials, on the other hand, are less popular as resonators, their main application areas being in, for example, actuating systems (stacked elements) in which they operate well below their natural resonances and in which the ability to generate high force or large displacements is more important. In other applications (for example high-performance ultrasonic transducers), high conversion efficiency and design versatility are important, and here PZT is ideal thanks to the ease with which it can be fashioned into almost any shape, and, in contrast to quartz, its ability to be polarized in any desired direction.

2.13 Pyroelectric effects

The polarization in piezoelectric materials is temperature dependent. The oriented structure of the electric dipoles gradually disappears with rising temperature. Within the safe operating temperature range the changes are reversible. When exposed to excessive heat permanent loss of polarization will occur. Changes in the alignment of the dipoles lead to charge displacements and electric fields.

In most applications this phenomenon is an unwanted side-effect which causes measuring errors or even failure of sensitive electronic components like MOSFETS by overvoltage.

In other applications the effect is very useful, for instance in infrared detectors.

Infrared radiation heats up the ceramic, the resulting voltage or charge is a measure for the level of the radiation.

In most cases however it is a nuisance. The interference mainly occurs in very low frequency or quasi-static applications. To suppress it parallel resistors are used to allow the charge to flow away. In sensors this causes an unwanted uplift of the lower cut-off frequency. In this section a qualitative as well as a quantitative overview of the pyroelectric effect will be given.

A measure for the effect are the so-called pyroelectric coefficients dP/dT and dE/dT .

For our PZT range the following values are typical:

$$\frac{dP}{dT} \approx 400 \times 10^{-6} \text{ C}/(\text{m}^2\text{K})$$

$$\frac{dE}{dT} \approx 20 \times 10^3 \text{ V}/(\text{mK})$$

Fig.2.19 and 2.20 show the results of measurements on PZT5A discs.

Room temperature was taken as a reference and temperature cycles were carried out at a rate of 3 K/min. When a specimen is heated to 100 °C for the first time a considerable irreversible change in polarization takes place. After a few cycles the changes become almost purely reversible.

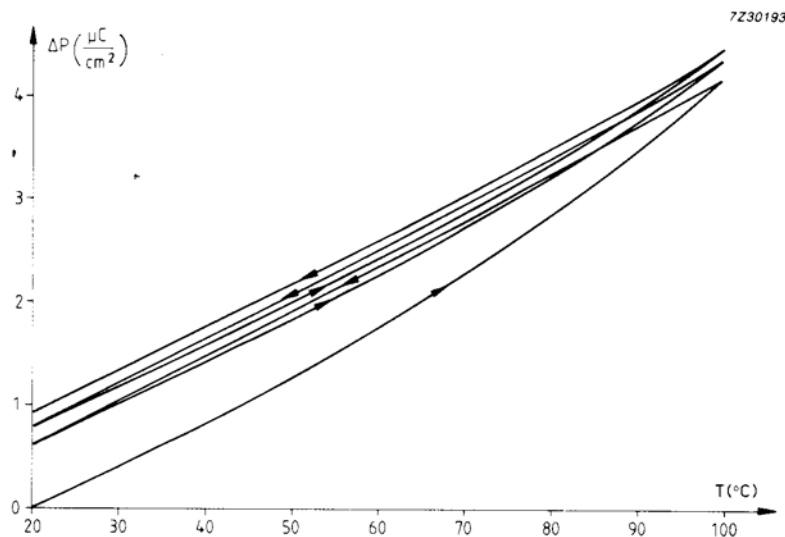


Fig.2.19 The polarization of PZT5A during temperature cycling

From Fig.2.20(a) it is clear that ΔP is almost a linear function of temperature. The curve for ΔE however deviates from being linear because the dielectric constant (E) is also a function of temperature.

The following example clearly demonstrates the importance and danger of the pyroelectric effect:

$$\Delta T = 10\text{K}$$

PZT5A disc of $\varnothing 10 \times 1 \text{ mm}$.

$$\Delta E = 20 \times 10^3 \text{ V/(mK)} \times 10 \text{ K} = 200 \times 10^3 \text{ V/m}$$

$$\Delta V = \Delta E \cdot h = 200 \times 10^3 \text{ V/m} \times 10^{-3} \text{ m} = 200 \text{ V}$$

Clearly this voltage would destroy a MOSFET amplifier stage immediately.

Figure 2.21 shows measured values of $(dP)/(dT)$ as a function of temperature for several PZT material grades. The average of all curves confirms the value of $400 \times 10^{-6} \text{ C/(m}^2\text{K)}$ mentioned before. The liberated pyroelectric charge for a temperature change can be calculated with the formula:

$$Q = \frac{1}{2} \left(\frac{dP}{dT} T_1 + \frac{dP}{dT} T_2 \right) \cdot (T_2 - T_1) \cdot A \quad (2.14)$$

where A is the surface area of the PZT-element.

Given a possible rate of temperature change, the leakage resistor necessary to keep the interference within limits can now be calculated. In critical applications material grades with the highest ratio between piezoelectric (d_{33}) and pyroelectric charge constant (dP/dT) should be used. PZT5A is the best grade in this respect.

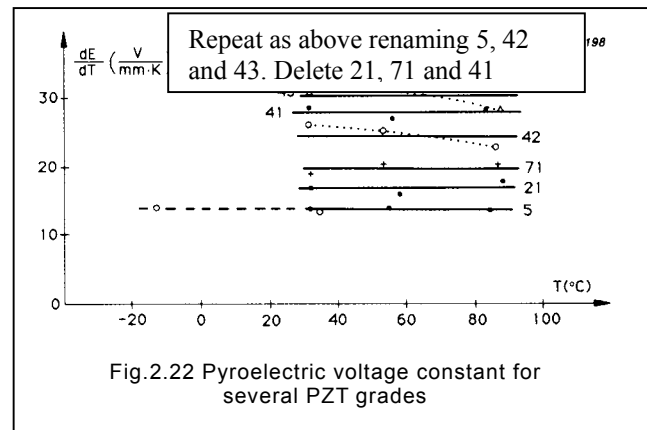
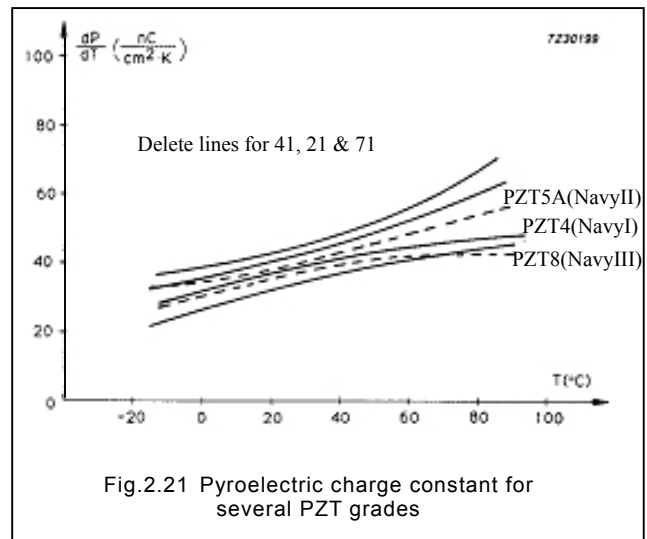
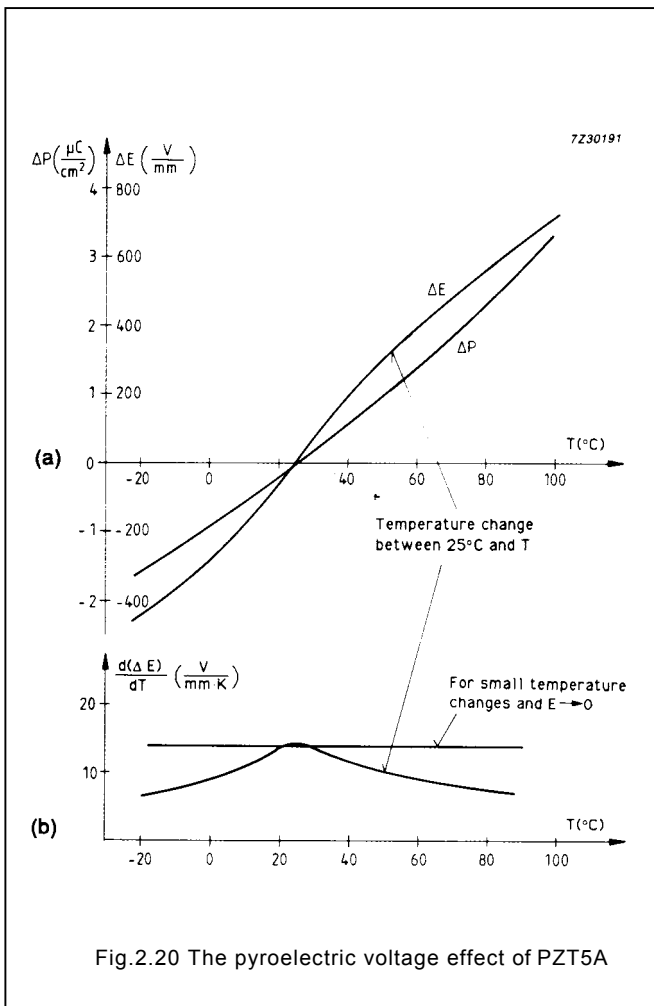
Figure 2.22 provides information about the pyroelectric constants of field-strength (dE/dT) for the range of PZT grades. These constants are important to predict their behaviour under open circuit conditions, as is the case in spark generators and often in acceleration sensors.

The generated pyroelectric voltage is given by:

$$U = \frac{dE}{dT} \cdot \Delta T \cdot h \quad (2.15)$$

h - height of PZT-element

In this case a measure for material quality is the ratio between the piezoelectric voltage constant (g_{33}) and the pyroelectric field strength constant (dE/dT).



3 GENERATORS

An important application area for PZT is in the conversion of mechanical energy into electrical energy, and this chapter describes the conditions under which PZT should be used to convert the maximum amount of energy.

A PZT cylinder can generate voltages that are high enough to draw a spark across an electrode gap [8], [9], and such sparks can be used to ignite combustible gases in for instance cigarette lighters or gas stoves (Fig.3.1).

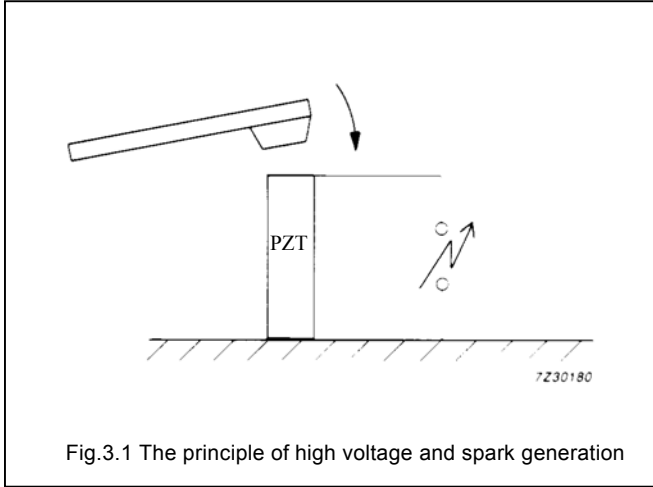


Fig.3.1 The principle of high voltage and spark generation

Moreover, a part of the energy generated by a PZT transducer can be stored in a capacitor and can be used to power a circuit (Fig.3.2).

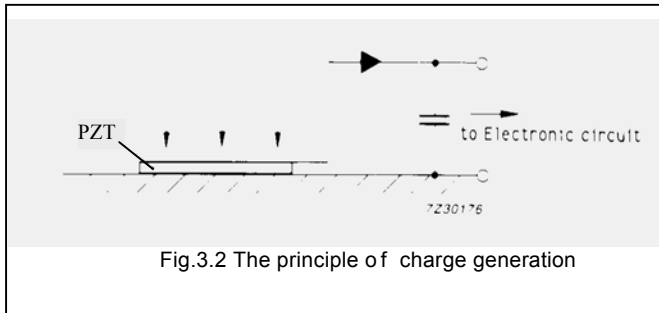


Fig.3.2 The principle of charge generation

In these applications, important factors governing performance are the shape of the PZT transducer, the manner in which the transducer is mounted and, of course, the nature of the electrical load.

A PZT disk for example, compressed between two metal surfaces will never be able to expand in the radial direction as readily as would a long, thin cylinder, which is only constrained at its ends and assumes a barrel shape on radial expansion. So the way in which the material is mounted will directly affect the energy conversion per unit volume. The general rule therefore is to allow the PZT body some freedom to expand radially since charge generation is directly coupled to deformation.

Another important parameter is the impedance of the load circuitry. If the charge is not allowed to flow away

quickly, the electrical field it generates will tend to act against depolarization. The time during which a force is applied has a marked influence on this, static or quasistatic forces tending to depolarize a material faster than dynamic forces of the same magnitude.

3.1 Static loading

3.1.1 Open circuit conditions

Consider a PZT cylinder of height h , polarized in the axial direction and with electrodes on its end faces. If an axial stress T_3 is applied, it will deform and hence charge will displace toward the electrodes. Under open circuit conditions ($D = 0$) the voltage U_3 is given by:

$$U_3 = -g_{33}hT_3 \quad (3.1)$$

A compressive stress (negative sign) will therefore generate a positive voltage across the transducer. To get an idea of the order of magnitude of the voltage to be expected, a 10 mm PZT5A cube ($g_{33} = 22 \times 10^{-3} \text{ Vm/N}$) subjected to a force of 5 kN will generate a voltage about 11 kV.

The total energy W_D fed into a PZT element by a mechanical source can be split up as follows: (no losses, open circuit)

$$W_D = W_m + W_e \quad (3.2)$$

where: W_m = mechanical deformation energy

W_e = energy stored in the electrical field in the ceramic

The latter may be withdrawn from the element as electrical energy.

The energy W_D can be simply expressed in terms of compliance S^D and the mechanical stress T by:

$$W_D = \frac{V}{2} s_{33}^D T_3^2 \quad (3.3)$$

in which V is the volume of the PZT element. W_e and W_m are given in terms of the coupling coefficient k_{33} by:

$$W_m = \frac{V}{2} (1 - k_{33}^2) s_{33}^D T_3^2 \quad (3.4)$$

$$W_e = \frac{V}{2} k_{33}^2 s_{33}^D T_3^2 \quad (3.5)$$

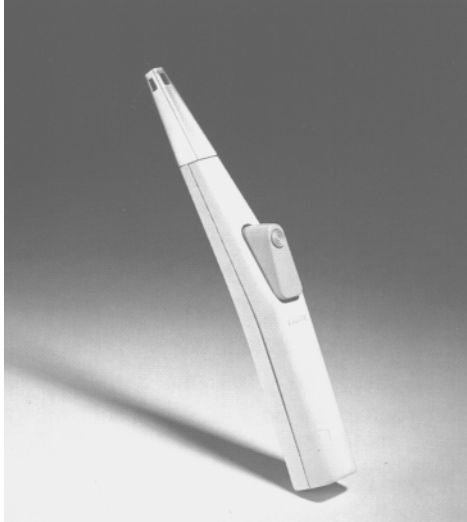
These equations show that for given material properties only V and T govern the energy conversion. If, therefore, in a particular application the force that can be applied is limited, the electrical energy generated can be increased by choosing a smaller surface area (equal volume). For example one can use a long thin cylinder instead of a short thick one.

With equations A9, A10, A14, A15 (appendix) and 3.1 W_e can be expressed as:

$$W_e = \frac{1}{2} \epsilon_{33}^T (1 - k_{33}^2) \frac{A}{h} U_3^2 = \frac{1}{2} \epsilon_{33}^S \frac{A}{h} U_3^2 - \frac{1}{2} (1 - k_{33}^2) C_0 U_3^2 \quad (3.6)$$

where ε_{33}^s and ε_{33}^T are defined in section 2.7, h is the height of the element, A the surface area and C_0 its capacitance at low frequency.

PZT-elements under compressive stress in open circuit conditions do not suffer from depolarisation. The induced field has the same direction as the poling field during polarization and the voltage increases almost linearly with the stress even up to very high load levels.



3.1.2. Electrically short-circuited systems

If a PZT element is compressed while its electrodes are short circuited, charge is generated by linear as well as nonlinear processes. In addition, at very high stress levels depolarisation occurs.

The charge density resulting from the linear piezoelectric effect caused by deformation of Weiss domains is determined by:

$$\frac{Q_3}{A} = D_3 = d_{33}T \quad (3.7)$$

where: Q_3 = total generated charge
 A = the surface area of the element
 D_3 = the dielectric charge displacement
 d_{33} = piezoelectric charge constant.

The calculated and measured charge displacements are in agreement only at very low voltages. This is due to the nonlinear character of the piezoelectric effect caused by reversible or irreversible displacement of the Weiss domain walls. As a consequence of this, an additional contribution to the charge displacement can occur, causing it to rise more strongly with increasing mechanical load than would be expected from the linear effect. Irreversible displacements cause depolarization and are only permitted in generators designed for one-time use. The occurrence of depolarization can be checked by measuring the charge developed during subsequent load cycles. If the curves match, no depolarization has taken place. For PZT8(Navy III), for instance, the maximum allowable static stress is 85×10^6 Pa under closed circuit conditions. The decrease of the coupling factor k_{33} remains below 5%.

Measurements made with PZT5A discs show (Fig.3.3) a maximum achievable charge density of 0.25 C/m^2 . The material is then almost completely depolarized. For very thin discs, where radial extension is blocked, about 10^9 Pa

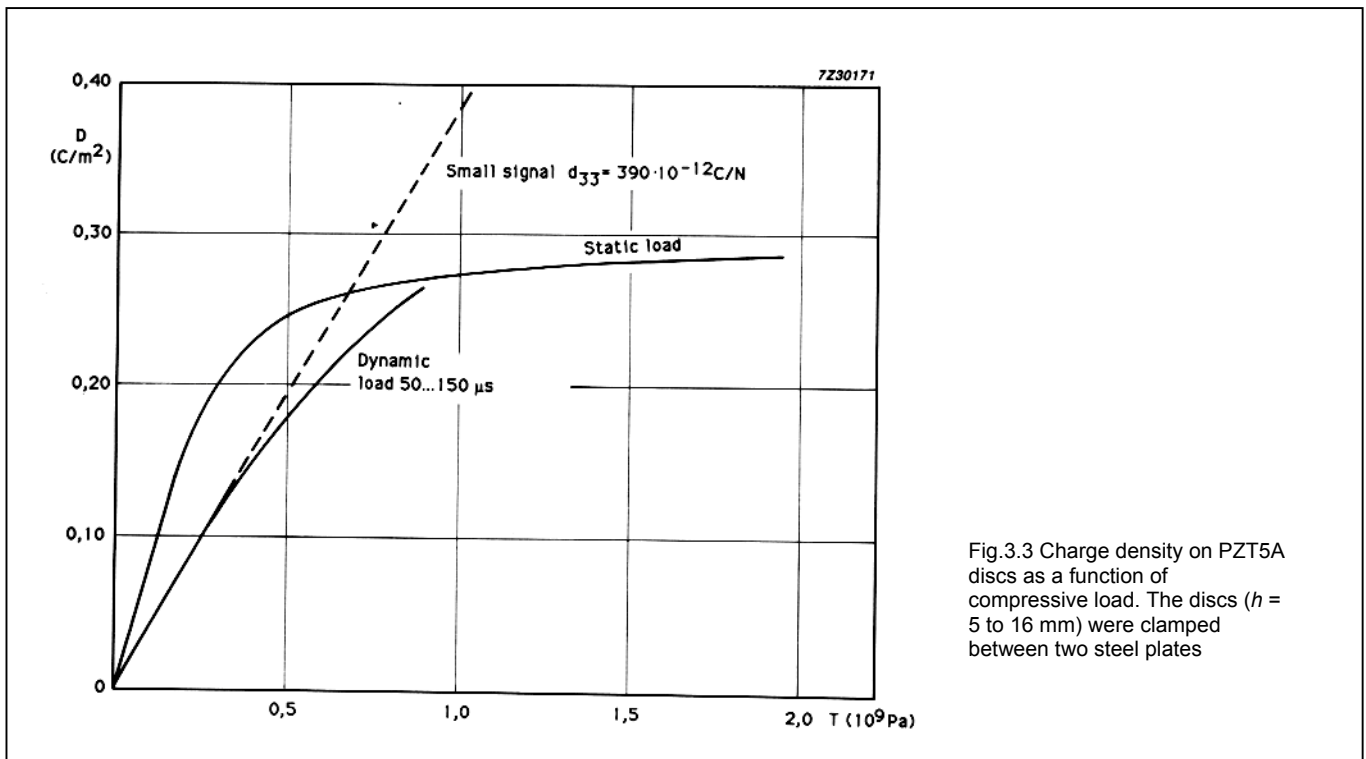


Fig.3.3 Charge density on PZT5A discs as a function of compressive load. The discs ($h = 5$ to 16 mm) were clamped between two steel plates

is needed to reach this condition. In the case of cylinders or cubes, 10^8 Pa is sufficient. These conditions apply for quasi-static as well as dynamic loading. However, for low stress levels there is a marked difference between quasistatic and dynamic loading because depolarization then also depends on the duration over which the load is applied.

In the design stage of a PZT-generator it should be established whether the generator is intended to function

- repeatedly, or
- once only, yielding the maximum possible energy or charge.

In the second case, the design should be such that the PZT-element is stressed at 10^8 to 10^9 Pa, statically or dynamically. The transducer will then be drained completely resulting in a charge density of about 0.25 C/m² on the electrodes.

3.1.3 Systems with finite impedance

In practical applications, it's important to fully exploit the available energy. Two main applications will be discussed from this point of view:

- solid state battery
- ignition of gases

3.1.3.1 Application with depolarization

In this type of application, the aim is to extract as much energy as possible from the PZT generator which may be depolarized in the process. The maximum energy density that can be achieved (≈ 1.2 W/cm³) is obtained under open circuit conditions. However, this energy is available for only a very short time because of flashover or dielectric breakdown. The very high voltage levels should be reduced by placing a capacitor in parallel with the generator. This capacitor, when charged, can also serve as a supply for an electronic circuit. For this purpose the circuit of Fig.3.4 can be used. To bring down the voltage to practical levels, the parallel capacitance C_p is generally much larger than C_0 of the PZT-element itself. Sometimes not more than 5 V is required for the electronic circuit (e.g. TTL circuitry). In the figure, diode D_1 prevents charge flowing back to the PZT-element upon decompression. D_2 protects diode D_1 against high reverse voltages which could occur if the material is not completely depolarized.

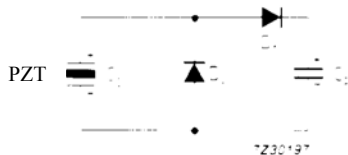


Fig.3 4 PZT generator with diodes and parallel capacitor

Unfortunately the parallel capacitor not only lowers the voltage level but also the available energy as can be seen from Fig.3.5. The reason for this is that the voltage decreases linearly with the total capacitance ($Q = UC$) whereas the energy is related to the square of the voltage ($W = \frac{1}{2} CU^2$).

$$\text{So: } W = \frac{C}{2} \times \frac{Q^2}{C^2} = \frac{1}{2} \times \frac{Q^2}{C}$$

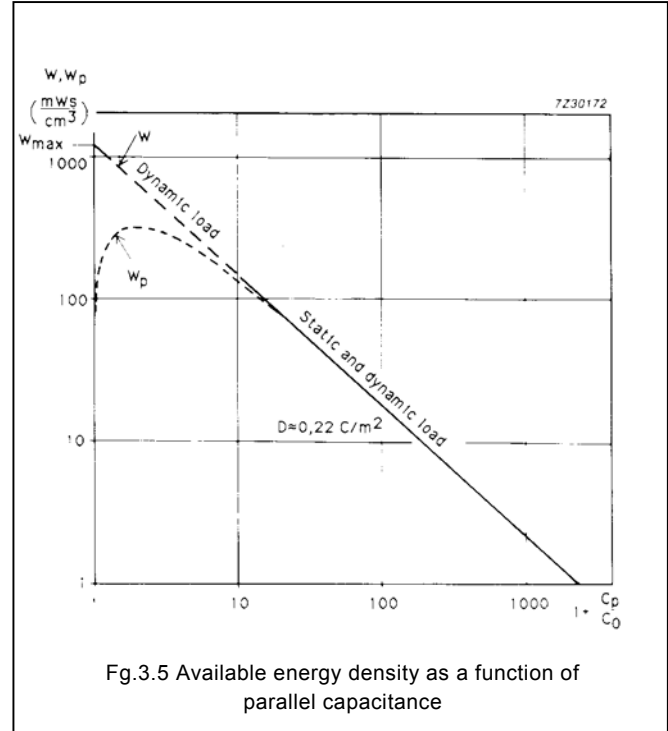


Fig.3.5 Available energy density as a function of parallel capacitance

In the following practical example we shall show how a parallel capacitor affects the available energy. Two PZT5A discs are stacked and electrically connected in parallel (diameter 16 inn, thickness 0.5 mm).

- Energy density $W_{max} = 1.2$ W/cm³
- capacitance $C_0 = 2 \times 7 \mu\text{F} = 14 \mu\text{F}$
- dielectric displacement $D = 22 \mu\text{C}/\text{cm}^2$
- surface area $A = 4 \text{ cm}^2$
- volume $V = 0.2 \text{ cm}^3$
- compressive stress $T = 10^9$ Pa.
- Generated charge $Q = D \times A = 22 \times 4 = 88 \mu\text{C}$
- Open circuit voltage

$$U = \sqrt{\frac{2wV}{C_0}} = \sqrt{\frac{2 \times 1.2 \times 0.2}{14 \times 10^{-9}}} = 5.86 \text{ kV}$$

at W_{max}

Available energy W is:

$$W = wV = 1200 \times 0.2 = 240 \text{ mWs}$$

With a parallel capacitance $C_p = 1 \mu\text{F}$ one obtains:

$$U = \frac{Q}{C_p} = \frac{88 \times 10^{-6}}{10^{-6}} = 88 \text{ V}$$

and the available energy is reduced dramatically

$$W = \frac{1}{2} C U^2 = \frac{1}{2} \times 10^{-6} \times 88^2 = 3.9 \text{ mWs}$$

Or, using Fig.3.5:

$$1 + \frac{C_p}{C_0} = 1 + \frac{10^{-6}}{14 \times 10^{-9}} = 72.4$$

$$W = mV = 24 \times 0.2 = 4.8 \text{ mWs}$$

The difference between both results is due to the fact that the graph is based on measured values, whereas the calculation is based on the average value of the generated charge ($22 \mu\text{C}/\text{cm}^2$).

It's possible to get a reduction of voltage without too much loss of energy by using a stack of thin discs. The capacitance C_0 will then be higher and the generated voltage lower so that a lower parallel capacitance is needed.

Applying this new 'multilayer technology' to the example quoted above, using comparable PZT material and a layer thickness of $50 \mu\text{m}$, we get the following results:

charge $Q \approx 1 \text{ mC}$

open circuit voltage $U \approx 600 \text{ V}$

capacitance $C_0 \approx 1.5 \mu\text{F}$

These are already more useful values with the impedance being better matched to the load. A stack of these $50 \mu\text{m}$ layers with a diameter of 5 mm and a height of 1 mm could charge a parallel capacitor of $1 \mu\text{F}$ to a voltage of 100 V , which represents an energy of 5 mWs and an energy density of around $250 \text{ mWs}/\text{cm}^3$.

The impedance can also be adjusted by means of a transformer (Fig.3.6). However to convert the same amount of electrical energy as in the abovementioned example its dimensions would have to be rather large. Nevertheless, by this method, or by using multilayer technology, practically all of the energy contained in the PZT transducer can be extracted and used.

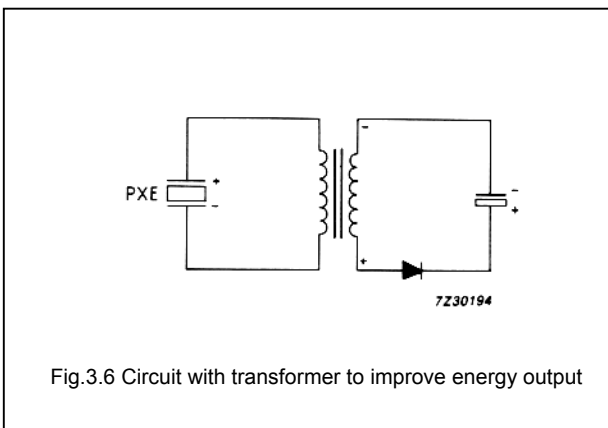


Fig.3.6 Circuit with transformer to improve energy output

3.1.3.2 Applications without depolarization

Another important application area for PZT generators is in the ignition of gases in pocket lighters, gas ovens or welding equipment. Of course, for these applications the piezoelectric device is expected to have a long service life, so depolarization is not permitted.

A piezoelectric ignition system is far less complex than those using permanent magnets or high-voltage transformers and capacitors. What's more, its volume is much less because the electrical part consists only of one or two PZT cylinders. For the same energy content these occupy almost the same volume as the capacitor alone in a standard electrical ignition system.

If a spark gap is connected across the piezoelectric element, flashover will occur as soon as the breakdown voltage of the gap has been reached. Up to the point of flashover, the PZT cylinder behaves as an electrically open system, but during discharge, the system is loaded with the (real) resistance of the conducting spark gap.

The electrical energy is released in a very short time (in around 10^{-7} s). The actual time depends on the cylinder capacitance, the length of the high-tension lead and the resistance of the spark gap. If, as is the case in practice, the cylinder remains connected to the mechanical source, and if the spark is still conductive, the PZT element is effectively short-circuited and so its compliance increases from s_{33}^D to s_{33}^E where:

$$s_{33}^E = \frac{s_{33}^D}{1 - k_{33}^2} \quad (3.8)$$

which means that the compressive strain of the cylinder can increase further with no increase of stress. This can't occur instantaneously, however. As soon as the spark gap breaks down, acoustic shock waves begin to move in from the ends of the cylinder. Their propagation speed is about 4 mm/ms , so this deformation is complete within a few microseconds. The additional mechanical energy fed into the cylinder by this effect can be converted into extra electrical energy W_{ea} given by

$$W_{ea} = \frac{V}{2} s_{33}^E k_{33}^4 T_3^2 = \frac{1}{2} \epsilon_{33}^T k_{33}^2 \frac{A}{h} U_3^2 \quad (3.9)$$

In practice the actual value of W_{ea} will depend greatly on the way in which the PZT cylinder is mounted, and on the way the compressive stress is applied.

The total energy available for the spark thus amounts

$$\text{to: } W_{tot} = W_e + W_{ea} = \frac{1}{2} \epsilon_{33}^T \frac{A}{h} U_3^2 + \frac{1}{2} C_0 U_3^2 \quad (3.10)$$

where C_0 is the cylinder capacitance at low frequency. The corresponding energy density $W_{tot} = W_{tot}/V$ can be calculated using equation 3.10 to give

$$w_{tot} = \frac{1}{2} \epsilon_{33}^T g_{33}^2 T_3^2 \quad (3.11)$$

3.2 Dynamic loads

In the so-called impact ignition system, the PZT element is stressed dynamically with a spring-loaded hammer mechanism.

In the simplest case of free impact between a hammer with an area A_H and a PZT cylinder with area A_C , and assuming that A_y and A_c are not too different, the maximum mechanical stress can be calculated from:

$$T_3 = u \frac{A_H Y}{A_C v + A_H v_{33}^D Y S_{33}^D} = u \frac{A_H Z_H Z_C^D}{A_H Z_H + A_C Z_C^D} \quad (3.12)$$

in which

u = impact velocity

V = velocity of pressure wave in the hammer

v_{33}^D = velocity of the pressure wave in the PZT (open circuit)

Y = the module of elasticity of the hammer material

S_{33}^D = compliance of the PZT material under open circuit conditions

Z_H = the specific acoustic impedance of the hammer material

Z_C^D = the specific acoustic impedance of the PZT material (open circuit) ($\approx 3.4 \times 10^7 \text{ kg/m}^2\text{s}$)

When the hammer strikes, a pressure wave is generated in both the PZT cylinder and the hammer. This wave is reflected a number of times, depending on the acoustical properties of the components. Until the flashover at the spark gap occurs, the PZT cylinder behaves as an electrically open system (Section 3.1.1), in which T_3 varies over the length of the cylinder. Equation 3.1, therefore, only applies to differential stretches of the cylinder and the total voltage would have to be obtained by integration over its length. For the design of an igniter, such a complicated calculation is not necessary. If the peak voltage is measured on an electrically open system, this value, inserted in equation 3.10, gives adequate information about the available energy due to linear effects. If additional nonlinear phenomena occur during flashover, the probability of ignition will only be improved.

3.3 Multilayer generators

The technique developed to make multilayer capacitors can also be used for piezoelectric ceramics. Thin layers of so called *green* ceramic are interleaved with silver-palladium electrodes, compacted, cut to size and then sintered.

Generators with layers as thin as 20 gm can be produced in this way. (Fig.3.7). With these devices, the large total surface area per unit volume means that the generated charge is high whereas the voltage is rather low (Fig.3.8).

These types of generator are ideal for use as a solid *state* battery for modern electronic circuits.

The parallel capacitance needed to bring the voltage down to the desired level can now be of the same order as the generator's own capacitance (C_0). The usable energy density reaches interesting levels (Fig.3.9).

Ideally the parallel capacitors (C_P) should have the same value as the generator itself (C_0). Under these conditions 28% of the theoretical maximum energy is available at the terminals of the parallel capacitor.

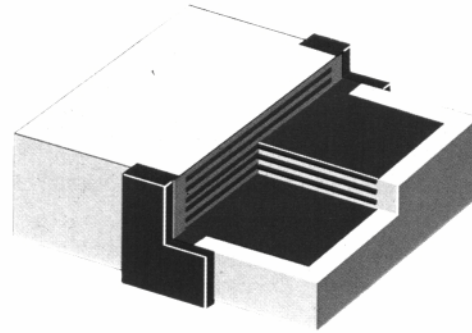


Fig.3.7 Multilayer generator

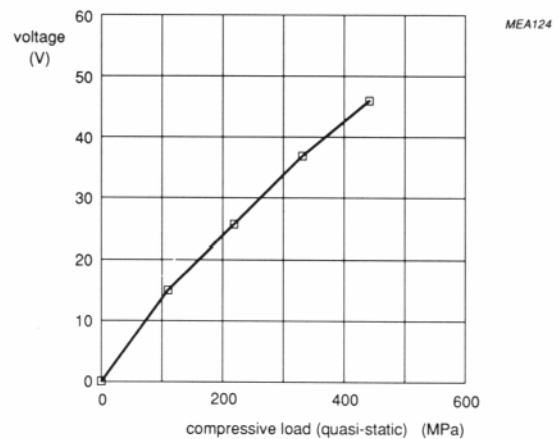


Fig.3.8 Output voltage as a function of compressive load

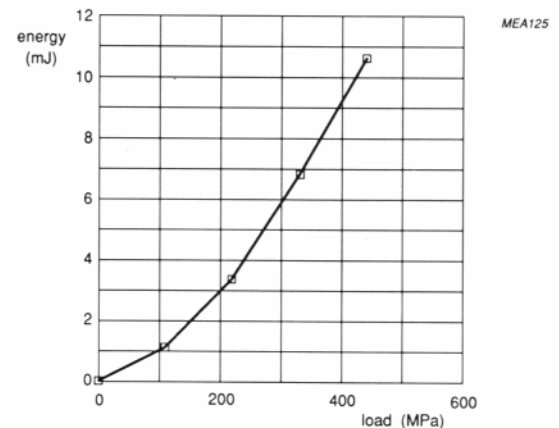


Fig.3.9 Energy density in multilayer generator as a function of load

4 SENSORS

The modern technical world demands the availability of sensors to measure and convert a variety of physical quantities into electrical signals. These signals can then be fed into data processing systems and electronically evaluated and processed. Sensors can therefore be regarded as links between the non-electrical environment and dataprocessing electronic systems.

Some of the quantities to be measured are mechanical, such as force, acceleration or pressure. PZT transducers are ideal for converting such quantities into electrical signals. Two fundamental types can be distinguished: the axial sensor and the bending sensor. In the axial sensor the force is exerted in the direction of the polarization (33mode). In the bending sensor (flexure element) the force acts perpendicular to the direction of polarization (31mode).

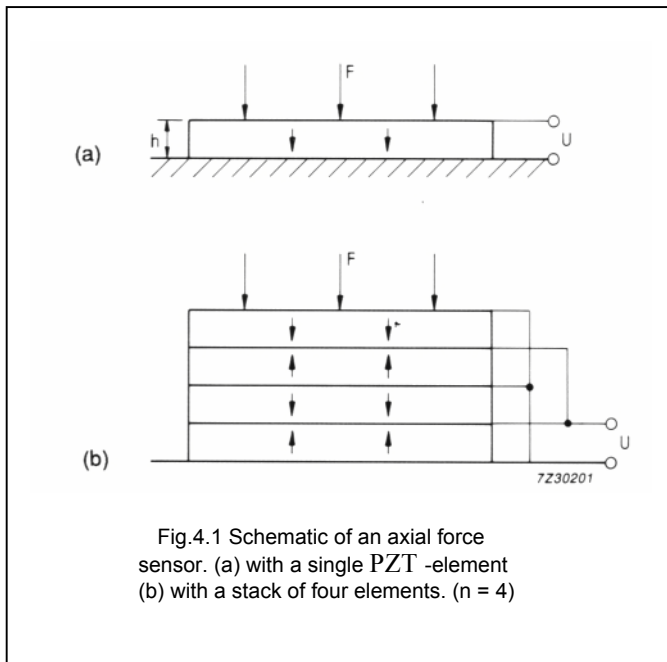
In addition to these PZT sensors, which make direct use of the piezoelectric effect for measurements, there is a wide range of acoustic measuring systems that incorporate PZT elements.

4.1 Axial sensors

4.1.1 Force sensors

Chapters 2 and 3 have already shown how the exertion of a force on a PZT transducer (Fig.4.1(a)) results in the generation of a charge

$$Q = -d_{33}F \quad (4.1 a)$$



This charge is completely independent of the dimensions of the PZT element (for explanation see section 2.8). However, if n PZT discs are stacked and connected electrically in parallel the result will be:

$$Q = -nd_{33}F \quad (4.1b)$$

since the force acts simultaneously on n platelets.

The open circuit voltage on a disc of height h is given by:

$$U_3 = -g_{33}hT_3 \quad (4.2)$$

In the case of the stack, the discs are connected in parallel, so the resulting voltage is the same. The advantage of a stack is more charge, higher capacitance and thus a lower impedance. Since the voltage increases almost linearly with mechanical stress, the PZT transducer can be used as force sensor.

Example

A force of 1 N is exerted on a PZT5A disc of diameter 10 mm and thickness 1 mm. The resulting mechanical stress is:

$$T_3 = - \frac{4}{100 \times 10^{-6} \pi} = - 1.27 \times 10^4 \text{ N/m}^2$$

The voltage generated (Eq.4.2) will be:

$$U = 22 \times 10^{-3} \times 10^{-3} \times 1.27 \times 10^4 = 280 \text{ mV}$$

This sensitivity of 280 mV/N is fully adequate for the majority of applications.

The capacitance of a PXE disc at low frequency is given by:

$$C_a = \frac{\epsilon_0 \epsilon_r A}{h} \quad (4.3)$$

(A = surface area)

For the disc in this example this means:

$$C_a = \frac{8.85 \times 10^{-12} \times 2000 \times 100 \times 10^{-6} \pi}{4 \times 10^{-3}} = 1.39 \text{ nF}$$

It should be kept in mind that charge is generated only when there is a change in the applied force. The charge will leak away across the input resistance of the instrument used to measure the signal and the resistance of the PZT - element itself. Because of this, it's not possible to use PZT sensors to measure a static force or pressure. The ability to measure low frequency signals is limited by the time constant formed by the combination of C_a and the input resistance of the electronic circuit. For instance to measure at a frequency of 10 Hz, a time constant of less than 1 s is necessary.

With the example of $C = 1.39 \text{ nF}$:

$$R \times C_a = 1 \text{ s} \\ R = \frac{1}{1.39 \times 10^{-9}} = 720 \text{ M}\Omega \quad (3.11)$$

which is already high, though not impossible with modern MOSFETs. If a lower input impedance is chosen, there are two ways to prevent the cut off frequency from rising:

- use a parallel capacitor (C_p);
- use more discs in parallel (stack).

A parallel capacitor, however, will also lower the signal level. The use of a charge amplifier is another possibility. In fact, such a device simulates a very large parallel capacitor.

4.1.2 Acceleration sensors

A PZT disc can operate as an acceleration sensor if it's clamped firmly between a seismic mass (M) and a base plate (Fig.4.2). It's also possible to allow the PZT element itself to act as the seismic mass. See, for example, Section 4.4 which describes a sensitive acceleration sensor comprising a PZT5A cube incorporated in a MOSFET circuit (an active knock sensor).

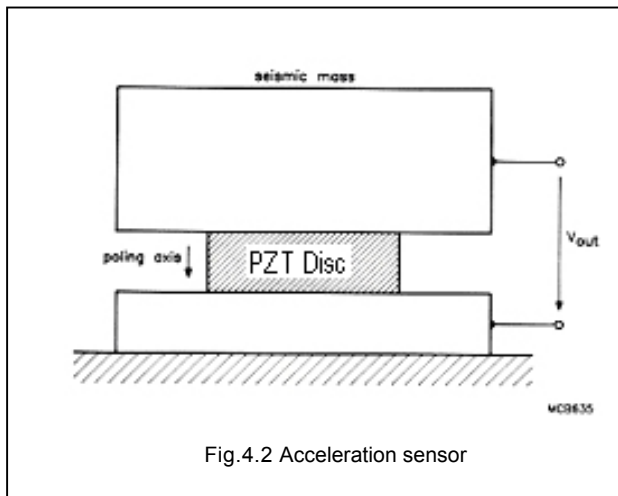


Fig.4.2 Acceleration sensor

During acceleration in the axial direction the seismic mass exerts a force on the disc

$$F = Ma \tag{4.4}$$

The mechanical stress T_3 in the PZT disc is given by:

$$T_3 = -a \frac{M}{A}$$

where: A = surface area
 a = acceleration.

Such an acceleration sensor is in effect a mass-spring system which can be characterized by an electrical equivalent circuit (Fig.4.3, see also section 2.9). This circuit can be simplified for frequencies far below the system resonant frequency. L_1 representing the seismic mass M , can be neglected so that the sensor is represented by the static capacitance C_0 and the "mechanical" capacitance C_1 of the spring (spring constant).

$$C_a = C_0 + C_1 \tag{4.6}$$

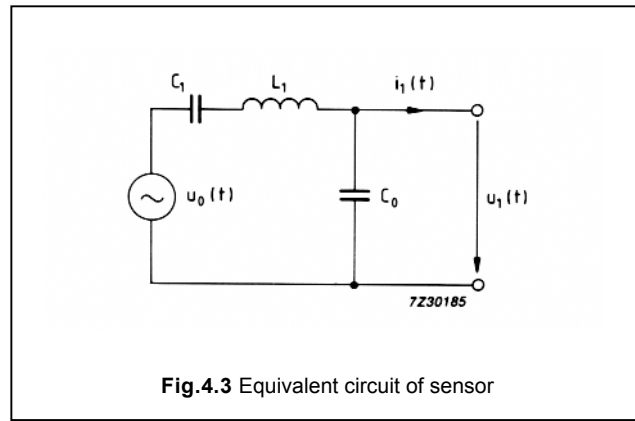


Fig.4.3 Equivalent circuit of sensor

The sensor is loaded by the input impedance (R_E, Z_E in Fig.4.2) of the amplifier. Open circuit voltage will be maintained if:

$$C_E \leq C_a$$

$$R_E \geq \frac{1}{\omega(C_a + C_E)} \approx \frac{1}{\omega C_a}$$

The sensitivity of PZT acceleration sensors is defined as the quotient of the output voltage or the generated charge (short-circuit) and the acceleration a , i.e.:

$$S_u = \frac{U}{a} \tag{4.7}$$

and for the charge

$$S_Q = \frac{Q}{a} \tag{4.8}$$

These sensitivities depend on frequency.

The fundamental frequency response is given in Fig.4.4. If the sensitivity, S_u or S_Q of a PZT sensor is specified, the value given relates to the horizontal, frequency independent, part of the response curve.

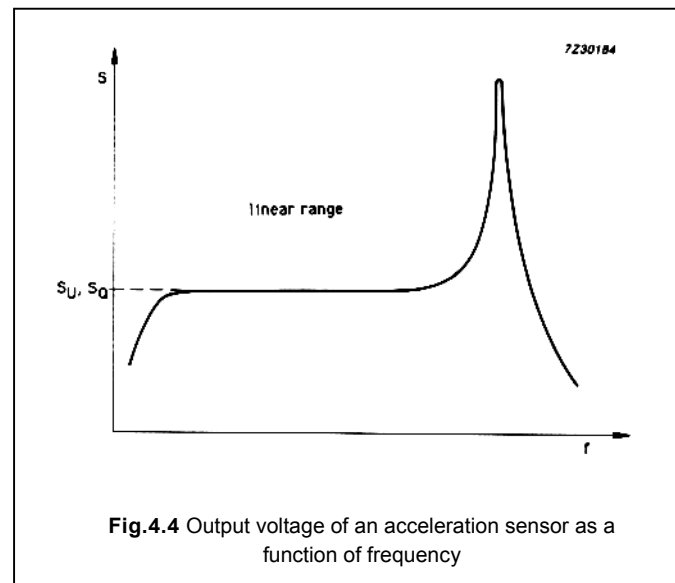


Fig.4.4 Output voltage of an acceleration sensor as a function of frequency

The lower (-3 dB) limit frequency f_L for this range can be calculated using the formula:

$$f_u = \frac{1}{2\pi R_E (C_a + C_E)} \quad (4.9)$$

A rule of thumb for the upper limit frequency f_u is:

$$f_u = \frac{1}{2} f_r \quad (4.10)$$

in which f_r is the first resonant frequency of the PZT sensor. This mechanical resonant frequency is given by:

$$f_r = \frac{1}{2\pi} \sqrt{\frac{C^*}{M + \frac{1}{3}m}} \quad (4.11)$$

where M = seismic mass
 m = mass of the PZT disc
 C^* = stiffness of PZT element

This stiffness can be calculated using the formula:

$$C^* = \frac{F}{\Delta h} = \frac{A}{sh}$$

The value of the compliance s depends on whether the PZT transducer operates under open-circuit or short-circuit conditions (see Section 2.7). For short-circuit conditions, s^E and C^E should be used to calculate the resonant frequency, whereas s^D and C^D should be used for the open-circuit case. The sensitivity can be calculated using Eqs 4.2 and 4.5. If the seismic mass M is much larger than the mass m of the PZT-disc one obtains:

$$U = g_{33} h \frac{a M}{A} \quad (4.13)$$

and

$$S_U = \frac{U}{a} = g_{33} \cdot \frac{h}{A} M \quad (4.14)$$

If m is not negligible compared with M , then $(M + 1/2m)$ should be substituted in the equation. If the seismic mass is only $1/2m$ because $M=0$ the following equation results:

$$S_U = g_{33} \frac{h}{A} \cdot \frac{m}{2} = \frac{1}{2} \rho g_{33} h^2 \quad (4.15)$$

ρ = density of PZT material

This formula shows that the sensitivity of a PZT sensor without seismic mass depends on the square of the disc thickness and is independent of the cross-sectional area. Substitution of the numeric values of ρ and g_{33} gives

$$S_u = 85h^2 \quad (h \text{ in metres})$$

or, if S_U in terms of the acceleration due to gravity ($g^* = 9.81 \text{ m/s}^2$)

$$S_u = 830 h^2 \text{ V/g}^*$$

which is the usual way to specify sensitivity for acceleration sensors.

The actual sensitivity is, in general, lower than that given in equations 4.14 and 4.15, since, even if R_E is very large ($=>\infty$), there will always be a finite external capacitance C_E . This will cause a drop in voltage sensitivity to:

$$S_{UE} = S_U \cdot \frac{1}{1 + \frac{C_E}{C_a}} \quad (4.16)$$

The sensor capacitance C_a can be calculated using Eq.4.3.

Example

An acceleration sensor as given in Fig.4.2 comprises a PZT5A disc of mass $m = 150 \text{ mg}$ and dimensions $A = 20 \text{ mm}^2$ and $h = 1 \text{ mm}$. The seismic mass $M = 20 \text{ g}$.

The open-circuit sensitivity is given by:

$$S_U = \frac{22 \times 10^{-3} \times 10^{-3} \times 20,075 \times 10^{-3} \times 9.81}{20 \times 10^{-6}} = 217 \text{ mV/g}^*$$

Taking into account a load capacitance of 40 pF and knowing that

$$C_a = \frac{8.85 \times 10^{-12} \times 2000 \times 20 \times 10^{-6}}{10^{-3}} = 354 \text{ pF}$$

lowers this sensitivity to

$$S_{UE} = \frac{217}{1 + \frac{40}{354}} = 195 \text{ mV/g}^*$$

It's interesting to compare the values calculated in this case with those of a quartz transducer of the same dimensions. The piezoelectric voltage constant of quartz is a factor 2.3 higher than that of PZT5A. The open-circuit sensitivity will therefore be higher by the same factor. However, the relative dielectric constant is much lower, 4.5 against 2000. With the assumed load capacitance of 40 pF, the resulting sensitivity for quartz will be only 9.6 mV/g*. In spite of this, the use of quartz transducers is advisable when low temperature dependence is required, for instance in measuring transducers. To find the upper limit frequency of the sensor we're discussing here, s_{33}^D must first be calculated. In the shortcircuit case for PZT5A, the compliance is given by:

$$s = s_{33}^E = 18 \times 10^{-12} / \text{Pa}$$

For open-circuit conditions one finds:

$$s = s_{33}^D = (1 - k_{33}^2) s_{33}^E = 9.4 \times 10^{-12} / \text{Pa}$$

$$(k_{33} = 0.69)$$

So, using Eq.4.12, the rigidity of the **PZT** disc under this condition is

$$C^D = \frac{20 \times 10^{-6}}{9.4 \times 10^{-12} \times 10^{-3}} = 2.12 \times 10^9 \text{ N/m}$$

The related mechanical resonant frequency will be:

$$f_r = \frac{1}{2\pi} \sqrt{\frac{2.12 \times 10^9}{20.05 \times 10^{-3}}} = 51.75 \text{ kHz}$$

According to Eq.4.10, the upper frequency limit is about half this value.

If the acceleration sensor is used without additional seismic mass ($M = 0$) this yields:

$$f_r = \frac{1}{2\pi} \sqrt{\frac{2.12 \times 10^9}{0.05 \times 10^{-3}}} = 1.04 \text{ MHz}$$

Almost the same result can be obtained by using Eq.2.13. However, since the PZT body is not vibrating freely but is fixed to a rigid base, twice the height h must be used in the formula:

$$f_r = \frac{N_3^D}{2h} = \frac{1850}{2 \times 10^{-3}} = 1 \text{ MHz}$$

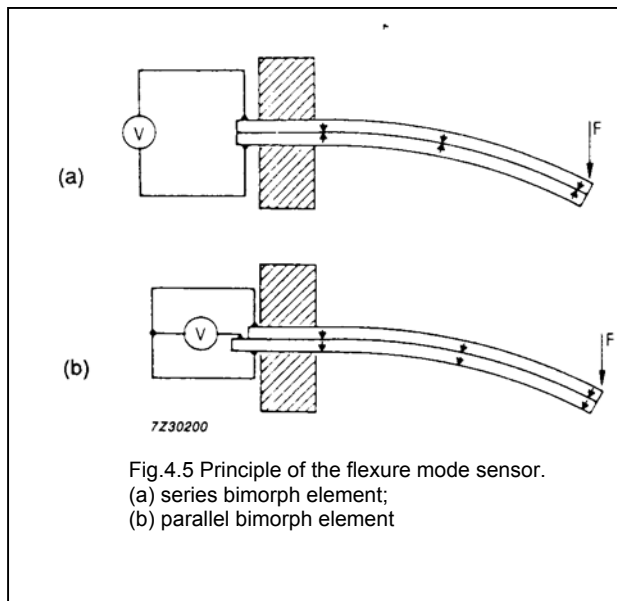
The considerations dealt with in this section and the example discussed show that PZT sensors have high stiffness, which leads to high resonant frequencies at adequate sensitivity.

4.2 Flexional sensors

4.2.1 Force sensors

Mechanical sensors can also take the form of a flexure element. These are based on the principle shown in Fig.4.5.

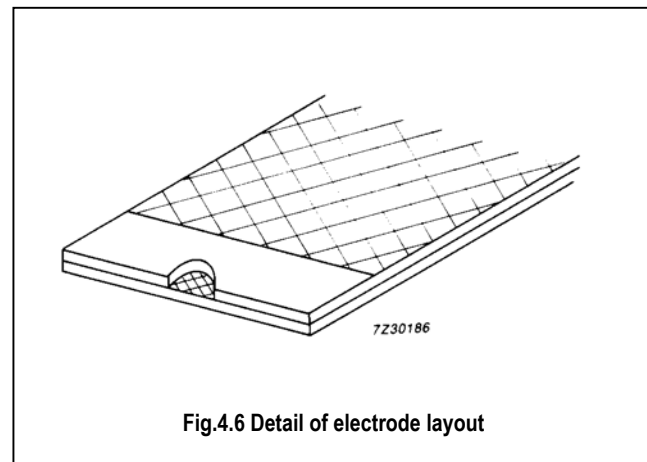
Two PZT strips or plates, polarized in their thickness direction, are bonded together to form what's known as a *bimorph*. The two plates can be polarized in opposite directions (series bimorph) or in the same direction (parallel bimorph). A possible mounting method is shown in Fig.4.5. One end is fixed to a base plate while the force to be measured acts on the other, free, end (cantilever mounting).



The force F causes bending and therefore a tensile force in the upper layer and a compressive force in the lower one. When the plates are of opposite polarity, the resulting electrical fields, and hence the voltages, have the same direction. The layers are electrically in series and can be contacted simply by attaching wires to their outer metallized surfaces (series bimorph).

Its favourable cost price and simple construction (which also incidentally largely compensates the pyroelectric effect), make the series bimorph the preferred type for sensors.

When the polarization is in the same direction, the generated fields have opposite signs. A parallel connection can be made by contacting the electrode on the inner surface of one of the strips (parallel bimorph). How this is realized in practice is shown in Fig.4.6.



Flexural-mode sensors have a far lower stiffness than axial sensors and therefore a lower resonant frequency. They also have a lower mechanical and electrical impedance, so they're better adapted to "soft" mechanical movements and, in general, require simpler amplifiers than axial sensors.

Table 4.1 gives formulas for calculating the most important mechanical and electrical properties of series and parallel bimorphs in sensor applications. All dimensions have to be entered in metres.

TABLE 1
Design data for series bimorphs

bending (m/N)	$7 \times 10^{-11} L^3 / Wh^3$
resonant frequency (Hz)	$400h / L^2$
charge output (C/N)	$4 \times 10^{-10} L^2 / h^2$
capacitance (F)	$2 \times 10^{-8} L_1 W / h$
voltage output (V/N)	$2 \times 10^{-2} L^2 / h L_1 W$

Example

A flexural-mode sensor uses a series bimorph of dimensions 10 x 4 x 0.6 mm (free length 7 mm). Its characteristic properties are calculated using the equations in Table 4.1.

Compliance

$$\frac{z}{F} = 7 \times 10^{-11} \times \frac{343 \times 10^{-9}}{4 \times 10^{-3} \times 0.216 \times 10^{-9}} - 28 \times 10^{-6} \text{ m/N}$$

Resonant frequency

$$f_r = 400 \times \frac{0.6 \times 10^{-3}}{49 \times 10^{-6}} = 4.9 \text{ kHz}$$

Output charge

$$\frac{Q}{F} = 4 \times 10^{-10} \times \frac{49 \times 10^{-6}}{0.36 \times 10^{-6}} = 55 \times 10^{-9} \text{ C/N}$$

Capacitance

$$C_a = 2 \times 10^{-8} \times \frac{10 \times 4 \times 10^{-6}}{0.6 \times 10^{-3}} - 1.3 \text{ nF}$$

Output voltage

$$\frac{U}{F} = 2 \times 10^{-2} \times \frac{49 \times 10^{-6}}{0.6 \times 10 \times 4 \times 10^{-9}} = 41 \text{ V/N}$$

Although generally the capacitance of PZT flexural elements is high, leading to a high time constant, it's often necessary to increase the time constant. This involves connecting a capacitor in parallel with the element, which also lowers the sensitivity. For instance a parallel capacitor of 250 nF (about 200 x 1.3 nF) would reduce the sensitivity by a factor of 200. With $RC = 1 \text{ s}$ we get, with $C_E = 250 \text{ nF}$, a resistance $R = 4 \text{ M}\Omega$ which is a reasonable value for a simple amplifier stage with long input leads.

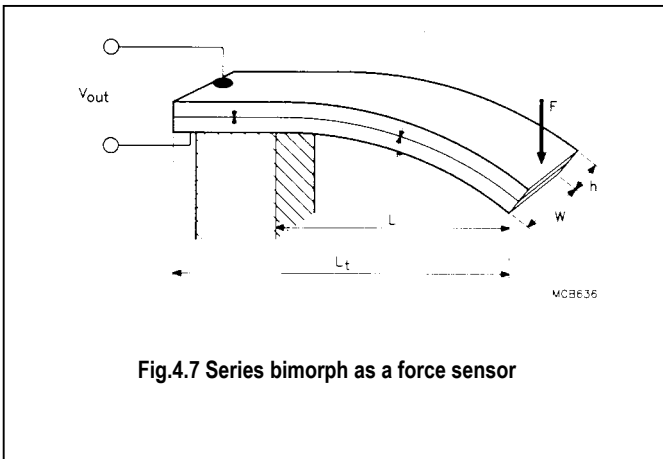


Fig.4.7 Series bimorph as a force sensor

4.2.2 Acceleration sensors

If a flexural element is subjected to an acceleration a , it bends in the manner shown in Fig.4.8. In the case of a series bimorph the output voltage is given by:

$$U = 50 \frac{l^3}{l_t} \cdot a$$

which, using the values of the example in the previous section and expressing the result in terms of g^* gives:

$$S_U = 50 \times \frac{343 \times 10^{-9}}{10 \times 10^{-3}} = 16.8 \text{ mV/g}^*$$

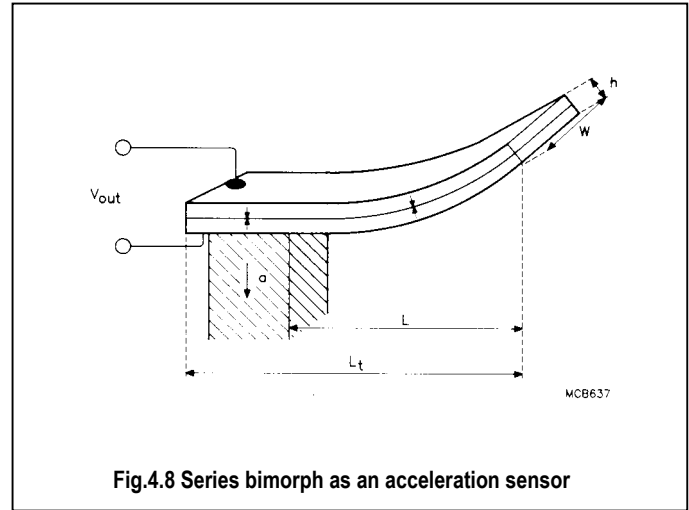


Fig.4.8 Series bimorph as an acceleration sensor

4.3 Temperature dependence of sensors

When designing a PZT sensor, it must be taken into account that the material constants g , d and e are temperature dependent.

Practical values of temperature coefficients (TC) for PZT5A are:

$$TC \ g_{33} = -0.2\%/K$$

$$TC \ d_{33} = 0.3\%/K$$

$$TC \ \epsilon_{33} = 0.5\%/K$$

Since $g = d / \epsilon^T$, the temperature coefficient of g can be taken as the difference between the temperature coefficients of d and ϵ^T .

The temperature dependence of the output voltage can be virtually eliminated by connecting a capacitor in parallel with the sensor. If the total capacitance of the assembly is increased to say 1.7 times that of the PZT sensor, the temperature coefficient of this total capacitance is reduced by the same factor. So the apparent TC ϵ_{33} decreases from 0.5%/K to 0.3%/K, the same value as $TC \ d_{33}$.

Since, as explained above, the temperature coefficient of g_{33} is the difference of $TC \ \epsilon_{33}$ and $TC \ d_{33}$, the output voltage is practically constant over a wide temperature range.

Another effect that must be considered here is the pyroelectric effect (see also Section 2.13). Sudden changes in temperature can cause relatively high voltages. These not only interfere with measurement, they can also destroy amplifier input stages (e.g. MOSFET). In series bimorphs, the pyroelectric effect is not a problem since it's compensated by the opposed polarisation in the constituent plates.

4.4 Practical applications

In this section we discuss two applications in car electronics that have already been put into practice. Since these PZT sensors are used in safety devices for passengers or car engines, they need to be highly reliable.

4.4.1 Knock sensors

High-speed knocking in car engines will cause damage and should therefore be avoided. In modern, high-efficiency engines with high compression ratios, lean mixtures and turbo-chargers, safety margins are very narrow. It's therefore essential to be able to detect excessive knocking to allow effective countermeasures to be taken.

The *knock sensor* is mounted against the engine. Axial acceleration sensors have proved quite effective because they are sturdy and easy to mount. Their task is to identify, in cooperation with filters and evaluation electronics, knock signals in the noise spectrum of the engine.

Upon positive identification, engine management parameters are regulated until knocking disappears. Figure 4.9 shows the usual construction of such an axial sensor. The constituent components are a PZT ring and a seismic mass, pre-stressed with a central bolt in a protective casing. The seismic mass exerts a force on the PZT disc during acceleration, thus generating an electrical signal.

Figure 4.10 shows an alternative design, the so-called *active knock sensor*. A small PZT cube combined with a FET-amplifier provides the signal. A low output impedance (which is less sensitive to interference) and a wide frequency range are the main features. In addition, because the PZT is not pre-stressed, this type of sensor is less prone to ageing

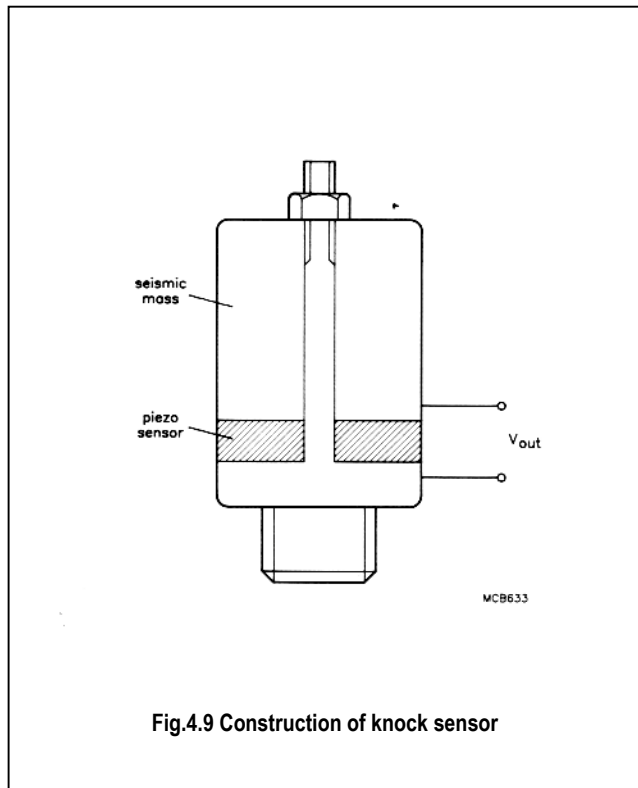


Fig.4.9 Construction of knock sensor

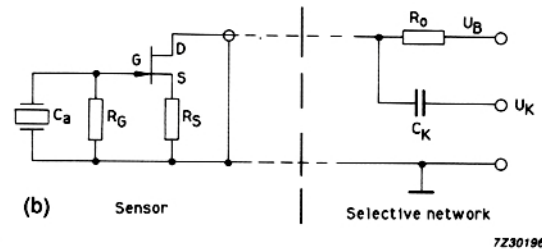
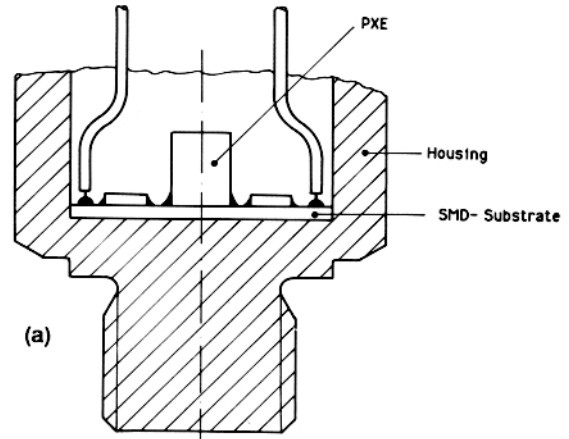


Fig.4.10 Principle of active knock sensor

4.4.2 Crash sensors

Another use of PZT in the car industry is in the so-called *crash sensor*.

This sensor has the task of detecting the start of a collision. To do this it's mounted on the chassis of the car and constantly monitors deceleration levels. A real collision shows a typical deceleration/time pattern. The sensor, supported by a dedicated IC, decides if there is a collision and then activates devices like safety belt tensioners or air-bag systems. Injuries to passengers can therefore be avoided. Figure 4.11 shows a modern crash sensor which operates with a flexural PZT5A element.

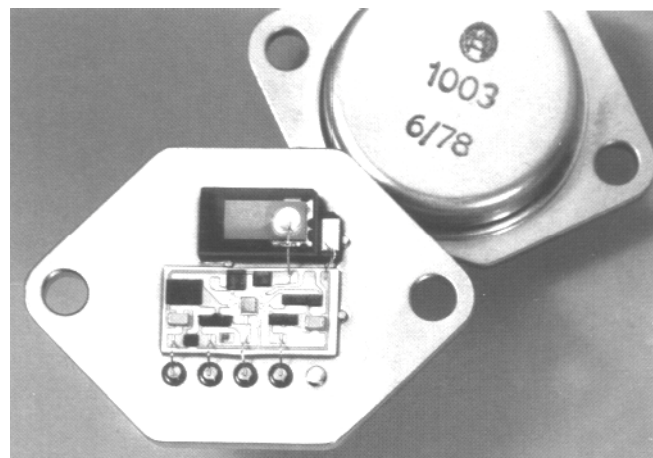


Fig.4.11 Acceleration sensor based on a PZT5A series bimorph. The dedicated electronic circuit activates the seat belt tensioner in case of a crash. (courtesy Robert Bosch GMBH)

5 ACTUATORS

PZT actuators convert electrical signals like voltages or charges into mechanical displacements or forces. The operating frequency range of actuators is from static up to about half the resonant frequency of the mechanical system. As for sensors, a reasonably linear relationship between input signal and movement is required. On the other hand, there is the special class of actuators, which is purposely driven at their resonant frequency, known as *ultrasonic transducers*.

These transducers convert electrical energy into mechanical energy and are treated in chapter 6.

PZT actuators can be divided in three main groups

- axial actuators (d_{33} -mode)
- transversal actuators (d_{31} -mode)
- flexural actuators (d_{31} -mode).

Axial and transversal actuators have high stiffness and are optimized for small movements and high forces. Flexural actuators (bimorphs), on the other hand cover the applications where larger movements are required.

If a voltage is applied to an actuator there will be a displacement. When this displacement is blocked, a force will develop, the so-called *blocking force*, which is, in fact, a measure of the stiffness of the actuator. Figure 5.1 gives a survey the possible stroke-blocking force combinations.

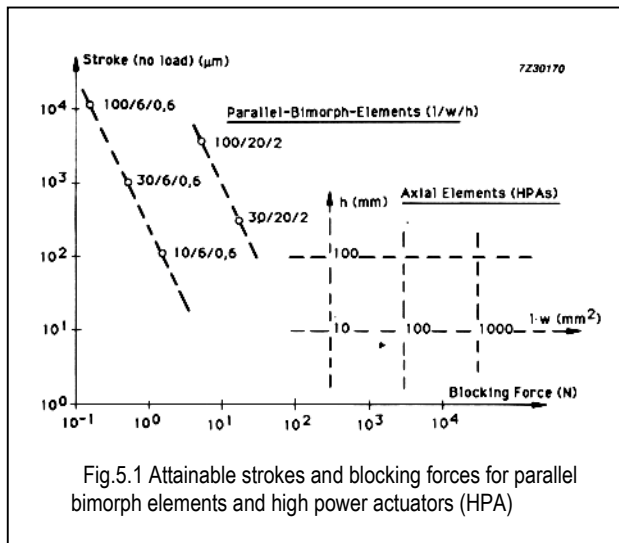


Fig.5.1 Attainable strokes and blocking forces for parallel bimorph elements and high power actuators (HPA)

5.1 Basic calculations on actuators

5.1.1 PZT -actuators at low field strengths and low loads

For low field strengths and loads the basic equations in Section 2 and Appendix A1 are fully applicable. First we'll discuss a simple axial actuator consisting of only one PZT element (Fig.5.2a) to get acquainted with its basic behaviour.

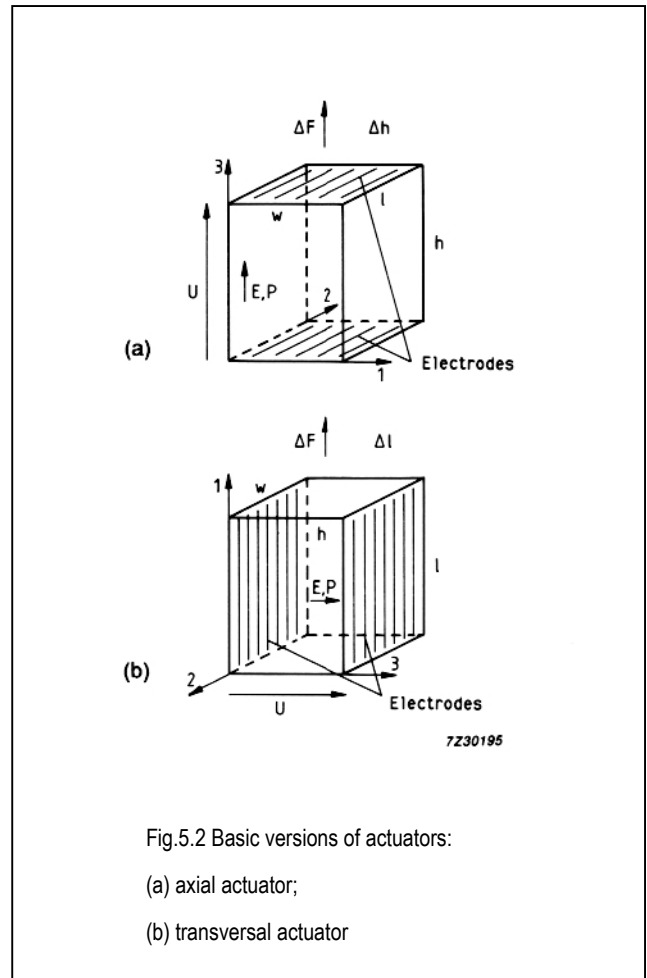


Fig.5.2 Basic versions of actuators:

(a) axial actuator;

(b) transversal actuator

Stroke for $\Delta F = 0$ (no load)

$$\Delta h = d_{33} U \quad (5.1)$$

Blocking force for $\Delta h = 0$ (force developed by a rigidly clamped PZT-element)

$$F_b = \frac{d_{33} l w}{s_{33}^E h} \cdot U \quad (5.2)$$

Stiffness (spring constant)

$$C_E = \frac{\Delta F}{\Delta h} = \frac{l w}{s_{33}^E h} \quad (5.3)$$

Resonant frequency for the free element with w and $l < h$

$$f_r = \frac{N_3^D}{h}$$

Resonant frequency when one end is attached to a base

$$f_r = \frac{N_3^D}{2h}$$

$$w_{tot} = \frac{1}{2} \epsilon_{33}^T g_{33}^2 T_3^2 \quad (3.11)$$

Figure 5.2(b) shows a transversal mode actuator. Its properties are:

Stroke for $\Delta F = 0$

$$\Delta l = d_{31} \frac{l}{h} \cdot U \quad (5.5)$$

Blocking force for $\Delta l = 0$

$$F_b = \frac{d_{31}}{s_{11}} w \cdot U \quad (5.6)$$

Stiffness (spring constant)

$$C^E = \frac{\Delta F}{\Delta l} = \frac{hw}{s_{11}l} \quad (5.7)$$

Resonant frequency for free element

$$f_r = \frac{N_1^E}{l} \quad (5.8)$$

Resonant frequency with one end clamped

$$f_r = \frac{N_1^E}{2l}$$

For cylindrical elements the term lw should, of course, be replaced by πr^2

A constant external force, from a pneumatic or hydraulic cylinder or a weight, for instance, will reduce the absolute length of the element. The deformation depends on the stiffness of the PZT element and on the magnitude of the force, but up to very high loads, the stroke and blocking force of the actuator will remain unaltered.

On the other hand, if the actuator is subject to an external force from a spring, its behaviour will be quite different since the strength of the external force increases as the actuator expands, and the stroke will depend on the spring constant C^L .

The influence of C^L on stroke and blocking force are given by:

$$\Delta F_L = \frac{\Delta F}{1 + \frac{C^L}{C^E}} \quad (5.9)$$

$$\Delta h_L = \frac{\Delta h}{1 + \frac{C^L}{C^E}} \quad (5.10)$$

Figure 5.3 explains these relations for an axial actuator. Without any external force or voltage applied, the height $h = h_0$. A voltage U in this case increases h to $h_0 + \Delta h$. With a constant force F' applied, the operating point is shifted. A voltage U then causes an increase in height of h' which is practically equal to Δh .

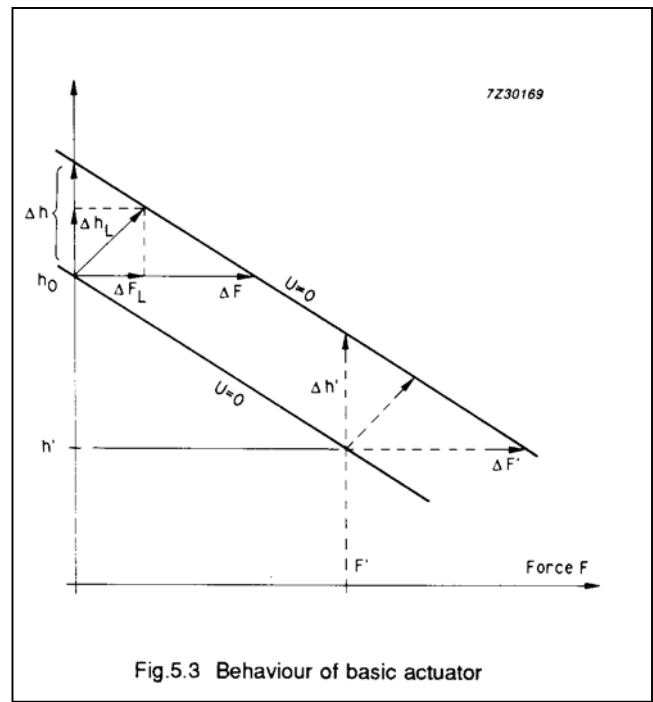


Fig.5.3 Behaviour of basic actuator

Loading with a spring force F_L , on the other hand, decreases the stroke to Δh_L .

Material data for the relationships given above can be found in Table 2.1. Data in this table allows the low signal behaviour of actuators to be calculated. All information applies to unimpeded elements, and when the actuator is clamped deviations from the quoted figures can be expected. Thin discs, for instance, are not free to move radially when they expand, so the force they can deliver and their stroke are reduced (by up to 30%).

5.1.2 Behaviour of PZT actuators at high field strengths

For most PZT materials, the charge constants d_{33} and d_{31} rise with increasing field strength. In Fig.5.4, their relative increase is given for PZT5A and PZT5K.

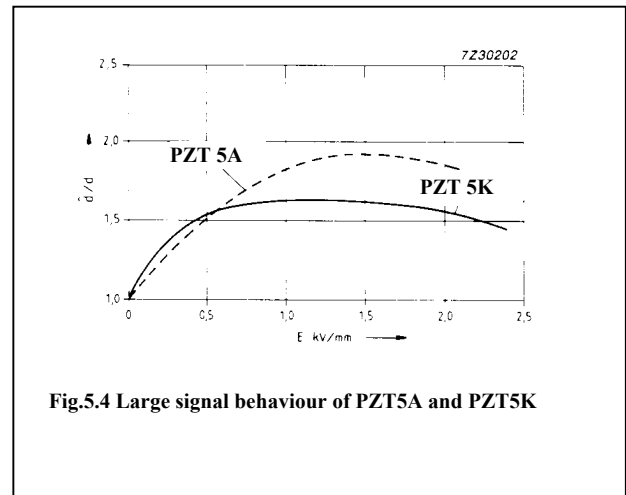


Fig.5.4 Large signal behaviour of PZT5A and PZT5K

At high fields strengths therefore, the stroke of a PZT actuator will be higher than that calculated from the equations of Section 5.1.1. Blocking forces also increase, though to a lesser extent. Both PZT5A and PZT5K show a steep increase of sensitivity with field strength.

The charge constants of material grades PZT4 and PZT8 are less dependent on field strength than those of PZT5A and PZT5K. Another difference between these two material groups can be found in the hysteresis behaviour. PZT5A and PZT5K have a much wider hysteresis loop and thus dissipate more heat during excursions.

In practice it's always difficult to predict the exact performance of an actuator. In particular, the manner of mounting and pre-stressing the material can have an important influence and measurements should always be the final decider of performance.

5.2 Composite actuators

Simple actuator elements, such as those shown in Fig.5.2 are only seldom used because of the very high voltages necessary to reach a practicable stroke. According to Eq.5.1, a voltage of 20 kV would be needed to reach a stroke of about 10 μ m. Such a voltage would no longer be controllable and switchable with readily available electronic components. If, on the other hand, the actuator is built from a large number of thin individual elements, electrically connected in parallel, operating voltages below 1000 V can be attained.

Still more advantageous are actuators with voltages below 100 V. These actuators are built up using the same multilayer technique that are used with ceramic capacitors. The advantage of low control voltages is obtained at the cost of high capacitances and operating currents, so when short reaction times are required, electrodes, connections and leads must be able to handle high currents.

Figure 5.5 shows a schematic drawing of a composite actuator. PZT discs, 0.3 - 1.0 mm thick, are stacked in the direction of the force and movement. This method of construction entails the disadvantage that many joints can considerably reduce the rigidity of the actuator. Only with a high mechanical pre-stress can the properties of a one-piece ceramic element be approximated.

Properties can be calculated using Eqs 5.1 to 5.4 by substituting nU for U and nh for h where n is the number of discs. If an extremely elastic spring is used for prestressing, as shown in Fig.5.6, stroke, blocking force and stiffness will be as predicted. Only the response time increases because of the added mass.

Pre-stressing springs of higher rigidity (for example a central bolt or tube around the actuator) act as a loading spring and thus reduce the performance of the assembly.

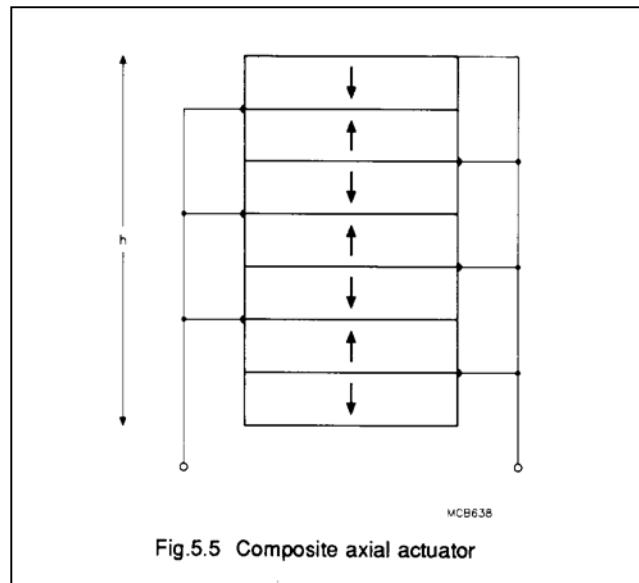


Fig.5.5 Composite axial actuator

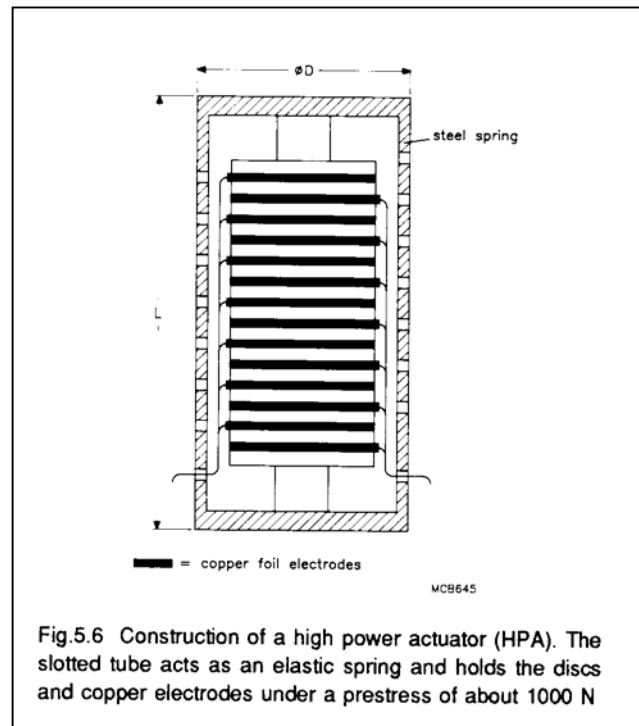


Fig.5.6 Construction of a high power actuator (HPA). The slotted tube acts as an elastic spring and holds the discs and copper electrodes under a prestress of about 1000 N

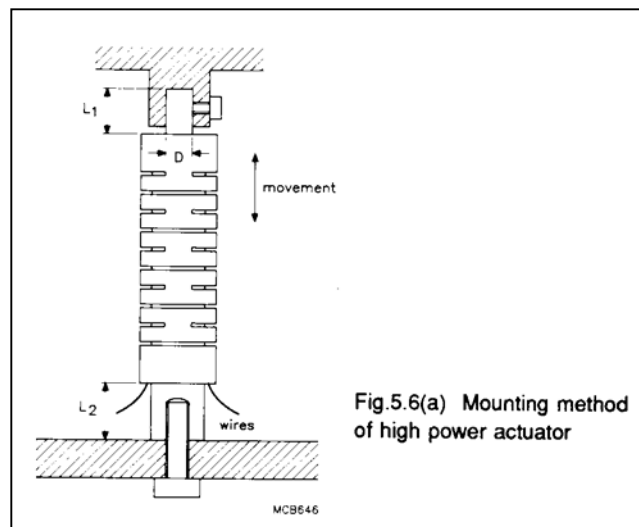


Fig.5.6(a) Mounting method of high power actuator

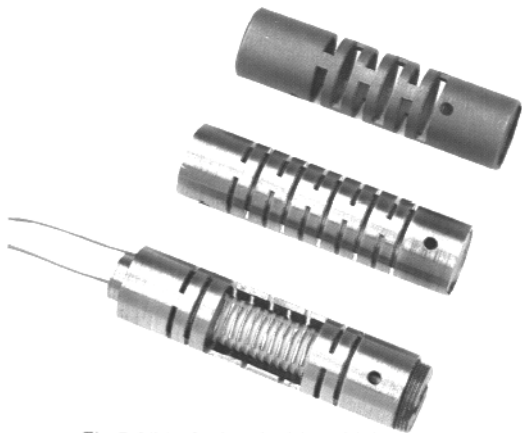


Fig.5.6(b) A view inside a high power actuator

A drawback of high mechanical pre-stressing is that it can lead to (partial) depolarization, especially during the time that no operating voltage is applied. If, however, grade PZT5K is used, the ceramic will be re-polarized by the operating voltage itself. This leads to the peculiar behaviour shown in Fig.5.7. After a long break from work, one or two cycles are required before reproducible values are obtained.

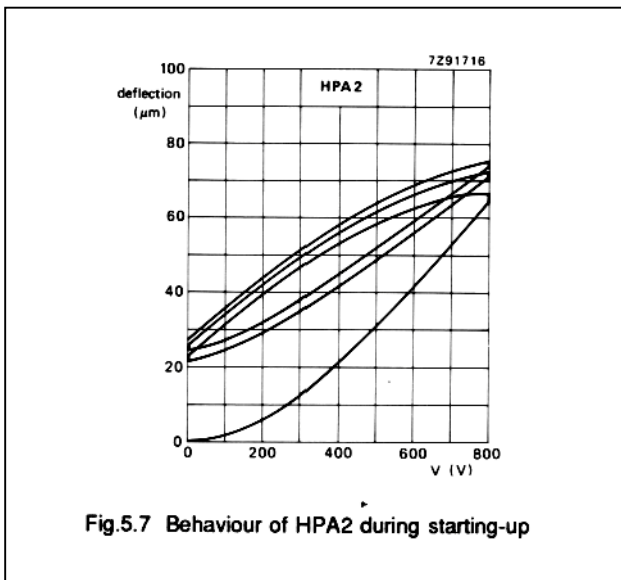


Fig.5.7 Behaviour of HPA2 during starting-up

Bonded stacks don't have this drawback, but they are more elastic since the glue lines cannot be made as thin as desired. What's more, since the tensile strength of ceramic is low, these non pre-stressed actuators must be protected against tensile forces, especially during pulse operations.

Figure 5.10 shows three high-power PZT-actuators (HPA) complete with elastic spring tubes. Table 5.1 gives data for this standard range.

Figure 5.8 shows the response of HPA2 to a squarewave voltage. Since charge constants d_{33} and d_{31} have positive temperature coefficients, the stroke of a PZT actuator increases with temperature. A typical curve for PZT5K is given in Fig.5.9.

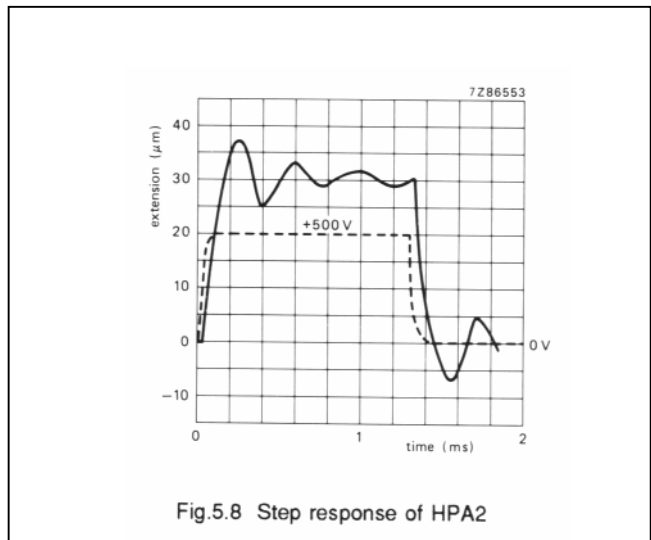


Fig.5.8 Step response of HPA2

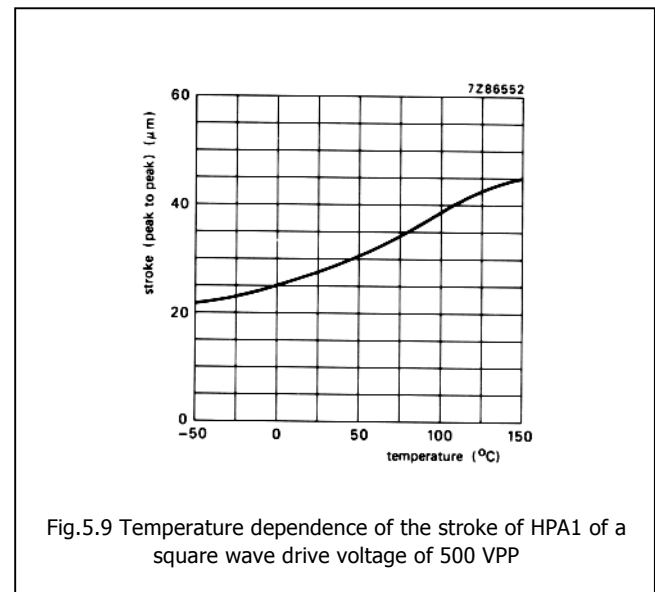


Fig.5.9 Temperature dependence of the stroke of HPA1 of a square wave drive voltage of 500 VPP

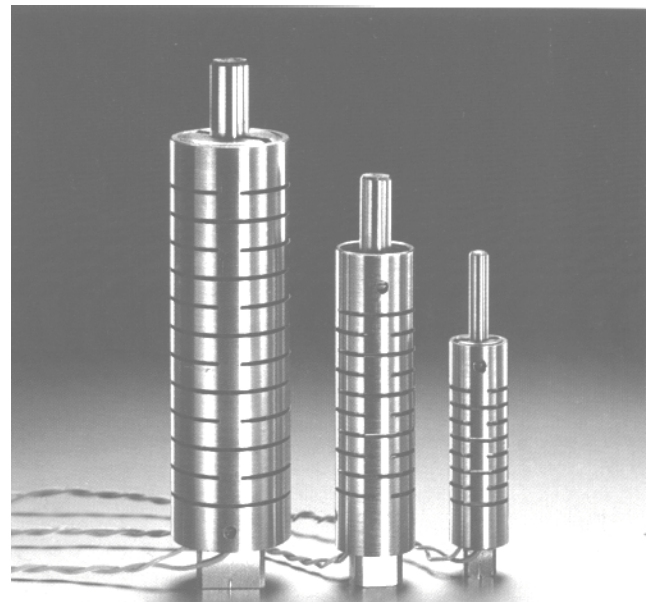


Fig.5.10 The range of High Power Actuators

TABLE 1
PZT high power actuators

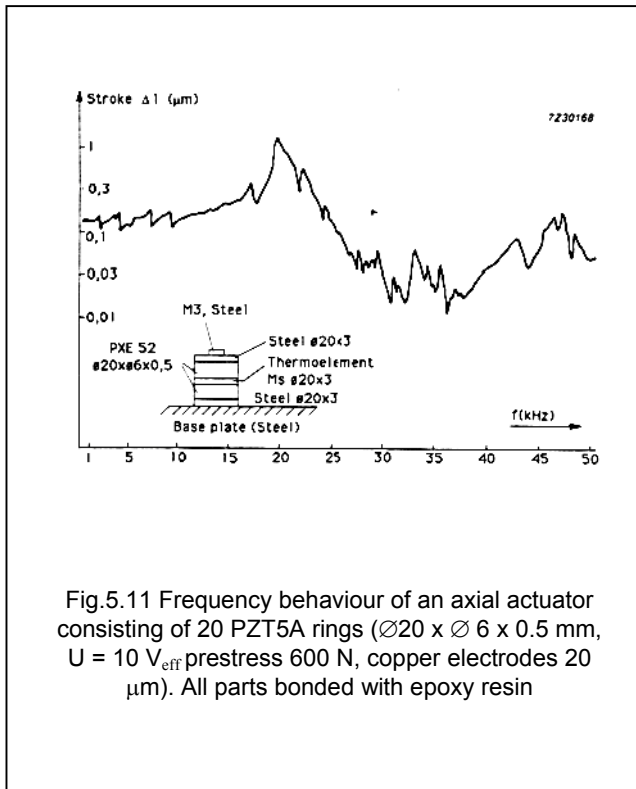
code 4322 020	1905	1906	1907
dimensions D × L (mm)	16 × 50	22 × 75	32 × 100
stroke 0 to 500 V (μm)	≈20	≈30	≈50
stroke 0 to 800 V (μm)	≈35	≈50	≈80
capacitance at 25 °C (nF)	≈100	≈250	≈800
stiffness (N/μm)	≈30	≈50	≈80
max. applied force (N)	2000	3000	5000

This standard range of HPAs is designed for applications where response times against high forces should be short, but repetition frequency is relatively low (up to 200 Hz). Such applications are found, for instance, in hydraulics, fuel injection valves and tool adjustment.

5.3 Actuators for higher operating frequency

During the design stage of actuators for high-frequency operation, two factors should be kept in mind. First, hysteresis losses in the materials heat up the actuator and limit the application range. Second, the construction should be as compact as possible to avoid spurious resonances below the main resonance of the actuator.

Figure 5.11 shows the frequency behaviour of a simple bonded axial actuator. Its basic resonant frequency lies at about 20 kHz (one end fixed). Below this frequency many additional, weaker, resonances occur, as a result of bending vibrations in the central bolt and in the test fixture.



For larger amplitudes and high frequencies, PZT8 is a suitable material grade - its hysteresis losses are much lower than those of PZT5K for instance. But the difference is not as great as might be expected from a comparison of their mechanical quality factors (Table 2.1). If two actuators of identical construction (Fig.5.11), one with PZT8, the other with PZT5K, are driven at the same amplitude, the difference in their heat dissipation is only a third what would be expected from Table 2.1. The reason for this is the higher sensitivity (d_{33}) of PZT5K which therefore requires a lower driving voltage and hence has lower dielectric losses.

The actuator in Fig.5.11 was tested at a constant amplitude of 1 gm. At 5 kHz, the temperature rose by 25 K for PZT5K and 10 K for PZT8. At the resonant frequency, lower drive voltages are needed and temperature rises are down to 4.5 K and 2 K respectively.

5.4 Drive circuitry

To fully exploit the fast response of high power actuators, it's essential to use drive circuitry that can deliver high currents at high voltage levels during short periods. Though there is no holding current because the PZT-actuator is essentially a capacitive device, power levels can be considerable if the actuator is switched at a high repetition rate. For instant HPA 3 of Table 5.1 has a capacitance of about 800 nF. At a driving voltage of 800 V, the energy per cycle is 0.26 J, which at 100 Hz operating frequency, means an output power of 52 W. It's not necessary, however, to dissipate all that power. With the right circuit design, up to 90% can be regained upon discharge of the actuator.

Fundamentally there are two options in driving an actuator: *voltage* or *charge drive*.

Voltage drive is easier from the circuit point of view. Its major drawback is that the expansion/voltage curve will show hysteresis and creep phenomena (Fig.5.12(a)).

With charge drive these effects are virtually absent. There is an almost linear relation between dielectric displacement and deformation (Fig.5.12(b)), but the circuitry for this drive mode is more complicated. The curves of Fig.5.12 have been measured on a composite high power actuator built up from 92 (diam. 20 x 0.5 mm) PZT5K discs.

Figure 5.13 shows a straightforward drive circuit based on two thyristors. The actuator is charged via thyristor Th1 and a current-limiting resistor R1, and discharged via Th2 and R2. The circuit is simple and handles high peak currents, so switching can be extremely fast. A drawback is that after switching on, Th1 shuts down when the current falls below the holding level. This disconnects the element from the supply and the voltage will start to decrease due to leakage. For long cycle times this would be unacceptable, but for fast switching, the circuit is quite satisfactory (Fig.5.16(b)).

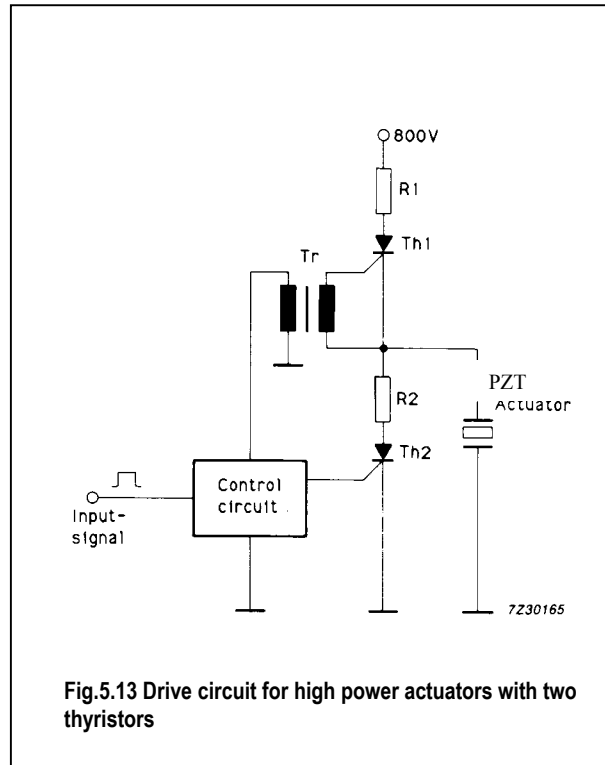
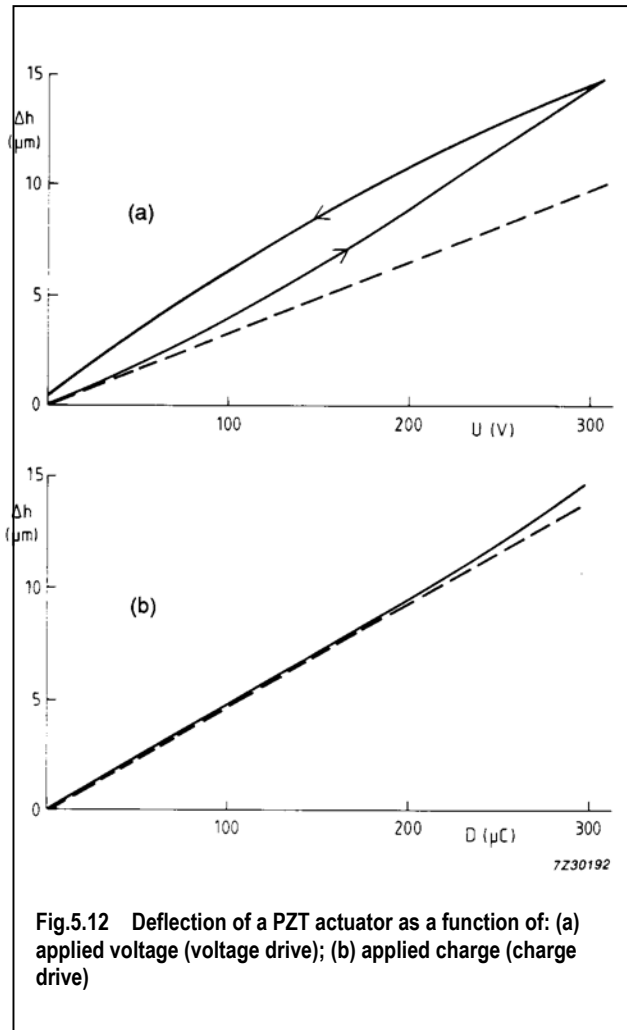
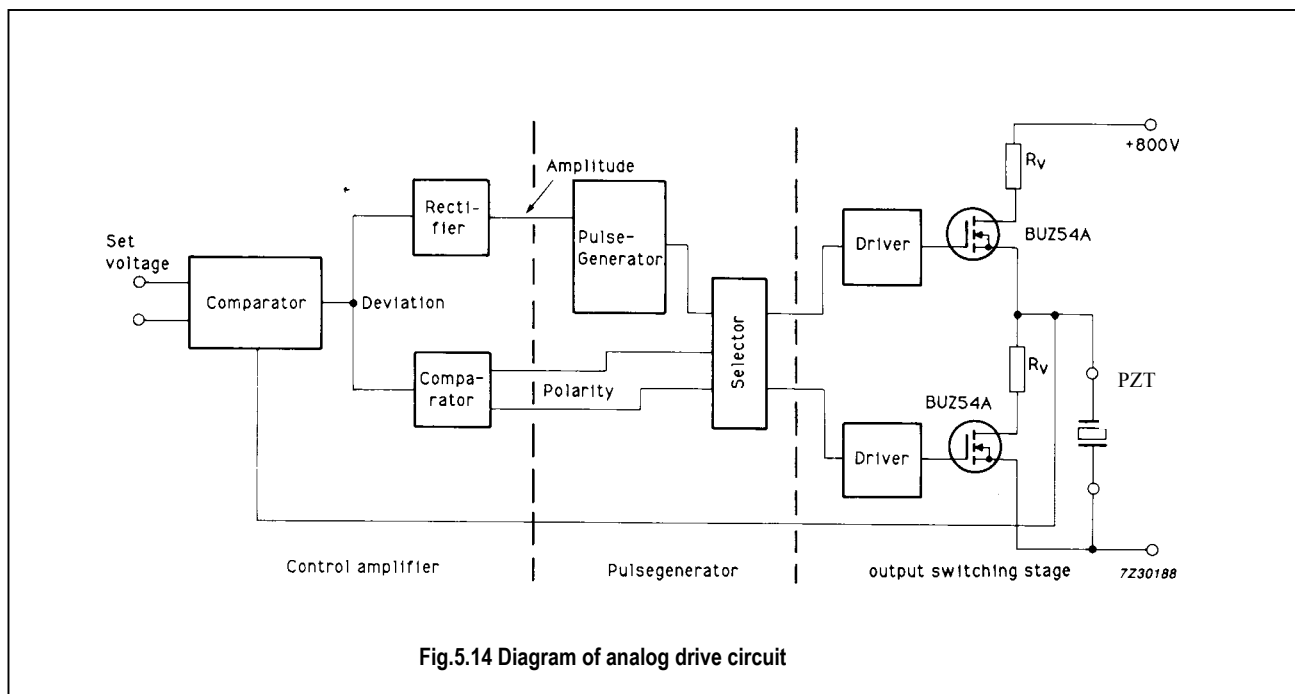


Figure 5.16(a) demonstrates the behaviour of the same HPA with analog voltage drive. After the fast response to the voltage step there is an increase of extension with time, apparently charge keeps flowing to the PZT-elements. If a continuous, controlled adjustment of the actuator is required, however, analog driving is essential.



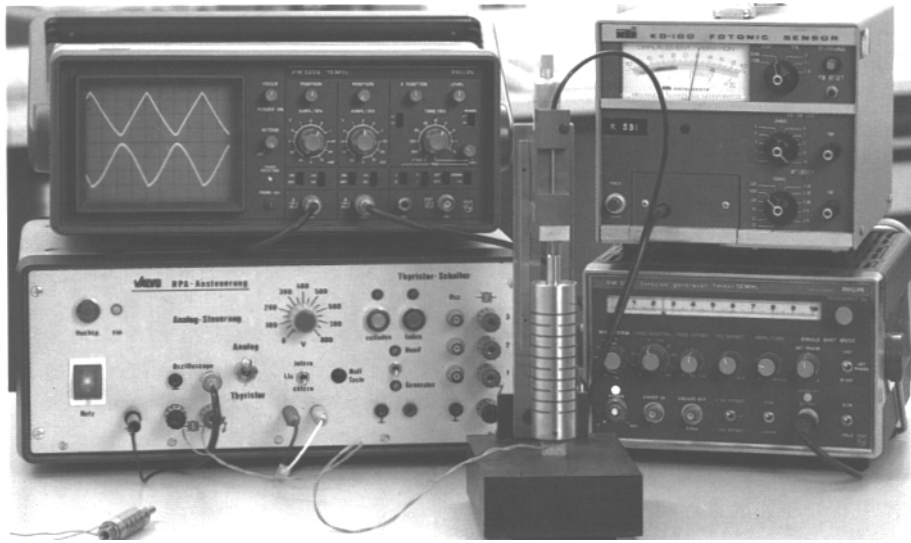
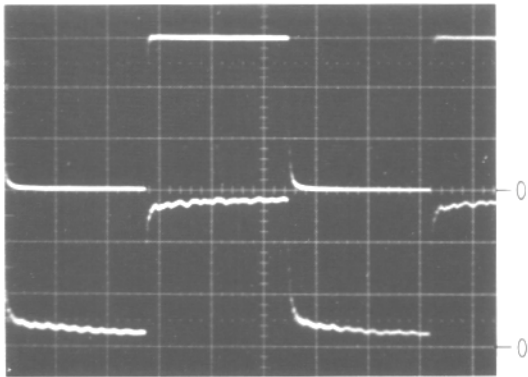
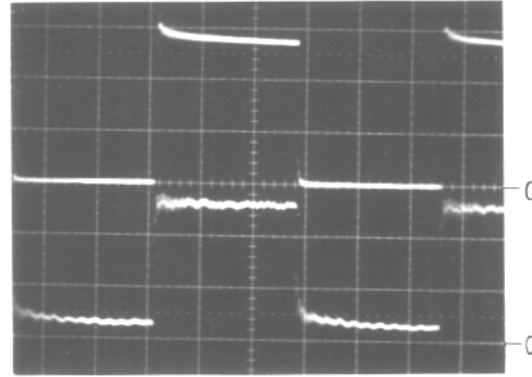


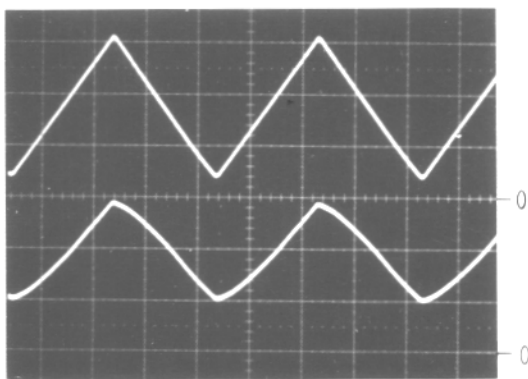
Fig.5.15 Measuring set-up for high power actuators



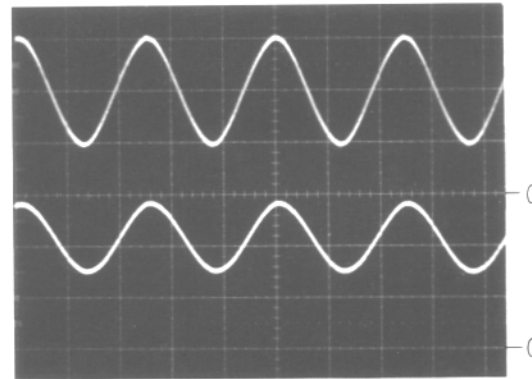
(a) in voltage drive



(b) in charge drive



(c) triangular wave



(d) sine wave

Fig.5.16 HPA response to a square wave

The principle of an analog voltage-drive circuit is given in Fig.5.14. Its power stage, consisting of two power MOSFETS, operates in switched mode with variable pulse duration. High peak currents can be handled in this way and power dissipation in the switches is kept low. The voltage on the actuator is compared with a preset voltage in the regulator stage of the amplifier. The actuator is then charged or discharged by variable amounts as required.

Figure 5.17 shows an analog charge-drive circuit. The current to the actuator causes a voltage drop across the 4.7 kΩ resistor and this is used as a feedback signal for the operational amplifier. The current to the actuator, and thus the charge is regulated according to the input voltage. This charge-drive circuit is particularly useful in cases where a good linearity is required (Ref.3)

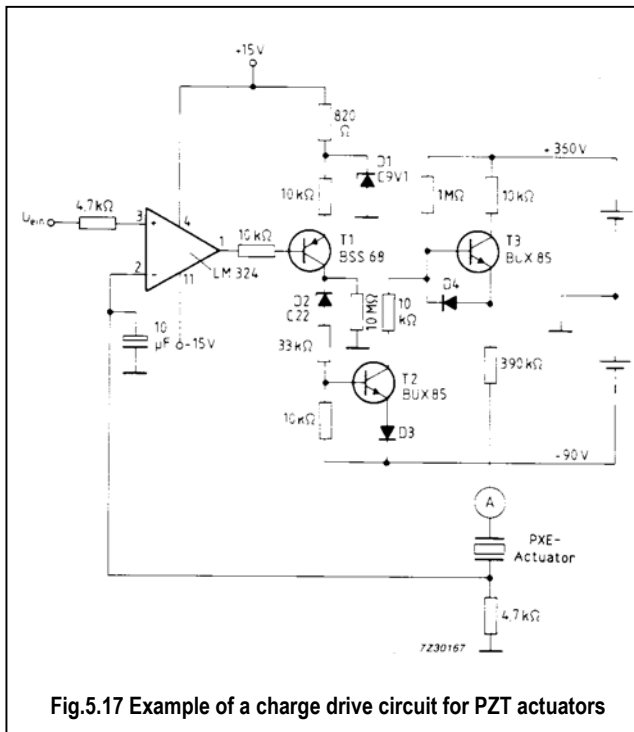


Fig.5.17 Example of a charge drive circuit for PZT actuators

If very precise and stable positioning is required, PZT actuators should always be used in a closed loop system in combination with a sensor. This could, for example, be an optical sensor like the *Fotonic Sensor* shown in Fig.5.15, which was used to produce the curves in Fig.5.16. Inductive sensors, interferometers or strain gauges can also be used to measure the absolute position and, if necessary, to adjust the voltages supplied to the actuator.

5.5 Flexure elements as actuators

A PZT-flexure element can also be used as an actuator. The operating principle is explained in Fig.5.18. A voltage is applied to the plates in such a way that one plate contracts while the other expands, and since the plates are glued together, they bow.

For this application we recommend the parallel bimorph (see Chapter 4). Both plates are polarized in the same direction and can be connected in parallel. This offers higher sensitivity and the possibility of applying a bias voltage (Fig.5.18) to generate an electric field parallel to the direction of polarization, thus eliminating the risk of depolarization.

Deflections possible with this actuator are high but blocking forces are relatively low. The elements are generally thin, long and compliant. Stiffness is low and so is the resonant frequency. Main properties are given in Table 5.2. All dimensions in metres and:

- h = thickness
- l_t = total length
- l = free length
- w = width
- z = deflection.

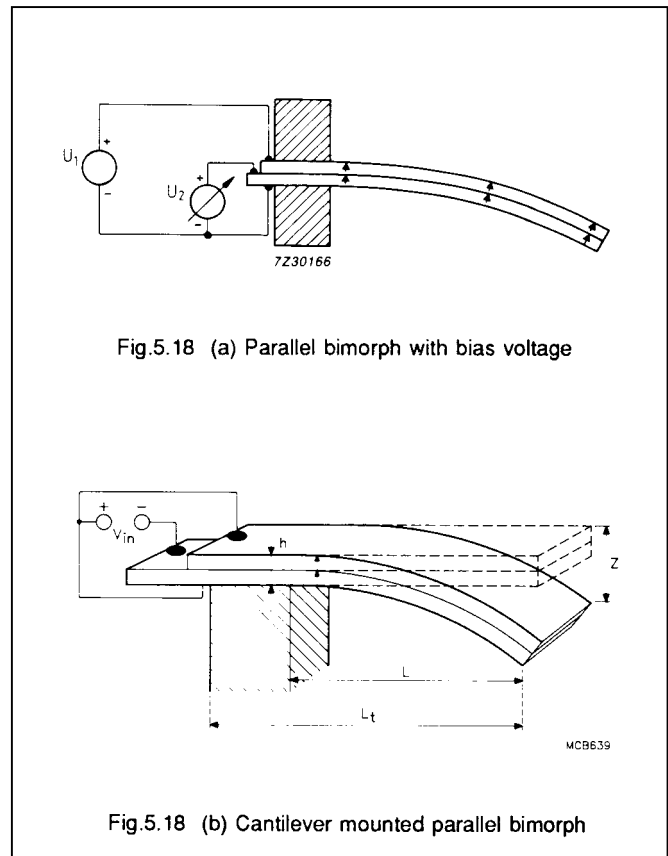


Fig.5.18 (a) Parallel bimorph with bias voltage

Fig.5.18 (b) Cantilever mounted parallel bimorph

TABLE 2
Design data for parallel bimorphs

deflection (m/V)	$9 \times 10^{-10} L^2 / h^2$
bending (m/N)	$7 \times 10^{-11} L^3 / Wh^3$
resonant frequency (Hz)	$400h / L^2$
charge output (C/N)	$8 \times 10^{-8} L^2 / h^2$
capacitance (F)	$8 \times 10^{-8} L_1 W / h$
voltage output (V/N)	$10^{-2} \times L^2 / h L_1 W$

Example

A flexure mode actuator is built up with a PZT5A parallel bimorph of dimensions 15 x 6 x 0.6 mm (free length 12 mm). The characteristic properties are calculated from the equations in Table 5.2.

Deflection:

$$\frac{z}{U} = 9 \times 10^{-10} \times \frac{144 \times 10^{-6}}{0.36 \times 10^{-6}} = 0.36 \times 10^{-6} \text{ m/V}$$

Resonant frequency:

$$f_r = 400 \times \frac{0.6 \times 10^{-3}}{144 \times 10^{-6}} = 1.67 \text{ kHz}$$

Capacitance:

$$C_a = 8 \times 10^{-8} \times \frac{15 \times 6 \times 10^{-6}}{0.6 \times 10^{-3}} = 12 \times 10^{-9} \text{ F}$$

Blocking force:

$$\frac{F_k}{U} = 10 \times \frac{0.6 \times 6 \times 10^{-6}}{12 \times 10^{-3}} = 3 \times 10^{-3} \text{ N/V.}$$

To give the designer a better overview of the possible combinations of deflection and resonant frequency, the following considerations might be useful.

Multiplying the deflection and resonant frequency above and inserting $U = E \cdot h/2$, we get:

$$zf_r = 0.18 \times 10^{-6} E.$$

This means that the product of deflection and resonant frequency is a constant for a given field strength. In practical applications this field strength is limited by the effects of depolarization and by flashover or breakdown.

For a DC field opposing the direction of polarisation, this limit is 300 V/mm. With alternating fields PZT5A can be used up to 500 V/mm, and if a bias field is used, the practical limit (in air) increases to 1 kV/mm.

So for an alternating voltage (500 V/mm) the resulting relation is:

$$zf_r = 90 \times 10^{-3} \text{ HZm.}$$

These relations are shown graphically in Fig.5.19. PZT5A flexure elements can never operate outside the boundaries given by the lines in this graph. Inside the boundaries, any combination of deflection and resonant frequency may be chosen by varying the free length and thickness of the bimorph.

For the actual design procedure, the graphs of Fig.5.20 are useful. Deflection z and resonant frequency f_r have been plotted against free length with height h of the bimorph as a parameter. Figure 5.20 is for $U = 150 \text{ V}$. Other voltages cause a parallel displacement of the family

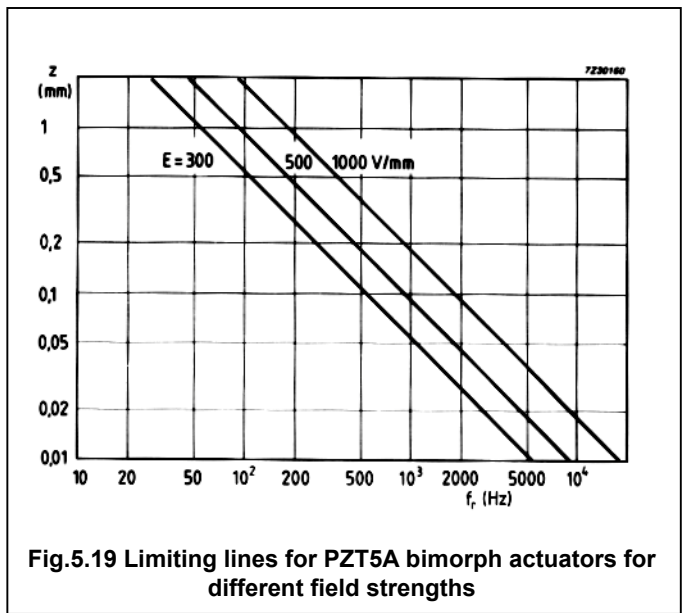


Fig.5.19 Limiting lines for PZT5A bimorph actuators for different field strengths

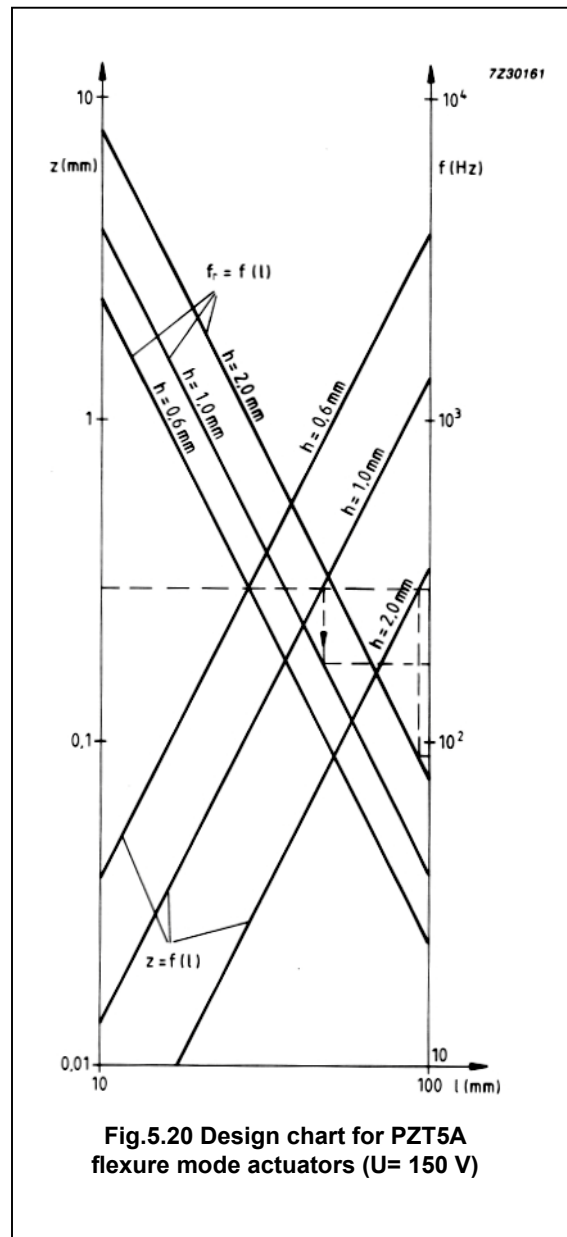


Fig.5.20 Design chart for PZT5A flexure mode actuators (U= 150 V)

Assume that a deflection of 0.3 mm is required. The horizontal dotted line ($z = 0.3$ mm) intersects the $h = 1.0$ mm line at a free length of 48 mm. The vertical dotted line intersects $h = 1.0$ mm line at resonant frequency $f_r = 175$ Hz. If a higher resonant frequency is required, a thinner actuator should be chosen - for example $h = 0.6$ mm. The dotted line then intersects at $l = 28.5$ mm and $f_r = 300$ Hz. A lower resonant frequency comes when the height of the bimorph is increased to, for instance, 2 mm. The graph then gives $l = 94$ mm and $f_r = 91$ Hz.

Blocking force, the remaining parameter, can be estimated by means of Fig.5.21. Here, force in newtons per unit width is plotted against free length with height h as parameter (width in metres). Again the graph is valid for $U = 150$ V.

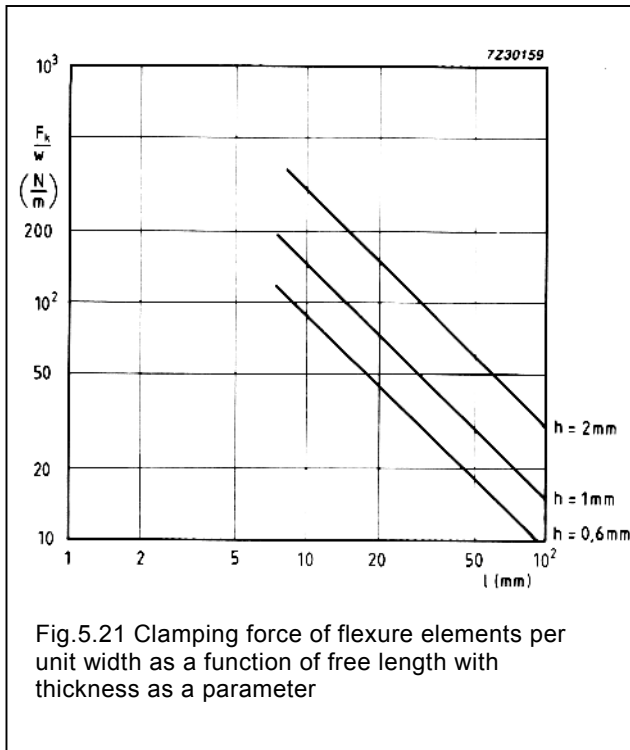
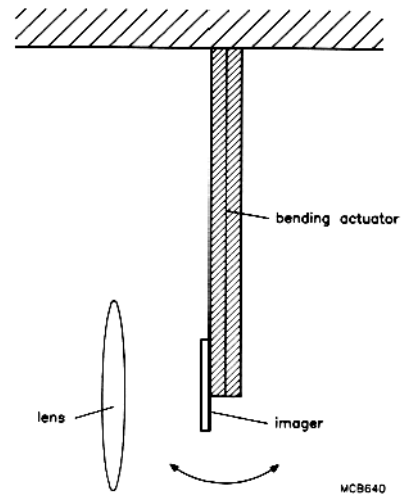
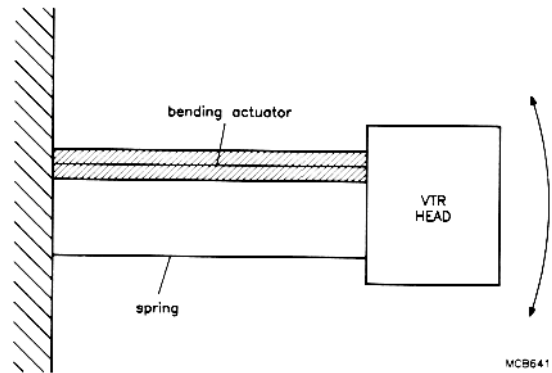


Fig.5.21 Clamping force of flexure elements per unit width as a function of free length with thickness as a parameter



- Reading aids for the blind.
- Actuating or controlling hydraulic valves.

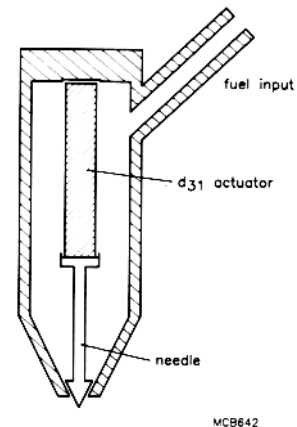
An example could be the new high-speed valves in fuel injection systems for car engines (Refs 4 and 5).

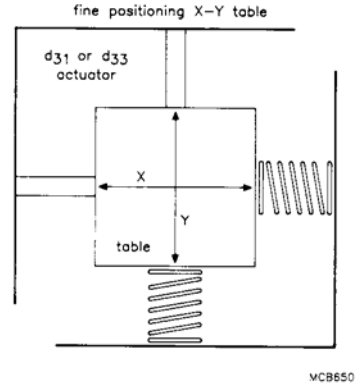
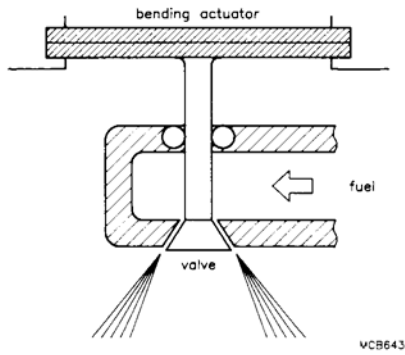
5.6 Applications

Though their movements are limited, PZT actuators have found applications in many fields. The following merit attention in particular.

- Optical instruments.

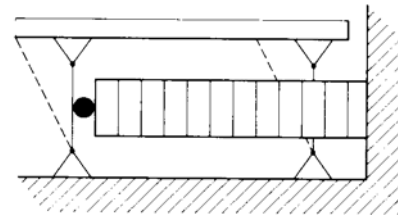
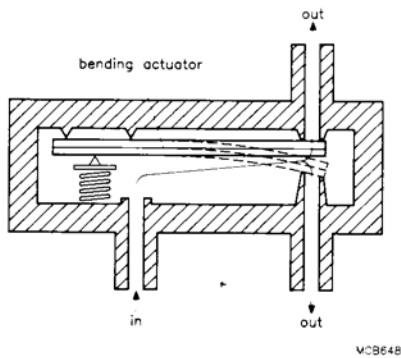
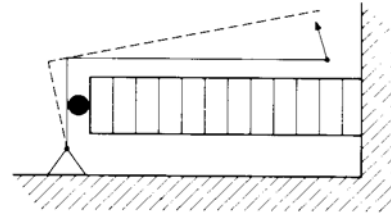
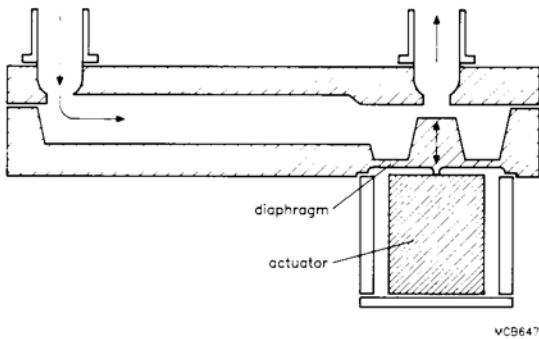
PZT-actuators are used to adjust the position of lenses or mirrors, often with nanometre precision. Movement is important in this application, force to a much lesser extent.





- Control of pneumatic valves.

In many applications, the movement of a PZT actuator is too small. Several methods are known for amplifying the stroke. Some examples are given below.



- Fine adjustment of machine tools.

Thanks to their high rigidity, these actuators are ideal for fast, precise adjustment of tools or even workpieces. By applying fixed voltage patterns, in phase with the rotation of a lath, high precision out-of-round work pieces become possible.

- Oscillation damping.

Undesired oscillations in machine tools can be damped by means of PZT-actuators operating in antiphase with the vibrations. This improves quality of the final product or avoids excessive wear of tools. It can also significantly reduce noise levels (Ref.6).

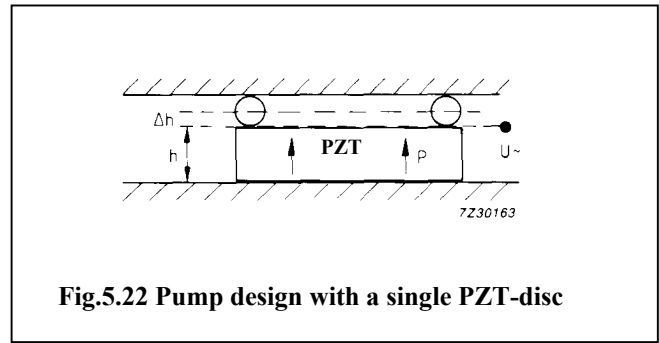
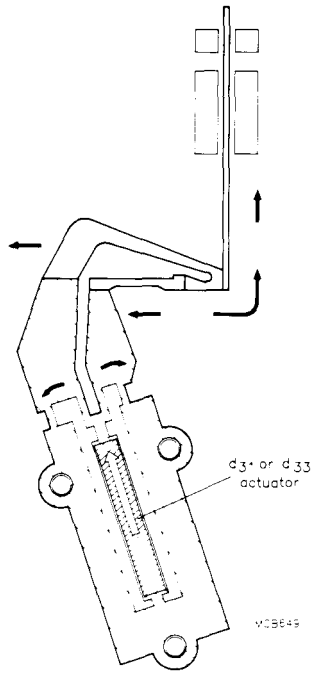


Fig.5.22 Pump design with a single PZT-disc

5.7 Piezoelectric pumps

The excursions of a piezoelectric element can be used to operate an input-output valve to control the transport of small volumes of gas or liquids.

In some cases valves are not even required. The dynamic properties of the fluid are often sufficient to generate a flow. The latter principle is applied in the so-called tubular ink-jet printer.

Table 5.3 shows what volume displacements and maximum pumping pressures can be achieved with the various PZT elements.

High pumping pressures, combined with low volumes, are possible with simple PZT-discs. With flexure elements, volumes up to several cubic millimetres are possible. Pumping pressures, however, are much lower.

TABLE 5.3

	volume displacement (mm ³)	blocking pressure (Pa)
PZT-disc	5.10 ⁻²	10 ⁷
PZT-tube	5.10 ⁻³	5.10 ⁶
flexure element (membrane)	5	10 ⁵

PZT discs

The maximum pumping pressure of a PZT disc can be calculated from Fig.5.22. The thickness of the disc will increase when an electric field is applied. To avoid depolarization, this field should preferably be aligned in the direction of polarization of the actuator.

If an AC-voltage supply is used, it may be necessary to add an additional DC-bias voltage.

The deformation of the disc caused by a field E is given by:

$$S = \frac{\Delta h}{h} = d_{33}E \quad (5.11)$$

$$\text{or: } \Delta h = d_{33}Eh = d_{33}U. \quad (5.12)$$

The change in height by a mechanical stress T is:

$$S = \frac{\Delta h}{h} = s_{33}T \quad (5.13)$$

$$\text{or: } \Delta h = S_{33}hT. \quad (5.14)$$

From these equations the stress T_b , and hence the pressure P_b , necessary to push back or block the movement caused by the piezo-electric effect can now be found:

$$T_b = P_b = \frac{d_{33}U}{s_{33}h}. \quad (5.15)$$

This relation is used to calculate the maximum pressure mentioned in Table 5.3.

The effective change in volume ΔV is calculated by multiplying Eq.5.12 by the surface area of the disc.

$$\Delta V = A\Delta h = d_{33}AU. \quad (5.16)$$

As a practical example of this, consider a PXE 5 disc 20 mm in diameter and 1 mm in thickness, to which a 300 V voltage is applied.

From Eq.5.15 the maximum pumping pressure is

$$P_b = \frac{390 \times 10^{-12} \times 300}{18 \times 10^{-12} \times 10^{-3}} = 6.5 \times 10^6 \text{ Pa}$$

or since 1 Pa = 10⁻⁵ bar:

$$P_b = 65 \text{ bar.}$$

For the volume displacement we get from Eq.5.16

$$\begin{aligned} \Delta V &= 390 \times 10^{-12} \times \frac{400\pi}{4} \times 10^{-6} \times 300 \\ &= 36.75 \times 10^{-3} \text{ mm}^3. \end{aligned}$$

If the applied voltage is only in the direction of polarization (DC or AC with bias), its practical limit is about 1 kV in this example. Pressure and volume displacement will then be about a factor 3 higher than calculated above.

PZT tubes

A radially polarized PZT tube can serve as a pump since the volume of the central hole decreases when a voltage is applied.

The general formula for this effect is:

$$\Delta V = -\frac{3}{2} d_{33} L R_i E$$

(R_i = inner diameter).

For a tube of PZT5A 10 mm long, an outer diameter of 1 mm, an inner diameter of 0.5 mm and a field $E=10^6$ V/m this becomes:

$$\begin{aligned} \Delta V &= -\frac{3}{2} \times 500 \times 10^{-12} \times 10^{-12} \times 0.5 \times 10^{-3} \times 10^6 \\ &= -5.9 \times 10^{-12} \text{ m}^3 = -5.9 \times 10^{-3} \text{ mm}^3 \end{aligned}$$

(voltage = 250 V).

The blocking pressure is given by:

$$P = \frac{1}{2} d_{33} \cdot \frac{R_o - R_i}{R_i} \cdot \frac{1}{s} \cdot E$$

where R_o = outer diameter
 s = compliance of PZT5A

In the present example, this maximum pressure would be

$$P = 4.7 \times 10^6 \text{ N/m}^2 = 47 \text{ bar.}$$

PZT flexure elements (membranes)

A membrane in this context is a round flexure element. It can be a combination of two discs of PZT (bimorph) or of a piezoceramic disc and a metal disc. An exact treatment of this type of pumping element is rather complicated. Empirical values and simplified formulas will be used to estimate volume displacements and pressures.

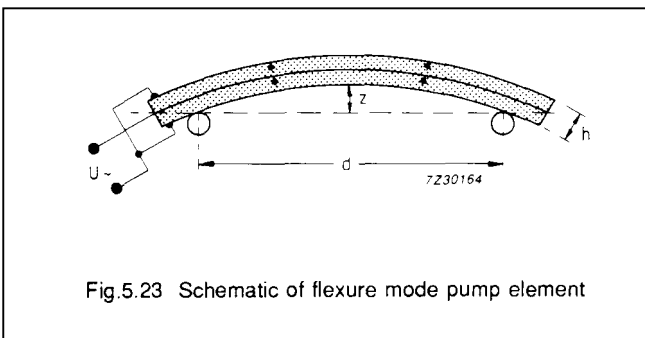


Fig.5.23 Schematic of flexure mode pump element

Deflection in the centre of a disc is given by:

$$Z_a = 10^{-10} \frac{d^2}{h^2} \cdot U \text{ (m)} \quad (5.17)$$

where d = diameter of disc

h = thickness of disc.

An approximate expression for the volume displacement is:

$$\begin{aligned} \Delta V &= \frac{\pi d^2}{4} \times 0.5 \times 10^{-10} \frac{d^2}{h^2} U \text{ (m}^3\text{/V)} \\ &\approx 4 \times 10^{-11} \times \frac{d^4}{h^2} U \text{ (m}^3\text{/V)}. \end{aligned} \quad (5.18)$$

The resilience is:

$$Z_p = 1.5 \times 10^{-10} \frac{d^3}{h^3} \text{ (m/N)}. \quad (5.19)$$

By combining Eqs 5.17 and 5.18 and integrating over the surface area of the membrane, the blocking pressure is found to be:

$$P_b \approx 8 \frac{h}{d^3} \cdot U \text{ (Pa)}. \quad (5.21)$$

Some practical examples:

- PZT 5A bimorph with:

$$h = 0.6 \text{ mm}$$

$$d = 25 \text{ mm}$$

$$U = 150 \text{ V.}$$

Displacement:

$$\begin{aligned} \Delta V &\approx 4 \times 10^{-11} \times \frac{d^4}{h^2} \times 150 \text{ m}^3 \\ &= 6.5 \times 10^{-9} \text{ m}^3 \\ &= 6.5 \text{ mm}^3. \end{aligned}$$

Blocking pressure:

$$\begin{aligned} P_b &\approx 8 \times \frac{h}{d^3} \times 150 \text{ Pa} \\ &\approx 5 \times 10^4 \text{ Pa} \\ &\approx 0.5 \text{ bar.} \end{aligned}$$

With a thicker bimorph, a higher pumping pressure can be obtained.

- PZT 5A bimorph with:

$$h = 1.2 \text{ mm}$$

$$d = 25 \text{ mm}$$

$$U = 300 \text{ V.}$$

Displacement $\Delta V \approx 3 \text{ mm}^3$.

Blocking pressure $P_b \approx 2 \times 10^5 \text{ Pa}$
 $\approx 2 \text{ bar.}$

A flexure element should be used when a relatively large volume displacement is required. A result of using this construction, however, is rather low pressure.

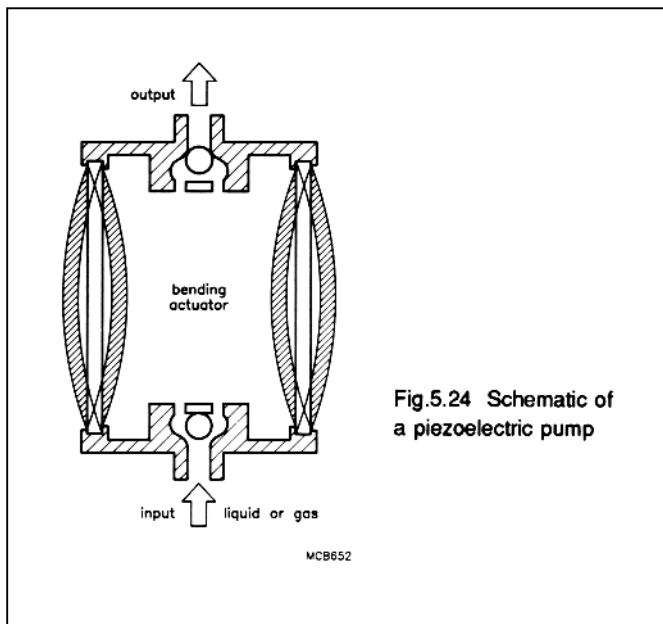


Fig.5.24 Schematic of a piezoelectric pump

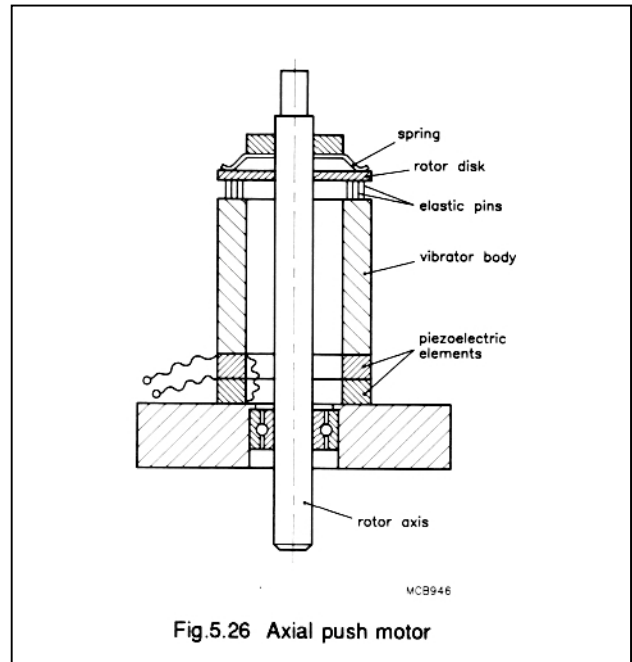


Fig.5.26 Axial push motor

5.8 Piezoelectric motors

Although piezoelectric actuators are only able to make small movements, these can be converted into large linear displacements or rotations using constructions called *piezoelectric motors*.

Three basic types can be distinguished:

- linear motor
- axial push motor
- travelling wave motor.

5.8.1 Linear motor

The basic construction contains three actuators (Fig.5.25). Two elements act as brakes or clamps, the third element causes the displacement. The operating cycle is as follows:

- brake 1 is activated
- actuator 2 elongates
- brake 3 is activated
- brake 1 unlocks
- actuator 2 contracts
- ... and so on.

This motor type is sometimes called an *inchworm*, a very appropriate name for this kind of movement. Speed can be regulated by varying step amplitude and frequency.

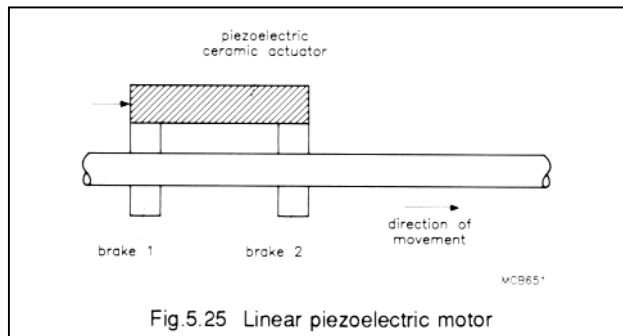


Fig.5.25 Linear piezoelectric motor

5.8.2 Axial push motor

A stator, built up with PZT-discs and metal cylinders, is brought into mechanical resonance. The axial movement is transformed into an elliptical movement against a rotor which is thereby put in motion (Fig.5.26).

5.8.3 Travelling wave motor

A ring of piezoelectric ceramic is glued to a stator ring. The ceramic is polarized in a special pattern (Fig.5.28). An alternating voltage is applied in such a way that resonance occurs (e.g. 40 kHz). A standing wave is generated. By regulating the phase difference between two groups of "islands", the standing wave can be set into rotation, clockwise or anti-clockwise. As a result, the castellated upper part of the stator ring performs elliptical movements against the surface of the rotor. This surface is coated with a special polymer to improve friction and keep wear within acceptable limits. This type of motor can be very flat (Fig.5.27).

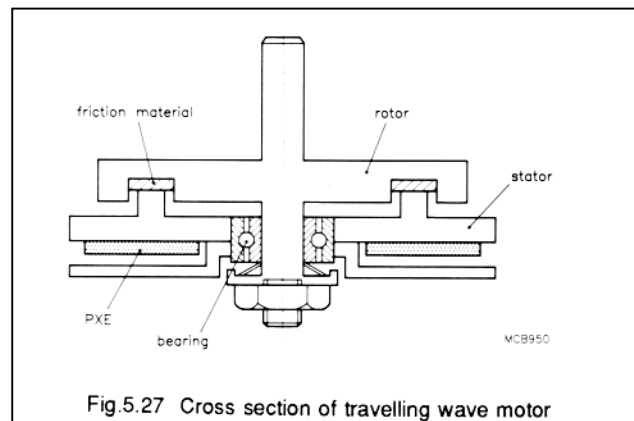


Fig.5.27 Cross section of travelling wave motor

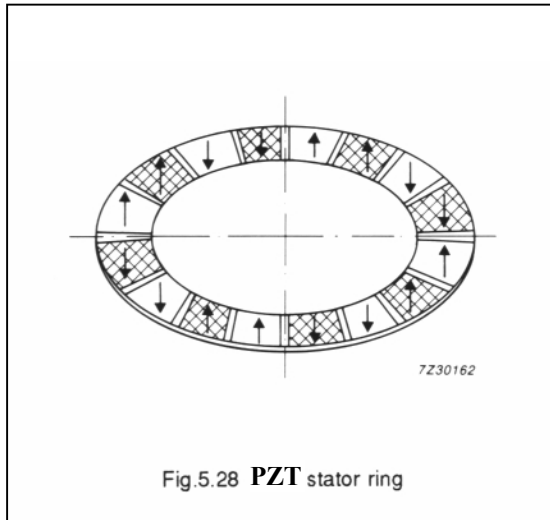


Fig.5.28 PZT stator ring

Major advantages of this motor are:

- high torque
- low RPM
- fast response times
- no brake necessary.

A drawback is that they need rather complicated electronic circuitry to drive them. What's more, the PZT element for the travelling wave type is not easy to produce and so is rather expensive. These motors should not therefore be seen as a replacement for simple electric motors. Their use is only feasible where their specific properties are of importance.

5.9 Multilayer actuators

5.9.1 Transversal mode (d_{31}) actuator

Multilayer actuators (Fig.5.29) can be produced with layer thicknesses as low as 20 or 40 μm . The manufacturing method is completely different from the classical process of sawing and electroding individual discs or plates (Fig.5.30). Because of the very thin layers of PZT, an electrical field strength of about 1 kV/mm can easily be reached for a drive voltage as low as around 50 V. The elongation per unit length or height is roughly the same as for of "classical" actuators. The difference is that the effect is reached for a much lower voltage.

The performance of a transversal d_{31} -mode type is shown in (Fig.5.31). Note that the element shortens for a drive voltage in the polarization direction.

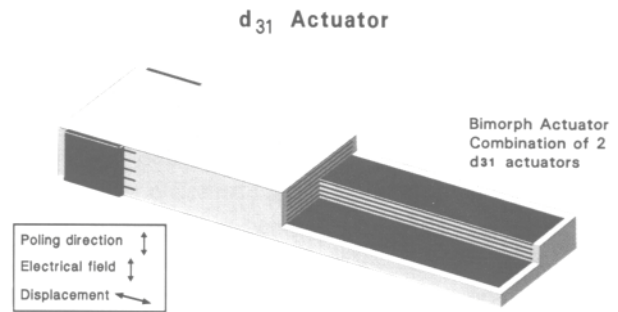


Fig.5.29 Transversal mode multilayer actuator

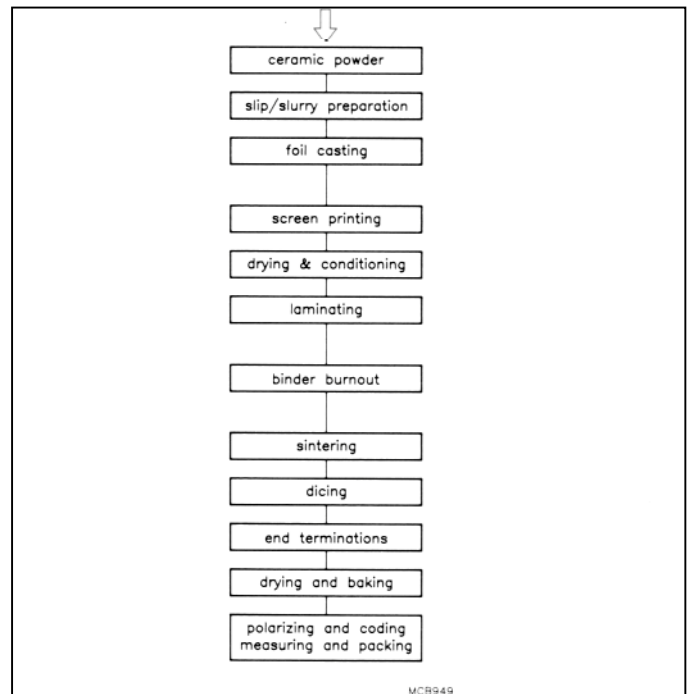


Fig.5.30 Flow chart of multilayer process

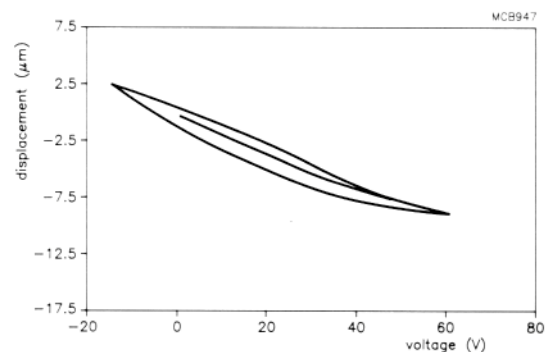


Fig.5.31 Performance of multilayer d_{31} -mode actuator

Axial mode multilayer actuators (d_{33} -mode)

As with "classical", axially-stacked actuators, the strain in the direction of polarization is twice as large as it is in the transverse direction. However, to get a large absolute elongation, the dimension of the actuator in the direction of polarization must be large as well.

For the multilayer process the thickness is currently limited to about 2 mm. Figure 5.32 shows the structure of such an element.

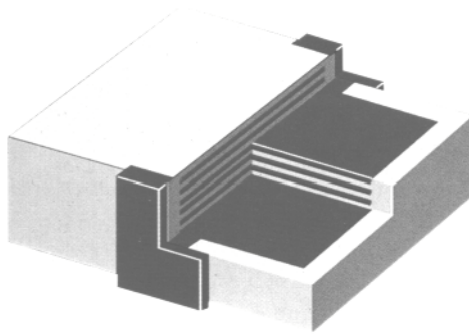


Fig.5.32 Axial mode multilayer actuator

Basically these elements can be built up in three ways:

- gluing a d_{31} actuator onto an inactive substrate, like a metal strip;
- combining a d_{31} -actuator with an unpolarized PZT layer;
- combining layers of piezoelectric ceramic with an intricate electrode structure so that the layers expand or contract like a classical bimorph element

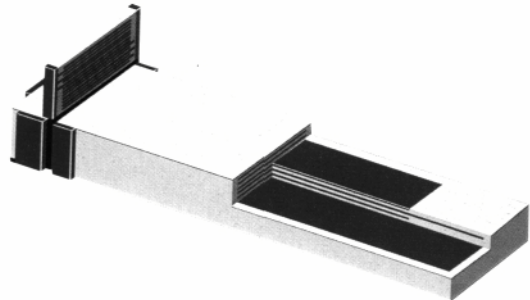


Fig.5.34 Multilayer parallel bimorph element

Since the maximum strain is around 10^{-3} at 50 V supply voltage, the absolute increase of its thickness will be about 2 μm .

For most practical applications it's necessary to stack several of these elements (Fig.5.33).

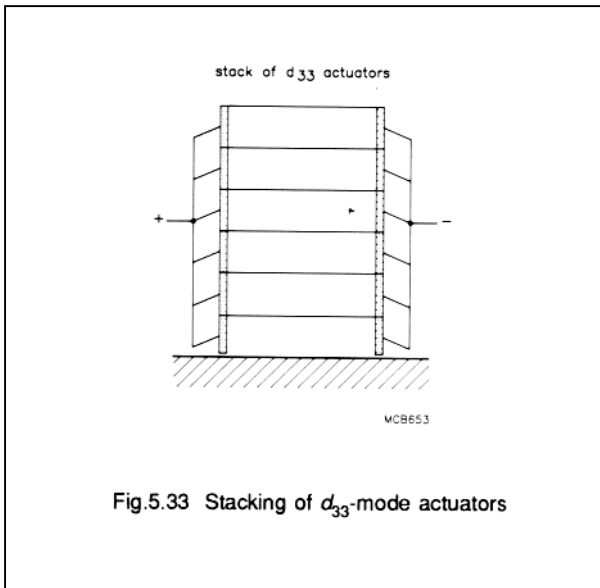


Fig.5.33 Stacking of d_{33} -mode actuators

Multilayer flexure mode actuators

The use of very thin piezoelectric layers results in flexure elements requiring much lower driving voltages than classical bimorph actuators.

Since again the maximum strain is around 5×10^{-4} for 1 kV/mm (as with discrete flexure elements), the general rule and formulas in this section also apply to multilayer elements.

Figure 5.35 shows the performance of a typical multilayer flexure mode actuator.

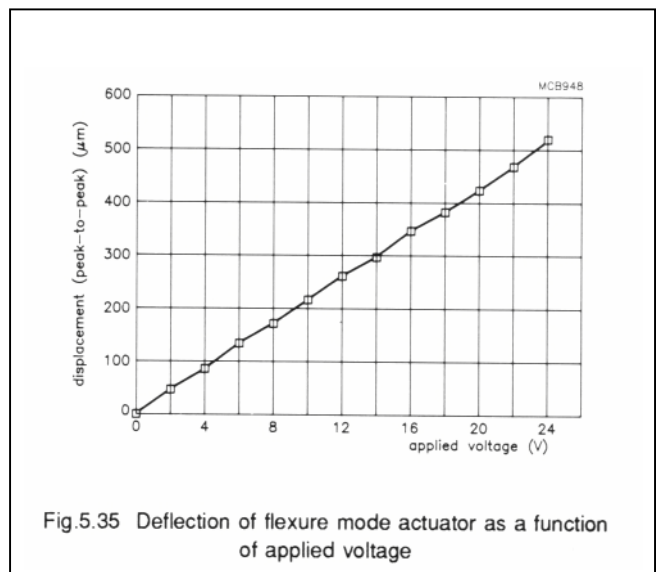


Fig.5.35 Deflection of flexure mode actuator as a function of applied voltage

6 TRANSDUCERS

6.1 Ultrasonic power

transducers 6.1.1 General

Most high intensity ultrasound applications, such as ultrasonic cleaning, require half wavelength transducers with resonant frequencies between 18 kHz and 45 kHz. The length in the main excursion direction of, say, a PZT4 transducer would therefore range from 9 cm to 3.5 cm since the sound velocity in this ceramic is approximately 3200 m/s. What's more, to reach the required output power level, the device would need a large surface area. The resulting single-piece ceramic block can present enormous manufacturing problems. And such blocks might be relatively inefficient anyway, since the whole transducer body would dissipate vibrational energy at a rate inversely proportional to the mechanical quality factor, Q_m , which is generally much lower in ceramics than it is in metals.

In a half-wavelength transducer, the stress amplitude reaches a maximum in the centre, the two end portions acting mainly as inert masses. These end portions can therefore be replaced by metal parts, which are cheaper and have a higher mechanical quality factor.

With high intensity transducers the overall electro-acoustic efficiency is of particular importance:

$$\eta \approx 1 - \frac{1}{1 + k_{\text{eff}}^2 Q_E Q_L} - \frac{1}{1 + \frac{Q_{m0}}{Q_L}} \quad (6.1)$$

(dielectric losses) (mechanical losses)

where: Q_{m0} = unloaded mechanical quality factor
 Q_E = electrical quality factor
 Q_L = quality factor due to the acoustic load alone.

The efficiency reaches a maximum when:

$$Q_L = \frac{1}{k_{\text{eff}}} \sqrt{\frac{Q_{m0}}{Q_e}} = Q_{Lopt} \quad (6.2)$$

then:

$$\eta_{\text{max}} = 1 - \frac{2}{k_{\text{eff}} \sqrt{Q_E Q_{m0}}} \quad (k_{\text{eff}} \sqrt{Q_E Q_{m0}} \ll 1) \quad (6.3)$$

It should be noted that at high drive levels Q_E and Q_{m0} can no longer be treated as constants - they are then often much lower than the low drive-level values.

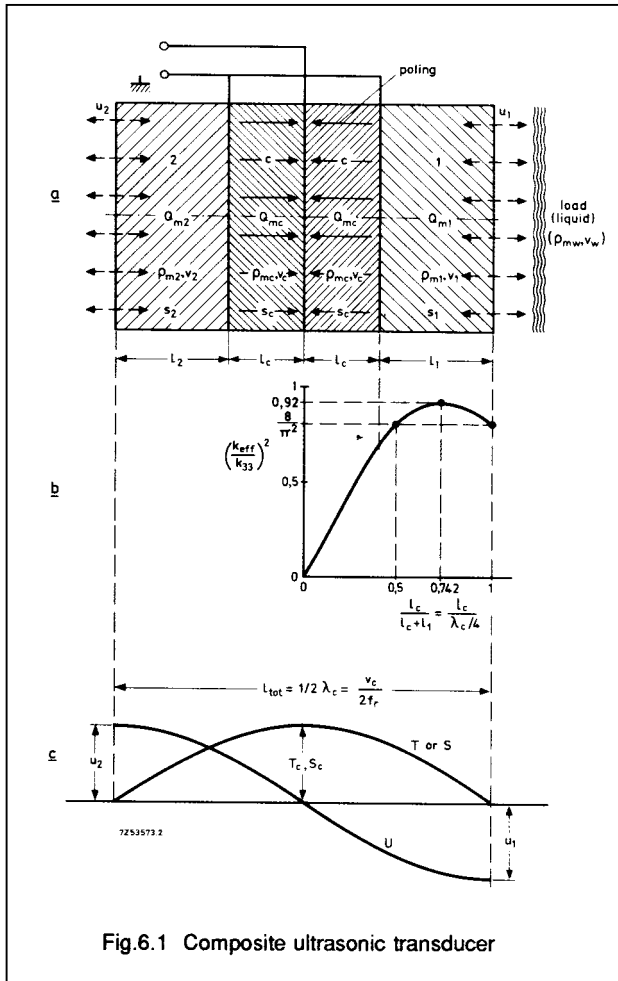


Fig.6.1 Composite ultrasonic transducer

6.1.2 Advantage of composite transducers

The mechanical quality factor Q_{m0} (no-load condition) of composite transducers is higher than that of single-piece transducers. In addition, owing to the better heat conductivity of the metal end pieces, the operating temperature of the ceramic components will be lower. So according to Eq.6.3, the overall electro-acoustic efficiency can be higher.

Another reason for the high efficiency of composite transducers is the fact that their piezoelectric coupling coefficient k_{eff} is not necessarily much lower than that of single-piece transducers. This is illustrated in Fig.6.1 in which the end portions 1 and 2 have the same acoustic properties and cross-sectional area as the central ceramic parts. In such cases, the excursion amplitudes u of the end faces 1 and 2 are equal ($u_1 = u_2$) as are their velocity amplitudes w . Consequently, the maximum attainable velocity amplitudes $(\omega_s u)_{\text{max}}$ at the end faces are related to the permissible stress amplitude in the central nodal plane $T_{c\text{max}}$ by:

$$(\omega_s u_1)_{\text{max}} = (\omega_s u_2)_{\text{max}} = \frac{T_{c \text{ max}}}{\rho_{mc} v_c} \quad (6.4)$$

where ρ_{mc} is the density of the ceramic material and v_c is the sound velocity in the material.

If end face 1 is loaded with a liquid (density ρ_w in which the sound velocity is v_w) into which it launches perfectly planar waves, Eq.6.4 is also valid for the particle velocity amplitude inside the liquid near face 1. The

maximum attainable ultrasound intensity in the liquid $I_{w \max}$ may be evaluated by inserting Eq.6.4 into the basic equation:

$$I_{w \max} = \frac{1}{2} (\omega_s u_1)_{\max}^2 \rho_{mw} v_w \quad (\text{W/m}^2). \quad (6.5)$$

If the end portions 1 and 2 have equal lengths and the same acoustic characteristics, the fractional bandwidths (B_F) of such a simple composite transducer are:

coil tuned:

$$B_{FLM} \approx \frac{k_{\text{eff}}}{\sqrt{1 - k_{\text{eff}}^2}} \quad (6.6)$$

single load:

$$B_{Fm} \approx \frac{1}{Q_{m0}} + \frac{2\rho_{mw} v_w}{\pi \rho_{mc} v_c} \quad (6.7)$$

double load:

$$B_{Fm} \approx \frac{1}{Q_{m0}} + \frac{2}{\pi} \cdot \frac{(\rho_{mw} v_w)_1 + (\rho_{mw} v_w)_2}{\rho_{mc} v_c} \quad (6.8)$$

In many cases the industrial application or the laboratory experiment requires much higher values of $I_{w \max}$ and B_{Fm} than those offered by the simple composite half wavelength transducer discussed so far. In the next section we shall discuss methods to improve these parameters.

6.1.3 Improving radiation intensity and bandwidth by means of different end sections

With an arbitrary material used for each end portion and the bond plane between the ceramic central portions maintained as the nodal plane (in which the stress amplitude T_c reaches a maximum of $T_{c \max}$), the simple amplitude and frequency relations of Section 6.1.2. and Fig.6.1 are no longer valid. The new equations can be conveniently expressed in terms of two numerical parameters q_i and G_i (i is either end portion 1 or 2):

$$q_i = \frac{\rho_{mc} v_c A_c}{\rho_{mi} v_i A_i} \quad (6.9)$$

where q_i is the ratio of the characteristic acoustic impedances (ρv multiplied by cross-sectional area) of the central and end portions, with cross-sectional areas A_c and A_i respectively. In practice, $A_i > A_c$ (Fig.6.2), and

$$G_i = q_i^2 - (q_i^2 - 1) \sin^2 \frac{\omega_s l_c}{v_c} \quad (6.10)$$

where G_i is the coefficient of gain, i.e. the ratio of gain in ultrasound intensity at the end faces to the gain in a homogeneous transducer (Fig.6.1) for constant T_c .

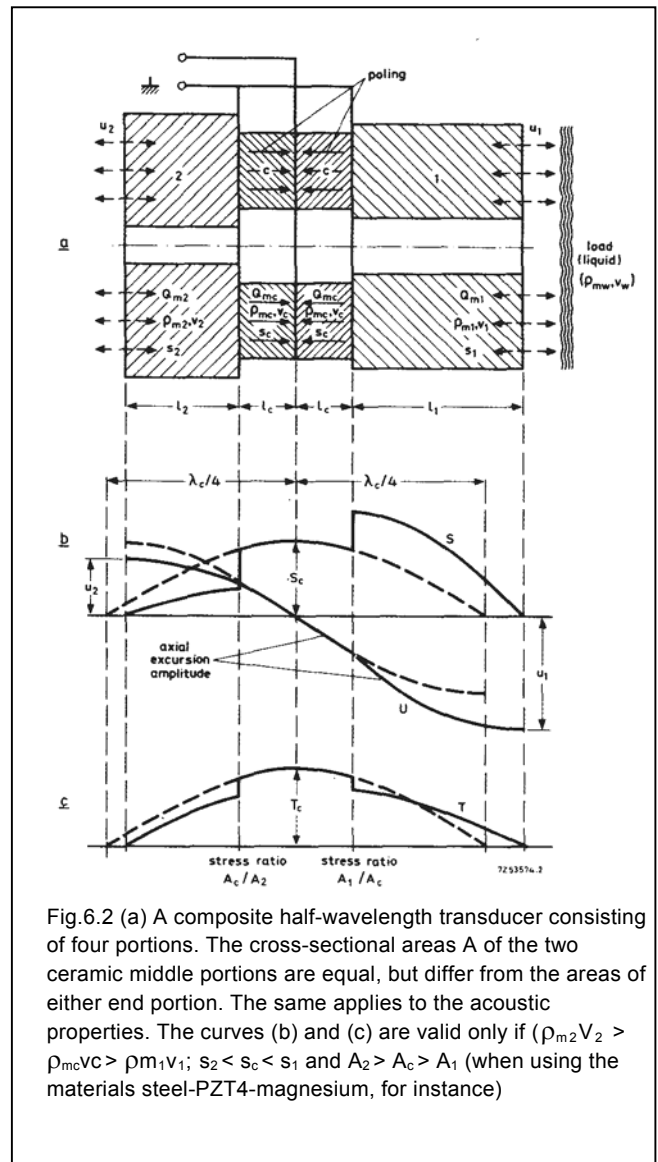


Fig.6.2 (a) A composite half-wavelength transducer consisting of four portions. The cross-sectional areas A of the two ceramic middle portions are equal, but differ from the areas of either end portion. The same applies to the acoustic properties. The curves (b) and (c) are valid only if $(\rho_{m2} v_2 > \rho_{mc} v_c > \rho_{m1} v_1; s_2 < s_c < s_1$ and $A_2 > A_c > A_1$ (when using the materials steel-PZT4-magnesium, for instance)

Both q_i and G_i are unity for the simple composite transducer discussed so far, but they are greater (less) than unity for up (down) transforming end portions. Obviously G_i ranges between q_i^2 and unity, and increases as the specific acoustic impedance $\rho_{mi} v_i$ decreases.

Using the above variables and assuming a load on both end faces we can write (see Eqs. 6.1, 6.2 and 6.5):

$$I_{wi \max} = \frac{1}{2} G_i \left(\frac{T_{c \max}}{\rho_{mc} v_c} \right)^2 (\rho_{mw} v_w)_i \quad (\text{W/m}^2) \quad (6.11)$$

$$B_{Fm} \approx \frac{1}{Q_{m0}} + \frac{2}{\pi} \cdot \frac{G_1 (\rho_{mw} v_w)_1 + G_2 (\rho_{mw} v_w)_2}{\rho_{mc} v_c} \quad (6.12)$$

The following resonant condition should be satisfied:

$$\tan \left(\frac{\omega_s l_i}{v_i} \right) \cdot \tan \left(\frac{\omega_s l_c}{v_c} \right) = q_i \quad (6.13)$$

Here both angles $\omega l/v$ range between 0 and $n/2$ radians and can be conveniently represented in a diagram using q_i as a parameter. An even clearer picture is obtained if the angles are multiplied by $2/\pi$, so that fractional lengths act as an ordinate and an abscissa:

$$\frac{2}{\pi} \cdot \frac{\omega_s l_i}{v_i} = \frac{l_i}{\lambda_i/4}, \quad \text{and} \quad \frac{2}{\pi} \cdot \frac{\omega_s l_c}{v_c} = \frac{l_c}{\lambda_c/4} \quad (6.14)$$

A family of $l_i/(\lambda_i/4)$ versus $l_c/(\lambda_c/4)$ curves for q_i values in the useful range of 0.4 to 4.0 is shown in Fig.6.3(a). All the corresponding G_i versus $l_c/(\lambda_c/4)$ curves are drawn in Fig.6.3(b).

These curves are very useful to the engineer for working out the first concept of a high intensity transducer as they provide a short-cut through the detailed calculations required for final design. It should be borne in mind that such detailed calculations require an appropriate choice of the material constants v_i and v_c (or λ_i , and λ_c). For instance, if diameter D of a mechanical transmission line increases to such an extent that the D -to- $\lambda/4$ ratio changes from unity to two, the effective phase velocity of extensional waves of the first mode already falls considerably below:

$$v_{bar} = \frac{1}{s \rho_m} \quad (6.15)$$

commonly called the *thin wire value*.

The correction needed on the value of v_{bar} depends on the value of Poisson's ratio of lateral contraction σ . Figure 6.4 gives the phase velocity of extensional waves in cylindrical bars in terms of v_{bar} for materials with $\sigma = 0.29$.

Table 6.1 contains numerical data on v_{bar} and other important properties of some materials that are of prime importance for high intensity transducers, either for high intensity end 1 ($G_1 > 1$) or for end 2 whose intensity is usually reduced ($G_2 < 1$) to have it radiate much less power when submerged together with active end 1. The table also gives the fatigue strength T_f and the maximum strain S_f . These are particularly important data if a bolt of one of the indicated metals is used for pre-stressing the transducer.

Combining the numerical data of Table 6.1 and the graphical data of Figs 6.2, 6.3 and 6.4, we arrive at the following conclusions:

- The combination of steel-PZT-magnesium is very favourable; the cheaper combination of steel-PZT-aluminium (duralumin) is also favourable but to a lesser extent. Aluminium (and magnesium) end portions can be upgraded by drilling holes or cutting slots in them.

- The sound velocity in PZT is relatively low. So the ratio of diameter-to-quarter-wavelength readily exceeds unity in 40 kHz to 50 kHz applications of the available PZT discs or rings. It's necessary, therefore, to take a

correction factor into account when determining the actual sound velocity, see Fig.6.4, for instance.

- When the diameter of a half-wave resonator is comparable to, or greater than, its length, *lateral* or radial mode resonances are possible whose frequency may (depending on the diameter-to-thickness ratio) be close to, or lower than the frequency of the fundamental, thickness mode. It's therefore generally best to have $D < \lambda/2$ wherever possible with this type of transducer.

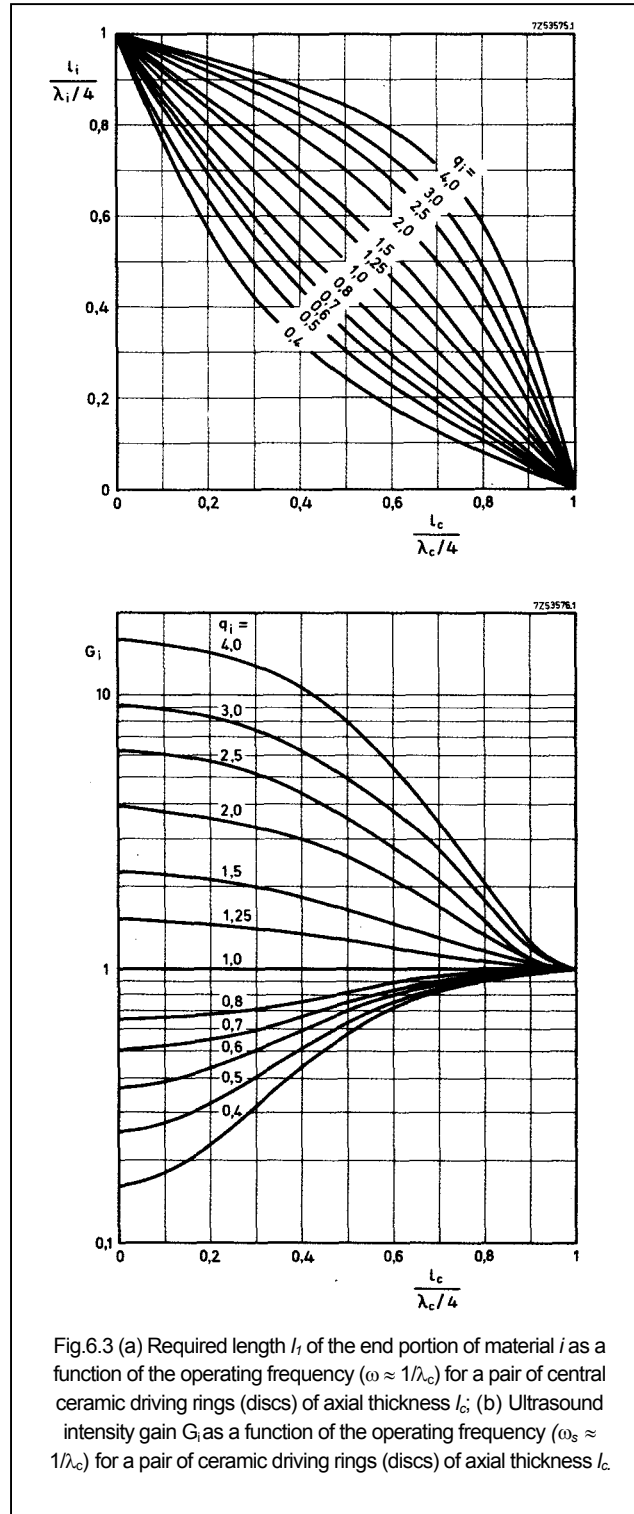


Fig.6.3 (a) Required length l_i of the end portion of material i as a function of the operating frequency ($\omega \approx 1/\lambda_c$) for a pair of central ceramic driving rings (discs) of axial thickness l_c ; (b) Ultrasound intensity gain G_i as a function of the operating frequency ($\omega_s \approx 1/\lambda_c$) for a pair of ceramic driving rings (discs) of axial thickness l_c .

TABLE 6.1

Physical properties of materials for high-intensity transducers

quantity	unit	materials for the moderate-intensity end portion 2			ceramic central portion c	materials for the high-intensity end portion 1		
		tool steel	aluminium bronze	brass	PZT4	titanium alloy	duralumin	magnesium alloy
ρ	10^3 kg/cm^3	7,85	8,50	8,30 ... 8,45	7,70	4,42	2,79	1,74
$v = 1/\sqrt{\rho}$	m/s	5250	4070	3240 ... 3400	= 2910	4900	5130	4800
ρv	$10^7 \text{ kg/m}^2 \text{ s}$	4,12	3,46	2,74 ... 2,82	2,24	2,17	1,43	0,835
$\rho_k v_k / \rho_{1,2} v_{1,2}$	-	0,58	0,69	0,85 ... 0,88	1,00	1,11	1,68	2,88
s	10^{-12} Pa^{-1}	4,6	7,0	10,5 ... 11,2	= 15,3	9,4	13,5	23,8
σ		0,29		0,35	= 0,30	0,36	0,34	0,28
$\Delta l / \Delta T$	$10^{-6} / \text{K}$	11 ... 16		18 ... 20	1 ... 4	9	23	26
$Q_m^{(2)}$		≥ 1400	≥ 17000	≥ 3000		≥ 24000	≥ 50000	
T_f	10^6 Pa	550	370	150		720	190	
S_f	10^{-3}	2,52	2,59	1,69		6,80	2,57	

¹⁾ Composition 90% Ti, 6% Al, and 4% V.

²⁾ Mechanical quality factors at approximately half the fatigue strength; the symbol \geq is valid for low intensities. See also Section 6.1.4.

According to Fig.6.3(b), we get the highest intensity gain G_i and the highest G_1/G_2 ratio (which may be of interest in totally immersed transducers) when the wavelength in the ceramic material is greater than 20 or 30 times the thickness of the ceramic disc or ring. In other words, the lowest possible resonant frequency should be chosen. However, there are two factors that count against the use of extremely low operating frequencies for a given pair of PZT discs (axial length $l_c = 6.35 \text{ mm}$).

1. The effective piezoelectric coupling factor becomes too low. Although the low-intensity end portion with $q_i < 1$ slightly improves coupling, the high-intensity end portion with $q_i > 1$ reduces coupling by roughly the same amount, so the total coupling doesn't differ much from that of a composite transducer with $q_i = 1$ (see Figs 6.6(a) and 6.1(b)). According to these curves we may write:

$$k_{eff} < 0.5k_{33} \text{ for } \lambda c > 25l_c,$$

i.e., for $f_s < 20 \text{ kHz}$ (for discs with $l_c = 6.35 \text{ mm}$).

2. The ultrasound intensity w in the liquid near radiating surface 1 is no longer given by Eqs 6.5 and 6.11 which only hold for planar waves in the liquid. At low frequencies, the radiated waves are no longer planar. If this effect is to be taken into account, the right-hand terms of Eqs 6.5 and 6.11 must be multiplied by the real part of a radiation coefficient. This coefficient is plotted in Fig.6.6(b) as a function of the diameter-to-wavelength ratio (in water). It's clear that at low frequencies, radiation drops more than linearly with the frequency, which is indeed a severe limitation. A moderate fall in ζ' may be welcomed however, as it is accompanied by less beaming. Therefore allowing a minimum ζ' of approximately 0.75, the minimum diameter of the radiating face would be about half a wavelength in the liquid load.

Since the liquid load adds a substantial effective mass to the transducer, a considerable mismatch results (see curve

ζ'' in Fig.6.6(b)). This mismatch can usually be allowed for in the circuit design. So in the case of a single pair of PZT rings 6.35 mm thick and with $D_c = 38.1 \text{ mm}$, and an aluminium or magnesium end portion with a diameter D_1 only slightly larger, the minimum operating frequency is 20 kHz. The same minimum frequency is also derived from coupling factor considerations. For frequencies below 20 kHz, the effective coupling factor can be improved by using more than one pair of rings.

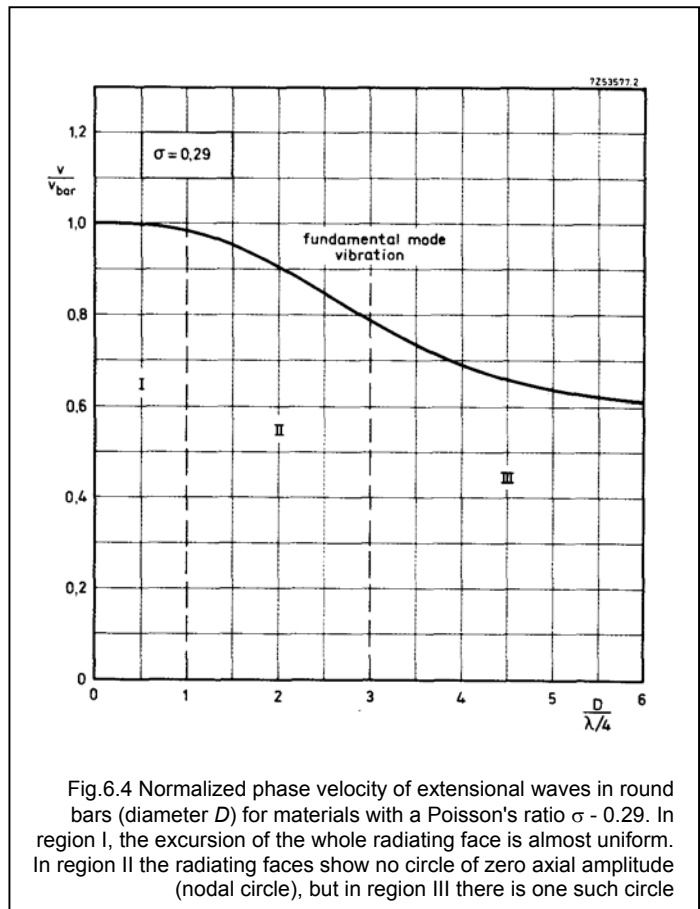


Fig.6.4 Normalized phase velocity of extensional waves in round bars (diameter D) for materials with a Poisson's ratio $\sigma = 0.29$. In region I, the excursion of the whole radiating face is almost uniform. In region II the radiating faces show no circle of zero axial amplitude (nodal circle), but in region III there is one such circle

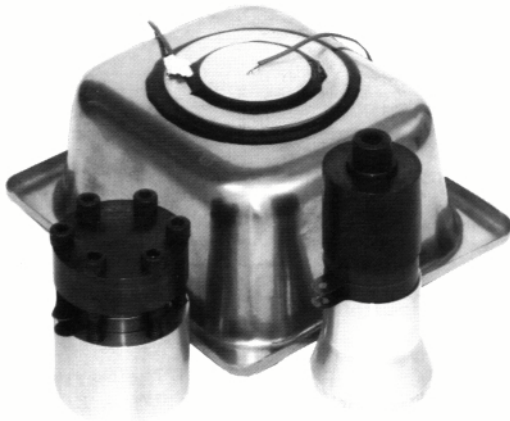


Fig.6.5 Some high-intensity ultrasonic transducers for cleaning applications (see also Figs.6.8, 6.9 and 6.10)

6.1.4 Performance of non-pre-stressed composite transducers

In Sections 6.1.2 and 6.1.3 we mentioned that the maximum radiation intensity is proportional to the square of $T_{c \max}$, the maximum permissible dynamic tensile stress amplitude. $T_{c \max}$ must always be greater than the fatigue strength T_f of the material present at or near the nodal plane where the stress amplitude reaches a maximum (see Fig.6.7(a)). The fatigue strength of both the piezoelectric ceramic (T_{fc}) and the bond material (T_{fb}) should be considered, i.e.:

$$\beta T_{fc} \geq T_{c \max} \leq \beta T_{fb} \quad (6.15)$$

where β can be considered a safety factor. Table 6.2 gives Approximate data on fatigue strength under conditions of negligibly small thermal stresses

TABLE 6.2
Fatigue strength amplitudes at ultrasonic frequencies

material	fatigue strength T_f $\times 10$ Pa
piezoelectric ceramic PZT4	20 – 30
hot-set epoxy cement	fresh 30 – 50 aged* 20 – 30
cold-set epoxy cement (Araldite)	fresh 20 – 30 aged* 10 – 20

* Shelf-aging under normal humid conditions. Aging in dry atmosphere would not reduce the fatigue strength significantly.

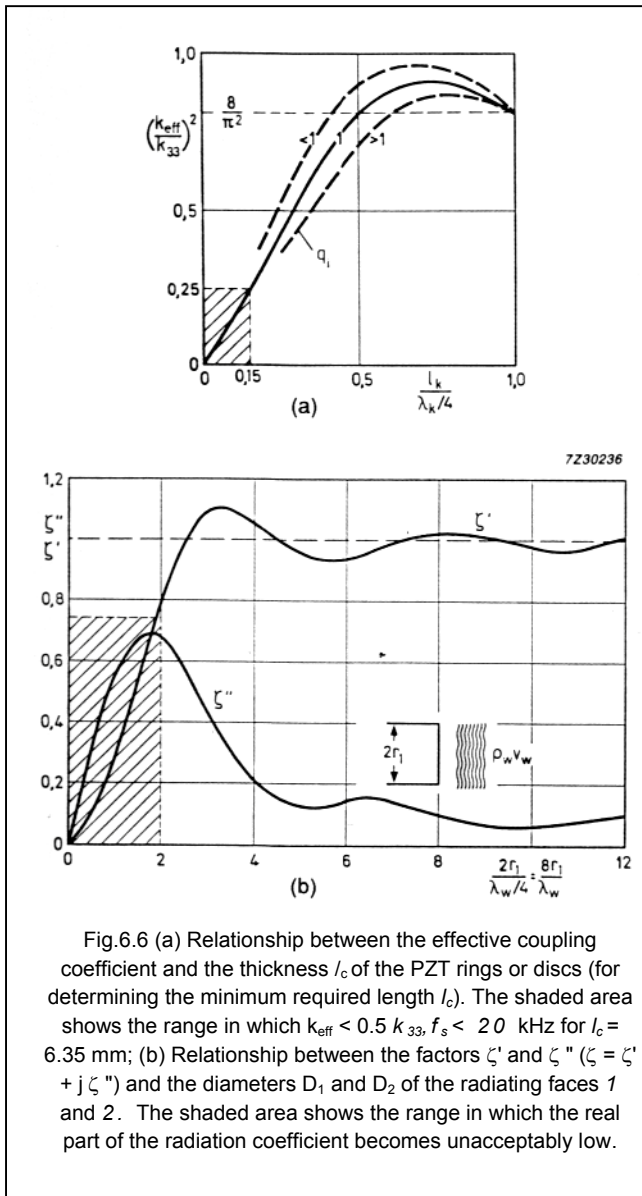


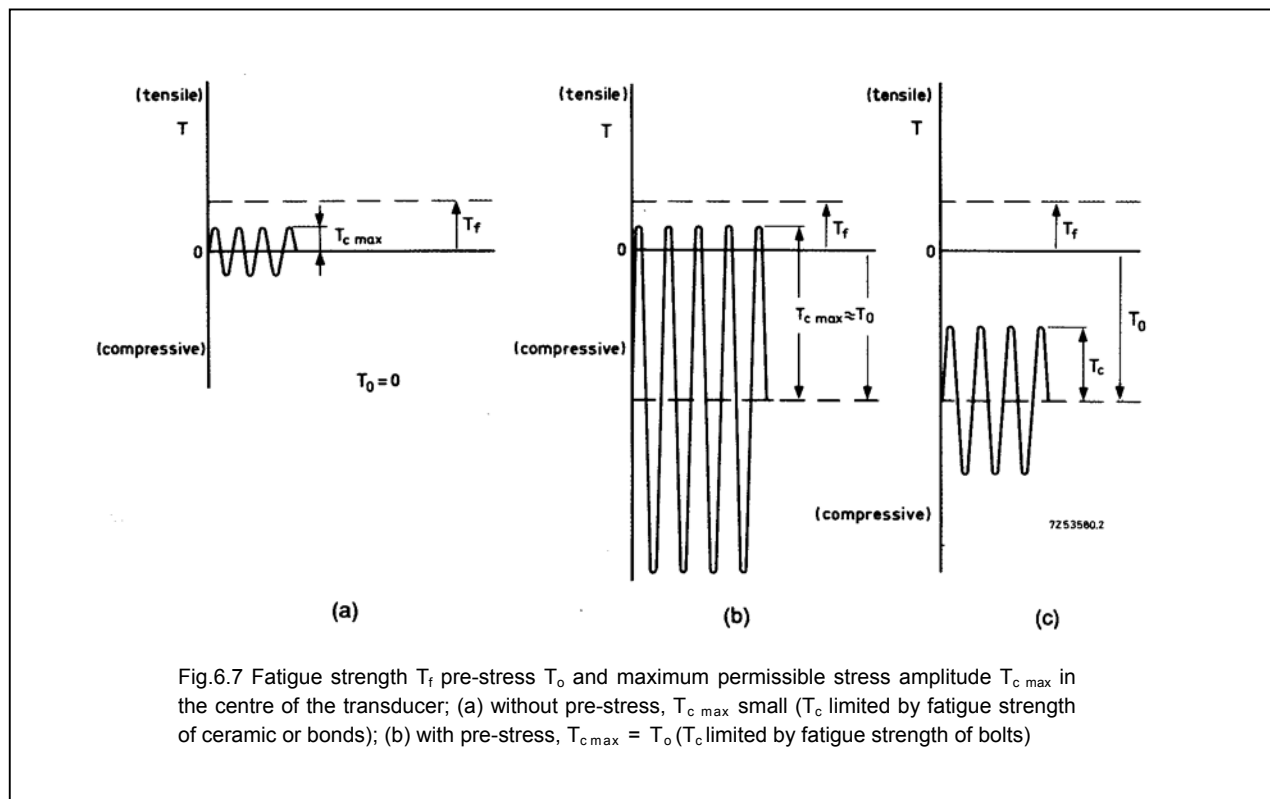
Fig.6.6 (a) Relationship between the effective coupling coefficient and the thickness l_c of the PZT rings or discs (for determining the minimum required length l_c). The shaded area shows the range in which $k_{\text{eff}} < 0.5 k_{33}$, $f_s < 20$ kHz for $l_c = 6.35$ mm; (b) Relationship between the factors ζ' and ζ'' ($\zeta = \zeta' + j \zeta''$) and the diameters D_1 and D_2 of the radiating faces 1 and 2. The shaded area shows the range in which the real part of the radiation coefficient becomes unacceptably low.

Sometimes the critical stress amplitudes, or fatigue strengths tabulated in Table 6.2, are not very reliable as they may be drastically reduced by static thermal stresses caused by the differing thermal expansion coefficients of the cemented parts. When cementing aluminium or magnesium to PZT4 (according to Table 6.2), a differential thermal strain of 20 or more ppm/K is to be expected, so that the curing of epoxy cement at, say, 150 °C, would lead to differential thermal radial stresses of approximately 50×10^6 Pa to 150×10^6 Pa. In other words, the surface layer of a large ceramic disc would be severely prestressed in the radial direction with the correct sign but in an uncontrolled, inhomogeneous way. Considering such illdefined conditions, which also exist when the transducer is dissipating large amounts of energy at high intensities, and allowing for a safety factor ($\beta = 0.5$, the resulting critical stress amplitude in the frequency range 20 kHz to 50 kHz would be no more than:

$$T_{c \max} \approx 4 \times 10^6 \text{ Pa}$$

Substituting this into Eq.6.5, and assuming a water load $p_{mw}v_w = 1.485 \times 10^6 \text{ kg/m}^2\text{s}$, we find for the attainable intensity:

$$I_{wi \max} = 2G_i \quad (\text{W/cm}^2)$$



The gain factor may be derived from Table 6.2 and Fig.6.3(b), i.e.:

$$I_{wi \max} \approx 10 \text{ W/cm}^2$$

(magnesium end portion with a gain G of approximately 5),

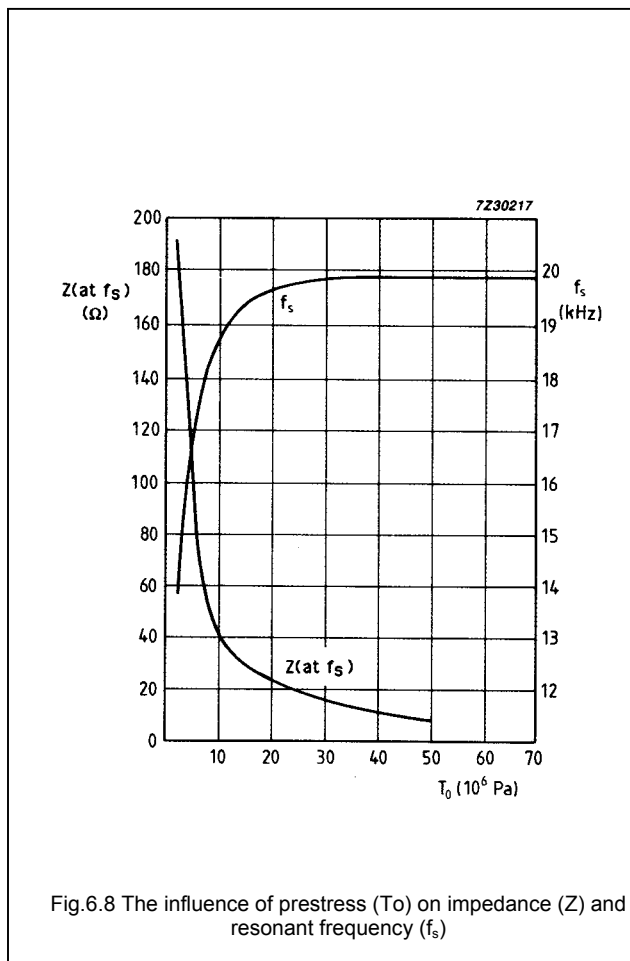
$$I_{wi \max} \approx 4 \text{ W/cm}^2$$

(duralumin end with a gain G of approximately 2).

6.1.5 Pre-stressed composite transducers (with applications)

As already explained, it's often useful to assemble high-power ultrasonic transducers from thin rings or discs of PZT material with metal end pieces to match. For many types of transducer used for ultrasonic cleaning, the power requirements are often so severe that the tensile strength of the ceramic material is inadequate for the high mechanical stress involved. This can be remedied by mechanically pre-stressing such transducers in the axial direction by means of one or more bolts, the useful amount of pre-stress T_0 being about $25 \times 10^6 \text{ Pa}$. Under these conditions, T_0 replaces $T_{c \max}$ in the intensity equation (Eq.6.II), as illustrated in Fig.6.7(b).

Figure 6.8 shows the impedance Z (at f_s), which is a good indication of the damping, and the resonant frequency (f_s) as a function of the pre-stress for a specific transducer design. At $T_0 = 25 \times 10^6 \text{ Pa}$, the resonant frequency has reached a stable value and the damping is acceptable (Ref.7).



Too high a pre-stress may cause the bolt to break. It could also cause major irreversible changes in the properties of the ceramic material (depolarization). What's more, repeated application and removal of the same mechanical pre-stress could cause the relationship between capacitance and stress, or between coupling factor and stress, to vary in an unreproducible manner. However, provided the prestress is kept below about 30×10^6 Pa, the variations are reasonably reproducible. Too low a pre-stress reduces efficiency because there is an increase in mechanical loss at the various interfaces.

Construction of two high intensity transducers

Figures 6.9(a) and (b) show two designs of high intensity transducer that have been thoroughly tested. Both of them can be built around PZT4 or PZT8. The design shown in Fig.6.9(a) consists of two PZT rings (in the centre) clamped between two end pieces by means of a bolt. The bolt is insulated from the centre electrode by means of a thin PVC sleeve. A transducer constructed in this way has a slightly higher efficiency than one in which the centre bolt is replaced by six or eight bolts around the circumference of the transducer (Fig.6.9(b) because the centre bolt construction allows for a more uniform and radially symmetric application of pre-stress to the PZT. However, the centre bolt assembly with its conical front portion may be more costly to produce, and its greater length may be a disadvantage where space is important.

If the transducer is bonded to the cleaning tank (usually of stainless steel), the temperature needed to harden the glue may be high enough to impair the properties of the PZT rings or discs. It's therefore advisable to first bond the front block of the transducer to the tank wall, and to complete the assembly after the bonding agent has had time to harden and cool. If the torque needed to tighten the bolt is not taken up by a holding tool applied to the coupling portion, there is a risk of the bonded joint to the tank being broken. The main advantage of the transducer of Fig.6.9(b), with bolts around the circumference, lies in its compactness, and in the possibility of first bonding the front portion to the tank and then assembling the transducer. The bolts can be tightened without overloading the bond because the torque for any one of the bolts is substantially lower than that required for the one large bolt in the transducer of Fig.6.9(a). A special holding tool is then not needed.

The PZT components used for the transducers shown in Fig.6.9 consist of two rings (outside diameter 38.1 mm, inside diameter 12.7 mm, thickness 6.35 mm) or two discs (38.1 mm diameter and 6.35 mm thick) of PZT4 or PZT8. The electrodes are of copper-beryllium alloy (250 μ m gauge), which has a high fatigue strength. The soldering tags must be damped with a pliable substance (e.g. silicone rubber) to prevent breakage due to fatigue, particularly if other materials, such as sheet copper, are

used. The steel cylinders (often of free cutting steel) should be protected against corrosion: chemically-protected or cadmium-plated steel or, even better, stainless steel can be used. The front portion radiating ultrasound can be made of duralumin or free cutting alloy (e.g., Al, Cu, Mg, Pb alloy). When assembling the transducer, it's important to apply the right amount of pre-stress (e.g., 25×10^6 Pa). There are various methods of measuring the stress, the most reliable way being to measure the charge generated in the PZT under short-circuit conditions. A capacitor of, say, 10 μ F (not an electrolytic one) is connected to the electrical terminals and to a DC voltmeter whose internal resistance should be at least 10 M Ω . This meter measures the charge generated as the bolts are tightened. If the total area of the PZT rings is, for instance, 2×10^{-3} m², and the piezoelectric charge constant $d_{33} = 290 \times 10^{-12}$ C/N (PZT4), the charge after pre-stressing is 14.5 μ C. Together with a capacitance of 10 μ F this results in a voltage of 1.45 V, which can easily be measured. With $R_i \approx 10$ M Ω ,

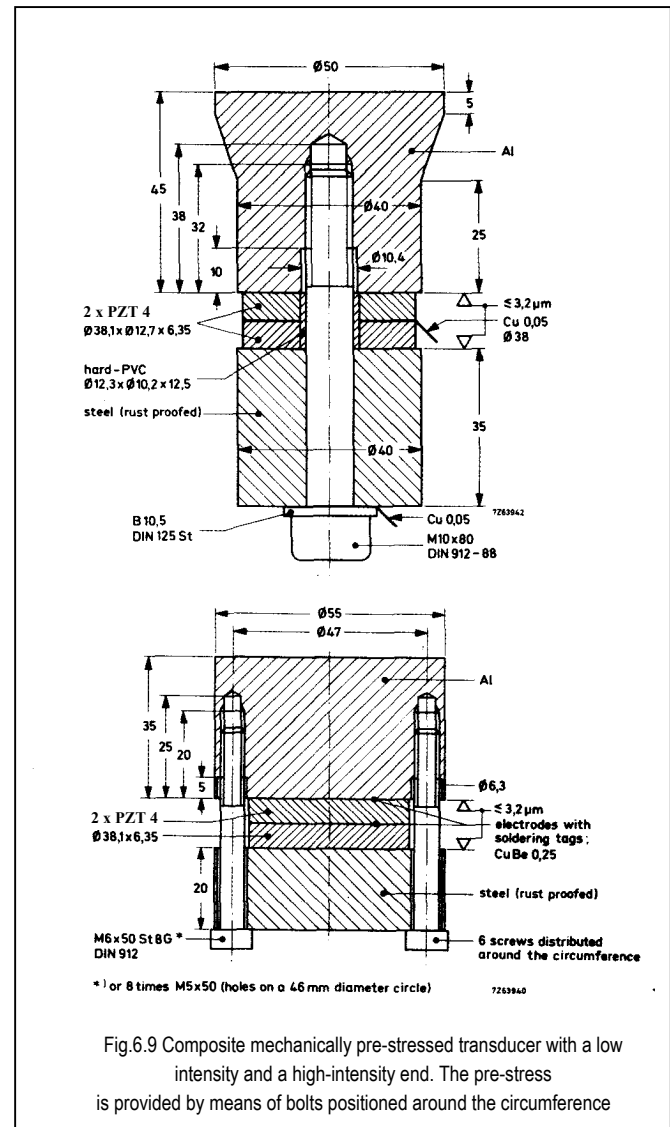


Fig.6.9 Composite mechanically pre-stressed transducer with a low intensity and a high-intensity end. The pre-stress is provided by means of bolts positioned around the circumference

a time constant of about 100 s is obtained and therefore the bolt must be tightened as quickly as possible (within a few seconds). This will not be necessary if $R_i \gg 10 \text{ M}\Omega$. A simpler method than charge measurement, though less accurate, is to use a torque wrench. (A torque wrench is always necessary for tightening multi-bolt transducers to ensure that the stress is applied uniformly). Since the torque required for a certain amount of pre-stress depends to a large extent on the finish of the transducer parts, this method is particularly recommended for series production where the components are always the same. The torque wrench must first be calibrated in some way, for instance, by charge measurement. To ensure a uniform pre-stress distribution in multi-bolt transducers, the bolts positioned diagonally across from each other must be tightened in turn, and the torque should be increased progressively by small increments until the required value is reached all round.

The forces taken up by the bolt, or bolts, to obtain a pre-stress of $25 \times 10^6 \text{ Pa}$ can be considerable: for PZT rings or discs of 38 mm diameter they amount to about 25 kN to 30 kN. When an AC voltage is applied to the transducer, the bolts will, of course, have to take up additional large alternating forces. Table 6.1 shows that titanium alloy combines the highest fatigue strength with extremely low losses (even at large excursions), and is therefore the best material for the bolts. The threaded end of the bolt and the thread in the metal end piece must be perfect, though they are positioned in the vicinity of a nodal point. Repeated assembly and dismantling reduces the torque required.

High intensity transducers in operation

Water load, tank wall, and bonding layer all reduce the transducer frequency slightly (the water load alone causes a frequency decrease of about 0.5 kHz in a centre-bolt transducer). The characteristic frequency of the tank and the water load usually give rise to several additional resonances. With a properly designed generator circuit the transducer will always operate close to its own resonant frequency.

Since the transducer capacitance C_0 might lead to a high reactive current, it's useful to compensate this capacitance with an inductance (see Appendix A), usually shunted across the transducer, but series connection is also possible. The required inductance is given by:

$$L = \frac{1}{4\pi^2 f^2 C_0} \quad (6.16)$$

where f is the operating frequency.

The impedance of a transducer thus compensated is almost real at the operating frequency. However, the tank and water resonances can again cause deviations. Cavitation occurring at high powers causes a reduction in impedance which becomes all the more pronounced when

the radiating plane of the transducer is brought into direct contact with the water. The change of impedance due to cavitation is much reduced when the transducer is bonded to the tank wall and radiates through it into the water.

The maximum permissible operating power depends to a large extent on the operating conditions (temperature, coupling to the tank, type of tank and its contents, and so forth). Reliable performance is ensured at an (electrical) input power of 50 W; at higher powers one must carefully consider heat loss and the stresses and strains involved. The overall efficiency is also governed by the operating conditions, but is usually better than 90%.

6.1.6 Disc transducers (bonded to a cleaning tank)

Construction of a PZT disc transducer

Pre-stressed composite transducers are not absolutely necessary for effective ultrasonic cleaning, good results are also obtained with PZT disc transducers bonded direct to the tank wall. The transducer itself consists of a PZT disc alone (PZT8), or a PZT disc and a metal disc bonded together. In the latter case the metal disc is positioned against the tank wall. Figure 6.10 shows such an arrangement.

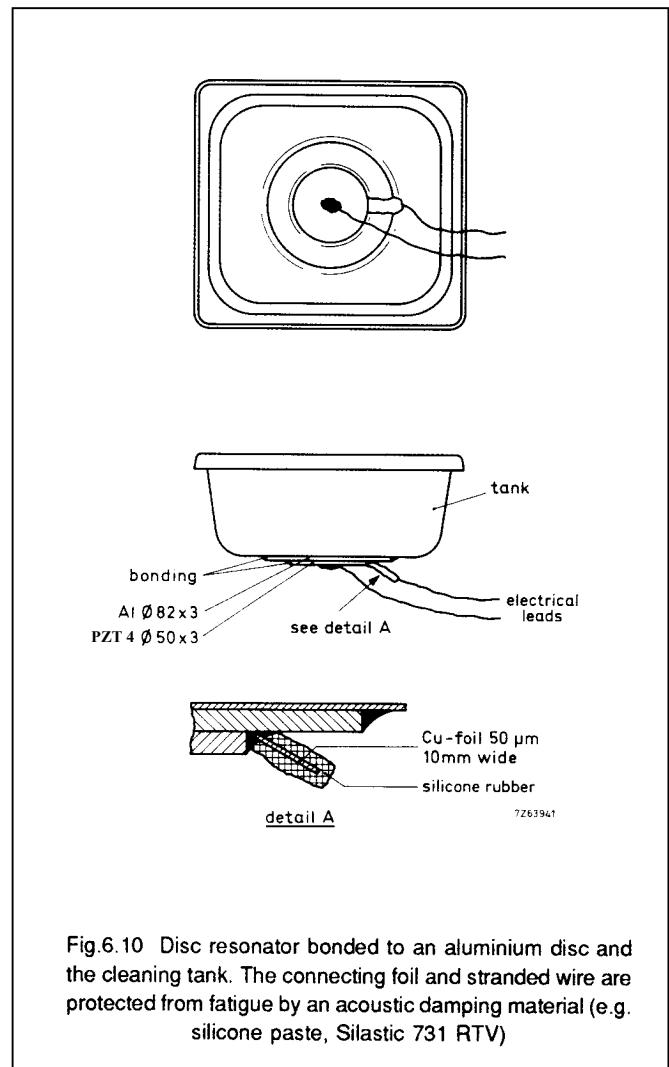


Fig. 6.10 Disc resonator bonded to an aluminium disc and the cleaning tank. The connecting foil and stranded wire are protected from fatigue by an acoustic damping material (e.g. silicone paste, Silastic 731 RTV)

When bonding a PZT disc direct to the tank, bear in mind that, apart from involving considerable losses, a thick bond impedes heat removal. It's therefore essential that the bond be as thin as possible. On the other hand, a bond that's too thin is liable to fracture, especially if heavy objects are dropped into the tank. Obviously a compromise must be made. A bond of defined thickness can best be made by reinforcing it with a fibre-glass or metal gauze about 0.5 mm thick. The thickness of the PZT disc cannot be chosen independently of the thickness of the tank wall. Stainless steel tanks with the usual wall thickness of 1 mm used in conjunction with 3 mm thick discs provide a satisfactory compromise between mechanical strength and efficiency.

A metal plate between the PZT disc and the tank (Fig.6.10), will protect the PZT and reduce losses. The metal disc may be aluminium or steel. Size for size, aluminium gives a greater electro-mechanical coupling factor than steel (and a better matching).

The PZT disc and the metal disc are usually of the same thickness their diameters are chosen to give them the same radial-mode resonant frequency. For optimum results, a PZT disc of, say 50 mm diameter, requires a steel or aluminium disc of about 82 mm diameter.

With both transducer types it's advantageous to use a tank without sharp corners (which tend to impede the spreading out of the ultrasound). The connections to the free electrode must be made with a soldered stranded wire. and contact to the bonded electrode is made with a compression bonded or soldered metal foil (beryllium copper. for instance).

To ensure reliable operation, all free ends of the stranded wire and the foil must be acoustically damped with a damping agent (such as silicone rubber).

The PZT disc bonded to the tank vibrates in the radial mode with an impedance of a few hundred ohms and radiates power mainly through the tank wall into the bath. On the other hand. transducers bonded to the tank with a metal plate in between exhibit various resonances between 40 kHz and 60 kHz and have impedances of several kilohms. The radial vibrations of the transducer apply shear forces to the tank wall, causing the wall to vibrate in flexure mode and thus radiating power into the liquid. Owing to mechanical feedback the transducer is caused to vibrate in a superimposed flexure mode.

Since the tank wall has in fact become part of the transducer, both form and thickness of the tank greatly influence the overall characteristics of the equipment.

Optimum results are possible only if the tank data is taken into account, which calls for a great deal of experimental work. The transducer data, such as operating frequency, impedance, and maximum efficiency, can be determined only after samples have been made.

Operating frequency and power

Ultrasonic cleaning tanks equipped with PZT disc transducers and constructed as shown in Fig.8.10 operate at about 50 kHz, which is somewhat higher than the radial mode frequency of the freely suspended disc (radial vibration $f_s \approx 45$ kHz for a disc of 50 mm diameter). The transducer can be safely driven at an electrical input power of 50 W and it exhibits no irreversible changes, but between 100 W and 150 W the transducer begins to show signs of permanent damage.

6.1.7 Driver circuits for high intensity transducers

The circuit described in this section is useful for laboratory experiments or during the design phase of a transducer. Operating frequency and output voltage are adjustable. The circuit is built up with three basic units (Fig.6.1](a):

- power supply
- sine wave generator
- power output stage with matching transformer.

Fig.6.1 1(b) shows the supply circuit for generating the necessary DC voltages.

The sine-wave generator in Fig.6.11(c) comprises a free-running^g oscillator that generates a triangular wave, and a sine-shaping network. The frequency adjustment operates with a ten turn potentiometer and with an additional potentiometer for fine-tuning. The oscillator frequency depends linearly on the setting of the potentiometer. The advantage of this type of oscillator is its simple frequency adjustment and its stability in amplitude even during frequency changes.

The power stage (Fig.6.11(d)) operates like a normal Hi-Fi power amplifier (class B). Its output transistors are Power MOSFETs to guarantee the required power level over the full frequency range. The maximum output voltage is limited by the supply voltage level. Generally this level is much too low to drive PZT -transducers. An output transformer is therefore used which offers a choice of floating output voltages to suit the connected transducer. The power transistors are protected by a current limiter. In overload situations, caused for instance by a mismatch between transducer and output, the current is limited to a prefixed level.

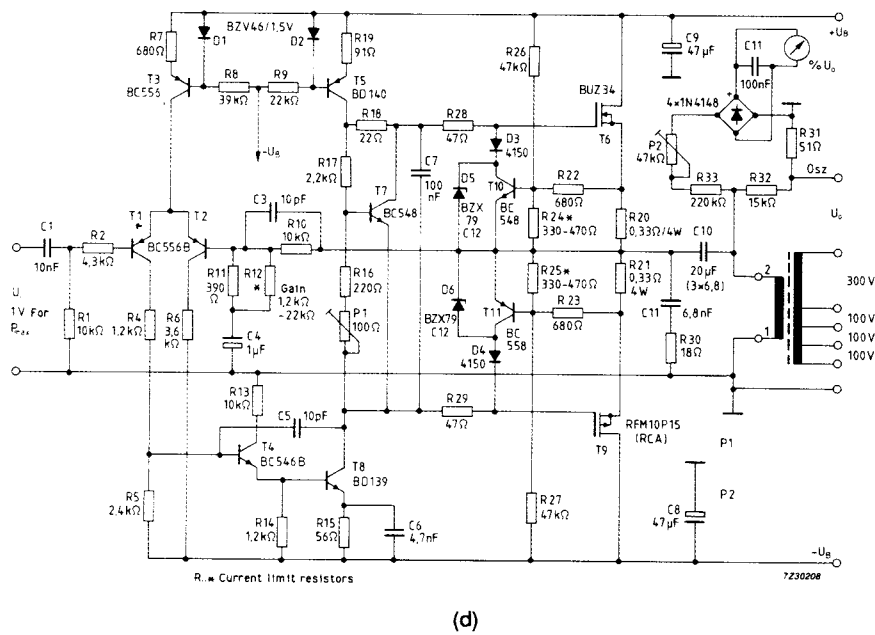
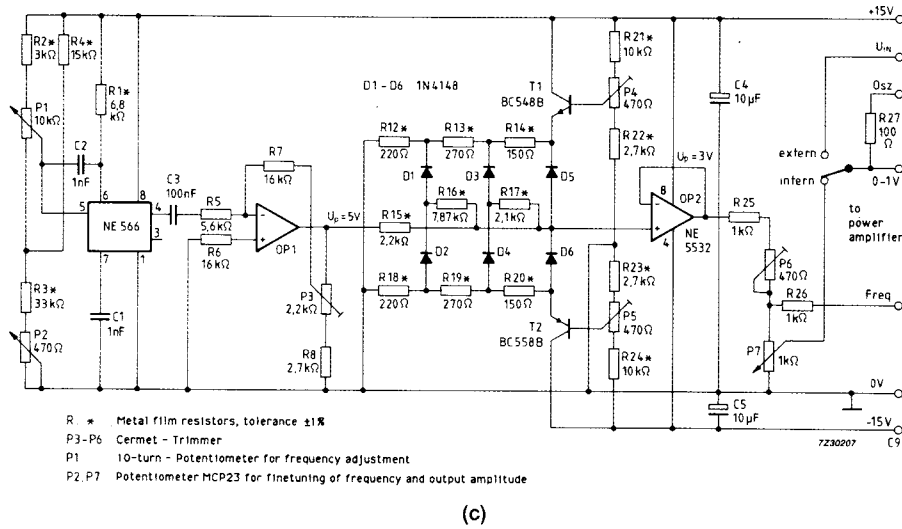
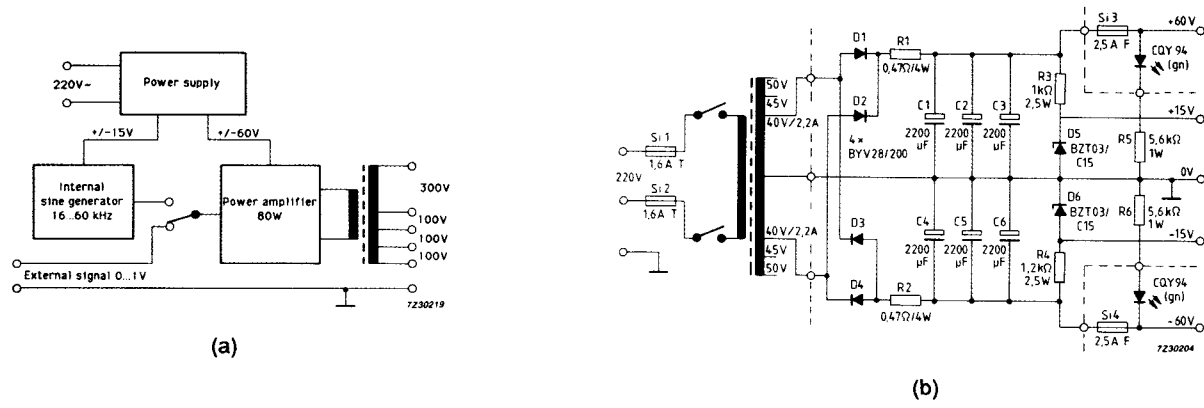


Fig.6.11 Drive circuit for high-intensity transducers.
 (a) block diagram (c) sinewave generator
 (b) power supply (d) power stage with output transformer

6.2 High intensity transducers with amplitude transformation

High intensity transducers as described in Section 6.1 can be used for many other applications like welding plastics, pulverizing liquids and ultrasonic drilling. For welding plastics, amplitudes of 15 to 60 μm (peak to peak) are required, depending on the internal mechanical losses of the material.

To reach such amplitudes, the normal longitudinal vibration on the end faces must be amplified by an amplitude transformer, also called a *horn* or *sonotrode* (Fig.6.12). With this the vibrational energy is concentrated on a smaller surface area, preferably not larger than the work piece. Such a horn is bolted to the end piece of a transducer and is usually made of a titanium or aluminium alloy to give it the required fatigue strength.

The horn must be tuned to a half wavelength ($\lambda/2$). Its length is somewhat larger than half the wavelength in the transducer at the resonant frequency since the propagation speed increases with decreasing surface area on the horn. If the horn has an exponential shape, the vibrational amplitude increases inversely with its cross sectional area.

Figure 6.12 shows a number of possible shapes. The curves give an impression of excursions and strain in the different horn types. In the case of the exponential horn, where the diameter in this example decreases with a factor 5, the vibrational amplitude increases by the same factor. The other shapes are less effective but are easier to manufacture.

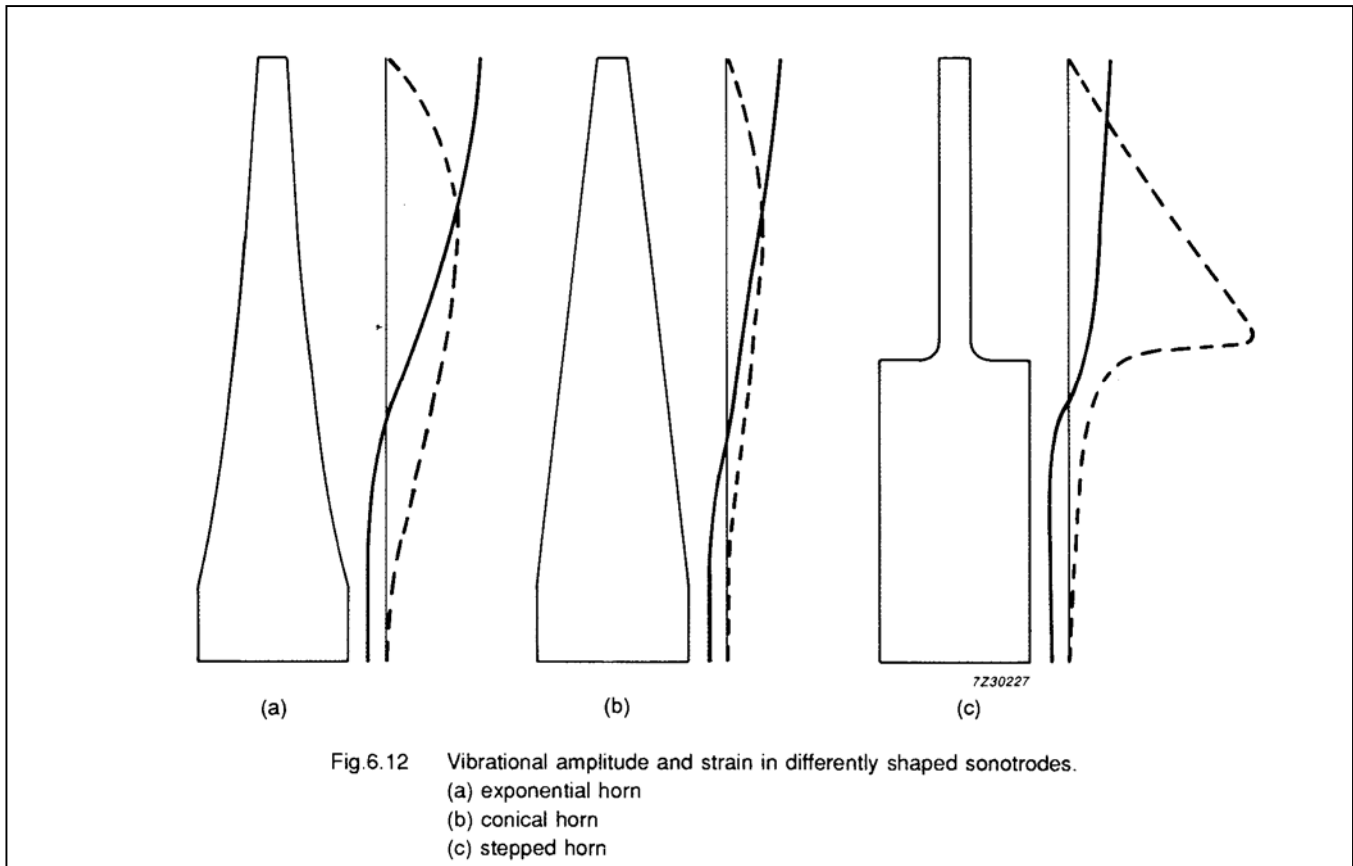
Considerable success has been obtained with several $\lambda/2$ horns in series and with horns several half wavelengths long. However, the influence of the damping in the workpiece on the vibrational amplitude increases with the transformation factor, so it's not possible to get unlimited increases in amplitude without taking this damping into account.

The horn must be tuned exactly to the frequency of the ultrasonic transducer. A standing wave should be established so that the tip of the horn vibrates with the maximum possible amplitude dictated by the geometry. The radial dimensions of the horn have little influence on the resonant frequency as long as these dimensions do not exceed a quarter wavelength ($\lambda/4$).

6.3 Pulverization of liquids

An important and interesting application of the stepped horn is the pulverization of liquids (Fig.6.13(a)). The fluid is pumped through the central hole of the horn and is pulverized into tiny droplets at its tip.

Another possibility is to generate compressional waves with a PZT -disc a few centimetres below the surface of a liquid. Small droplets will then separate from the surface (Fig.6.13(b)).



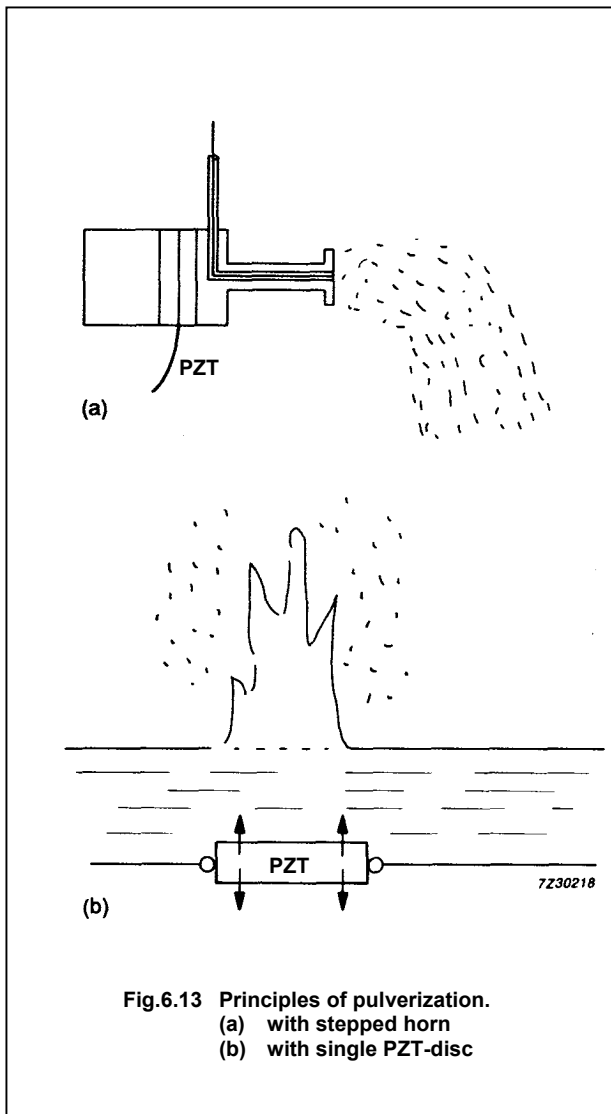


Fig.6.13 Principles of pulverization.
 (a) with stepped horn
 (b) with single PZT-disc

The peak in the distribution of the droplet diameter depends on the excitation frequency f_a and is given by:

$$d_h = 0.73 \sqrt[3]{\frac{T}{\rho f_a^2}} \quad (6.17)$$

where: T = surface tension of the fluid

ρ = its density

f_a = the operating frequency.

As can be seen from this formula, the particle size decreases with increasing frequency. In the case of water with $T = 72.9 \times 10^{-3} \text{ N/m}$, $\rho = 1000 \text{ kg/m}^3$ and $f_a = 50 \text{ kHz}$, the size of the droplets centres around $d_h = 22.5 \text{ }\mu\text{m}$. For a frequency of 2 MHz the particle size has decreased to 1.9 μm . Droplets of this diameter are small enough to form a free floating mist, and are ideal for air humidifiers.

6.36.3.1 Pulverization of liquid by an ultrasonic transducer with amplitude transformer

When ultrasound is radiated in a liquid, capillary waves form at its surface. The frequency f_c of these waves is half

that of the transducer (f_a). At a sufficiently high energy level, droplets start to separate from the surface of the liquid. Their diameter is given by Eq.6.17.

The throughput of pulverized liquid depends on several parameters. For example, it increases linearly with the radiating surface area. For this reason, it is very effective to provide the horn with a dish-shaped end piece to increase the surface area.

Sometimes the design of the disc causes its bending resonance to occur at the frequency of the transducer, causing large increases in its amplitude. In most cases, however, the bending-mode resonance occurs as a higher frequency than the axial resonance. The disk then vibrates with a constant amplitude resulting in more predictable behaviour.

Figure 6.14 shows a PZT -ultrasonic pulverizer. It comprises two PZT4 rings ($\text{Ø } 15 \times \text{Ø } 6 \times 3 \text{ mm}$), two electrode foils of copper-beryllium alloy and two machined Cr-Ni steel parts. The piece parts are threaded to allow a strong, prestressed, construction of the transducer (torque 7 Nm). Glued connections would not be strong enough. The stepped horn is an integral part of one of the machined parts. Its end face is dish-shaped to increase the throughput volume.

The mounting method is critical for reliable operation of the transducer. It should preferably be fixed in the nodal plane by a special disc (Fig.6.14(c)) or by the tube through which the fluid is dispensed (Fig.6.14(a)).

The finished transducer is a half-wavelength resonator with amplitude transformation by the stepped down diameter of the horn. The excursion of the disk is approximately 12 μm at a driving voltage of 50 V (RMS). The amplitude is the same over the total area of the disk so that, provided supply is sufficient, the liquid is evenly pulverized from the whole surface.

The maximum throughput of pulverized liquid is a function of the vibrational amplitude, which in turn depends on the applied voltage.

The throughput is limited by the power dissipation in the transducer. A temperature rise up to 150 °C is the limit because depolarization of PZT starts at that temperature. Maximum applied power depends on cooling conditions. In this respect, of course, the dispensed fluid itself has a cooling effect as well as the blower necessary to disperse the pulverized liquid.

Typical data for a pulverizer as shown in Fig.6.14 would be:

capacitance	1.1 μF
axial resonant frequency	53 kHz
impedance at resonance	= 200 Ω
driving voltage	50 V
power consumption	6 W
k_{eff}	0.20
droplet diameter (water)	22 μm
throughput (water)	2 l/h

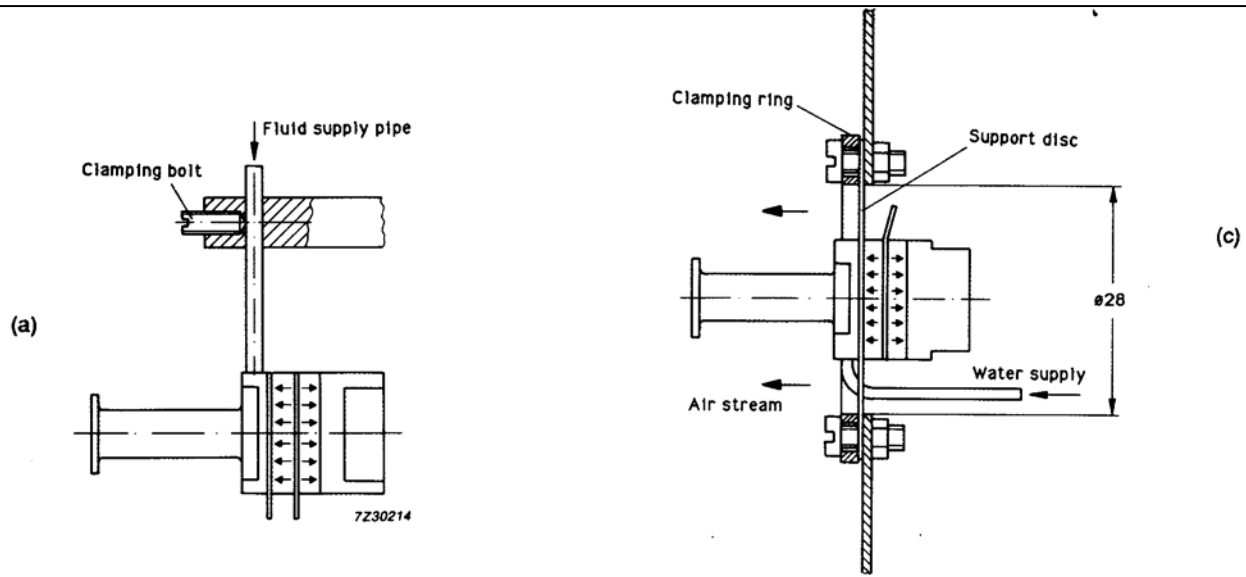
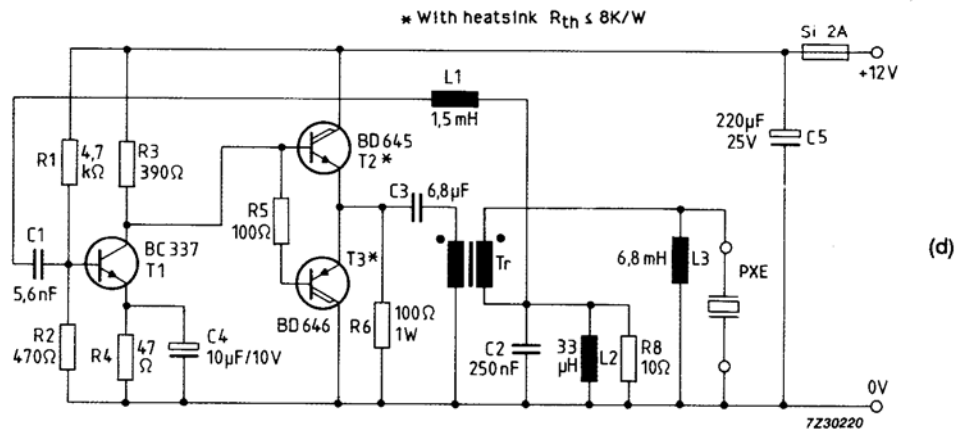
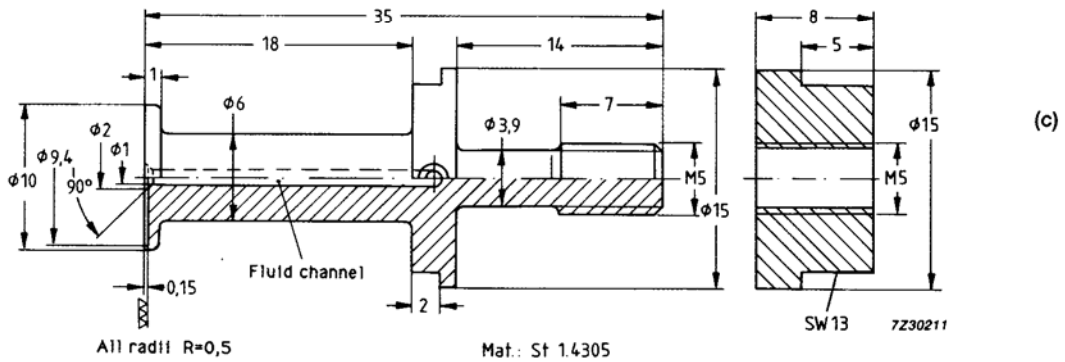
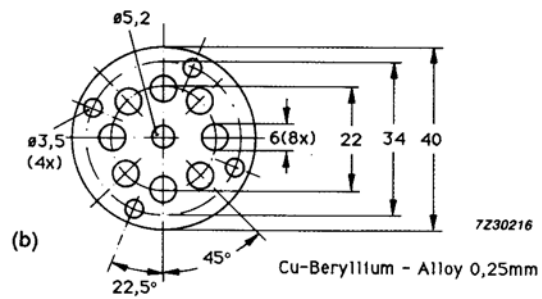


Fig. 6.14 Ultrasonic transducer for pulverization of liquids.
 (a) fixation at the fluid supply pipe.
 (b) CrNi-steel parts of the transducer.
 (c) mounting with special CuBe-membrane
 (d) Drive circuit for liquid pulverizer



The maximum drive voltage without additional forced cooling is 80 V (RMS). The pulverization rate for water will then be about 3 l per hour.

To get a higher throughput, the size of the transducer should be increased to reduce the operating frequency. However, the diameter of the droplets will then increase too, and this could be a drawback for many applications since these larger droplets will tend to fall down before evaporating completely.

Figure 6.14(d) shows a drive circuit. The oscillator requires a supply voltage of 12 V. Transistor T_1 , drives the output stage consisting of two darlington's T_2 and T_3 . The operating frequency is determined mainly by the mechanical properties of the transducer which is connected to the secondary winding of the transformer. Near its series resonance, the impedance of the transducer is practically real, which fulfils the oscillating requirements of the circuit. The feedback voltage is taken from resistor R_8 . The feedback loop comprises two LC-filters, L_1 and C_1 (series) and L_2 and C_2 (parallel), which suppress unwanted vibrational modes.

Because of the low output impedance of the oscillator, the transducer is voltage driven at a level depending on the turns ratio of the transformer. In the present case a turns ratio of 1:12 provides optimum results. Under these circumstances the transducer consumes 6 W. At a supply current of 1 A this means a circuit efficiency of 50%.

6.3.2 Pulverization at very high frequencies

A different method uses a PZT -disc mounted some centimetres below the surface of a liquid. If the disc is 1 mm thick, it resonates at about 2 MHz.

Ultrasound is radiated towards the surface, pressure builds up, resulting in a kind of fountain that focuses the energy and releases minute droplets into the air. At this frequency the average droplet diameter is $1.9\mu\text{m}$. This is small enough to form a free floating mist that evaporates before settling down. This is a very desirable characteristic when used in air humidifiers - its major application.

6.4 Ultrasonic air transducers

6.4.1 Applications and basic requirements

Ultrasonic air transducers can be used both for generating and for receiving ultrasound. When operating in *impulse-echo* mode, a single transducer can perform both functions. In most cases, however, an installation comprises two transducers: a transmitter and a receiver. By separating these functions, a transducer can be optimized for its task. Main application areas are distance measurement and intruder alarms.

Some examples of the numerous applications are:

- level detection in silos and containers
- distance measurement between cable or railway cars to maintain safety distances.

- parking aid for cars and trucks
- intruder alarms.

A transducer for operation in pulse-echo mode has to fulfil some requirements on range and bandwidth. The range is a function of the generated acoustic power and operating frequency of the transducer.

The maximum output power depends on the mechanical and thermal constraints of the design. The operating frequency can be obtained by a proper choice of the dimensions. For a long-range transmitter/receiver, the damping in air should be as low as possible, which calls for a rather low frequency. However, for good spatial resolution and directivity, the frequency should be as high as possible. For each individual application a compromise must be made.

For accurate distance measurement, especially over short range, the length of the pulses should be short. The transducer's bandwidth is therefore an important design parameter. The following relations hold to a rather good approximation (see Fig.6.15):

$$\tau \approx 1/B_{6\text{dB}}$$

$$l_i = t_i v$$

$$t_i > 2\tau$$

$$l_i > 2 \tau v$$

Where $B_{6\text{dB}}$ is the 6 dB bandwidth of the transducer (Hz), T is the rise and fall time (s), t_i the impulse time (s), l_i the impulse length (m) and v the sound velocity in air (344 m/s).

In impulse-echo mode, two conversions take place (electrical-acoustical and acoustical-electrical). In that case the relations still hold if instead of the 6 dB bandwidth the 3 dB bandwidth is used in the formulas.

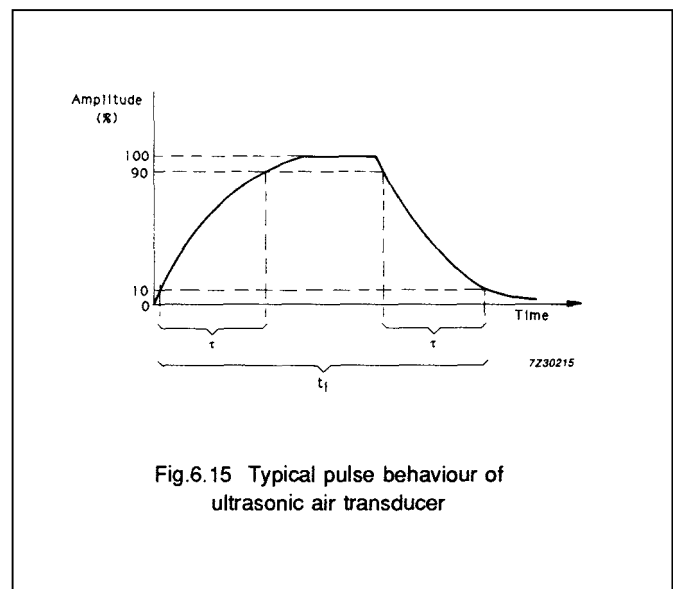


Fig.6.15 Typical pulse behaviour of ultrasonic air transducer

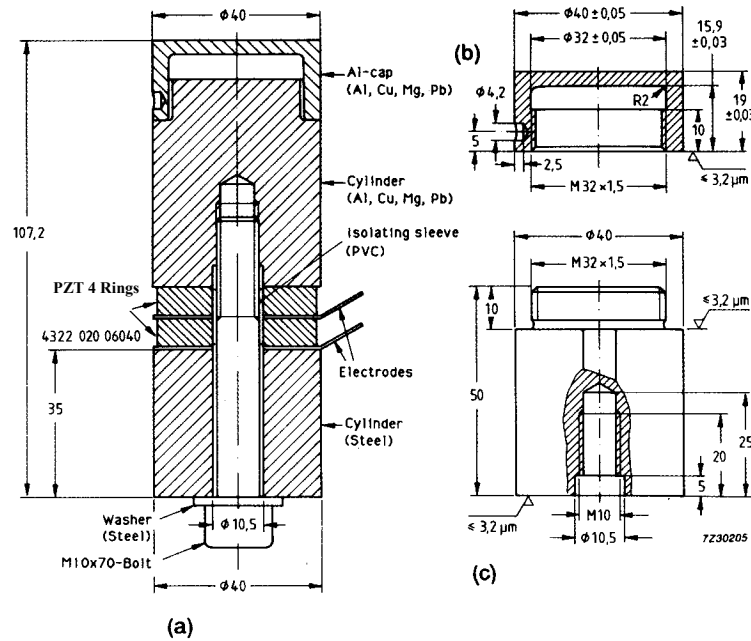


Fig.6.16 Construction of ultrasonic air transducer.
 (a) assembly
 (b) aluminium cap
 (c) aluminium alloy front part

6.4.2 Mechanical construction of a transducer

Figure 6.16 shows the construction of a transducer. Two PZT4 rings generate axial vibrations in the pre-stressed construction (resonance 1), and these are transferred to the flexure-mode resonator attached to one of the end portions. The flexure-mode resonator consists of an aluminium cap which behaves like a membrane clamped on its circumference. The amplitude of the vibration is amplified by the flexure mode resonator which provides a better match to air than a rigid cylindrical resonator.

The resulting two resonances and their coupling are chosen such that a very wide total bandwidth is obtained. This effect is enhanced by an electrical resonant circuit consisting of the transducer capacitance and an external tuning inductor. In this way the transducer, which normally has two separated narrow band resonances, has acquired wideband characteristics. However, the stronger damping means that the electro-acoustic efficiency is lower than it is in the narrow-band mode.

The mechanical pre-stress of this transducer is provided by a 10 mm bolt. The required force is 25×10^3 N, which calls for a torque of 60 to 90 Nm when the device is first assembled. If it ever has to be reassembled, this torque decreases to approximately 50 Nm for the same prestress. A more reliable way to adjust the required prestress, therefore, is to measure the liberated charge on the PZT-rings ($Q = 13 \mu\text{C}$). Finally, the aluminium cap should be firmly mounted using a spanner.

Assembled in this way the transducer will have following electrical properties:

(a) without AL-end cap (one resonant frequency)

$$f_s = 22.1 \text{ kHz} \quad |Z_s| = 30 \Omega$$

$$f_p = 23.7 \text{ kHz} \quad |Z_p| = 130 \text{ k}\Omega$$

$$C (1 \text{ kHz}) = 3.2 \mu\text{F}$$

(b) with end cap (two resonant frequencies)

$$f_{s1} = 18.7 \text{ kHz} \quad |Z_s| = 110 \Omega$$

$$f_{p1} = 19.3 \text{ kHz} \quad |Z_p| = 30 \text{ k}\Omega$$

$$f_{s2} = 23.2 \text{ kHz} \quad |Z_s| = 70 \Omega$$

$$f_{p2} = 23.9 \text{ kHz} \quad |Z_p| = 70 \text{ k}\Omega$$

Figure 6.17 shows a typical admittance curve.

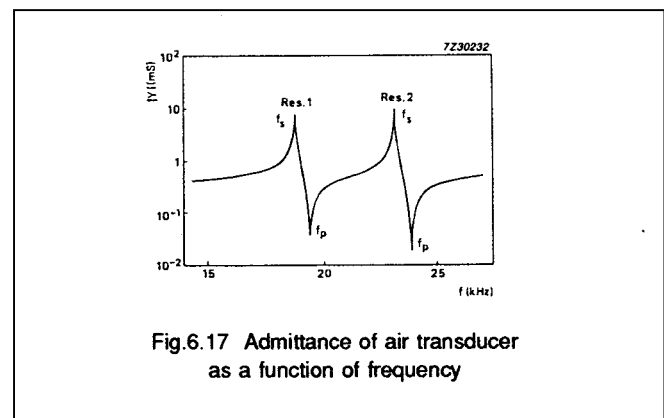


Fig.6.17 Admittance of air transducer as a function of frequency

6.4.3 Acoustical properties

The frequency behaviour of the transducer is the same in transmitting and receiving mode, but electrical circuitry connected to the transducer can influence this behaviour. This section gives curves for the transmitting function. Curves for the receiving function have the same shape, only conversion figures differ.

Figures 6.18, 6.19 and 6.20 illustrate how the properties of the transducer vary with load resistance. The illustrations relate to the following conversion figures:

- transmitter: $p(1\text{ m})$ sound pressure at 1 m distance (Pa)
- receiver: s sensitivity (mV/Pa).

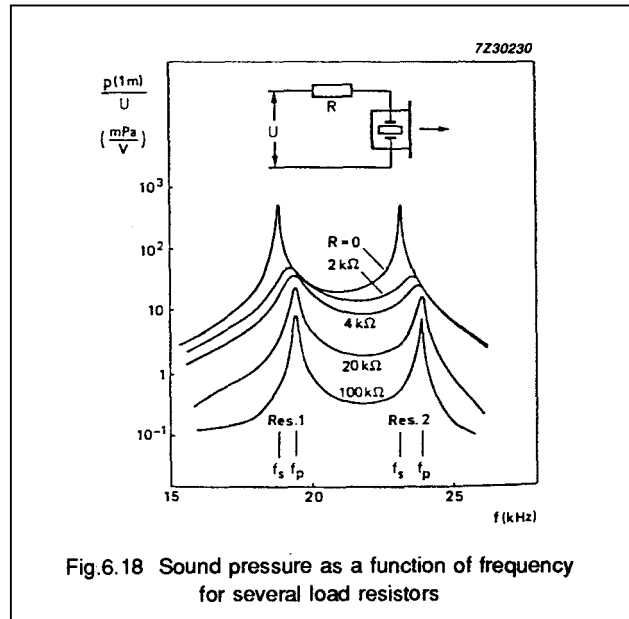


Fig. 6.18 Sound pressure as a function of frequency for several load resistors

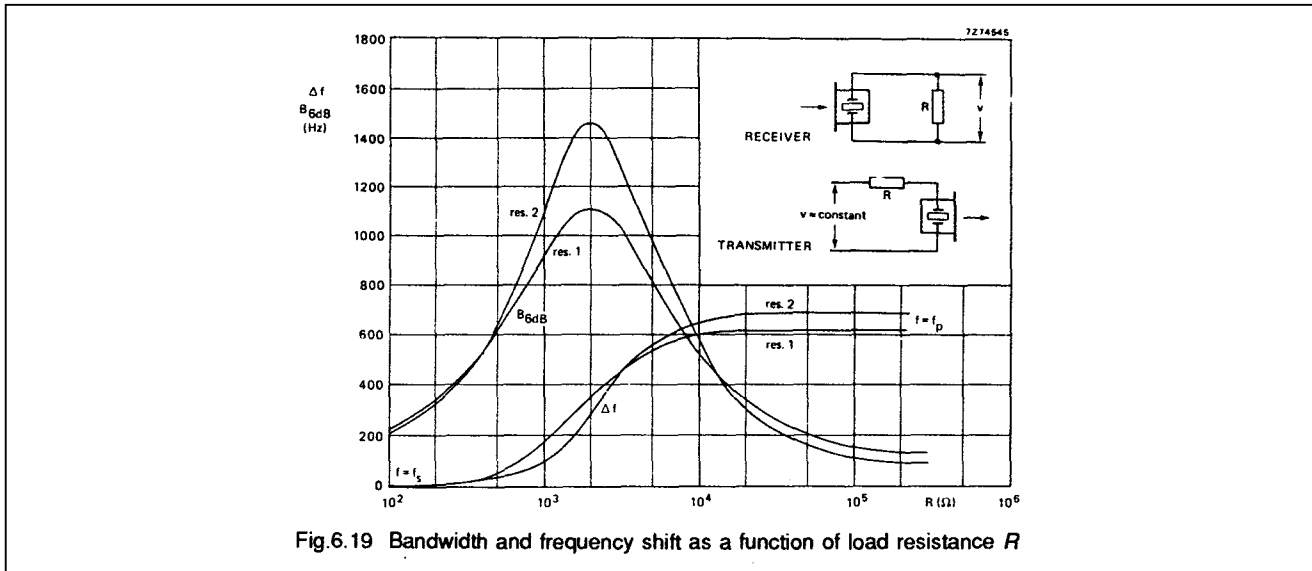


Fig. 6.19 Bandwidth and frequency shift as a function of load resistance R

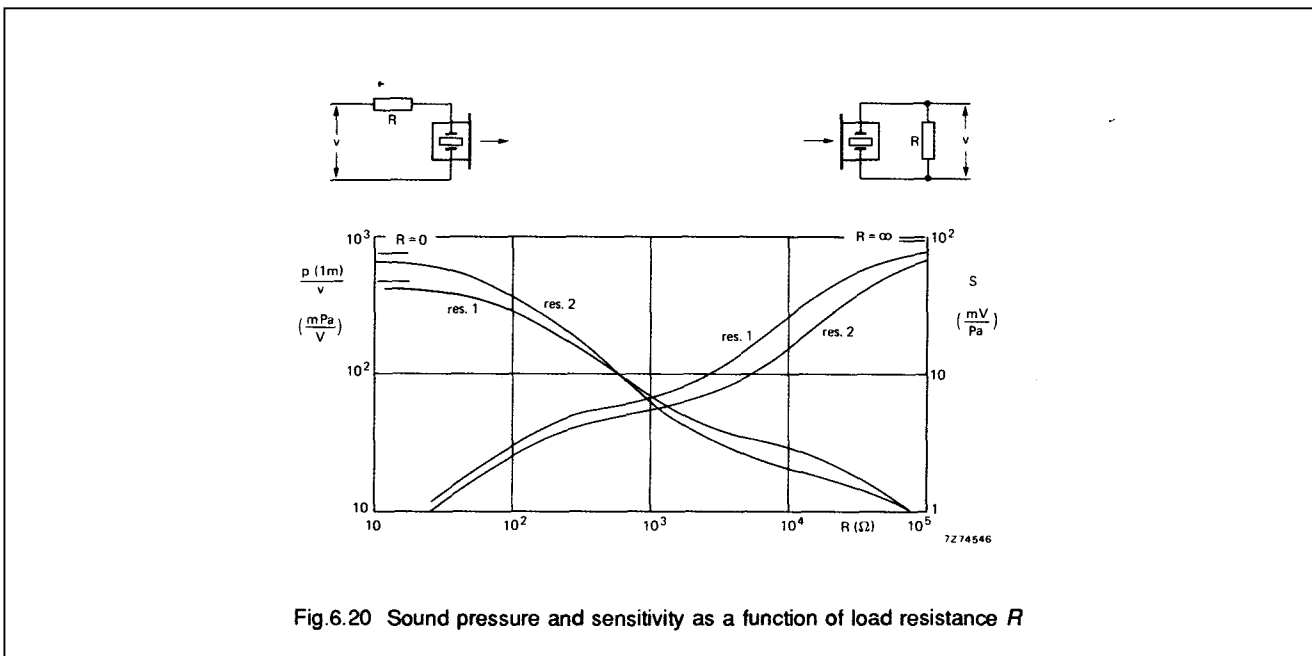


Fig. 6.20 Sound pressure and sensitivity as a function of load resistance R

The frequency behaviour of the transducer in combination with a parallel or series tuning inductor is shown in Figs 6.21 and 6.22. Table 6.3 gives data for some special operating conditions and Fig.6.23 shows the pulse response. The directivity characteristics of this particular transducer are:

- 34° total angle for -3 dB
- 48° total angle for -6 dB.

The measured characteristics agree well with the theoretical relations presented in this section.

TABLE 6.3
Transducer properties under different operating conditions

		frequency	bandwidth	sound pressure coefficient	sensitivity	minimum pulse duration	minimum pulse length
		f (kHz)	B_{6dB} (kHz)	$p(1\text{ m})/U$ (mPa/V)	e (mV/Pa)	2τ (ms)	l_i (cm)
$R = 0$	resonance 1	18,7	$\approx 0,1$	470	-	≈ 20	≈ 670
$R = 0$	resonance 2	23,2	$\approx 0,1$	750	-	≈ 20	≈ 670
$R = \infty$	resonance 1	19,3	$\approx 0,1$	-	100	≈ 20	≈ 670
$R = \infty$	resonance 2	23,9	$\approx 0,1$	-	90	≈ 20	≈ 670
$R = 2,2\text{ k}\Omega$	resonance 1	19,1	1,1	46	9	1,8	60
$R = 2,2\text{ k}\Omega$	resonance 2	23,5	1,4	36	7	1,4	47
$L_p = 17,5\text{ mH}$, $R = 4\text{ k}\Omega$		21	7,4	19	6,3	0,27	9
$L_s = 14,7\text{ mH}$ $R = 1\text{ k}\Omega$		21	7,3	32	3,2	0,27	9

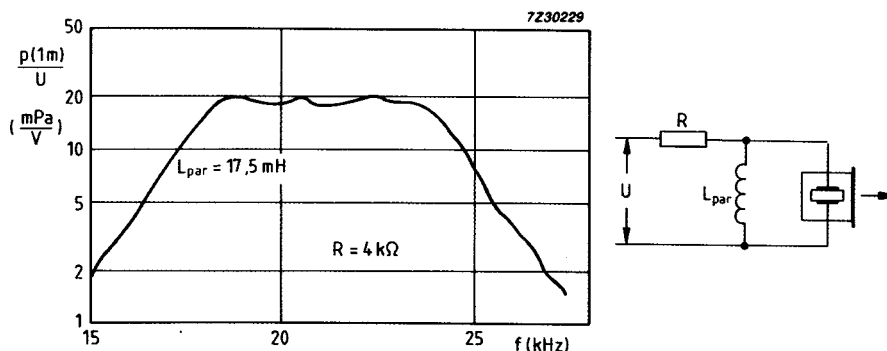


Fig.6.21 Frequency behaviour with parallel inductor.
($L_{par} = 17.5\text{ mH}$, $R = 4\text{ k}\Omega$)

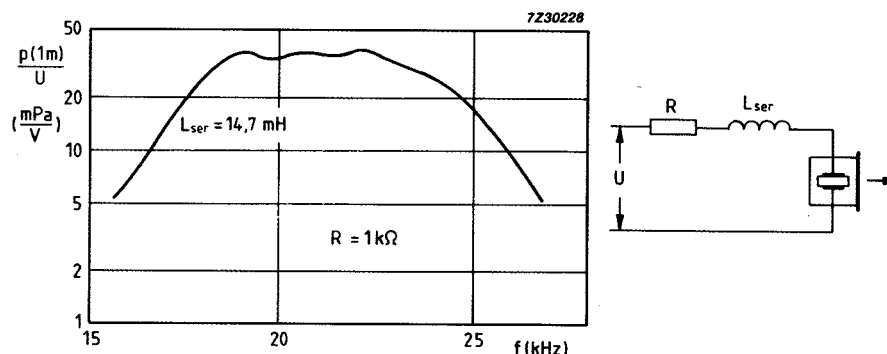


Fig.6.22 Frequency behaviour with series inductor.
($L_{ser} = 14.7\text{ mH}$, $R = 1\text{ k}\Omega$)

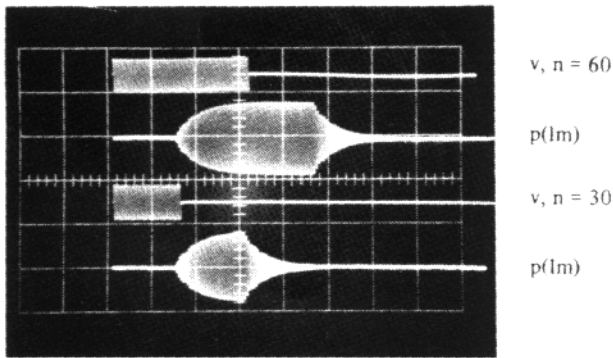


Fig.6.23(a) The transducer in pulse operation.
 ($f = 19.1 \text{ kHz}$, $R = 2.2 \text{ k}\Omega$)
 drive voltage 50 V/unit scale
 sound pressure 1 Pa/unit scale
 time base 1 mS/unit scale

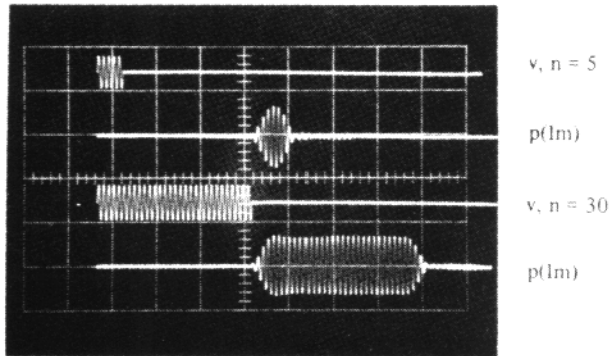


Fig.6.23(b) Pulse operation at 21 kHz.
 ($L_{par} = 17 \text{ mH}$, $R = 4 \text{ k}\Omega$)
 drive voltage 100 V/unit scale
 sound pressure 1 Pa/unit scale
 time base 0.4 ms/unit scale

6.4.4 Range

The practical range in air of the ultra-sound transducer described here is lower than theory would indicate.

The relation between damping (D) and distance (l) is:

$$D=20 \log l+\delta l$$

where δ is the absorption coefficient in air ($\delta = 0.6 \text{ dB/m}$ at 20 kHz). The detection level of the broad-band receiving transducer is about 10^{-3} Pa . For a transmitting sound level of $p(1 \text{ m}) = 10 \text{ Pa}$, a damping of 80 dB is therefore still acceptable. According to the formula this damping is reached at a distance between transmitter and receiver of 70 m.

In practice, air currents and temperature gradients in air cause strong variations. This results in a shorter practical range for reliable transmission. It's possible, however, to improve the performance of transducers by focusing with reflectors or by using a narrower bandwidth. Ranges up to 100 m can be obtained in this way. For pulse-echo measurements the corresponding range would be 50 m.

It should be noted that wide-band transducers require a relatively high level of input power. With a tuning inductor of 17.5 mH and a resistance of 4 k Ω , the coefficient of sound pressure $p(1 \text{ m})$ is $19 \times 10^{-3} \text{ Pa/V}$. For a sound pressure of 10 Pa a voltage level of 526 V must be applied. The resulting power consumption will be $V^2/R \approx 70 \text{ W}$.

In many applications, the frequency dependence of reflection and absorption of ultrasonic radiation are important design parameters. For long range, low frequency is an advantage, since damping in air rises steeply with frequency. Practical half-value distances l (the distance over which the sound pressure drops to half its original value) are given in the following table:

f (kHz)	δ (dB/m)	l (m)
20	0.6	10
50	2	3
100	3	2

Air temperature, humidity and pollution have their influence on the half-value distance. If the object to be detected has the same dimension as the wavelength used, *fringing* may occur. As a result detection becomes unreliable and a higher operating frequency must be used.

6.4.5 Power limitations

A good indicator of the operating power level on the transducer is the current consumption or the radiated acoustical power. The voltage is not a good indicator, since its value depends strongly on losses. For the transducer described above with:

100 Pa/A for resonance 1

70 Pa/A for resonance 2

sound pressure limit $p(1 \text{ m})$ and current are:

$p(1 \text{ m}) = 15 \text{ Pa}$ or 0.15 A (res. 1)

$p(1 \text{ m}) = 40 \text{ Pa}$ or 0.6 A (res. 2)

The sound pressure limit in impulse-echo mode is approximately:

$p(1 \text{ m}) \approx 30 \text{ Pa}$.

For continuous operation, heat dissipation often leads to a further limitation.

In wide-band mode the voltage across the tuning inductor can reach such high values that the high-voltage limitations of the PZT must be taken into account.

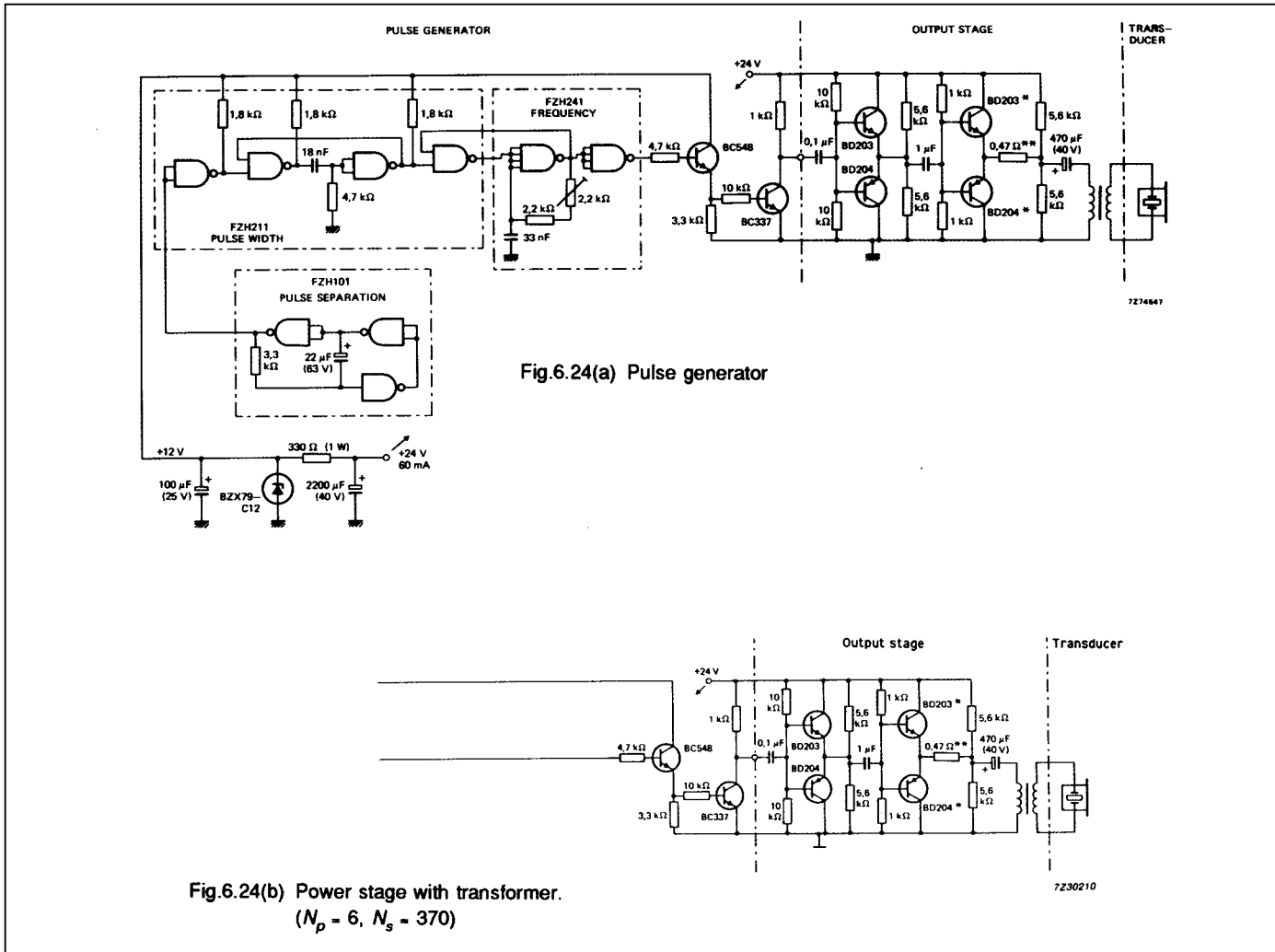


Fig.6.24(a) Pulse generator

Fig.6.24(b) Power stage with transformer.
($N_p = 6, N_s = 370$)

6.4.6 Circuitry for a pulse generator

A generator for pulse-mode transducers delivers the required power (70 W for 10 Pa) only in short bursts. The continuous power consumption is therefore kept relatively low (24 V and 60 mA). The output stage should have a low stand-by current and a low impedance because of the high turns ratio (1:62) of the output transformer. For optimum matching, the output impedance should be $4 \text{ k}\Omega / 62^2 \approx 1 \Omega$

The pulse generator is designed for a delay time of 200 ms and a burst of 300 μs. Delay time and burst length can be adjusted by choosing different values for the capacitors and resistors.

If greater precision is needed in setting the delay time, the electrolytic capacitor (22 μF) should be replaced by a foil type capacitor. After every change in the delay and burst length settings, the output stage must be checked for overheating. The generator frequency can be adjusted with the 2.2 M potentiometer. Figure 6.25 shows the performance measured with a second transducer tuned as a receiver.

direct radiation reflected signal subsequent reflections

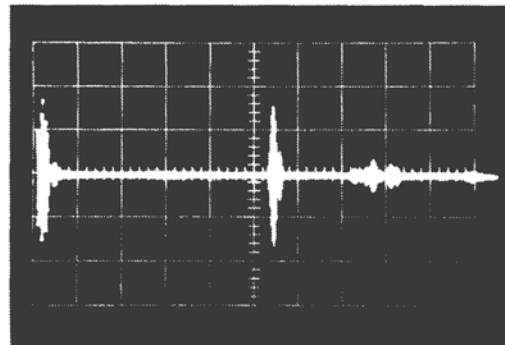


Fig.6.25 Output signal of receiving transducer.
($R = 4 \text{ k}\Omega, L_{par} = 17.5 \text{ mH}$)
reflector distance 1.80 m
voltage 10 mV/unit scale
time base 2 ms/unit scale

6.5 Flexure-mode ultrasonic air transducers

6.5.1 Flexure-mode transducers with metal membranes

Thin metal-disc flexure resonators, driven by glued-on PZT discs, as well as PZT bimorph flexure elements, have proven to be excellent devices for producing and receiving ultrasound. The main reason for this is that they can be well matched to the low acoustic impedance of air, and hence have a relatively high electro-acoustic efficiency (up to 10%).

Figure 6.26 shows some radially symmetric types of ultrasonic air transducer plus their respective modes of vibration. In each case, the PZT disc is bonded to a metal plate so that the composite assembly deflects in the manner shown during operation (broken lines). If the (mechanical) resonant frequency of this resonator is the same as frequency of the voltage applied, the amplitude of deflection, and hence the ultrasound radiation into the ambient air, is at a maximum.

Without further precaution, the resonator shown in Fig. 6.26(a) will exhibit simultaneous counterphase amplitudes which partly suppress the radiated sound waves, leading inevitably to a very low acoustic output. However, if the outer areas of the resonator are screened off as far as the vibrational nodal circle by means of a resilient sound-absorbing material (such as foam rubber or cork), which can function as the mounting at the same time, only the central area of the resonator will radiate sound. (Alternatively, the central area may be screened off.) A drawback of this simple type of ultrasonic transducer is its open construction which is not suitable for use in humid and dusty environments. Section 6.4 describes another transducer that is basically the same.

Though the transducer shown in Fig. 6.26(b) is efficient, it also has an open construction, making it unsuitable for operation in humid and dusty atmospheres. However, the diaphragm types shown in Figs 6.26(c) and 6.26(d), in which the resonator is edge-supported, can have a closed construction, making them extremely sturdy and highly resistant to the effects of dust and humidity. An additional advantage of these transducers is the fact that their (mechanical) resonant frequency can be changed relatively simply by machining. The type shown in Fig. 6.26(c) still operates satisfactorily at high frequencies (> 40 kHz), and shows good directivity and beaming characteristics (large ratio between membrane diameter and ultrasound wavelength in air). For the transducers of Figs 6.26(a) and (b), the diameter of the PZT disc is not critical. However, for the types (c) and (d), the diameter of the PZT disc should be no greater than 0.35D and 0.25D respectively (D being the diameter of the metal diaphragm).

The mechanical resonant frequency f_{sn} of the flexure elements discussed so far can be approximated by:

$$f_{sn} = k_n \frac{h}{D^2} \quad (6.19)$$

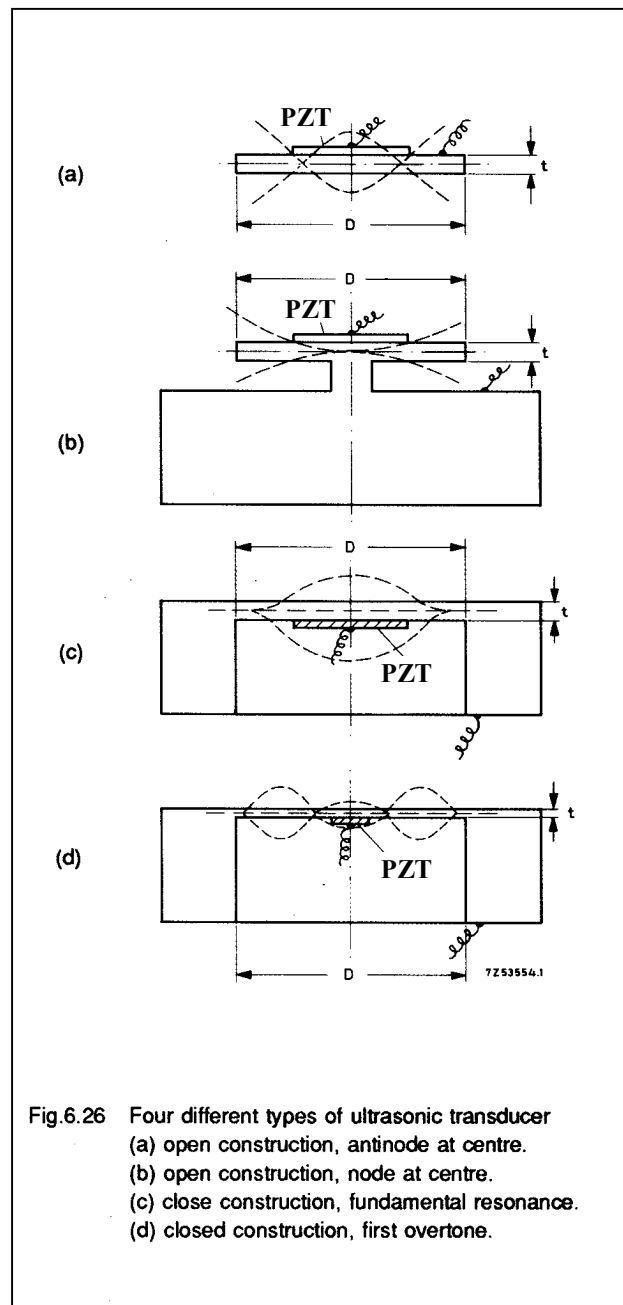


Fig. 6.26 Four different types of ultrasonic transducer
 (a) open construction, antinode at centre.
 (b) open construction, node at centre.
 (c) close construction, fundamental resonance.
 (d) closed construction, first overtone.

where h is the thickness and D the diameter of the metal disc or diaphragm, and k_n is a material constant depending on the mounting method and the mode of vibration (n indicates the order of the overtone).

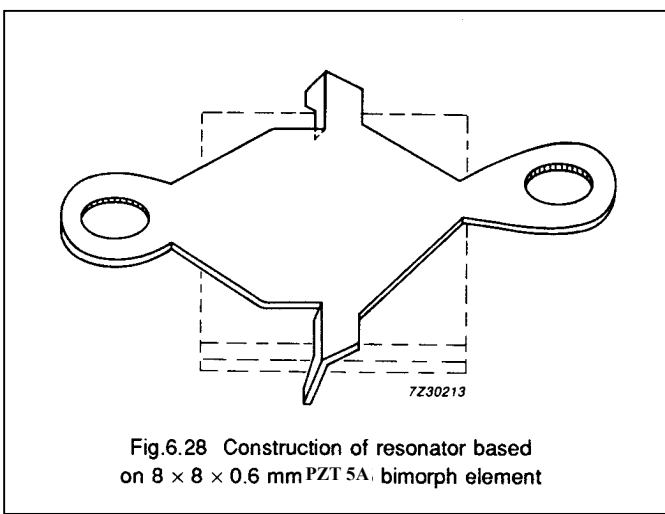
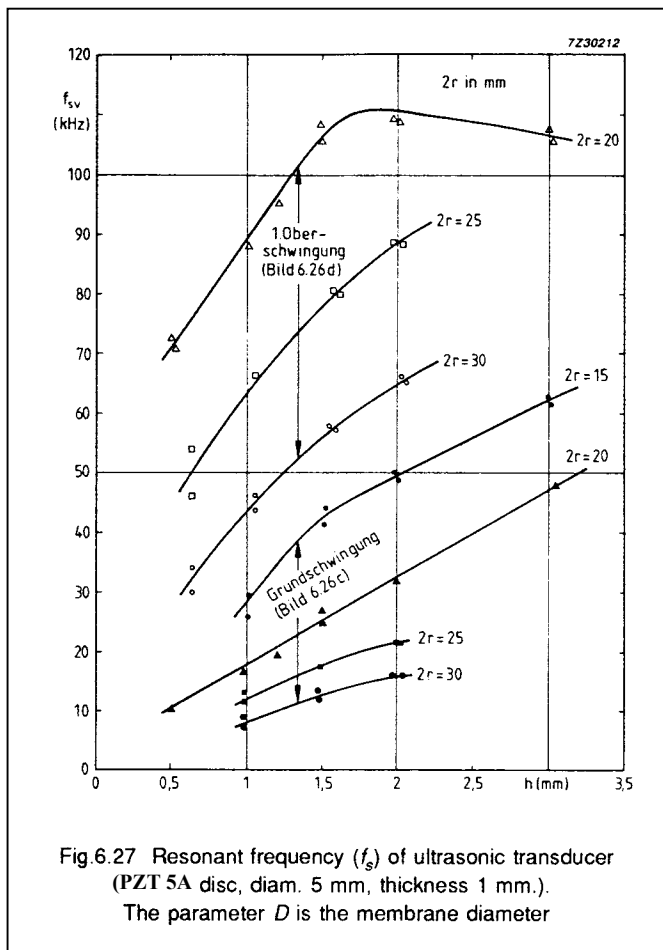
For an edge-clamped aluminium or steel diaphragm without bonded PZT disc, k has the following (theoretical) values:

fundamental resonance $k_0 = 10^4$
 Hz.m, (Fig. 6.26 (c))

first overtone $k_1 = 4.10^4$
 Hz.m, (Fig. 6.26 (d))

However, the PZT disc will itself influence the (mechanical) resonant frequency, so the above values are not usually very accurate and it's best to measure the actual resonant frequency.

The curves of Fig.6.27 show the results of a number of measurements performed on aluminium discs of various dimensions. All discs were edge-clamped, and a disc of PZT5A (10 mm diameter, 1 mm thick) was glued to the centre of each.



Bimorph flexure elements based on the above principle have a greater coupling factor and a greater sensitivity than other types where the PZT element is glued to a metal diaphragm or plate.

Figure 6.29(a) shows that the ultrasonic transducer has a sharp resonance. The electrical behaviour of the transducer can be adequately explained by means of the equivalent circuit shown in Fig. 6.29(b).

There are two characteristic frequencies:

- the series resonant frequency at which the admittance of the transducer reaches a maximum.
- the parallel resonant frequency at which the admittance of the transducer reaches a minimum.

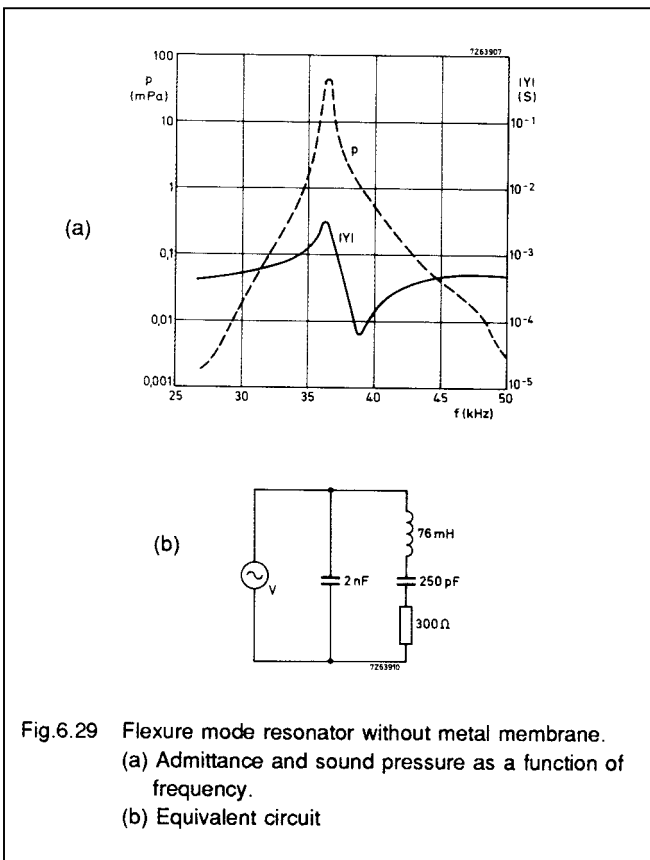


Fig.6.29 Flexure mode resonator without metal membrane. (a) Admittance and sound pressure as a function of frequency. (b) Equivalent circuit

6.5.2 Bimorph flexure elements without metal membrane

Figure 6.28 shows an ultrasonic air transducer based on a square bimorph PZT flexure element. A specially designed metal plate at the top keeps the PZT element centred between two opposite edges, and a similar plate at the bottom (rotated through 90° with respect to the top plate) does the same with the other two opposite edges. These two metal plates also serve as the electrical contacts. The central area of the PZT element vibrates in counterphase with its edges causing a certain amount of cancelling of the radiated ultrasound and hence very low efficiency. This is remedied by shielding the central area of the PZT element with a metal plate to prevent direct radiation from the centre. A secondary - and welcome - result is that sound diverted laterally by the plate undergoes a phase conversion and so reinforces the radiation from the corners of the square element.

The transducer characteristics depend strongly on the electrical load for which, so far, we have only assigned a real value R . This resistance can be regarded as the input resistance of a microphone amplifier, or the internal resistance of a transmitter generator since the characteristics of the two working conditions do not differ much. When there is effectively no electrical load ($R \ll |Z_S|$ or $R \gg |Z_p|$), the transducer has a quality factor of about 60, which means a 3 dB bandwidth of about 0.6 kHz.

Figure 6.30 shows how the maximum response frequency f_m varies with R , the load resistance (see also Eq.A33 in Appendix A3). The maximum response frequency is the frequency at which the microphone sensitivity or the sound pressure of the transmitter reaches its maximum. Figure 6.30(b) shows the bandwidth. Note that f_m shifts from f_s to f_p as the load increases, whilst at $R = 2\text{ k}\Omega$ a maximum bandwidth of about 3 kHz is established. The corresponding value of f_m is located about mid-way between f_s and f_p .

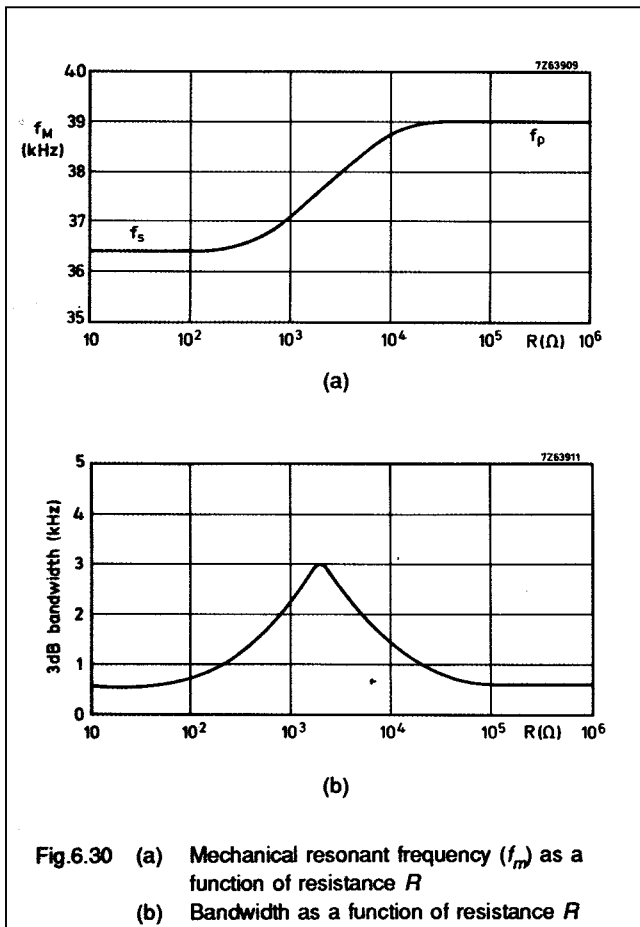


Figure 6.31 shows the voltage V and the electrical output power P generated when the transducer is operated as a receiver (sound pressure 0.1 Pa). The relationship between the electrical output power and the load resistance R provides a clear indication that in the range of values of R from 100 Ω to 50 k Ω , efficiency remains fairly constant. The same applies when the transducer is driven as a sound transmitter.

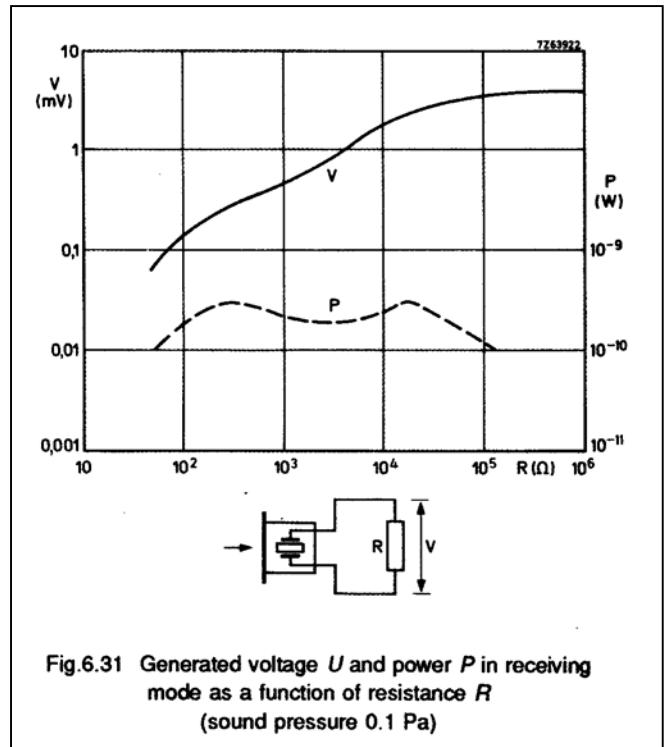
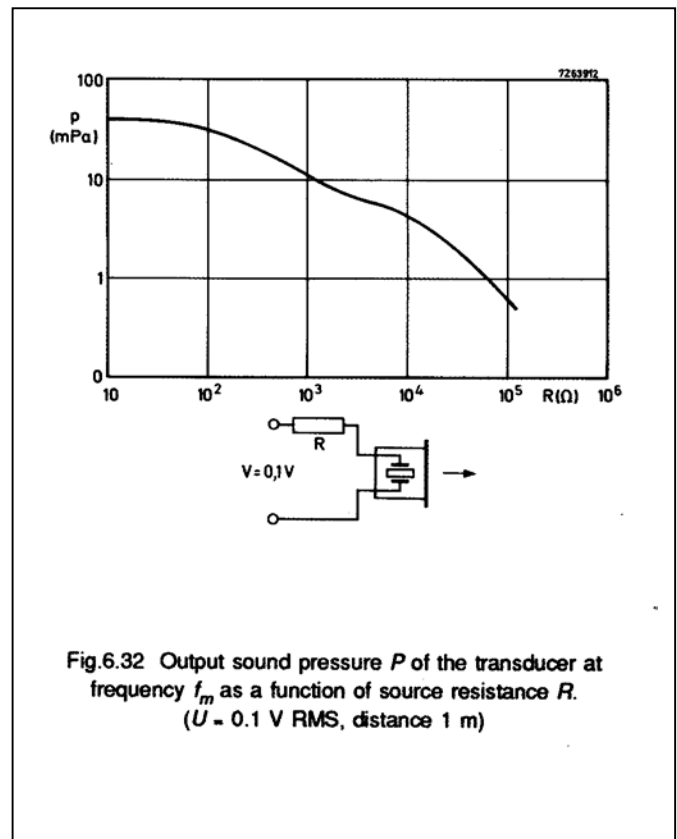
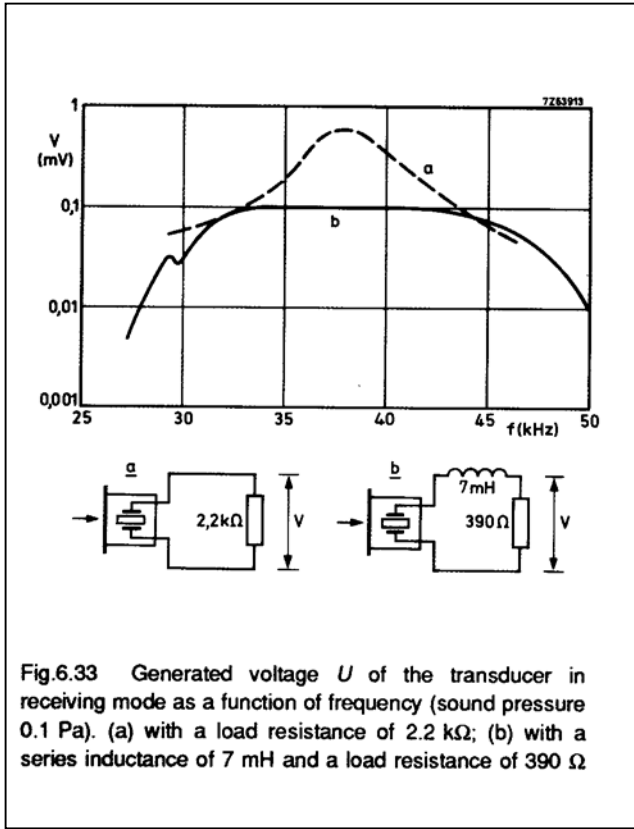


Figure 6.32 indicates the sound pressure obtained at a distance of 1 m at $V = 0.1\text{ V RMS}$. It should be noted that during transmitter operation the sound pressure drops not only by $1/l$ (where l is distance) but also by damping by about 1,4 dB/m due to absorption by air (half-value distance $\approx 4\text{ m}$).



The bandwidth of the transducer can be expanded considerably if, apart from the load resistance R , an inductance of about 7 mH is connected in parallel (L_{par}) or in series (L_{ser}) with the transducer (Fig.6.33). This inductance differs slightly from the one calculated with Eq.2.10 since here the acoustic effect of the cover plate has been taken into account. A flat response curve is obtained by choosing a load resistance of 390 Ω (series coil), or 10 k Ω (parallel coil).



Whereas the sensitivity of a transducer microphone is about 1 mV/Pa with a series inductance ($R = 390 \Omega$) and 5 mV/Pa with a parallel inductance ($R = 10 \text{ k} \Omega$), the sound pressure (at a distance of 1 m) produced by a transmitter at $V = 0.1 \text{ V}$ RMS is 0.007 Pa for series connection and 0.002 Pa for parallel connection. From what has been said so far it will be clear that when designing the electronic circuitry associated with these transducers, the input and output impedances must be given due consideration.

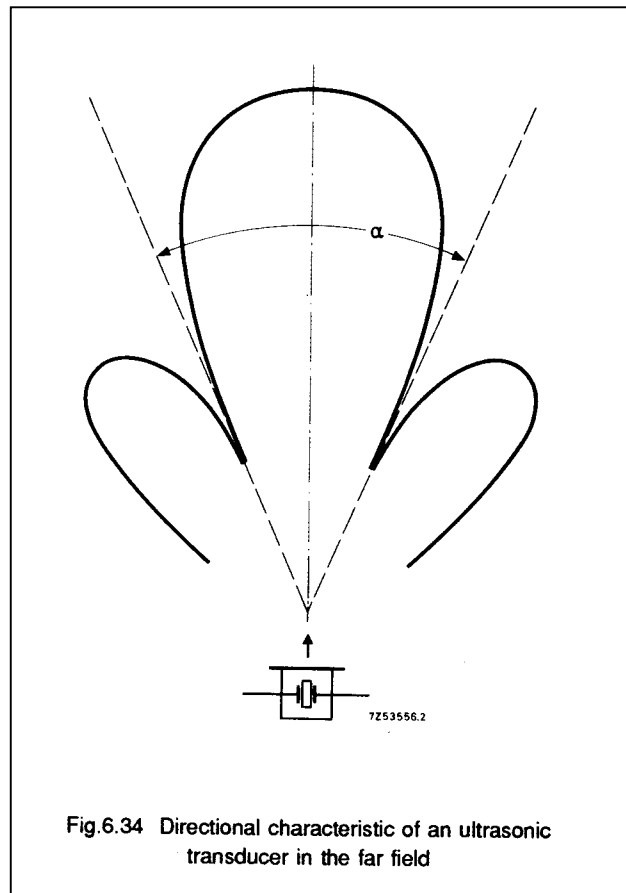
6.5.3 Directivity and sound pressure

If a flexure transducer is to function as a transmitter, it's essential to know the directivity of the radiated sound. (Likewise, one needs to know the directional characteristic when it is used as a microphone.) For the so-called 'far field', i.e., distance $> D^2/2\lambda$, this directivity depends on the diameter D of the radiating area, the vibrational amplitude distribution over that area, and the wavelength λ in air

(Fig.6.34). For cases in which $\lambda < D$, the total angular width, α , of the main sound beam directed along the axis of symmetry can be calculated quite accurately from D and alone:

$$\sin \alpha/2 \approx \lambda/D \approx \frac{v}{Df} \quad (6.20)$$

where v is the velocity of sound in air (344 m/s at 20 °C), and f is the operating frequency. So if $\lambda \ll D$ one gets a narrow beam and good directivity. At the same time, a number of funnel-shaped lobes occur. The above relationship no longer applies if $\lambda > D$, because the directional characteristic then assumes a spherical form. It's also possible to get beaming by means of a concave acoustic reflector. In that case, the diameter of the reflector must again be much greater than the wavelength.



In general, a narrow sound beam is required because it reduces interference and the chance of undesired transducer couplings, for instance, via reflecting objects outside the main beam. On the other hand, a narrow beam can be made to deviate from its original path between transmitter and receiver under the influence of turbulence. The narrower the beam and the greater the distance, the more significant is this deviation likely to be.

6.6 Compact ultrasonic air transducer

Figure 6.35 shows a very compact air transducer. A PZT5A disc 5 mm in diameter and 0.5 mm thick is glued into a TO-39 transistor housing. The resonant frequency of the transducer in the assembly is about 38 kHz. The minimum impedance (at f_r) is $1.5\text{ k}\Omega$ and the generated sound pressure for a driving voltage of 3 V_{eff} is 0.04 Pa at a distance of 1 m . Figure 6.36 shows the impedance and the sound pressure as a function of frequency. The maximum sound pressure coincides with the series resonance (f_s) and with the minimum in the impedance curve provided no extra resistor is added between generator and transducer. With an external series resistor of $10\text{ k}\Omega$, the maximum sound pressure decreases and the frequency shifts towards the parallel resonance (f_p).

The transducer can also be used as an ultrasonic microphone. In that case the sensitivity will be about 10 mV/Pa ($R_i > 10\text{ M}\Omega$). The capacitance at 1 kHz is approximately 600 pF .

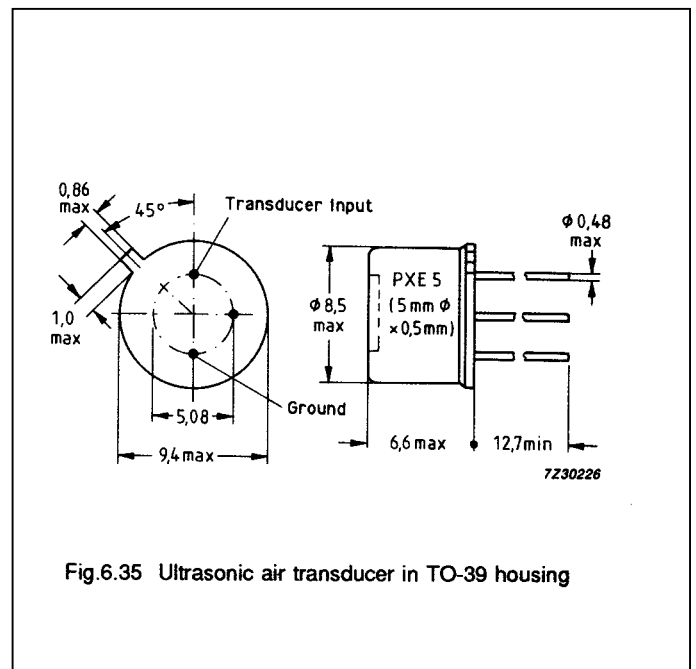


Fig.6.35 Ultrasonic air transducer in TO-39 housing

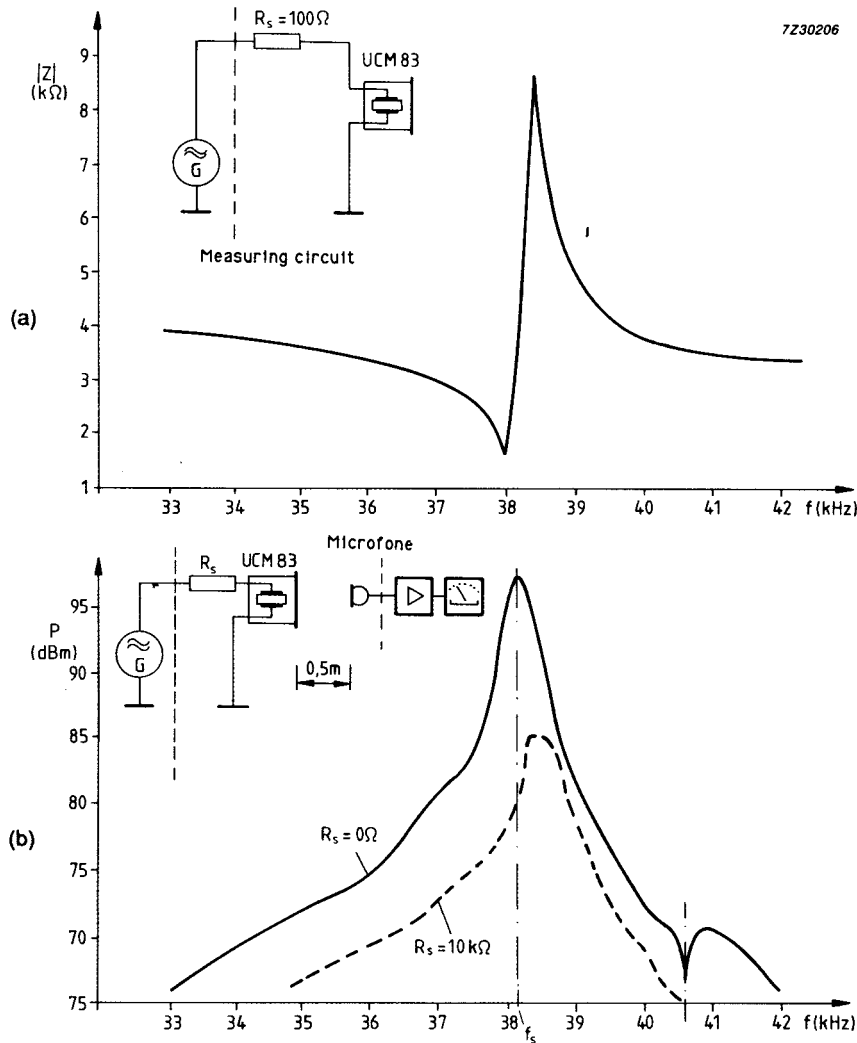


Fig.6.36 Frequency spectrum of air transducer in TO-39 housing (drive voltage 5 V RMS).
 (a) impedance as a function of frequency; (b) sound pressure as a function of frequency.
 (courtesy: HOLTHAUSEN GMBH)

6.7 Sound transducers (buzzers)

PZT -flexure mode elements can also be designed to generate audible sound. Such *tone generators* have several advantages over electromagnetic buzzers.

Their simple flat design and low energy consumption make them ideal for use in battery powered equipment where limited space is available and a high sound level is required. As with PZT ultrasonic transducers they are reliable and maintenance-free.

6.7.1 Design of buzzers

The housing construction of a sound generator has a profound effect on the attainable sound level and its cost effectiveness. The damping should be low, but the construction must be air-tight, especially when used in conjunction with a Helmholtz resonator.

The flexure element itself usually consists of a thin PZT -disc glued to a suitable metal membrane. When an alternating voltage is applied, the membrane bends periodically because of the deformation of the piezo-ceramic disc, causing the system to vibrate with the frequency of the driving voltage.

If the frequency of the applied signal coincides with the mechanical resonant frequency of the system, the amplitude of the vibration increases and the sound output reaches a maximum. The sound level can be sufficient for many practical applications.

The design of the sound generator can be as shown in Fig.6.26(c) but also as in Fig.6.37 which gives the following possibilities:

- The membrane is clamped on its nodal line. The movement is not influenced by the clamping which results in a high Q-factor and vibrational amplitude. A drawback is that the outer parts of the membrane would radiate sound in antiphase with the central part. This would lead to interference phenomena. The housing is therefore designed in such a way that no sound from the outer part can escape.
- A membrane, which is clamped on its circumference, vibrates at approximately the same frequency as the nodal design of a). However there is more interaction with the housing, causing a decrease of the Q-factor and amplitude. An advantage is that the whole surface vibrates in phase.

The housing generally needs to be more massive to rigidly fix the membrane, and variations in the clamping can easily effect the performance.

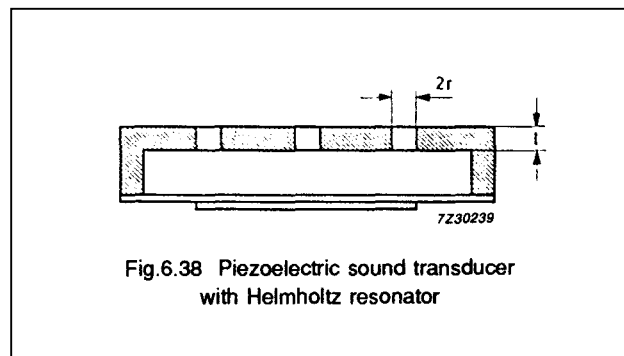
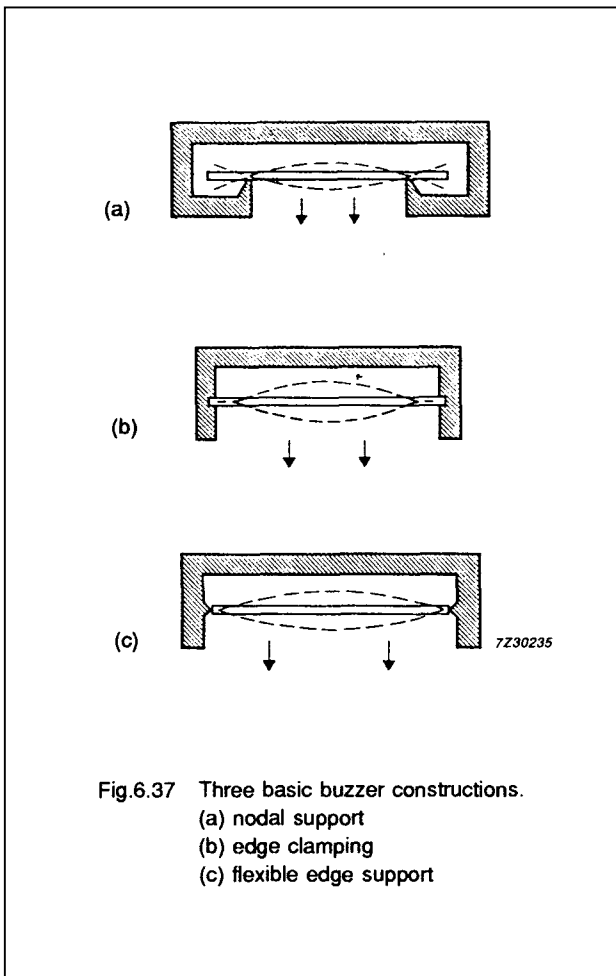
- In this design, the membrane is not clamped but only pinched at its outermost circumference in a flexible material such as rubber. In this way angular movements are still possible. The resonant frequency of this construction is only half that of the other designs. This is excellent for a sound transducer but the construction can be rather critical.

6.7.2 Helmholtz resonators

The acoustic impedance of a sound transducer is often not well adapted to that of the surrounding air. Energy transfer is therefore not optimum resulting in a rather low sound level.

The cavity inside the housing can, however, be designed in such a way that its acoustic impedance matches that of the membrane (Fig.6.38), resulting in a much improved sound output. Such a design is called a *Helmholtz resonator*. Its function can be explained as follows:

- The air volume in the housing absorbs and releases potential energy during pressure variations (capacitor) -
- The mass of the air in the holes picks up kinetic energy when moving (inductance).



Resonance occurs just like in a electrical LC-circuit. The resonant frequency is given by:

$$f_r = \frac{v}{2\pi} \sqrt{\frac{n\pi r^2}{V \left(l + \frac{\pi r}{2} \right)}} \quad (6.21)$$

- where: V = sound velocity (344 m/s)
 n = number of holes
 r = radius of the holes
 l = length of the holes
 v = volume of the housing

If the Helmholtz resonator has nearly the same resonant frequency as the flexure element, coupling occurs, resulting in a broader resonance, just as with coupled electrical oscillators. Because of the greater bandwidth, the peak output level is reduced, but the transducer is now able to handle a wider frequency range (Fig.6.39). This capability is used in multi-tone buzzers for telephone

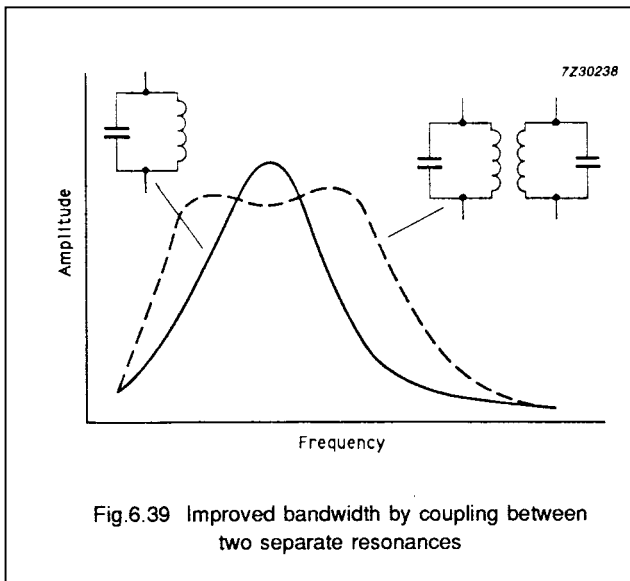


Fig.6.39 Improved bandwidth by coupling between two separate resonances

For transducers with Helmholtz resonators, the dimensions of the housing must be well defined. The frequency behaviour is a function of resonant frequency, damping of the Helmholtz resonator and flexure element, and of the coupling between them.

6.7.3 Drive circuits for PZT sound transducers

PZT sound transducers may be powered from the mains or by batteries. The circuit designs depend on the application, but generally the circuits can be divided into three groups:

(a) Circuits with feedback loop

PZT -sound generators driven by this type of circuit vibrate at their resonant frequency. The bandwidth is narrow, but the mechanical Q-factor is high, resulting in low energy

consumption. This means they are suitable for battery operation. The layout of the drive circuitry is very simple if the PZT -disc is provided with a special feedback electrode (Fig.6.40). If this is not provided, the circuit can be based on the so-called *Pierce oscillator* or a multivibrator whose frequency is controlled by the PZT flexure element. Manufacturing tolerances do not play a major role in this design.

The system is self-stabilizing the resulting frequency will not always be exactly the same.

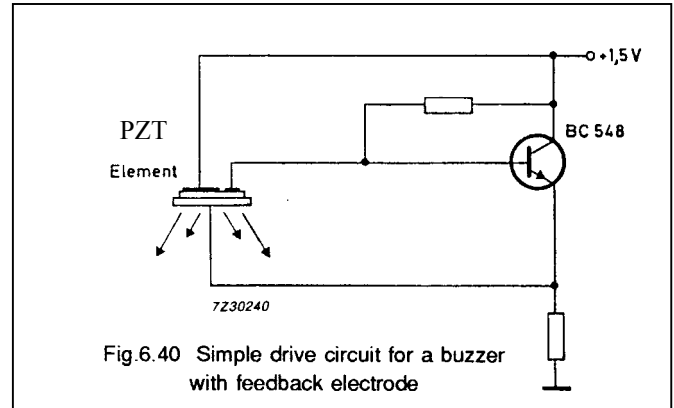


Fig.6.40 Simple drive circuit for a buzzer with feedback electrode

(b) Circuits with a fixed frequency

This design calls for a transducer with a large bandwidth. Regardless of manufacturing tolerances and influences of temperature, the transducer must operate at a fixed frequency set by the circuit. This is often assured by means of a Helmholtz resonator. For clocks and watches, the frequency is obtained from the quartz oscillator in conjunction with a frequency divider. For non-portable equipment, the mains voltage can be used via a 470 kΩ series resistor and a trigger diode.

(c) Circuits with parallel inductors

Figure 6.41 shows the basic principle of this design. When the current through the inductor is switched off, voltages much higher than the supply voltage are induced and cause the PZT -element to vibrate at its own resonant frequency. Because of this, variations in the transducer construction hardly influence the sound level. The same result can be obtained by applying a square wave of high amplitude, though since the square wave contains a broad frequency spectrum, overtones will be then generated.

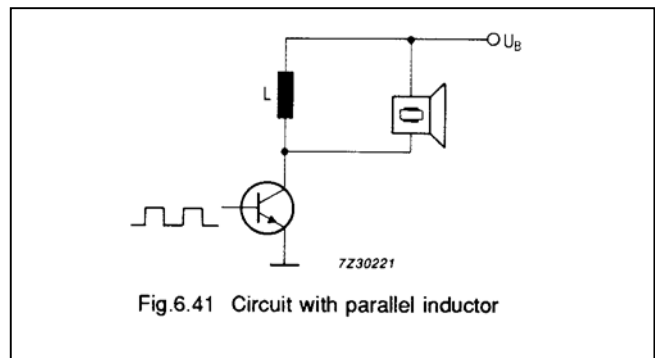


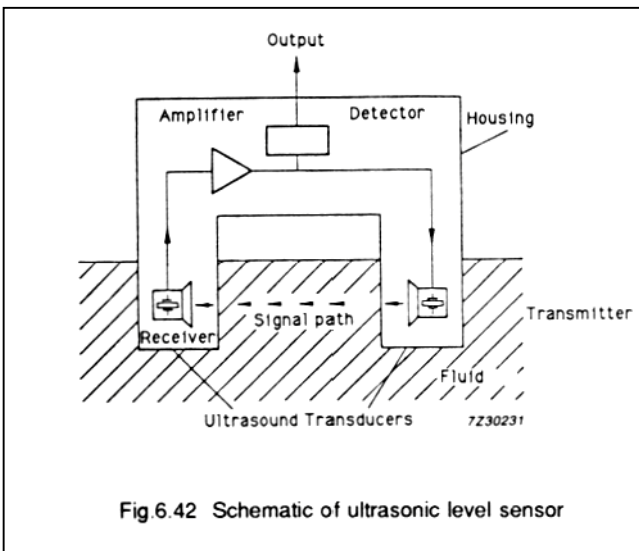
Fig.6.41 Circuit with parallel inductor

6.8 A fluid level sensor

Level sensors are often required nowadays for sensing the level of fluids such as oil and water, and of hydraulic fluids. In motor vehicles, in particular, the number of level sensors is increasing, to monitor the brake- and cooling fluid level, for example, or the level of the engine and gearbox oil, and of the windscreen-washer fluid.

It would be ideal to have just one type of sensor able to work with all these fluids, a sensor which is also inexpensive, reliable and mechanically robust.

A sensor based on the difference in sound transmission between two PZT -transducers in a liquid and in air has the potential to fulfil these requirements. Figure 6.42 shows the principle and Fig.6.43(a) shows a prototype with and without plastic moulding (epoxy resin). In Fig.6.43(b) one can identify the PZT5A discs ($\varnothing 5 \times 0.5 \text{ mm}$) that have been used as transducers, and the construction method.

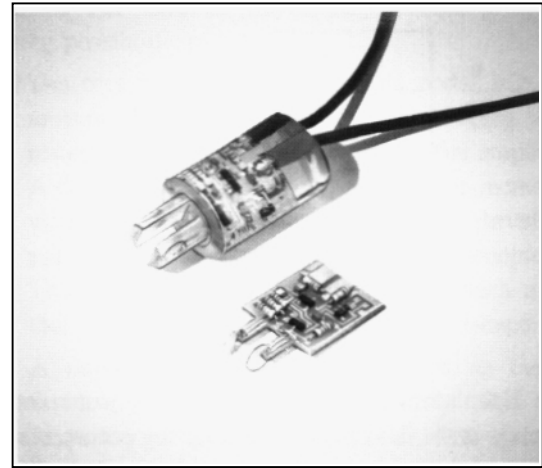


The PZT discs are clamped in a slit in the PCB and then soldered. When there is liquid between the two transducers the acoustic coupling should be high, whereas with air the coupling should be as low as possible. The transducers must therefore be highly directive with little or no coupling via the housing.

Figure 6.44 gives measured results for two discs of diameter 5 mm and thickness 0.5 mm. The thickness-mode resonance of these discs is about 4 MHz. At this frequency, the wavelength in water is only 0.4 mm, which results in a high directivity.

At 4 MHz the distance between the signal levels with and without fluid is as high as 55 dB. Below 1 MHz the situation is less favourable so a high-pass filter will be required in the electrical circuit.

The distance between the two fingers of a level sensor must not be too small, otherwise drops of fluid may adhere to it and fill the gap. For practical designs, a distance between 3 and 5 mm is adequate.



(a)

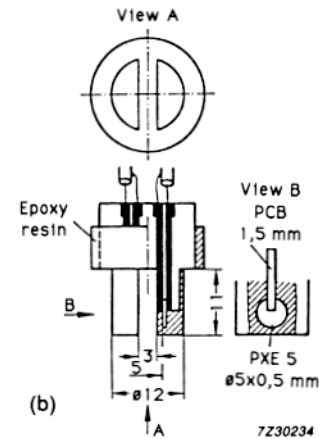


Fig.6.43 Level sensor in surface mount technology (SMT).
(a) assembled sensor before and after potting;
(b) detail of construction

Figure 6.45 shows a practical circuit. Basically it's an oscillator that drives one PZT -disc (S2) with the other (S1) in its feedback loop. The gain is about 40 dB. When the device is immersed in liquid, the coupling between S1 and S2 is better than -40 dB and the circuit oscillates. The rectified oscillator signal causes the second transistor to block and the LED to switch off.

Figure 6.26(c) shows a completely different design using a flexure element. The behaviour at resonance of such an element in air is different from its behaviour when immersed in a liquid. The resonant frequency will shift and damping (which depends on viscosity) will be much higher in the liquid. Readout for this sensor is usually more complicated and requires central electronic processing, but it does offer the advantage of allowing the sensor to operate at higher temperatures.

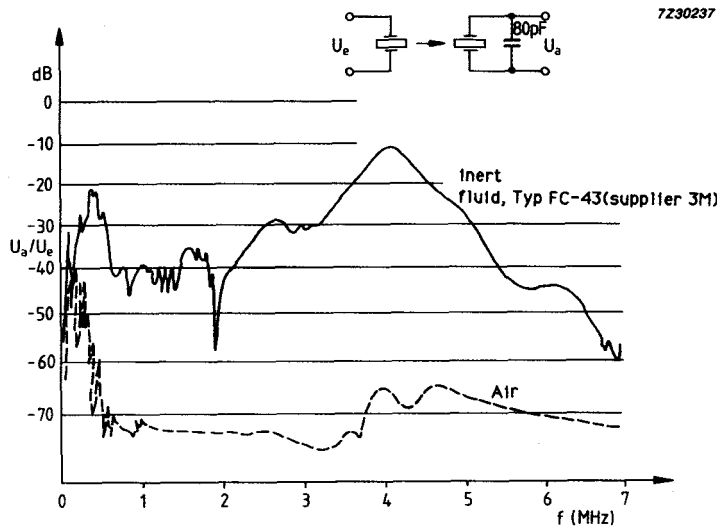


Fig.6.44 Attenuation for the transducer pair in liquid and in air

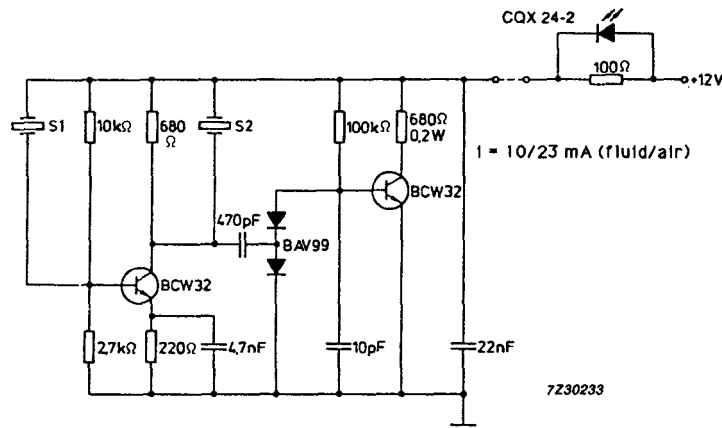


Fig.6.45 Circuitry for the level sensor

6.9 PZT delay lines

6.9.1 General

There are several electronic systems that require electrical signals to be delayed for periods of up to several milliseconds without a substantial loss of the information contained in the signal. Electrical transmission lines with either lumped or distributed components cause considerable attenuation and distortion, and are rather bulky.

Modern acoustic delay systems operate with an electro-mechanical transducer which converts the electrical signal into an acoustic signal that's converted back into an electrical signal after having travelled over an appropriate distance through an acoustic delay medium, which may be either solid or liquid. For analog signals it's important for the energy conversion in the transducer to be linear and reversible to ensure satisfactory restoration of the delayed electrical signal.

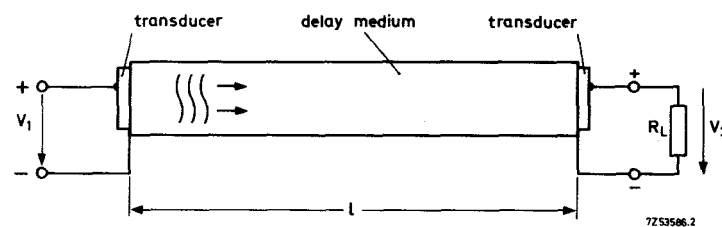


Fig.6.46 Principle of a delay line

With these systems, the delay depends almost entirely on the transit time of the acoustic wave. The velocity of sound in liquids and solids is between 1 km/s and 5 km/s, whereas the velocity of electromagnetic waves in dielectrics is about 10^5 times as high. Compact mechanical structures are therefore quite suitable for providing delay times of a few milliseconds.

Though ultrasonic delay lines are basically information storage devices, they are quite valuable for many other applications. They are practically indispensable when long delays or high fidelity, or both are required. Bandwidths of no less than 80% of the carrier frequency are quite common; so are delays of several milliseconds.

An ultrasonic delay line must satisfy the following requirements: long (and sometimes variable) delay with precise control, accurate preservation of pulse or modulation envelope shape (wide bandwidth and linear performance), a minimum of spurious signals, very moderate attenuation, compactness and stability under varying ambient conditions of temperature, humidity and vibration.

The main application area of such delay lines is in PAL- and SECAM colour television receivers. A further application is in video recorders as a drop-out compensator.

In PAL-system TV-receivers, the (R-Y) signal must be delayed 64 ps on alternate picture lines. Phase errors in the (R-Y) signal are corrected by taking the average of both signals. In SECAM-receivers, the (R-Y) and (B-Y) signal are delayed alternately in order to have them available at the same instant in time.

6.9.2 Solid delay lines

A solid ultrasonic delay line consists of a slice of quartz or potassium-lead glass through which the signal is propagated as an acoustic wave, launched and received by electro-acoustic transducers.

The delay depends on the total distance the wave travels in the medium. Reflections are used to keep dimensions within limits. The velocity of sound in the delay medium varies little with temperature. PZT-transducers are soldered or glued to the surface of the glass body. For good electromechanical efficiency, the thickness of the bonding layer should be maintained between half and a quarter wavelength, or it should be kept extremely thin

With high coupling piezo-ceramics, e.g. PZT703, devices with a large 3 dB-bandwidth and low damping can be constructed. In practice, a matching network consisting of a parallel coil is used to improve the transfer function of the delay line.

The coil (L_{par}) produces an electrical parallel resonance f_e given by:

$$f_e = \frac{1}{2\pi} \sqrt{\frac{1}{L_{par} C_0}}$$

With C_0 = clamped capacitance of the transducer. With for instance, $f_e/f_s = 0.7, 1.0, 1.4$ (f_s being the acoustical series resonant frequency), and a load resistance R_L given by

$$Q_e - 2\pi f_s R_L C_0 = 2$$

a PZT transducer pair with a piezoelectric coupling coefficient $k \approx 0.6$ then gives the three transfer functions drawn in Fig.6.47. Similar functions, but then for $Q_e = 5$, are shown in Fig.6.48, so that the influence of the load resistance becomes apparent. The conclusion is that the passband of the transducer pair, and hence of the total delay line can be shifted and shaped by an appropriate choice of Q_e and f_e (R_L and L_{par}).

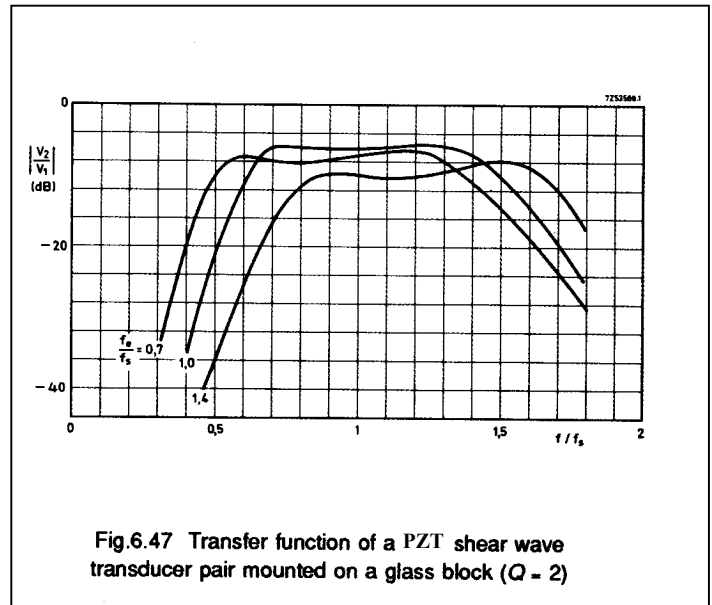


Fig.6.47 Transfer function of a PZT shear wave transducer pair mounted on a glass block ($Q = 2$)

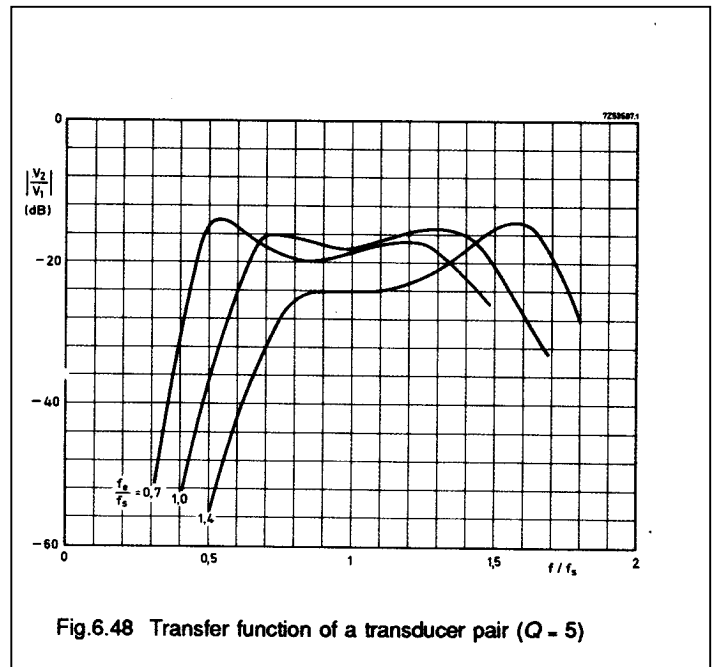


Fig.6.48 Transfer function of a transducer pair ($Q = 5$)

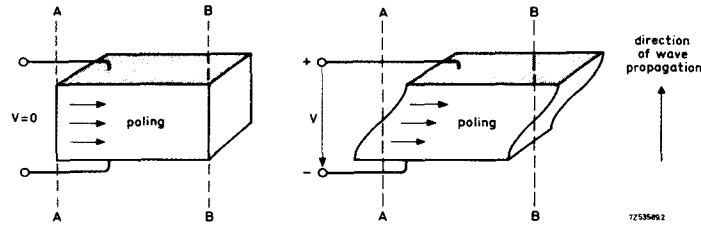


Fig.6.49 PZT transducer operating in the shear mode

6.9.3 Modes of vibration

The transducers used to transmit and receive waves in the delay line are PZT703 platelets which have been soldered to the glass body. Owing to the large coupling factor of PZT703 ($= 0.66$), it's possible to build delay line with a broad bandwidth and at the same time relatively low damping.

As shear waves are propagated more slowly than compressional waves, they are usually preferred where small dimensions are required. The ratio of the velocities of propagation of these two modes is given by:

$$\frac{V_c}{V_{sh}} = \sqrt{\frac{2(1 - \sigma)}{1 - 2\sigma}} \quad (6.23)$$

where σ is Poisson's ratio for the delay medium. This velocity ratio is approximately 1.6 and 1.7 for materials with $\sigma = 0.17$ (fused silica) and $\sigma = 0.225$ (isopaustic potassium-lead-silicate glasses) respectively.

Figure 6.49 shows the deformation, with magnitude exaggerated, of a transducer operating in the shear resonant mode. In a shear transducer, the poling direction must be perpendicular to the direction of the alternating electric field, and so parallel to the electrode surfaces, as shown in Fig.6.49.

6.9.4 Directivity

Most delay-line transducers have a large aperture (20 or more wavelengths wide), and are therefore highly directional. This permits the use of ray paths intricately folded by repeated reflection to obtain a long delay in a small volume of material. The side lobes of the radiation pattern can give rise to spurious signals which follow 'stray' paths to arrive with unwanted delays. These can be minimized by careful geometrical design, accurate machining, and by coating the delay medium at appropriate points with absorbent materials such as epoxy resins or solder.

For a planar rectangular radiator with sides a and b which produces a shear stress amplitude p_0 in the semi-infinite medium with which it is in contact, the shear stress amplitude p of the radiated wave (of wavelength λ) at a distant point whose radius vector r forms angles $\pi/2 - \alpha$

and $\pi/2 - \beta$ with the a and b directions of the radiator, is given by the relation:

$$p = p_0 \cdot \frac{ab}{r\lambda} \cdot \frac{\sin\{(\pi a/\lambda) \cdot \sin\alpha\}}{(\pi a/\lambda) \cdot \sin\alpha} \cdot \frac{\sin\{(\pi b/\lambda) \cdot \sin\beta\}}{(\pi b/\lambda) \cdot \sin\beta} \cdot \exp\{-j2\pi f(t - r/v)\} \quad (6.24)$$

with v = the velocity of sound.

Evidently zeros occur at $\alpha_n = \pm n\lambda/a$ and $\beta_m = \pm m\lambda/b$, where n and m are positive integers.

In this distant region, the so-called *far field* or Fraunhofer region, the wavefront is approximately spherical, and the amplitude varies along the axis inversely with the distance from the radiator. However, the expression is only valid for a distant point in a long and very thick delay block in which the beam can spread freely. In fact, the conditions are significantly different where long lines are concerned. Dimension b of the transducer is usually almost equal to the vertical thickness of the plate of delay material, so the wavefront cannot spread vertically, and a partially guided wave is produced. The beam spread still occurs in the plan view and such a delay plate has a cylindrical wavefront with the following shear stress distribution:

$$p = p_0 \cdot \frac{a}{\sqrt{r\lambda}} \cdot \frac{\sin\{(\pi a/\lambda) \cdot \sin\alpha\}}{(\pi a/\lambda) \cdot \sin\alpha} \cdot \exp\{-j\pi f \cdot (t - rv)\} \quad (6.25)$$

In practice, many delay lines don't work with a relatively large transducer separation l . In other words they don't operate in the far field, but somewhere in the transition region between the far field and the near field, or Fresnel region. This near field extends from the transmitting transducer over a distance l_n ($l_n = l_{near}$) along its axis which is expressed by the following relations:

for the a direction:

$$l_n \approx a^2/2\lambda = f a^2/2v \quad (6.26)$$

for the b direction:

$$l_n \approx b^2/2\lambda = f b^2/2v \quad (6.27)$$

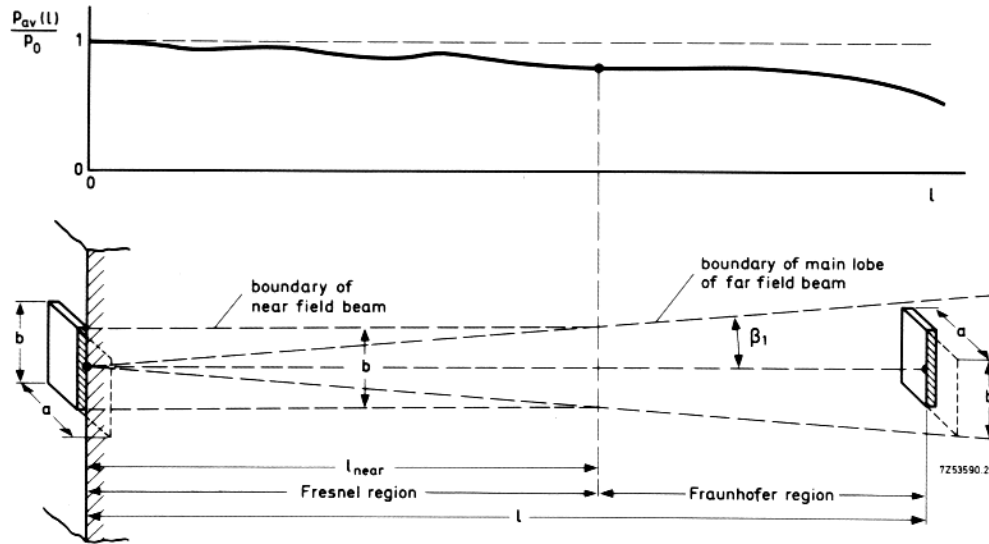


Fig.6.50 Near field and far field beam pattern

Details are shown in Fig.6.50 which also illustrates the average shear stress p_{av} integrated in phase and amplitude over area ab of a receiving transducer at a distance l from a similar transmitting transducer.

Optimizing the ratio of main delayed signal amplitude to worst spurious response amplitude (often called the 'third time around' signal) usually leads to the following preferred dimensions:

$$l_n \approx (0.7 \text{ to } 1.0)l = (0.7 \text{ to } 1.0)\tau v, \quad (6.28)$$

hence

$$a \approx b \approx \sqrt{1.7\tau f} \quad (6.29)$$

The velocity of shear waves in special isopaustic glass is about $2500 \text{ m/s} = 2.5 \text{ mm}/\mu\text{s}$.

6.9.5 DL 711 delay line

Compared with older types of delay line, the DL 711 is very small and light. These improvements result from making the delay line in the form of a thin plate, and giving it oblique end faces to produce multiple reflections.

Figure 6.51 shows the dimensions and shape of the glass plate used for the DL 711 delay line and the path followed by the ultrasound waves. The PZT transducers are bonded to the oblique faces. Delay can be adjusted by trimming the length of the plate (dimension = 30 mm).

Figure 6.52 shows the delay line stripped of its plastic encapsulation. The glass plate is about a wavelength thick and thus forms a waveguide in the thickness dimension, causing the wave-front to be cylindrical. Consequently beam losses caused by spread are less than in older types of delay line in which the wavefront is spherical.

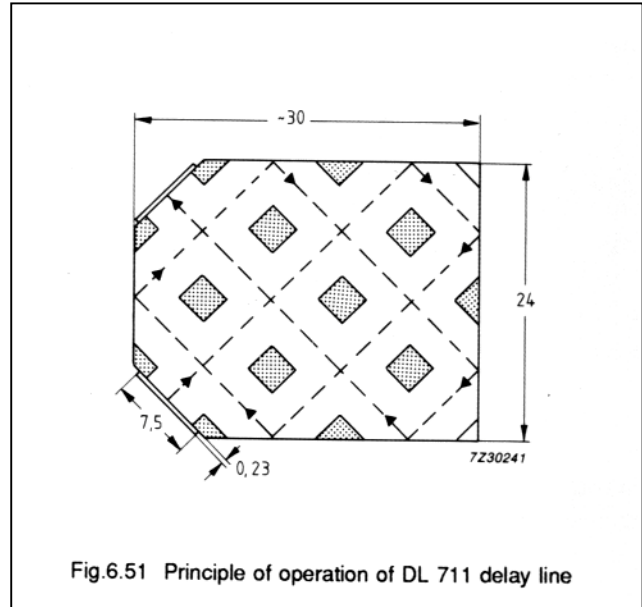


Fig.6.51 Principle of operation of DL 711 delay line

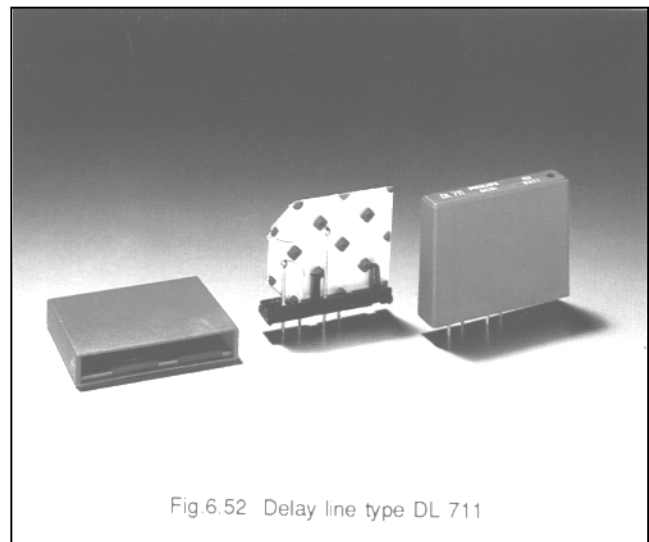


Fig 6.52 Delay line type DL 711

To allow the surface area of the glass plate to be very small, the sound wave is reflected seven times in the DL 711.

Repeated reflections mean more undesired stray waves, but these can easily be suppressed in this type of delay line. Areas of the two glass plates not on the path of the main beam are provided with a damping medium. Stray waves incident on these areas are heavily damped (e.g. 35 dB at frequencies between 3.9 MHz and 4.7 MHz).

The delay medium is a potassium-lead-silicate glass which, by careful selection of its composition, provides a delay almost independent of temperature (isopaustic) over a wide temperature range. Thermal expansion is compensated by a corresponding variation in propagation speed of the ultrasound wave.

The poling direction of the PZT703 transducer is parallel to the longitudinal axis (the long side) of the delay line, which results in a shear wave polarized in the same direction and causes the ultrasound wave to be propagated perpendicular to the longitudinal axis. The glass particles within the range of the ultrasound wave will then move parallel to the glass plate surfaces but perpendicular to the direction of propagation.

Under no-load conditions (in free air) the series - resonant frequency of the PZT703-transducer used for the delay line is about 4.4 MHz. The thickness h of the transducer is calculated as:

$$h = \frac{N_5^E}{f_s} \approx \frac{1025}{4.4 \times 10^6} \approx 230 \mu\text{m}.$$

Remark: Because of some depolarization during soldering and grinding operations, the value of N_5^E used in this formula is higher than the 920 m/s given in Table 2.1.

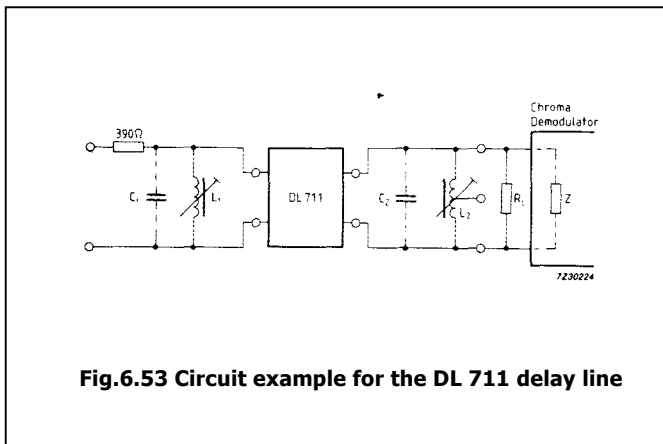


Fig.6.53 Circuit example for the DL 711 delay line

The transducers have no acoustic feedback and are electrically tuned to about the carrier frequency (mid-band frequency) by means of parallel coils. They are terminated by a resistance $R_L = 390 \Omega$, which yields a quality factor of about 2.5. The resulting 3 dB bandwidth ranges from 3.43 to 5.23 MHz.

6.10 PZT -transformers

Piezoelectric transformers are an alternative to wire wound magnetic transformers. They behave differently and have a number of advantages, e.g. they're lighter and smaller, and they have excellent electrical isolation and no magnetic stray flux. For these reasons they've been used as high voltage generators in TV sets. Their drawbacks are that they have only moderate voltage stability under load and their characteristics vary somewhat with temperature.

A PZT -transformer always consists of two transducers generally combined in a single piezo-ceramic body. Figure 6.54 shows two designs, but other configurations like rings or discs are possible. One transducer (input side) transforms the electrical energy into mechanical energy, while the second transducer (output side) converts mechanical energy back into electrical energy.

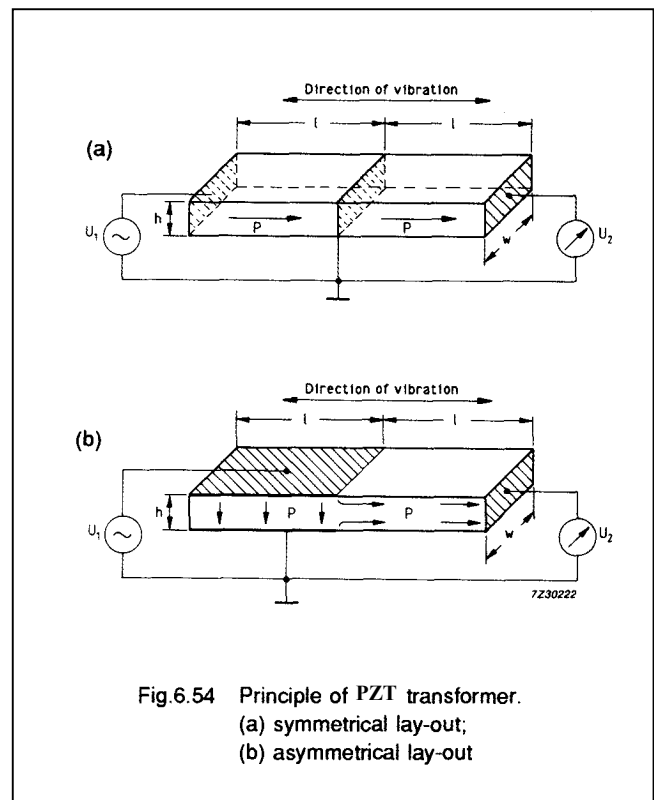


Fig.6.54 Principle of PZT transformer.
(a) symmetrical lay-out;
(b) asymmetrical lay-out

Piezoelectric transformers generally operate in resonant mode. Therefore, geometry, piezoelectric constants and mechanical quality factor govern their behaviour.

The transformer voltage ratio (U_2/U_1) is determined by the dimension of the transducers, their effective coupling factors (k_{eff}) and the mechanical quality factor (Q_m) by:

$$\frac{U_2}{U_1} \approx k_{eff1} \cdot k_{eff2} \cdot Q_m$$

Electrical loading of the PZT -transformer decreases the quality factor, which leads to a strong load dependence of the voltage ratio.

Figure 6.55 shows an approximate equivalent circuit and Fig.6.56 illustrates the computed behaviour of a symmetrical transformer as a function of the secondary load resistance R_2 .

For very high resistances (no load) the voltage ratio is high, but the efficiency is zero.

If the load resistance R_2 is optimally matched to the output capacitance ($R_2 = 1/(\omega C_{o2})$), the efficiency reaches a maximum (≈ 1). The voltage ratio, however, is only $\sqrt{2}$ and the output power shows a minimum. This is because the damping of the transformer increases with R_2 and also reaches a maximum for $R_2 = 1/\omega C_{o2}$. For higher values of R_2 , the damping decreases again, leading, at least to begin with, to higher output power.

With asymmetrical transformers, voltage ratio also depends on the geometry. By suitable choice of geometry, therefore, it's possible with this type of transformer to get high ratios with optimal matching and high efficiency.

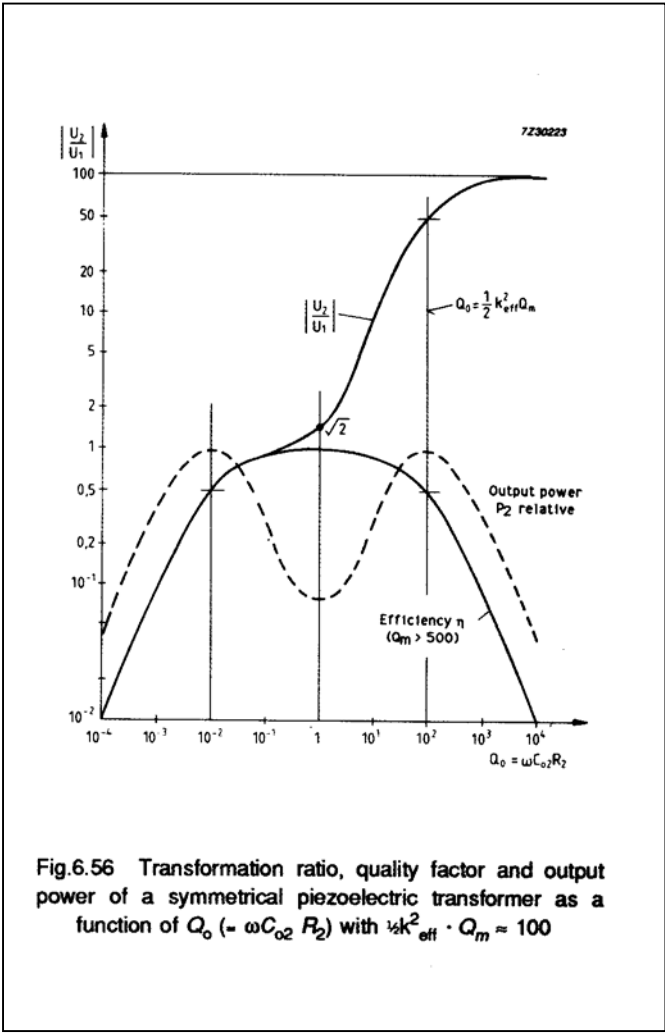
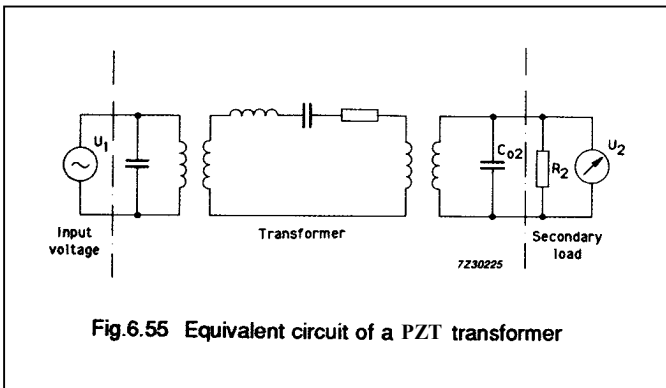


Fig.6.56 Transformation ratio, quality factor and output power of a symmetrical piezoelectric transformer as a function of $Q_0 (= \omega C_{o2} R_2)$ with $\frac{1}{2}k_{eff}^2 \cdot Q_m \approx 100$

7 COMBINED APPLICATIONS

The designs described in this section use PZT transducers both as a transmitter and a receiver, clearly demonstrating the reversible nature of the piezoelectric effect.

Typical examples are ultrasound echo sounders (in air or water), flow meters and the so-called key-finder.

7.1 Echo sounders

7.1.1 General

Ultrasound echo sounders operate of the following principle.

A short pulse of ultrasound is transmitted by the PZT transducer in the direction of the object that need to be located. The waves will be reflected by the object and can be picked up by the receiver. For economy, one transducer is normally used for both transmitting and receiving. The system is electronically switched between transmitting and receiving functions (Fig.7.1). The interval between transmitting and receiving pulses provides a measure of the distance to the object and can be shown on a display.

This operating principle requires a minimum distance between transducer and object. The transducer cannot receive properly before the vibrations caused by the transmission have subsided. The ultrasound pulse should therefore be as short as possible, which calls for a high operating frequency and a large bandwidth. A high operating frequency also means that the transducer can be smaller and more compact.

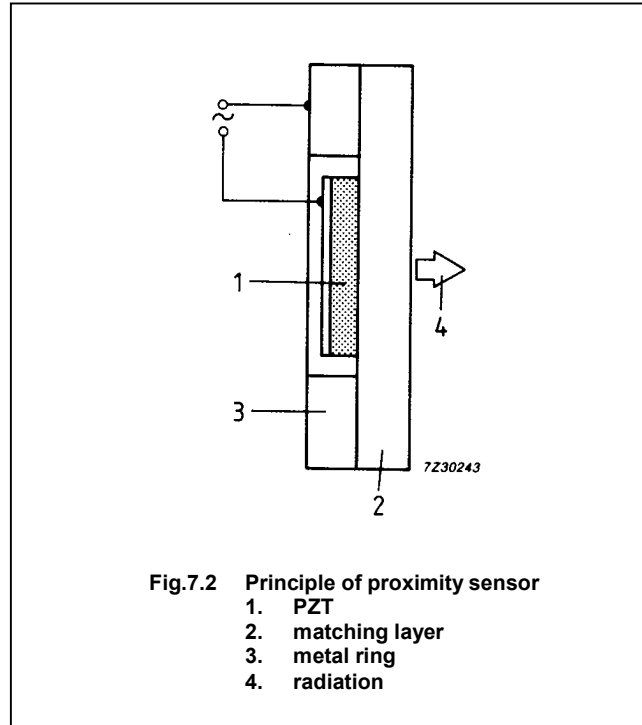
In practice, an echo sounder operating at 200 kHz will have a minimum detection distance of 0.2 m in air. Modern ultrasound devices, like those used in the medical field, operate at several megahertz. These can detect down to the millimetre region, but because of the much higher attenuation at this frequency, their maximum range is limited (see also 6.4.4).

The maximum range depends strongly on the construction of the transducer itself. For a simple echo sounding system, as used on small boats, the maximum range will be about 100 m at an operating frequency of 200 kHz.

7.1.2 Ultrasound proximity switch

An echo sounder can be used as a proximity switch by setting a detection threshold in the pickup circuitry. However, below a distance of 0.2 m the system is no longer reliable and inductive or infrared proximity switches should be considered.

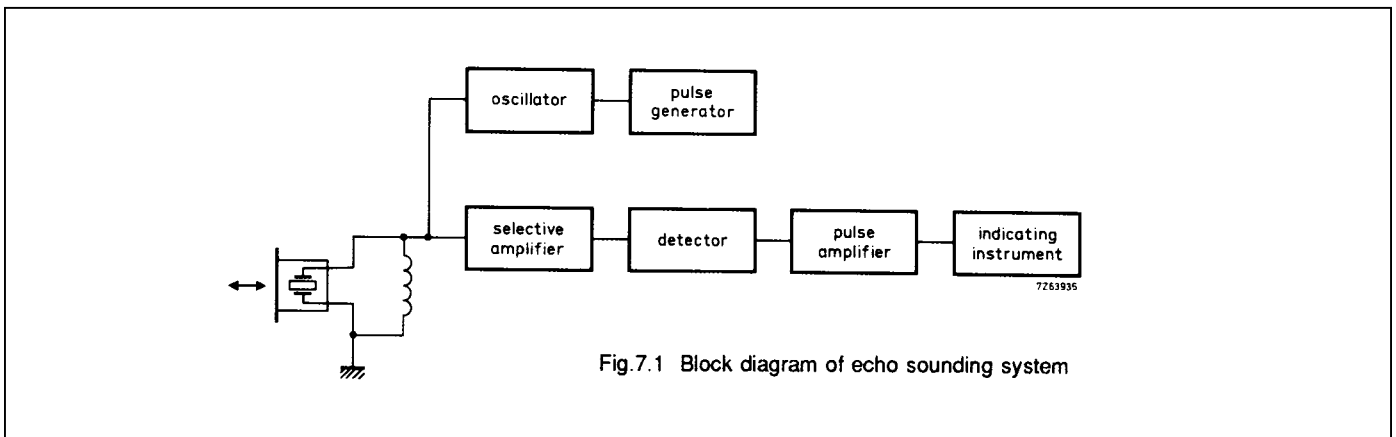
Figure 7.2 shows the basic construction of the proximity switch Ultrasound BERG®.



The piezo-ceramic disc is surrounded by an aluminium alloy ring and covered with a layer of acoustical impedance matching foam. Ultrasound is radiated only from the surface with the matching layer. The directivity is high, beam width is only 5°.

This device can be used as a proximity switch, with the object to be detected acting as a reflector. Another use is for safeguarding an entrance using a fixed mirror. Any object interfering with the beam will be detected.

® Trade mark of Siemens A.G.



7.1.3 Distance measurement in water using ultrasound

Nowadays small ships and boats of all types are fitted with simple but reliable echo sounding equipment, primarily for measuring the depth of water below the keel. Some types of equipment can also be used for detecting fish and, if the sound beam is radiated obliquely, underwater obstructions such as reefs and sandbanks can be detected in time to take avoiding action.

Maximum range

The simple echo sounder systems employed in small boats are usually designed to have a maximum depth range of about 100 m. The range depends on the electronics used, the power output of the transducer and the sensitivity of the receiver. It also depends strongly on the design of the transducer.

Operating frequency

Ideally one wants the smallest possible transducer in an echo sounder, which means high operating frequency. High frequencies are also more suitable for short pulses, which are of particular interest in shallow waters because both minimum measuring distance and resolution depend on the duration of the ultrasound pulse. On the other hand, sound absorption in sea water increases steeply with frequency, and hence a compromise must be found.

For the equipment under consideration (maximum range 100 m), the optimum frequency lies between 150 kHz and 200 kHz. The minimum distance that can be measured is typically 30 cm; resolution should be about half of this figure.

Bandwidth

As the ultrasound pulses become shorter, the bandwidth of the transducer must expand. However, it should not be too broad otherwise selectivity and, consequently, the signal-to-noise ratio will suffer. The required 3 dB bandwidth is about 10 kHz to 15 kHz, corresponding to a mechanical quality factor Q of about 15.

Directivity characteristic

The directivity characteristic of the transducer has an influence on several aspects of echo sounder performance. The range can be increased by concentrating the ultrasound into a narrower beam. At the same time smaller objects are more easily detected. However, this leads to the drawback that the reflected sound intensity will fall off more sharply as the boats heels over, and the depth indicated by the instrument will also increase due to the oblique angle of the transducer. The transducer must be so designed that it radiates only downwards, otherwise there may be interfering echoes from the boat itself or from the surface turbulence of the wake. The directivity characteristic should show the smallest possible side lobes; large side lobes tend

to make the directivity of the main beam ineffective. A suitable 6 dB beam width would be 10° to 30° .

It should be borne in mind that the effective beam width of the transducer becomes smaller if the transducer has the double function of transmitting and receiving: a

6 dB transducer beam width will mean a 12 dB beam width for the complete system.

The ultrasound transducer in echo sounding systems

The higher frequencies required for medium and short range echo sounding could be produced by long cylinders vibrating in the axial 33-mode. The vibrations of the end faces resemble those of a piston and the harmonics are well separated in frequency. However, for the frequency range in question, the radiating area of such transducers is small compared with the acoustic wavelength. This results in the directivity characteristic being almost spherical. Though this can be overcome by mounting several transducers in an array to give a narrower beam, the assembly is then inconvenient and cumbersome. One could instead use a disc whose diameter is large compared with its thickness and drive this at thickness resonance. This would also give a piston-like motion with adequate directivity and a good separation of harmonics, but to achieve a true thickness resonance in this frequency range, the diameter of the disc would be inconveniently large.

A much simpler, cheaper and more compact transducer can be made with a disc whose thickness and diameter are comparable. This results in the resonance being rather complex, because there is then coupling between vibration in the radial and thickness directions and there are several resonances occurring in the required frequency range. However, one of these has some resemblance to a true thickness mode and gives a highly directive beam. The most effective thickness-to-diameter ratio for such a transducer is about 0.4. This gives a strong 'thickness type' resonance reasonably well separated from its neighbours. The frequency of this resonance is largely governed by the thickness of the disc, but the directivity is governed by its diameter, the variation of vibration amplitude across its surface and the working frequency. The admittance graph of Fig.7.3 illustrates the case of a transducer designed to meet the present requirements using a PZT8 disc 31.75 mm in diameter and approximately 14.3 mm thick. The fourth resonance, with $f_s = 151$ kHz, is of the 'thickness type' and is well suited for transducer application because the electromechanical coupling factor is relatively large and the separation from the third and fifth resonance is quite adequate. What's more, the strong axial component of vibration gives good acoustic coupling to water and these disc dimensions give the required directivity characteristic.

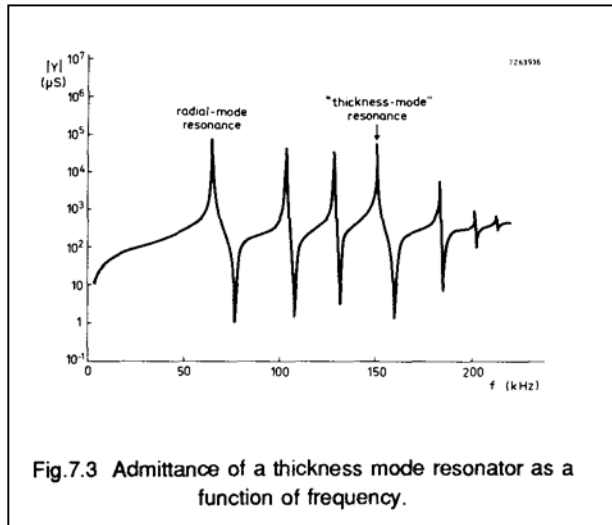


Fig.7.3 Admittance of a thickness mode resonator as a function of frequency.

The transducer must be properly housed to ensure satisfactory functioning of the echo sounder. Figure 7.4 shows a prototype transducer and housing. The PZT disc is mounted in a cup sealed with a moulding compound. Since the transducer must be sensitive in the forward direction only, it would be useful if only the front face of the PZT disc were coupled to the water, the other face and the cylindrical wall of the disc being isolated by air. However, it's found that such a design lacks mechanical strength and that, owing to the low damping, the radial resonances can interfere with the operating resonance. So in general, only the back of the PZT disc is isolated, and not its cylindrical wall. An isolating medium often used is foam rubber which is acoustically equivalent to a layer of air.

The radiating face of the PZT transducer must be protected by an interface layer. Optimum results are obtained if the thickness of the protective layer equals $1/4\lambda$, where λ is the acoustic wavelength in the interface medium. The better acoustic matching this gives increases the bandwidth significantly. For optimum matching, the interface should have a specific acoustic impedance between that of PZT and of sea water. Many synthetic materials, such as epoxy resins and other plastics, fall within this range. In most synthetic materials the propagation speed of sound is between 2.10^3 m/s and 3.10^3 m/s. For the required frequency range (150 kHz to 200 kHz) the optimum layer thickness is about 3 mm.

When selecting the moulding compound for the complete transducer (see Fig.7.4) the following properties should be considered:

- low sound absorption
- adhesive power and elasticity (protection against mechanical damage);
- tolerance to (sea) water and sunlight,
- smooth surface to reduce the growth of algae, and to facilitate cleaning.

A synthetic material is best for the housing for acoustic and economic reasons; metal housings involve resonance problems. However, a brass casting can be much stronger than synthetics.

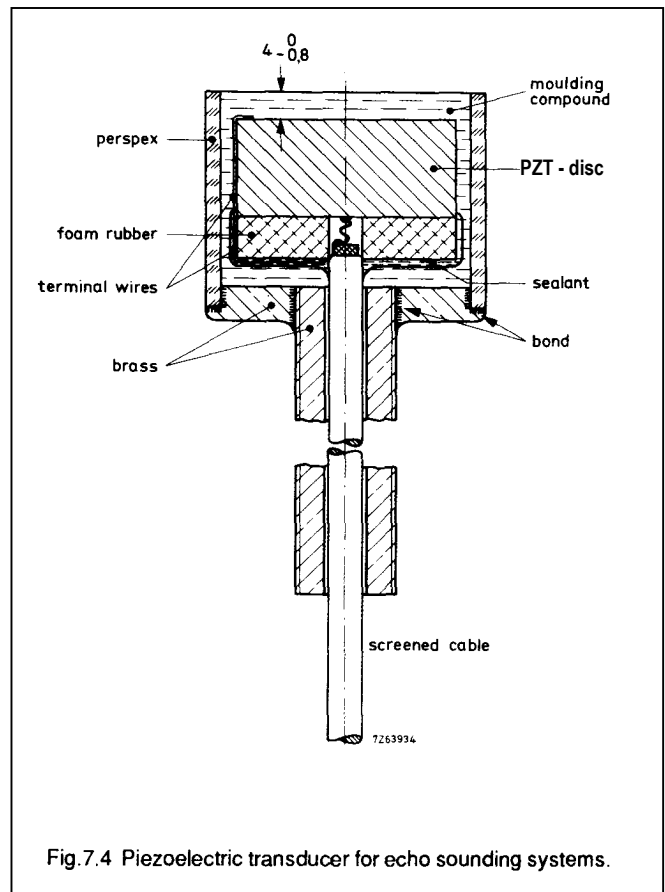


Fig.7.4 Piezoelectric transducer for echo sounding systems.

Electrical matching

The overall transducer impedance has a high capacitance content, much of which comes from the long connecting lead. Good load matching and improved bandwidth are obtained by means of inductive tuning (see Chapter 2.9).

A transducer is characterized by the following quantities:

- frequency (usually the series resonant frequency f_s)
- parallel inductance L_P (tuning);
- impedance of the tuned transducer $|Z_S|$ at f_s ;
- 6 dB bandwidth,
- directivity characteristic.

Other important data are the minimum pulse duration that can be transmitted (which depends on the bandwidth), and the sensitivity, which is a function of the transducer parameters and the terminating impedance. The sensitivity can be derived from the response of the transducer to a fully reflected acoustic pulse at a measured distance.

With this data, the behaviour of the transducer can be calculated fairly accurately. For short range (< 10 m), the echo intensity depends almost solely on distance and on the reflection coefficient of the sea bed. For greater distances the absorption of ultrasound by the water must also be taken into account. At 175 kHz this is about 0.06 dB/m, or 12 dB when operating in a (sea) water depth of 100 m (total path length = 200 m).

7.2 Flow meters

With two PZT -transducers positioned as in Fig.7.5, it's possible to measure the velocity of gases and fluids. Both transducers transmit short pulses simultaneously and then switch to receiving mode immediately. In static media, both delay times are, of course, the same. When there is a flow, pulses are speeded up or delayed by an amount depending on the direction. Delay times are then given by:

$$t_1 = \frac{l}{v + w}, t_2 = \frac{l}{v - w} \quad (7.1)$$

where l is the measuring distance. Flow velocity w is found to be:

$$w = \frac{l}{2} \left(\frac{1}{t_1} - \frac{1}{t_2} \right) \quad (7.2)$$

This equation doesn't contain the sound velocity so this need not be known.

The flow velocity calculated from Eq.7.2 is valid only for the trajectory of the ultrasound waves - the centre of the pipe in Fig.7.5.

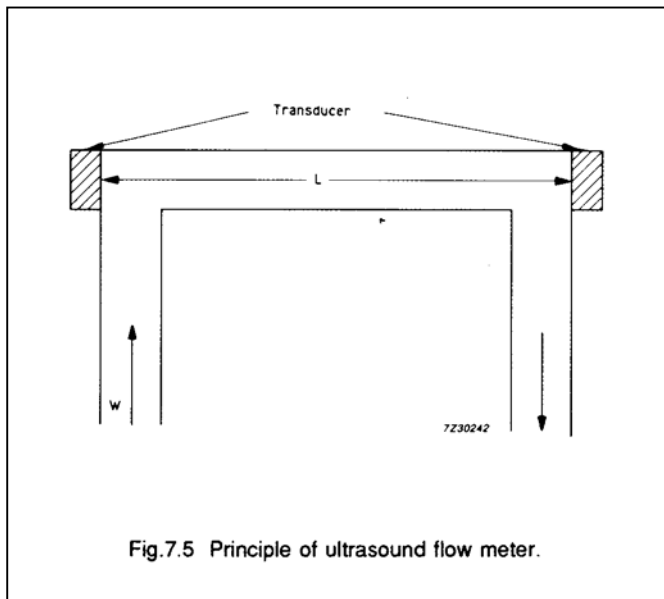


Fig.7.5 Principle of ultrasound flow meter.

Often it's more important to know the average flow velocity, which is a measure of volume throughput (Ref.8). With the transducers positioned as in Fig.7.6, the beam of ultrasound traverses areas with different flow velocities.

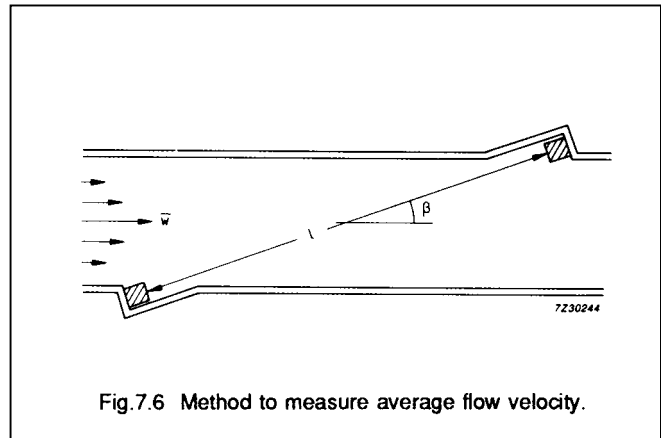


Fig.7.6 Method to measure average flow velocity.

The delay is then a measure for the average flow through the pipe.

$$\bar{w} = \frac{l}{2 \cos \beta} \left(\frac{1}{t_1} - \frac{1}{t_2} \right) \quad (7.3)$$

Sound velocity in a medium is generally a function of temperature, which, in turn, varies with time. Obviously Eqs 7.2 and 7.3 are only independent of sound velocity if it remains constant between the two delay measurements. This can only be expected when both measurements are executed simultaneously.

To improve resolution, different measuring principles based on phase differences or the Doppler-effect are often used.

7.3 Key-finder

A recent application where the PZT -transducer is used as a transmitter as well as a receiver is the so-called 'key-finder'. This is a compact device that, attached to a bunch of keys, reacts to whistling of the owner by emitting penetrating bleeps. This, of course, makes it a lot easier to find the keys.

Figure 7.7 shows the construction of the device. A metal membrane with a glued-on PZT -disc is clamped in a housing in such a way that two Helmholtz resonators with different resonant frequencies are formed.

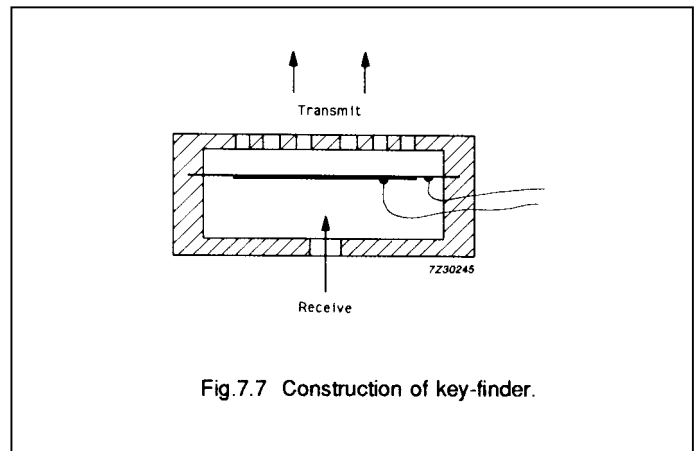
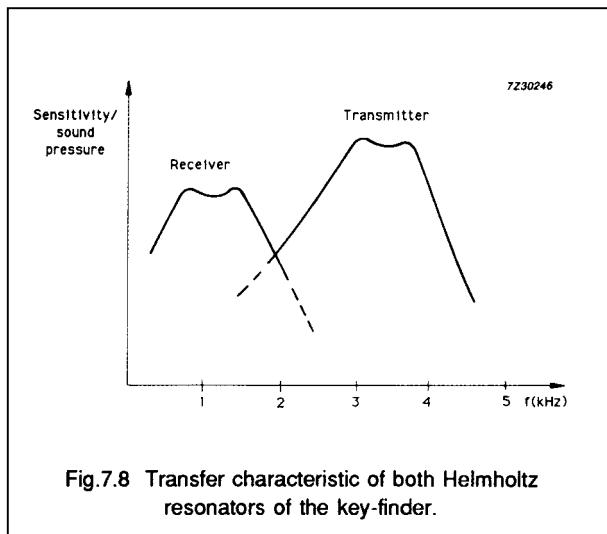


Fig.7.7 Construction of key-finder.



The transfer characteristic therefore shows two peaks, the first is used to receive, the second to transmit.

The peak sensitivity for receiving is situated around 1 kHz. When a whistle of such a frequency is received, the circuit switches to transmit and a penetrating, modulated sound with a frequency between 3 and 4 kHz is produced.

After completion of the series of bleeps the circuit immediately switches back to receive.

8 TESTING PZT DISCS AND PLATES

8.1 General

This chapter describes methods to check the piezoelectric charge- and voltage-constants, polarity and coupling factors of PZT products.

The measuring methods are based on following formulas:

$$E = -g_{33} T \quad (8.1)$$

$$Q = -d_{33} F \quad (8.2)$$

The charge constant d_{33} and the voltage constant g_{33} are related via the dielectric constant of the ceramic by:

$$d_{33} = g_{33} \epsilon_{33}^T \quad (8.3)$$

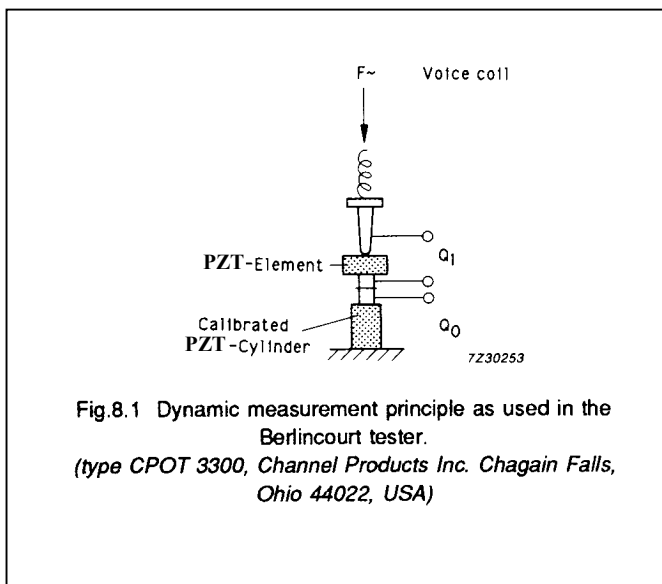
These formulas are valid for PZT -elements stressed in the same direction as their polarization and with the electrodes on the end faces perpendicular to this direction.

For most measurements, only compressive forces are used, which, by definition, have a negative sign. So the electrode that was positive during the polarization will have a positive charge induced on it. Normally this electrode is marked. Upon relaxation of the force, the charge is re-absorbed by the piezoelectric material. A tensile force would induce a negative charge on the marked electrode.

Several methods of measuring charge constant, voltage constant and polarity will be described. The effective coupling coefficient (k_{eff}) will be derived from the resonance behaviour.

8.2 Dynamical methods

With the so-called *Berlincourt* tester, an alternating (e.g. 50 Hz) force is applied to the unknown PZT -element and to a calibrated PZT -cylinder (Fig.8.1) by means of a loudspeaker coil for example. The amplitudes and phases of the voltages from both PZT -elements are compared.

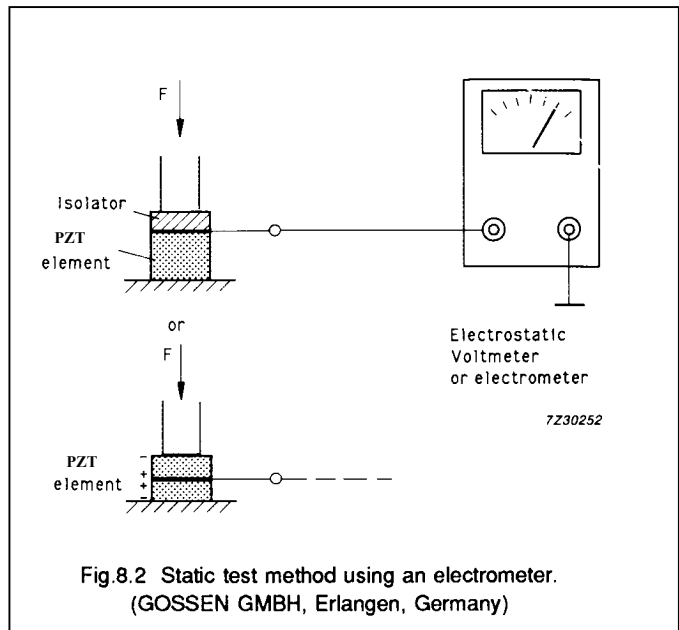


This method is used by many manufacturers to measure polarity and charge constants of piezoelectric products.

A drawback of this method is that the forces are rather low. So the values measured give low-signal properties of the material. Often this is not enough information to predict the actual performance of a piezo device operating at high force levels.

8.3 Quasi static method

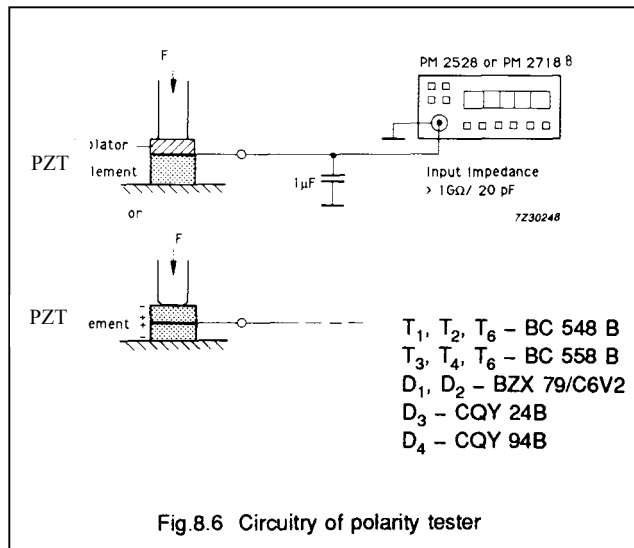
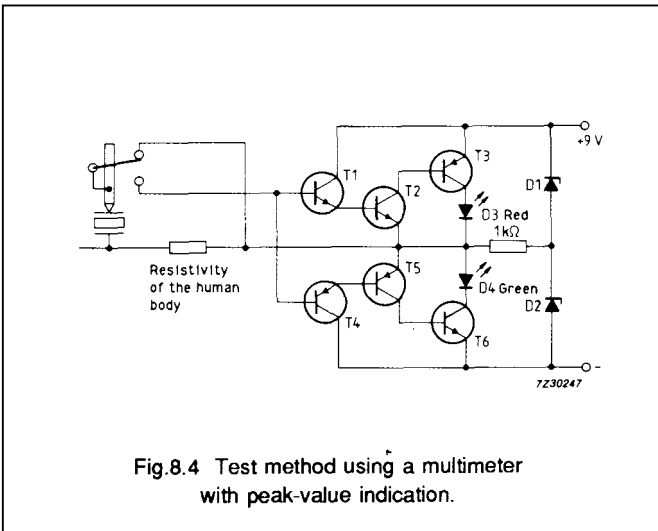
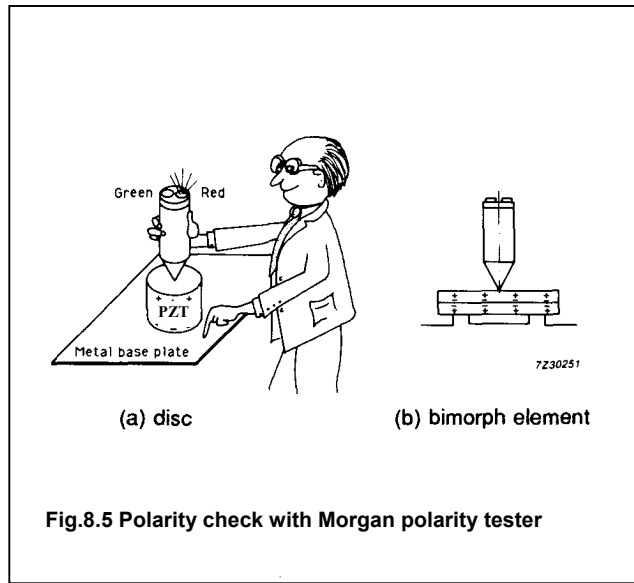
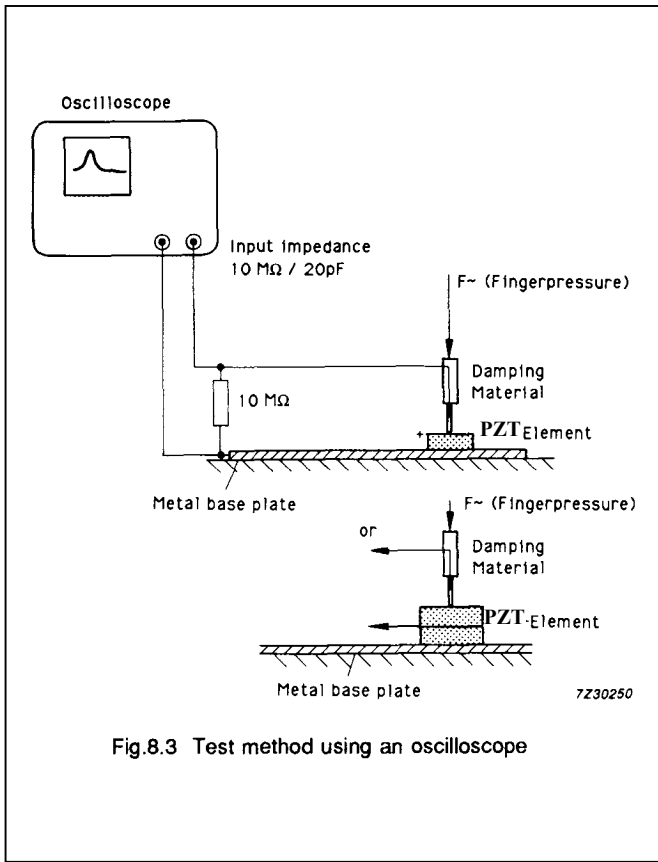
If only polarity needs to be checked, this is a popular method with the advantage that it can be carved out using standard laboratory equipment.



A difficulty might be the low capacitance of the PZT element, which means that the voltage must be measured with equipment having a very high input impedance to give a long enough RC-time (Fig.8.2).

An isolated contact pin is placed on the surface of the product to be tested and then tapped manually (Fig.8.3). The manual tapping should be done via some isolating material with high mechanical damping (e.g. rubber or soft PVC). Because of the mechanical damping, the force will be mainly compressive, no ringing occurs. Since the tapping force is somewhat variable, only polarity can be checked in this way.

The output can be measured on a standard oscilloscope. The high input impedance of this instrument together with the lag introduced by the screen phosphors and the eye's persistence of vision make it possible to observe the positive or negative excursions on the screen.



The sensitivity of PZT is very high. A compressive stress of 1 MPa (10^6 N/m^2) generates a field of about 20 V/mm in PZT5A. For a product of 010 x 3 mm this means that 80 N of force will give rise to a voltage of about 60 V. Forces in this range can easily be applied by hand without any special equipment.

Another way would be to use a modern multimeter (e.g. PM2528). In peak detection mode, the maximum signal observed within a given time frame will be displayed. Input impedances are often so high that RC-times as long as 10 seconds can be attained. With "reproducible" tapping, not only the polarity but also the voltage constant can be estimated with some accuracy.

Morgan's polarity tester

This simple hand-operated instrument is useful for checking the polarity of a PZT element.

The device under test should be placed on a conductive surface. The operator touches this surface with one hand and positions the tester on top of the PZT element (Fig. 8.5). The resistance of the human body is used to close the electrical circuit (no danger!). Then the tester should be pressed down slowly but positively. The switch closes and the charge on the PZT element activates either transistor T_1 or T_4 and the red or green LED lights up. Red means that the electrode on top is the positive one. The RC-time of the circuit is about 0.5 sec. During the period the force is applied, certain variations are unavoidable (the human influence). As the force is released, a negative charge is induced on the positive electrode causing the green LED to flicker. Since this could be misleading, only the indication as the force is being applied should be taken into account.

8.4 The effective coupling factor (k_{eff}) derived from resonance behaviour

The effective coupling factor, k_{eff} is a measure of the piezoelectric quality of a PZT body.

The piezoelectric element is clamped gently between two contacts, preferably in its centre, so that it can vibrate freely (Fig.8.7). An alternating voltage is then applied, for instance by means of an impedance analyser (HP 4192A or 4194A for example), and the frequency is swept through a range around the expected resonant frequency of the element.

Figure 2.12(b) shows the resulting impedance variation. This can be described as follows:

- a steady decrease according to $1/\omega C$
- a sharp decrease to a minimum Z value,
- followed by a sharp increase towards a maximum in the impedance curve,
- levelling off to a slope of $1/\omega C$ again.

This impedance curve comes from the mechanical behaviour of the piezoelectric element.

At low frequencies the element vibrates in phase with the applied voltage. Since electrically the element acts as a capacitor, the impedance decreases linearly with $1/\omega C$.

At a specific frequency (f_m), a mechanical resonance occurs. Here the alternating voltage is exactly in phase with the vibration of the PZT body. The amplitude is multiplied by a factor Q_m (mechanical quality factor). The high strain levels in the PZT cause large charge displacements and thus high current levels. The impedance decreases to a low level.

The minimum level is governed by internal losses and the resistance of leads and electrodes. In the equivalent circuit (Fig.2.11) this is represented by a series resonance (f_s) of L_1 and C_1 , which occurs at practically the same frequency as f_m .

When the frequency is increased still further, the difference in phase between the applied voltage and the mechanical vibration grows. The impedance reaches a maximum for a phase shift of 180° (at f_n). The vibration is then almost entirely suppressed, the voltage generated by the PZT element is in anti-phase with the applied voltage and almost prevents the current from flowing.

In the equivalent circuit, this phenomenon is represented by the parallel resonance of C_0 , C_1 and L_1 (frequency f_p).

Modern impedance analyzers (e.g. HP 4192A) can be combined with a computer and programmed to find f_s , f_p , Z_{min} and Z_{max} . The effective coupling factor k_{eff} then follows from the formula:

$$k_{\text{eff}} = \sqrt{\frac{f_p^2 - f_s^2}{f_p^2}}$$

It's also possible to determine k_{eff} of more complicated devices like bimorphs or PZT discs or plates glued on some substrate.

Depending on the construction different values of k_{eff} will be found. The translation to the *absolute* quality level is often very complicated or impossible. However k_{eff} is always a useful *relative* measure for the effectiveness of a device.

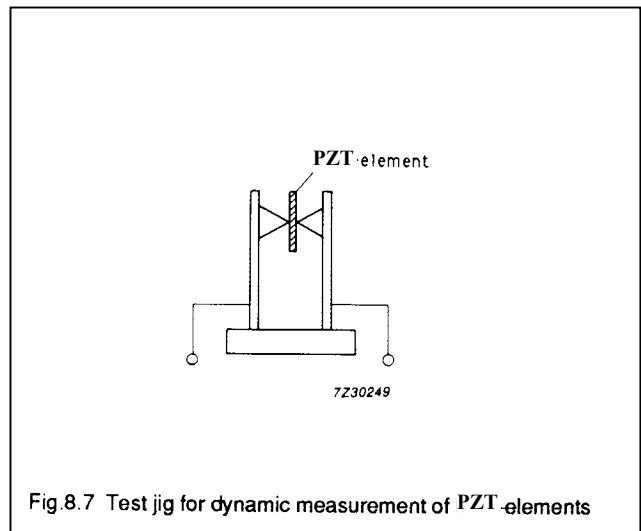


Fig.8.7 Test jig for dynamic measurement of PZT elements

APPENDIX A: MATHEMATICAL RELATIONS

A.1 Piezoelectric relations

The electrical behaviour of an unstressed medium under the influence of an electric field is defined by two quantities - the field strength E and the dielectric displacement D . Their relationship is:

$$D = \epsilon E \quad (A1)$$

in which ϵ is the permittivity of the medium.

The mechanical behaviour of the same medium at zero electric field strength is defined by two mechanical quantities - the stress applied T and the strain S . The relationship here is:

$$S = sT \quad (A2)$$

in which s denotes the compliance of the medium.

Piezoelectricity involves the interaction between the electrical and mechanical behaviour of the medium. To a good approximation this interaction can be described by linear relations between two electrical and mechanical variables:

$$\begin{aligned} S &= s^E T + dE \\ D &= dT + \epsilon^T E \end{aligned} \quad (A3)$$

The choice of independent variables (one mechanical, T , and one electrical, E) is arbitrary. A given pair of piezoelectric equations corresponds to a particular choice of independent variables. In a similar way it is possible to arrive at the following formulae:

$$E = -gT + \frac{D}{\epsilon^T} \quad (A4)$$

$$S = s^D T + gD$$

$$E = -hS + \frac{D}{\epsilon^S} \quad (A5)$$

$$T = c^D S - hD$$

$$D = dS + \epsilon^S E \quad (A6)$$

$$T = c^E S - eE$$

In these equations, S^D , S^E , ϵ^T , ϵ^S , d and g are the main practical constants and they require further explanation. The superscripts to the symbols denote the quantity kept constant under boundary conditions. For instance, if by short-circuiting the electrodes the electric field across the piezoelectric body is kept constant, superscript E is used. By keeping the electrode circuit open, the dielectric displacement is kept constant and superscript D is used. So S^D and S^E are the specific elastic compliances (strain per unit stress) for a constant electric charge density and constant electric field respectively. Terms ϵ^T and ϵ^S are the permittivities (electric displacement per unit field strength) at constant stress and constant strain respectively.

In reality, Eqs A3 to A6 are tensor equations with, in the general case, 3 electrical quantities (in the X, Y and Z directions) and 6 mechanical ones including the shear about the three axes. So, of each piezoelectric parameter, up to 18 varieties can exist and are indicated by subscripts.

For piezoelectric materials the direction of polarization is usually taken to be that of the Z-axis (direction 3).

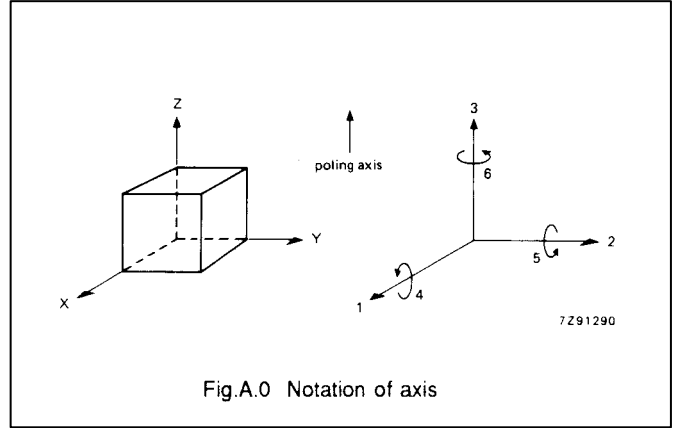


Fig.A.0 Notation of axis

In practical cases, only a limited number of combinations are important.

Examples

- d_{33} is the strain in the 3-direction per unit applied field in the 3-direction, the piezoelectric body being mechanically free and not subjected to fields in the 1- and 2-direction.
- g_{31} is the field developed in the 3-direction per unit stress applied in the 1-direction when there are no other external stresses.
- k_{31} denotes the coupling coefficient between the stored mechanical energy input in the 1-direction and the stored energy converted in the 3-direction or vice versa.

It follows from Eqs A3 and A4 that there are two ways of defining the piezoelectric constants d and g . So d can be defined as a quotient of either S and E or D and T . Similarly g can be defined from two other quotients (see Table A1).

Terms C^D and C^E are the elastic stiffnesses (stress per unit strain) and h and e piezoelectric constants. They are seldom used in practice and therefore these four constants are not given in the material tables.

It can easily be demonstrated that the two units given for d and for g are dimensionally the same. The relations between electrical and mechanical variables are based on energy equations. For instance Eqs A3 lead to:

$$\frac{1}{2}ST - \frac{1}{2}s^E T^2 + \frac{1}{2}dET = w_1 + w_{12} \quad (A7a)$$

and

$$\frac{1}{2}DE - \frac{1}{2}dET + \frac{1}{2}\epsilon^T E^2 = w_{12} + w_2 \quad (A7b)$$

W_1 , W_2 and W_{12} are the mechanical-, electrical- and piezoelectric energy density. The coupling factor is defined (Ref.9) as:

$$k = \sqrt{\frac{W_{12}^2}{W_1 W_2}} \quad (A8)$$

By substitution of energy terms from Eqs A7:

$$k^2 = \frac{d^2}{s^E \epsilon^T} \quad (A9)$$

From Eqs A3 and A4 it follows that

$$d = \epsilon^T g \quad (A10)$$

and

$$s^D = s^E \left(1 - \frac{d^2}{s^E \epsilon^T} \right) \quad (A11)$$

In a similar manner, the following relationships come from Eqs A4 and A5:

$$g = s^D h \quad (A12)$$

and

$$\epsilon^s = \epsilon^T \left(1 - \frac{d^2}{s^E \epsilon^T} \right) \quad (A13)$$

In combination with Eq A9 this leads to:

$$s^D = s^E (1 - k^2) \quad (A14)$$

$$\epsilon^s = \epsilon^T (1 - k^2) \quad (A15)$$

and from Eq A15 it follows that:

$$k^2 = \frac{\epsilon^T - \epsilon^s}{\epsilon^T} \quad (A16)$$

Where this coupling factor applies to a PZT element with random dimensions it's referred to as effective coupling factor (k_{eff}). Because of the tensor character of the above equations, k_{eff} describes energy conversion in all directions. When only conversions in specific directions are taken into account, the resulting coupling factor is indicated by subscripts.

Multiplication of Eq.A16 by $E^2/2$ demonstrates that k_{eff}^2 can be expressed as a quotient of energy densities.

$$k_{eff}^2 = \frac{\frac{1}{2}\epsilon^T E^2 - \frac{1}{2}\epsilon^s E^2}{\frac{1}{2}\epsilon^T E^2} \quad (A17)$$

TABLE A1
Definition of the constants d and g

constant	definition	S.I. units*		
d	dielectric displacement developed	coulombs/metre ²	or	C
	applied mechanical stress ($E = \text{constant}$)	Pa		N
	strain developed	metres/metre	or	m
	applied field ($T = \text{constant}$)	volts/metre		V
g	field developed	volts/metre	or	Vm
	applied mechanical stress ($D = \text{constant}$)	Pa		N
	strain developed	metres/metre	or	m ²
	applied dielectric displacement ($T = \text{constant}$)	coulombs/metre ²		C

Note: It can be shown that both units for the same constant are of the same dimensions. In the S.I. system of units they are also numerically identical.

In this equation $\frac{1}{2}e^T E^2$ represents the total stored energy density for the freely deforming PZT body ($T=0$). The term $\frac{1}{2}e^T E^2$ represents the electrical energy density when the body is constrained ($S=0$). The difference between these two terms (numerator) equals the stored, converted, mechanical energy.

This energy can often be extracted and the unconverted energy can also be recovered. Although a high k is desirable for efficient transduction, k^2 should not be thought of as an efficiency since this is defined as the ratio of the *usefully* converted power to the input power. Properly tuned and matched piezoelectric ceramic transducers operating at resonance can achieve efficiencies of well over 90%.

The same reasoning can be applied to the equivalent circuit of a piezoelectric transducer (Fig.2.11). Under stationary conditions the energy is stored in both capacitances. The mechanical energy in C_1 and the electrical energy in C_0

Equations (A17) transforms to:

$$k_{\text{eff}}^2 = \frac{C_1}{C_0 + C_1}$$

By using equations:

$$f_s = \frac{1}{2\pi} \sqrt{\frac{1}{L_1 C_1}} \quad (2.7)$$

and:

$$f_p = \frac{1}{2\pi} \sqrt{\frac{C_0 + C_1}{L_1 C_0 C_1}} \quad (2.8)$$

this ratio can be expressed as a function of series- and parallel resonant frequency,

$$k^2 = \frac{f_p^2 - f_s^2}{f_p^2} \quad (A19a)$$

So it's possible to derive the coupling factor from these resonant frequencies. As an approximation, when $k_{\text{eff}} \ll 1$ one may write:

$$k_{\text{eff}}^2 \approx 2 \frac{f_p - f_s}{f_s} = 2 \frac{\Delta f}{f_s} \quad (A19b)$$

When mechanical and electrical variables act only in specific directions, subscripts are added to the coupling factor, indicating the direction of the driving force (or field) and that of the resulting effect. The resonant frequencies are derived from the applicable vibration mode.

Example 1

Assume that forces act only in direction 1 and the electrical energy is available in direction 3.

The coupling factor between these variables is given by:

$$k_{31}^2 = \frac{d_{31}^2}{s_{11}^E \epsilon_{33}^E} \quad (A20)$$

Example 2

When an electrical field is applied to a PZT disc in direction 3, radial forces act in direction 1 and 2, leading to radial vibrations. Equations A3 now give:

$$S_1 + S_2 = 2 (s_{11}^E + s_{12}^E) T_1 + 2d_{31} E_3 \quad (A21a)$$

$$D_3 = 2 d_{31} T_1 + \epsilon_{33}^S E \quad (A21b)$$

The planar coupling factor is according to Eq.A8:

$$k_p^2 = \frac{2 d_{31}^2}{\epsilon_{33}^E (s_{11}^E + s_{12}^E)} \quad (A22)$$

Poisson's ratio is a measure of the compressibility of the medium:

$$\sigma^E = - \frac{s_{12}^E}{s_{11}^E} \quad (A23)$$

Combined with Eq.A22 this leads to:

$$k_p^2 = \frac{2 k_{31}^2}{1 - \sigma^E} \quad (A24)$$

The coupling factors in these examples refer to specific directions. Constraints in other directions are not taken into account, although they are there in most real products. To measure these special coupling factors samples should have specific shapes. Therefore they only appear in datasheets and catalogues to specify material properties.

A.2 Coupling coefficient chart

The graph of Fig.AI shows the relationship between the various material coupling coefficients and the relative frequency interval between f_s and f_p for the relevant fundamental resonance. The curves are related to three different modes of vibration.

- Thin-walled ring resonators in uniform radial vibration:
 k_u as a function of $\Delta f/f_s$.
- Half-wavelength resonators: wave propagation perpendicular to the AC field: $k_{\lambda/2\perp}$ as a function of $\Delta f/f_s$;
wave propagation parallel to the AC field:
 $k_{\lambda/2\parallel}$ as a function of $\Delta f/f_p$.
- Planar (radial) thin disc resonators:
 k_p as a function of $\Delta f/f_s$.

The effective coupling coefficient of an arbitrary type of resonator is given by the mathematical relation:

$$\frac{k_{\text{eff}}^2}{1 - k_{\text{eff}}^2} = \frac{f_p^2 - f_s^2}{f_s^2}$$

Since for a thin ring the coupling coefficient k_u is given

by:
$$\frac{k_u^2}{1 - k_u^2} = \frac{f_p^2 - f_s^2}{f_s^2} \quad (\text{A25})$$

it follows that

$$k_{\text{eff}} = k_u.$$

For resonators of the types (b) and (c), consisting of one piece and provided with full electrodes, we have:

$$k_{\text{eff}} \approx 0.9k. \quad (\text{A26})$$

Equations pertaining to FigA1

The curves in Fig.A 1 have been calculated using the more complicated mathematical relations given below which are valid only when the resonance is sufficiently strong for the following condition to be met:

$$\left| \frac{Y_{\text{max}}}{Y_u} \frac{f_u}{f_s} \right| \geq 10$$

in which the term Y_u is the admittance at a frequency f_u far below f_s .

$$\left. \frac{k_{mneff}^2}{1 - k_{mneff}^2} \right\} - 2 \frac{\Delta f}{f_s} \left(1 + \frac{1}{2} \cdot \frac{\Delta f}{f_s} \right) \equiv \frac{f_p^2 - f_s^2}{f_s^2} \quad (\text{A27})$$

$$\frac{k_{mnu}^2}{1 - k_{mnu}^2}$$

$$\frac{k_{mn\lambda/2\perp}^2}{1 - k_{mn\lambda/2\perp}^2} = \frac{\pi}{2} \left(1 + \frac{\Delta f}{f_s} \right) \tan \left(\frac{\pi}{2} \cdot \frac{\Delta f}{f_s} \right) \quad (\text{A28})$$

(if wave propagation is perpendicular to the AC field);

$$k_{mn\lambda/2\perp}^2 = \frac{\pi}{2} \left(1 - \frac{\Delta f}{f_p} \right) \tan \left(\frac{\pi}{2} \cdot \frac{\Delta f}{f_p} \right) \quad (\text{A29})$$

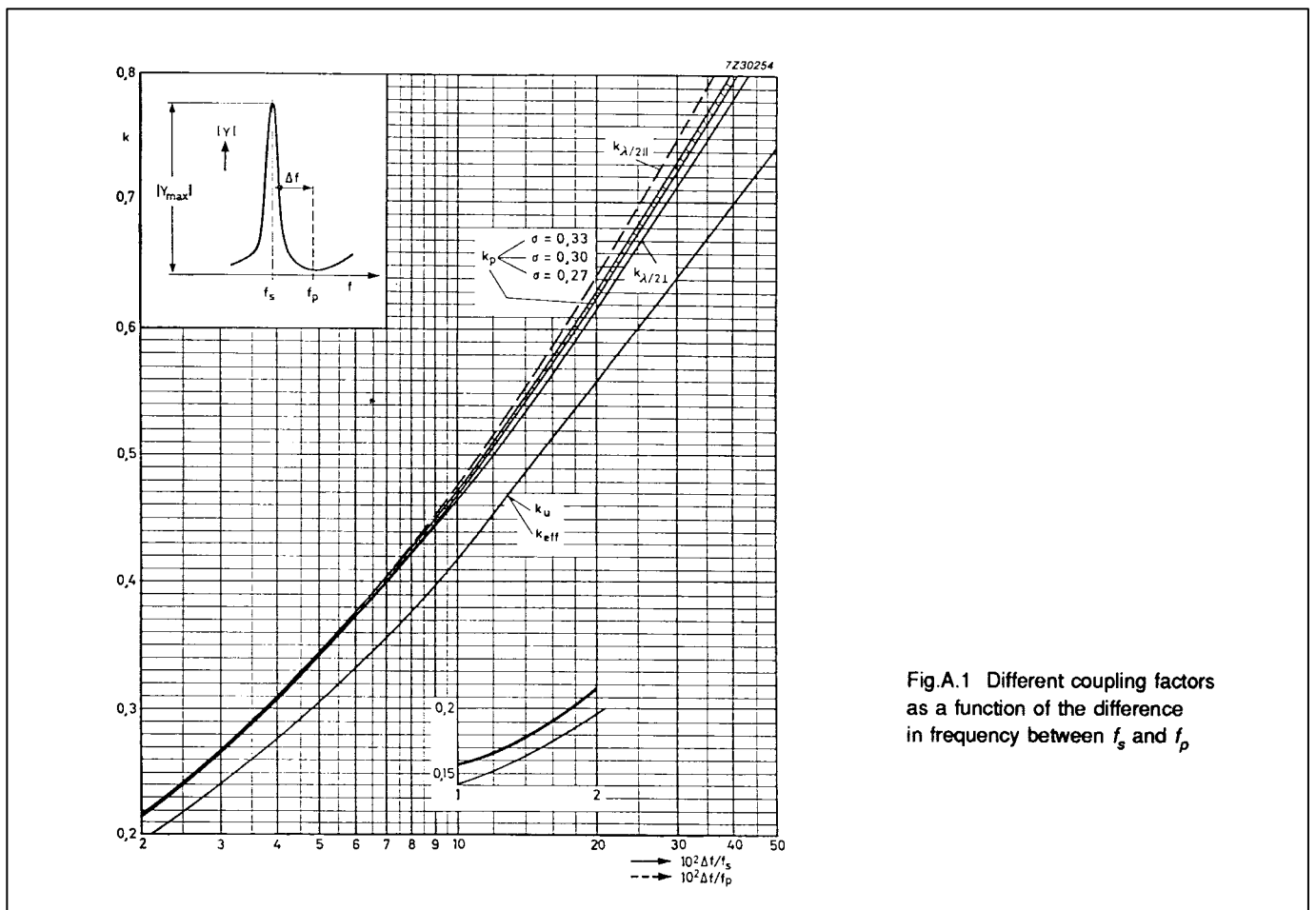


Fig.A.1 Different coupling factors as a function of the difference in frequency between f_s and f_p

(if the wave propagates in the same direction as the AC field, e.g., for $k_{33} \lambda/2$ and $k_{t \lambda/2}^2$);

$$\frac{k_p^2}{1 - k_p^2} = \frac{1 - \sigma_{12}^E}{1 + \sigma_{12}^E} \quad (\text{A30})$$

$$- \frac{R_1}{1 + \sigma_{12}^E} \left(1 + \frac{\Delta f}{f_s} \right) \frac{J_0 \left\{ R_1 \left(1 + \frac{\Delta f}{f_s} \right) \right\}}{J_1 \left\{ R_1 \left(1 + \frac{\Delta f}{f_s} \right) \right\}}$$

where J_0 and J_1 represent the zero-order and first-order primary Bessel functions.

The term $R_1 = \omega_1 r / v$ is the lowest positive root of the equation

$$(1 - \sigma_{12}^E) J_1(R) = R J_0(R)$$

in which r is the radius of the disc, v is the velocity of sound in the plane of the disc with zero AC field, and $\sigma_{12}^E = S_{12}^E / S_{11}^E$. For example, $R_1 = 2.05$ for $\sigma_{12}^E = 0.30$ (Ref.10).

A.3 Measurement of mechanical resonant frequency and quality factor

Figure A2 shows the basic circuits to measure admittance and impedance as a function of frequency. The quality factors can be derived from the 3 dB bandwidth.

$$Q_m^E = \frac{f_s}{\Delta f_s(3 \text{ dB})} = \frac{f_s}{f_2 - f_1} \quad (\text{A31})$$

$$Q_m^D = \frac{f_p}{\Delta f_p(3 \text{ dB})} = \frac{f_p}{f_4 - f_3} \quad (\text{A32})$$

(valid only when $k^2 Q_m > 10$. For explanation of f_1, f_2, f_3 and f_4 refer to Fig. 2.12)

The equivalent circuits of transducers that operate as sound receivers (microphones) or sound transmitters, are given in Fig.A3.

Apart from f_s and f_p there is a maximum response frequency f_m of the transducer, at which the modulus of its transfer function reaches a maximum. This is the frequency at which the microphone has maximum sensitivity and at which a transmitter gives maximum sound output. The frequency f_m , the bandwidth and the output power are influenced by the external resistance R_i , which can be either the input impedance of the microphone amplifier or the internal impedance of a generator. When $k_{\text{eff}} \ll 1$, which it is in most practical cases, the following holds:

$$f_M = f_s + \frac{f_p - f_s}{1 + 1/Q^2} \quad (\text{A33})$$

(with $Q = \omega_s C_0 R$)

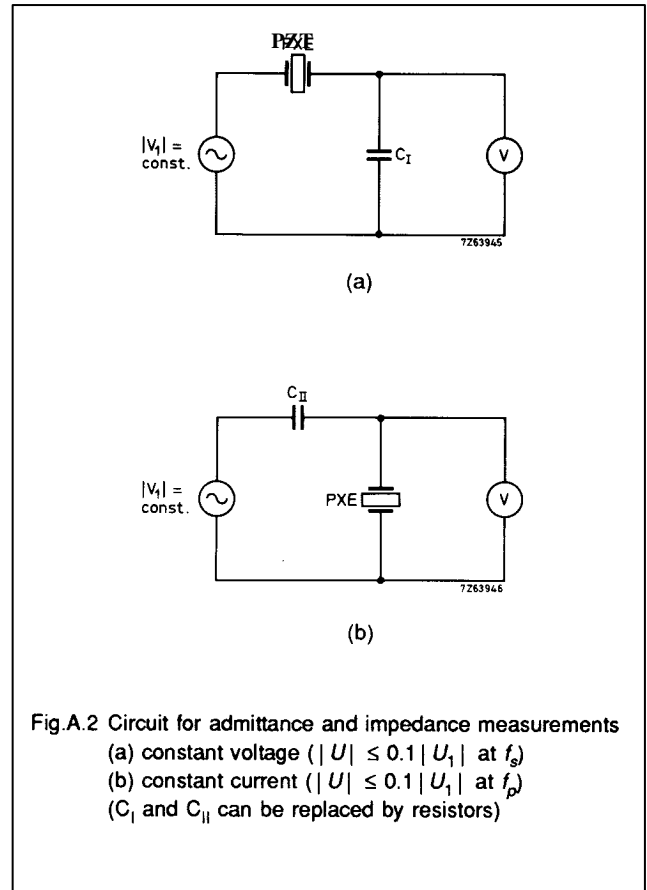


Fig.A.2 Circuit for admittance and impedance measurements
(a) constant voltage ($|U| \leq 0.1 |U_1|$ at f_s)
(b) constant current ($|U| \leq 0.1 |U_1|$ at f_p)
(C_I and C_{II} can be replaced by resistors)

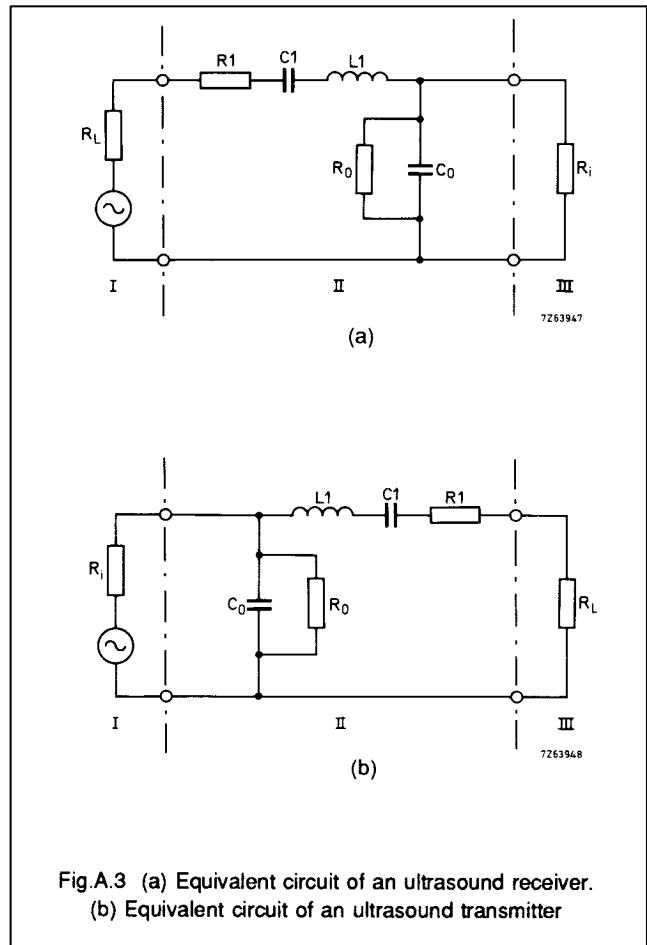


Fig.A.3 (a) Equivalent circuit of an ultrasound receiver.
(b) Equivalent circuit of an ultrasound transmitter

So:

$$f_M = f_s \text{ for } Q \ll 1$$

(short circuit conditions, R_i small)

$$f_M = f_p \text{ for } Q \gg 1$$

(no-load conditions, R_i large)

For $Q = 1$ the frequency f_M is midway between f_s and f_p .

The approximate bandwidth can be calculated from:

$$(\Delta f_M)_{3dB} = (\Delta f_s)_{3dB} \cdot \left(1 + \frac{Q Q_m^E k_{eff}^2}{1 + Q^2} \right) - \frac{f_s}{Q_m^E} \left(1 + \frac{Q Q_m^E k_{eff}^2}{1 + Q^2} \right) \quad (A34)$$

Near to f_p this equation loses accuracy (compare with Eq.A32).

Maximum bandwidth is obtained when $Q_m = 1$ with:

$$(\Delta f_m)_{3dB} = (\Delta f_s)_{3dB} \left(1 + \frac{Q_m^E k_{eff}^2}{2} \right) \quad (A35)$$

Optimum power matching is also obtained when $Q = 1$ with $k_{eff}^2 Q_m^E \leq 2$.

Matching can be considerably improved by means of inductive tuning.

When $k_{eff}^2 Q_m^E > 2$, optimum matching may be achieved at two different values of R_i . Matching to minimum impedance at f_s with $R_i \approx |Z(f_s)| \approx R_1 + R_{L1}$ or to maximum impedance at f_p with $R_i \approx |Z(f_p)|$.

A4 Frequency constant for thick discs

Some applications, like echo sounders, use PZT transducers in the form of discs where the thickness (h) and diameter (d) are of the same order. Vibration modes will therefore not be easy to predict by means of the frequency constants given for the materials. These apply to either thin discs or long bars.

To solve this problem, we have measured f_s of a number of PZT5A discs with various thickness-to-diameter ratios (short circuit conditions, $E = 0$).

Resonant frequencies found are multiplied by h and d respectively and then plotted in a graph. For discs with constant h/d -ratio, all resonant frequencies lie on a straight line. Basic resonances and overtones are numbered and connected by the curved lines.

Specific frequency constants from the data sheets, valid for very high or very low h/d -ratios, are marked in the graph.

$$\begin{aligned} N_p^E &= 2000 \text{ Hz m} \\ N_3^D &= 1850 \text{ Hz m} \\ N_3^E &= \frac{1}{2} V_3^E = \frac{1}{2\sqrt{\rho S_{33}^E}} = 1340 \text{ Hz m} \end{aligned} \quad (A36)$$

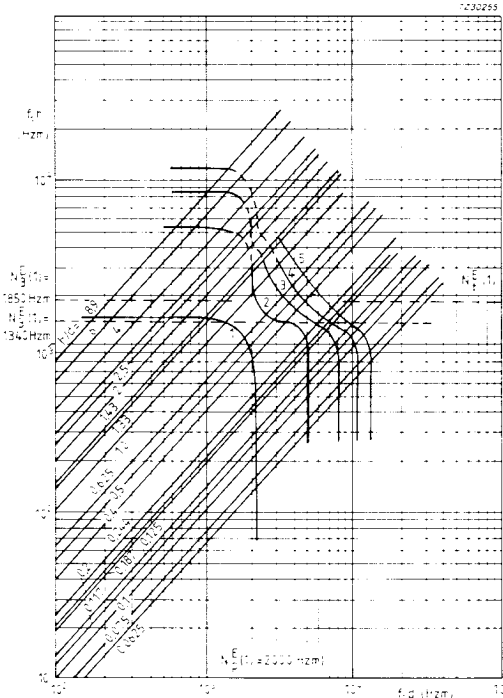
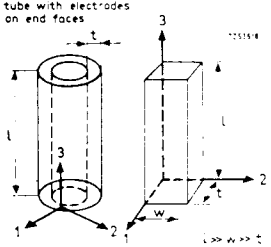
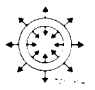
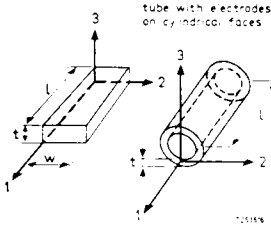
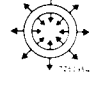

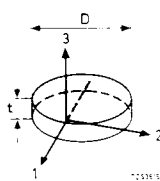
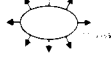


Fig.A.4 Frequency constants of PZT5A discs and cylinders with the h/d ratio as a parameter

APPENDIX B: COUPLING FACTORS AND FREQUENCY CONSTANTS FOR 4 DIFFERENT MODES OF VIBRATION

In literature, the symbol N_3 (frequency constant for length mode with parallel excitation) is often used to indicate the constant for thickness mode. Here the symbol N_T will be used for this mode.

resonant element with electrodes	biasing polarization	a.c. field and polarization	main component of a.c. stress and strain	conditions satisfied	pertinent coupling factor and frequency constant vibrational mode
	↑	↑ ↓ E_3, D_3	↑ ↓ T_3, S_3 (axial direction in tube)	$S_1 = S_2 = 0$ $T_1 = T_2 = 0$	$(k_{33})T_1T_2 = k_{33}$ $(N_T^E)T_1T_2 = N_3 = f_l t$ length mode with parallel excitation
			parallelepiped T_1, S_1  tube T and S in radial direction	$S_2 = S_3 = 0$ $T_2 = T_3 = 0$	$(k_{31})S_2S_3 = k_{31}^*$ $(N_1^E)S_2S_3 = N_1^* = f_r t$ thickness mode with transverse excitation
	↑	↑ ↓ E_3, D_3	 tube T and S in radial direction parallelepiped ↑ ↓ T_3, S_3	$S_1 = S_2 = 0$ $T_1 = T_3 = 0$	$(k_{33})S_1S_2 = k_t$ $(N_3^E)S_1S_2 = N_t = f_r t$ thickness mode with parallel excitation
			 T_1, S_1 (axial direction in tube)	$S_2 = S_3 = 0$ $T_2 = T_3 = 0$	$(k_{31})T_2T_3 = k_{31}$ $(N_1^E)T_2T_3 = N_1 = f_l t$ length mode with transverse excitation
	↑	↑ ↓ E_3, D_3	 T_1, S_1 (radial direction) (also T_2, S_2 in circular direction)	$S_3 = 0$ $T_3 = 0$	$k_{31} \sqrt{2(1-\sigma)} = k_p$ $N_p^E = N_p = P_r D$ planar mode with transverse excitation
			↑ ↓ T_3, S_3	$S_1 = S_2 = 0$ $T_1 = T_2 = 0$	$(k_{33})S_1S_2 = k_t$ $(N_3^E)S_1S_2 = N_t = f_r t$ thickness mode with parallel excitation

APPENDIX C: BONDING TECHNIQUES

C.1 Gluing

In most applications, PZT elements have to be fixed to some substrate. The three principal methods to do so are:

- clamping
- gluing
- soldering.

Clamping is often found to be an unreliable method. The function of the PZT element is, of course, to move. It is very difficult to stop the minute vibrations that will sometimes allow the element to "walk" out of the clamp.

Soldering has the advantage of giving a conductive connection. A drawback is that the movement will cause fatigue in the bond.

Gluing is usually the best approach. Modern epoxy- or acrylate glues, in particular, provide strong yet still flexible joints between adjacent surface. There is no fatigue and operating temperatures up to 150 °C are no problem for some of the glues (e.g. AT131, AV8, AV118 from Ciba Geigy).

These glues are hot setting. Where this is a problem or fast curing is essential, general-purpose epoxys like UHU-plus, Araldite Rapid etc. can be used with good results, though the temperature range is limited.

Electrical contact between the substrate and the electrode on the PZT is nearly always required. One possibility is to use conductive glue, usually an epoxy filled with particles. A drawback of these glues is that they are so heavily loaded with conductive particles that the glue line is often weak. What's more, the fact that the glue has a "three-dimensional" conductivity can lead to short-circuits.

Another way is to roughen one of the surfaces to be glued. If the glue is cured under a pressure of say 10^5 Pa (10^5 N/m²), many point contacts between the surfaces will be formed. This method, however, is not very reproducible.

A better way is to mix nickel powder¹⁾ with a well-defined particle size of about 10 µm into the glue (≈10% by weight). Again pressure during curing must be applied.

Since the nickel particles are almost ideal spheres (carbonyl-nickel process) they tend to form a monolayer between the surfaces.

Because of the pressure, thousands of point contacts will provide a reliable electrical connection. Only around 2% of the surface area is occupied by the nickel spheres so the quality of the glue line is hardly influenced. Moreover, the volume percentage of the nickel particles is so low that there is no risk of short circuit by excess of glue. This is a real one dimensionally conductive glue.

¹⁾ Inco Europe Ltd., Thames House Millbank, London SW 1 P4QF

Depolarization during gluing

Hot setting epoxy glues give high quality bonds. Temperatures during curing can be so high that they affect the piezoelectric activity of the element. The following indicates the extent of the potential damage

PZT5A

1 hour, 170 °C @ k_{eff} - 10%

1 hour, 210 °C @ k_{eff} - 20%

PZT4

1 hour, 200 °C @ k_{eff} - 10%

1 hour, 280 °C @ k_{eff} - 20%

C.2 Soldering

The electrodes on our PZT elements are of nickel or silver.

The nickel electrodes are vacuum-evaporated (layer thickness 0.2 - 0.5 µm), the silver electrodes are burnt in silver paste (layer thickness about 5 µm). Soldering on these surfaces is possible. Recommendations are given below.

Soldering of contact wires

Silver electrodes:

Occasionally it will be necessary to remove a surface layer of silver sulphide which is formed by contact with a polluted atmosphere. An efficient tool for this operation is a so-called glass brush. After removing the layer, use a small soldering iron and adjust the tip temperature to 250 °C to 300 °C. SnPb 60/40 can be used as a solder. Keep soldering time as short as possible (3 ± 1 second) and use a lightly activated resin as a flux²⁾

Nickel electrodes:

To solder to the nickel plated surface, the iron temperature should be at least 400 °C. In combination with the activated resin this high temperature helps to remove the oxidized top layer quickly. Again keep soldering time short (3 sec. max.) to reduce the heat flow to the ceramic as much as possible.

If depolarization occurs, it will only be very local if these guidelines are followed.

2)

"Fluitin", SnPb 60/1532

"Billiton", SnPb 60/RS4

"Multicore", SnPb 60/366

LITERATURE

1. CADY, W., Piezoelectricity, Dover Publications, New York, 1964.
2. MASON, W., Piezoelectric Crystals and their Applications to Ultrasonics, D. Van Nostrand, New York, 1950.
3. "IRE Standards on Piezoelectric Crystals: The Electromechanical Coupling Factor", Proc. IRE, 46:764 (1958).
4. "IRE Standards on Piezoelectric Crystals: Measurements of Piezoelectric Ceramics, 1961 ", Proc. IRE, 49:1161 (1961).
5. "IRE Standards on Piezoelectric Crystals: Determination of the Elastic, Piezoelectric, and Dielectric Constants - The Electromechanical Coupling factor, 1958". Proc. IRE 46 (1958) No. 4, pp. 764-778.
6. JAFFE, B., COOK, W. Jr. and JAFFE, H., Piezoelectric Ceramics, Academic Press, New York, 1971. 7. BERLINCOURT, D., in Ultrasonic Transducer Materials, MATTIAT, O., ed., Plenum Press, New York, 1971.
8. NEWCOMB, C. V. and FLINN, I., Improving the Linearity of Piezoelectric Ceramic Actuators. Electronic Letters 18 (1982), no. 11, pp. 442-444.
9. NEWCOMB, C. V., Piezoelectric Fuel Metering Valves. Second International Conference on Automotive Electronics, London 1979, Conf. Publ. no. 181.
10. CROSS, R. K., LARKA, P., O'NEILL, C. G., Electronic Fuel Injection for Controlled Combustion in Diesel Engines. SAE Technical Paper Series 810258. 11. HULST, A. P., On a family of high-power transducers. Ultrasonics International 1973, Conf. Proc., pp. 285-294.
12. MERKULOV, L. G., Design of Ultrasonic Concentrations. Soviet Physics-Acoustics 3 (1957), pp. 246-255.
13. MEISSER, C., Heat Meter Employs Ultrasonic Transducer. Control Engineering, May 1981, pp. 8789.